Author:
Li, Yikui

Title:
The spatiotemporal organisation as a means of control of regulatory T cell functions in autoimmunity

The spatiotemporal organisation as a means of control of regulatory T cell functions in autoimmunity

Yikui Li

A dissertation submitted to the University of Bristol in accordance with the requirements for award of the degree of Doctor of Philosophy in the Faculty of Life Sciences

School of Cellular and Molecular Medicine

June 2020

Word count: 44,280

Abstract

$CD4^+$ effector (Teff) and regulatory (Treg) T cells play different roles in the immune system. Teffs promote innate and adaptive immune responses, while Tregs suppress immune responses, maintain immunological tolerance and prevent autoimmune diseases. Naïve $CD4^+$ T cell can be induced *in vitro* to become Teffs or inducible Tregs (iTregs). This work focused on comparing the spatiotemporal organisation of T cell signalling intermediates upon activation of Teffs and iTregs, using the Tg4 murine model of experimental autoimmune encephalomyelitis. Live cell imaging data of Tg4 Teffs were previously acquired. Compared to Teffs, iTregs were found to show impaired spatiotemporal patterning of LAT, TCR-ζ and F-actin, suggesting their activation to be defective. T cell-APC couples formed by iTregs were found to be less stable. iTregs show a reduced ability to secrete IFN-γ and tend to secrete more IL-10 than Teffs. To investigate whether iTreg function can be controlled by proximal T cell signalling, CTLA-4 and PD-1 coinhibitory pathways, the spatiotemporal distribution of LAT during iTreg activation were manipulated.

Results show that blocking CTLA-4 and PD-1 significantly inhibited iTreg generation. Dual blockade of CTLA-4 and PD-1 was found to improve cell coupling and partially enhance LAT accumulation at the T cell-APC interface. Previous work has shown that fusing LAT with the PKC-θ V3 or Vav1 SH3SH2SH3 domain enhances LAT central accumulation at the interface under attenuated T cell stimulation. Here we show that in iTreg activation, fusion with PKC-θ V3 excessively enhanced LAT overall accumulation at the interface, but slightly reduced their IFN-γ and IL-10 secretion, while fusion with Vav1 SH3SH2SH3 fully restored LAT overall accumulation at the interface, and slightly enhanced IL-10 secretion. Both conditions improved cell coupling. These data indicate that blocking coinhibitory pathways and enhancing LAT spatiotemporal organisation improve iTreg activation, but regulate their immunosuppressive function to a small extent.

Author’s declaration

I declare that the work in this dissertation was carried out in accordance with the requirements of the University's Regulations and Code of Practice for Research Degree Programmes and that it has not been submitted for any other academic award. Except where indicated by specific reference in the text, the work is the candidate's own work. Work done in collaboration with, or with the assistance of, others, is indicated as such. Any views expressed in the dissertation are those of the author.

SIGNED: ..... DATE:.....

Acknowledgements

First I would like to express my sincere gratitude to my supervisor Prof. Christoph Wülfing, for his dedicated support and guidance. Thank you for always being there for me and answering my endless (sometimes silly) questions. I would like to thank Dr. Lindsay Nicholson and Dr. David Morgan for their support and kindness. Your advice was always helpful and decent. Thank you all for showing me what a good researcher should be.

Further, I would like to thank many great people in the Wülfing, Morgan, Wooldridge, and Amulic labs. I would like to thank Helen Tunbridge, as without your initial effort I would not have been able to work on this project. Danielle Clark and Rachel Ambler helped and taught me a lot when I first came to Bristol. Grace Edmunds was always willing to help and encouraging. Many thanks go to Laura McMillan and Sin Lih Tan who were great listeners and teachers. I would like to thank Silvia Cirillo for helping me with my experiments. I am very thankful to Carissa Wong who has always been a great friend and helped me out many times. A huge thank you to Jiahe Lu, Hanin Alamir, Emily Milodowski, Lea Knezevic and Jorge Huete Carrasco for being so kind and supportive, we had a great time in the lab. I will definitely miss those great football games I had with Fernando Manuel Ponce Garcia and Ore Francis. I enjoyed chats with Christopher Rice and Drinalda Cela, who were always inspiring and helpful.

Great flow cytometry experts like Andrew Herman and Lorena Sueiro Ballesteros made it possible for me to finish my Ph.D. Thank you both and I have been so lucky to have you two around during my study. Special thanks to Alan Hedges for being extremely patient with me and helping me with statistics.

Many thanks to Shanshan Liu, who has been so cheerful and encouraging during my writing. Chats with you always kept me motivated.

To my sisters, Lingnan and Manhua, thank you so much for your support and patience. You have been taking care of me for years and it is so reassuring to have you around.

Finally, I sincerely thank my patients for your encouragement and love. I know no matter where I go and what I choose to do, you will always support and believe in me. I'm very lucky to have you as my parents.

Table of contents

List of figures

List of tables

Abbreviations

AIRE	Autoimmune regulator
ANOVA	Analysis of variance
APC	Antigen presenting cell
Arp2/3	Actin-related protein 2/3
BBB	Blood-brain barrier
BCR	B cell receptor
CAR	Chimeric antigen receptor
CD	Cluster of differentiation
CFA	Complete Freund’s adjuvant
CNS	Central nervous system
cSMAC	Central supramolecular activation cluster
CTLA-4	Cytotoxic T lymphocyte antigen-4
CTV	CellTrace Violet
DAG	Diacylglycerol
DC	Dendritic cell
DIC	Differential interference contrast
DMEM	Dulbecco’s modified Eagle’s medium
DNA	Deoxyribonucleic acid
EAE	Experimental autoimmune encephalitis
EDTA	Ethylenediaminetetraacetic acid
ER	Endoplasmic reticulum
ERK	Extracellular signal-regulated kinase
FACS	Fluorescence activated cell sorting
F-actin	Filamentous actin
FBS	Foetal bovine serum
Foxp3	Forkhead-winged-helix transcription factor 3
FSC	Forward side scatter
GM-CSF	Granulocyte-macrophage colony-stimulating factor
Grb2	Growth factor receptor-bound protein 2
GRAP2 (Gads)	Grb2-related adapter protein 2
HA	Haemagglutinin
ICAM-1	Intercellular adhesion molecule-1
IFN	Interferon
Ig	Immunoglobulin
IL	Interleukin
ITIM	Immunoreceptor tyrosine-based inhibitory motif
iTreg	Induced Treg

Itk	IL-2 inducible tyrosine kinase
ITSM	Immunoreceptor tyrosine-based switch motif
LAG-3	Lymphocyte activation gene-3
LAP	latency-associated peptide
LAT	Linker of activated T cells
Lck	Lymphocyte specific protein tyrosine kinase
LFA-1	Lymphocyte function associated antigen-1
MAPK	Mitogen-activating protein kinase
MBP	Myelin basic protein
MFI	Median fluorescence intensity
MHC	Major Histocompatibility
MOG	Myelin oligodendrocyte glycoprotein
MS	Multiple sclerosis
mTEC	Medullary thymic endothelial cell
Nck	Non-catalytic region of tyrosine kinase adaptor protein 1
NF-κB	Nuclear factor κB
NK cells	Natural killer cells
NLR	NOD-like receptors
PAMP	Pathogen-associated molecular pattern
PBS	Phosphate buffered saline
PD-1	Programmed cell death protein-1
PD-L1	Programmed cell death protein ligand-1
PD-L2	Programmed cell death protein ligand-2
PFA	Paraformaldehyde
PIP_2	Phosphatidylinositol 4,5 bisphosphate
PIP_3	Phosphatidylinositol 3,4,5 trisphosphate
PI3K	Phosphoinositide 3-kinase
PKC	Protein kinase C
PLP	Proteolipid protein
PMA	Phorbol myristate acetate
PRR	Pattern-recognition receptor
pSMAC	Peripheral supramolecular activation cluster
pTreg	Peripheral Treg
RA	Rheumatoid arthritis
RAG	Recombination activating gene
RasGRP	Ras guanyl nucleotide-releasing protein
RNA	Ribonucleic acid
RPMI	Roswell park memorial institute medium

SCF	Stem cell factor
SH2/3 domain	Src-homology 2/3 domain
SHP-1/2	Src-homology region-2 domain containing phosphatase-1/2
SLE	Systemic lupus erythematosus
SLP-76	SH2 domain containing leukocyte protein of 76kDa
SSC	Side scatter
STAT	Signal transducer and activation of transcription
TCR	T cell receptor
TGF	Transforming growth factor
Th cells	T helper cells ($CD4^+$ T cells)
TIGIT	T cell immunoreceptor with immunoglobulin and ITIM domains
TIM-3	T-cell immunoglobulin and mucin-3
TLR	Toll-like receptor
Tr1	Type 1 regulatory cells
Treg	Regulatory T cell
tTreg	Thymically derived Treg
Vav1	Vav guanine nucleotide exchange factor 1
WASP	Wiskott-Aldrich syndrome protein
ZAP-70	Zeta-chain associated protein kinase-70

Chapter 1 Introduction

1.1 Innate and adaptive immune immunity

The human body protects individuals from infections and diseases caused by microorganisms including bacteria, fungi and viruses. As a product of evolution, the immune system of vertebrates not only protects the host from invasions of exogenous pathogens but also functions in a sophisticated fashion to maintain immune homeostasis. It comprises of two powerful lines of defence: the innate and adaptive immune system. When microbes invade, the innate immune system initiates efficient responses to recognise and eliminate the potential pathogens. This first barrier can discriminate self and non-self antigens. If the innate immune system is breached, recognitions of pathogens will be presented further, and adaptive immune responses are triggered. Activated B cells will secrete antibodies targeting these intruders and T cells can produce signalling proteins (cytokines) for reinforcement and induce apoptosis of infected cells. It is of note that none of these events can be properly executed if the host cannot identify pathogens at the beginning of the battle, and mechanisms of recognition lie within the immune receptors.

The innate immune system comprises various cells including macrophages, dendritic cells (DCs), mast cells, neutrophils, eosinophils and natural killer (NK) cells. With germline-encoded pattern-recognition receptors (PRRs), they can recognise pathogen-associated molecular patterns (PAMPs) from microorganisms (1). There are mainly four classes of PRRs including the Toll-like receptors (TLRs), NOD-like receptors (NLRs), RIG-like receptors (RLRs) and C-type lectin receptors (CLRs) (2). Endogenous signalling induced by the ligation of PRRs mediates inflammatory responses, provides costimulatory signals for T cell activation, and promotes effector T cell (Teff) differentiation (3).

Two main components of the adaptive immune system are T and B cells, and they express T cell receptors (TCRs) and B cell receptors (BCRs) on their cell surface respectively. T cells originate from common lymphoid progenitors from the bone marrow or foetal liver and mature in the thymus, while B cells originate from haematopoietic stem cells in the foetal liver which migrate to bone marrow after birth (4, 5). Mature T and B cells translocate to lymph nodes and the spleen where adaptive immune responses can be initiated, usually by receiving signals from the innate immune system (4).

B cells can efficiently differentiate into plasma cells and secrete pathogen-specific antibodies to promote neutralisation of pathogens after their BCR binds a cognate antigen (6). Moreover, B cells are also capable of presenting antigens to T cells (7).

T cell recognition is a key part of triggering effective adaptive immune responses. A TCR binds a specific antigen presented by an antigen presenting cell (APC), via its major histocompatibility complex (MHC). MHC class I molecules are expressed by many mammalian cells while MHC class II molecules are expressed mainly on APCs including DCs, B cells, and macrophages (8). T cell-APC interactions are required for T cell activation and differentiation, and cytotoxic T cells expressing cluster of differentiation 8 (CD8) are associated with MHC class I while helper T cells expressing CD4 are associated with MHC class II.

1.2 T cell differentiation and maturation

Common lymphoid progenitors enter the thymus and do not express TCRs, CD4, and CD8, termed double negative thymocytes (9). Double negative thymocytes can become T cells expressing either αβ or γδ TCRs (10). During the development of αβ T cells at the double negative stages, they initially express a pre-TCR consist of a non-rearranging pre TCR-α and a TCR-β chain which undergoes V(D)J gene recombination regulated by RAG proteins (9, 11). After several rounds of cell divisions, the pre-TCR-α is replaced by a newly rearranged TCR-α, and cells during this stage often start to express CD4 and CD8. Subsequently, a large number of $CD4^+$ $CD8^+$ thymocytes bearing a mature αβ TCR are generated (9). These double positive cells then first make contact with cortical thymic epithelial cells (cTECs) presenting self-peptides. If these cells express a TCR with a poor affinity for self-peptide MHC complexes, delayed apoptosis of these cells will be induced (death by neglect) (9). Double positive thymocytes expressing TCRs with intermediate affinity for self-peptide MHC complexes become CD4 or CD8 lineage-committed and then enter the medulla (positive selection) (12). They interact with medullary thymic endothelial cells (mTECs) which express numerous genes representing all tissues from the body. This is regulated by the autoimmune regulator (AIRE) (13), allowing the elimination of thymocytes which respond to self-peptides from all tissues with high affinity (negative selection or central tolerance). Cells expressing TCRs with intermediate affinity for self-peptides will eventually survive and differentiate into $CD4^+CD8^-$ or $CD4^-CD8^+$ single positive T cells (9, 14). Some T cells with high affinity for self-peptides leave the thymus and become regulatory T cells (Tregs) (15).

Mature naïve $CD4^+$ and $CD8^+$ T cells then leave the thymus and enter lymphoid sites. Upon activation, $CD8^+$ or cytotoxic T cells eliminate target cells by secreting cytokines such as tumour necrosis factor-α (TNF-α) and interferon-γ (IFN-γ), releasing granzymes and perforin, and inducing apoptosis via the Fas pathway (16). Activated $CD4^+$ or T helper (Th) cells differentiate into different subsets.

1.3 $CD4^+$ T cell subsets

Initially, APCs present peptide antigens to $CD4^+$ naïve T cells via TCR and peptide-MHC (pMHC) interactions, with the assistance of CD4 as a co-receptor. Moreover, with signals from costimulatory molecules (mainly CD28) and cytokines secreted by APCs, $CD4^+$ T cells can be fully activated. Depending on cytokines on-site, the strength of TCR signals, APC cell types, and costimulatory molecules, $CD4^+$ T cells can differentiate into different T helper cell (Th) lineages including Th1, Th2, Th17, Treg, T follicular helper (Tfh), Th9 and Th22 T cells (17, 18). Th cell differentiation is regulated by master regulators and signal transducer and activator of transcription (STAT) family members (19). Here we describe four of these subsets.

1.3.1 Th1 cells

Activation of naïve $CD4^+$ T cells in the presence of interleukin 12 (IL-12) and IFN-γ, drives Th1 cell differentiation (19), and strong TCR signals enhance Th1 but not Th2 responses (20). Th1 cells secrete IFN-γ, as a signature cytokine, and other pro-inflammatory cytokines including TNF-α and TFN-β (21, 22). The T-box transcription factor (T-bet) and IL12-induced STAT4 are important transcription factors for Th1 cell development and they both induce IFN-γ production of Th1 development (17, 22). IFN-γ plays roles in both innate and adaptive immune responses including upregulating expression of TLR4 (23), activating macrophages (24), enhancing phagocytosis (25), mediating immunoglobulin G (IgG) class switching (26), and stimulating $CD8^+$ T cell responses in viral infections (27). IFN-γ promotes the assembly of subunits (LMP2, MECL-1, and LMP7) of the immunoproteasome, which presents antigenic peptides to $CD8^+$ T cells during immune responses (28). Moreover, IFN-γ induces transporter-associated antigen processing (TAP) by upregulating expression of TAP1 and TAP2 subunits (29). Expression of MHC class I and II molecules on the cell surface can also be upregulated by IFN-γ (24). IFN-γ or IFN-γ receptor 1 knockout mice are susceptible to bacterial, parasitic, and viral infections (24).

IFN-γ-secreting Th1 cells are often associated with autoimmune diseases including type 1 diabetes, multiple sclerosis (MS), and rheumatoid arthritis (RA) (30). Experimental autoimmune encephalomyelitis (EAE), which is a mouse model for MS, has been widely applied to study autoimmune immune diseases in the central nervous system (CNS) and MS has been long considered to be mediated by IFN-γ secreting Th1 cells (31). After the discovery of Th17 cells in 2005, studies have revealed that their signature cytokine IL-17A and IL-17F play important roles in the development of EAE (32). The presence of Th17 cells and increased expression of IL-17A, IFN-γ, granulocyte-macrophage colony-stimulating

factor (GM-CSF) secreted by these cells have been observed in MS patients (33). Both Th1 and Th17 cells contribute to the pathogenesis of EAE and MS, but at different stages (34).

1.3.2 Th2 cells

Th2 cells secrete IL-4, IL-5, IL-9, IL-10 and IL-13 and their polarisation is induced by IL-4 and IL-2 with a weak TCR signal (17, 20, 21). Th2 differentiation is regulated by GATA3 and IL-4-induced STAT 6 (17). Th2 cells regulate immune responses against extracellular infections such as helminths and IL-4 is involved in IgE switching and production by B cells (17).

Overactive Th2 responses can lead to chronic inflammatory diseases such as asthma, which is associated with airway hyperresponsiveness and allergic inflammation in the lung (35).

1.3.3 Th17 cells

Differentiation of Th17 cells is regulated by the transcription factor RORγt, STAT3 and several cytokines. Naïve $CD4^+$ T cells can be induced into Th17 cells in the presence of transforming growth factor beta (TGF-β) and IL-6 or IL-21 and their expansion is promoted by IL-1 and IL-23 (36). IL-17 secreted by Th17 cells can promote pro-inflammatory cytokine (e.g. IL-1 and TNF-α) and chemokine secretion which activates and recruit macrophages to the site of infection (36). IL-17 promotes granulopoiesis by upregulating the release of granulocyte colony-stimulating factor (G-CSF) and expression of membrane-bound stem cell factor (SCF) (37). Elevated G-CSF levels induced by IL-17 also increase mobilisation of mature neutrophils from the bone marrow (38). Additionally, Th17 cells secrete IL-21 and IL-22. IL-21 can induce differentiation of activated B cells into plasma cells and enhance the cytotoxic activity of both NK cells and $CD8^+$ T cells (39), and IL-22 plays a key role in mucosal host defence against bacterial infection in the lung (40).

Moreover, Th17 cells and related cytokines are involved in the development of a wide range of autoimmune diseases including systemic lupus erythematosus (SLE), type I diabetes, RA and MS (41). IL-23, which induces Th17 differentiation shares the same p40 subunit of IL-12 and together with IL-17 and IL-21 secreted by Th17 cells contribute to the induction of EAE (42). Both Th1 and Th17 cells are able to induce EAE, and the ratio of Th1 to Th17 cells can determine whether T cell infiltration and inflammation will occur in the brain or spinal cord (43).

1.3.4 Regulatory T cells

$CD4^+$ regulatory T cells (Tregs) have been discovered, categorised and investigated for over the past 40 years. They are mostly known for their ability to suppress immune responses, maintain self-tolerance and play roles in helping tumour cells escape immune surveillance (44-47). In 1995, Sakaguchi *et al* (45) identified a subpopulation of $CD4^+$ T cells in mice expressing IL-2 receptor α-chains (CD25) which play roles in maintaining self-tolerance. Elimination of these $CD4^+$ $CD25^+$ T cells (about 10% of peripheral $CD4^+$ T cells) leads to inflammatory lesions in different organs and causes autoimmune diseases. Subsequently in 2003, forkhead-winged-helix transcription factor 3, Foxp3 was found to be specifically expressed in $CD4^+$ $CD25^+$ Tregs and define this Treg population (46, 48). Treg suppression can be induced via cell to cell contacts (e.g. Tregs constitutively express cytotoxic T lymphocyte antigen-4 (CTLA-4) which competes with costimulatory molecule CD28 for binding CD80/86), IL-2 deprivation, immunosuppressive cytokines (e.g. IL-10 and IL-35) and molecules (e.g. adenosine) (49) (Figure 1.1). Recently, Ovcinnikovs *et al* show that Tregs recruit CTLA-4 to the cell membrane and rapidly capture CD80/86 of APCs via trans-endocytosis upon stimulation (50).

$CD4^+$ $CD25^+$ $Foxp3^+$ Tregs can be naturally derived from the thymus (tTregs), generated peripherally *in vivo* (pTregs) and induced *in vitro* (iTregs) in the presence of TGF-β and IL-2 (51-53). Unlike tTregs and pTregs, Treg-specific DNA hypomethylation does not occur in Treg-specific demethylated regions (such as the *Foxp3* conserved non-coding sequence 2 (CNS2) region) of iTregs, and their Foxp3 expression is unstable (54-56). Naturally occurring tTregs are capable of suppressing self-reactive T cells escaping from negative selection thus play important roles in maintaining self-tolerance (57). It has been reported that a high-affinity TCR which recognises a cognate peptide and CD28 costimulation are both required for tTregs development (15, 58). pTregs exist in the periphery, such as the intestine and liver, where they are generated under weak TCR stimulation with IL-2, TGF-β or retinoic acid (59, 60). Low dose administration of antigen enhances pTreg induction, and increased DC activation impedes this process (61). Moreover, strong TCR stimulation and CD28 costimulation can inhibit iTreg generation (62, 63). A recent study suggests that efficient iTreg induction requires optimal TCR stimulation strength (64). It was shown that 1.0 μg/ml anti-TCRβ antibody leads to a higher frequency of iTregs, compared with 0.1 and 10 μg/ml anti-TCRβ, but a high concentration of anti-TCRβ antibody stabilises Foxp3 expression in iTregs by inducing demethylation of conserved non-coding sequence 2 (CNS2) of the *Foxp3* locus. These studies reveal that different signal strengths of TCR and costimulation are required in the development of tTregs, pTregs and iTregs. Unstable Foxp3 expression of iTregs is one major issue for applying iTregs for therapeutic approaches (65). In general, iTregs can be generated by stimulating naïve $CD4^+$ $CD25^-$ T cells with anti-CD3

antibody in the presence of APCs and TGF-β, or with plate-bound anti-CD3 and anti-CD28 antibodies in the presence of TGF-β and IL-2 (51, 66). IL-2 is required for TGF-β mediated iTreg induction (66).

Apart from $CD25^+$ $Foxp3^+$ Tregs, two other $CD4^+$ Tregs subsets were reported. Type 1 regulatory (Tr1) T cells were discovered when a specific peptide was repeatedly presented to naïve $CD4^+$ T cells with IL-10 in the culture (67). Tr1 cells secrete high level of IL-10 and are capable of suppressing naïve T cell proliferation but do not express Foxp3 (68). Coexpression of CD49b and lymphocyte-activation gene 3 (LAG-3) can identify Tr1 cells in mouse and human (69).

The third subset of $CD4^+$ Tregs, Th3 cells were identified from an EAE mouse model after oral administration of MBP (70). They secrete TGF-β, IL-4 and IL-10 and suppress EAE. Th3 cells are $Foxp3^-$ cells and express latency-associated peptide (LAP) in humans and mice (71). Nevertheless, numerous studies over the last few decades have focused on $CD4^+$ $CD25^+$ $Foxp3^+$ Tregs for their various mechanisms of suppression and therapeutic potential for autoimmune diseases and cancer (72).

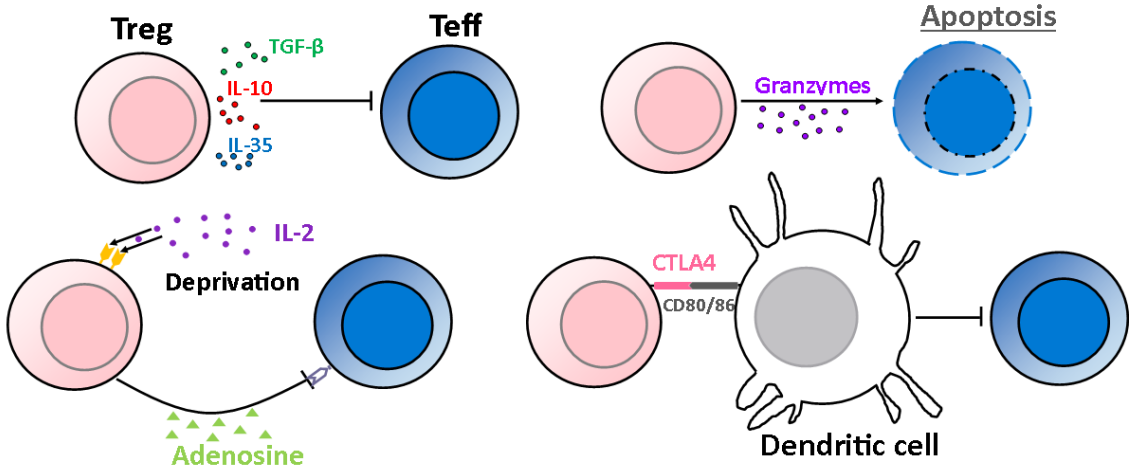

Figure 1.1 Basic mechanisms of Treg suppression

1. Tregs secrete inhibitory cytokines such as IL-10, TGF-β and IL-35 to inhibit Teff proliferation and differentiation. 2. Tregs release granzymes to induce T cell apoptosis. 3. Tregs express a high level of CD25 (IL-2Rα) which leads to IL-2 deprivation and generate adenosines that induce immunosuppression. 4. Tregs express CTLA-4 on the cell surface which binds CD80/86 to inhibit Teff activation by CTLA-4 trans-endocytosis.

1.4 Immune tolerance and autoimmunity

Most T cells recognising self-antigens with high affinity are deleted by the central tolerance (negative selection) or converted into Tregs. However, central tolerance is imperfect, as some autoreactive T cells with a low affinity for self-pMHC can escape from central tolerance (73). The fact that these cells normally do not trigger autoimmune responses indicates that additional modifications exist in the periphery, known as peripheral tolerance. There are several mechanisms of peripheral tolerance including keeping these autoreactive cells from cells expressing autoantigens, downregulating T cell responses by tolerogenic APCs, Treg suppression, peripheral deletion of autoreactive T cells, and expression of coinhibitory molecules on self-reactive T cells (74). If the balance of tolerance and immunity is broken, autoimmune cells could induce immune responses against healthy cells and lead to autoimmune diseases. Autoimmunity could be triggered by various factors including genetic background, tissue damage, hidden or new self-antigens, inflammation and infections (75). A wide range of autoimmune diseases have been studied for decades and based on the tissue involved, they can be categorised into organ-specific diseases (e.g. MS) and systemic diseases (e.g. SLE) (75).

1.5 Multiple sclerosis

MS is a chronic inflammatory disease affecting the brain and spinal cord, characterised by various clinical symptoms including cognitive impairment, impaired vision, tremor, vertigo, weakness and pain (76, 77). Based on the dominant phenotype, MS can be classified into five forms including relapsing-remitting MS, clinically isolated syndrome, radiologically isolated syndrome, primary-progressive MS and secondary-progressive MS (78). Infiltration of autoreactive T and B cells into the brain result in inflammations, demyelination and axonal injury in MS patients (79). Myelin associated autoantigens, such as myelin basic protein (MBP), myelin proteolipid protein (PLP) and myelin oligodendrocyte glycoprotein can be recognised by self-reactive T cells thus lead to immune responses (80, 81). Autoreactive T and B cells are initially activated and differentiated in the periphery, possibly by molecular mimicry, bystander activation, recognition of novel and CNS sequestered autoantigens (76). Activated $CD8^+$ T cells, Th1 cells, Th17 cells, B cells and innate immune cells pass through the blood-brain barrier (BBB) and enter the CNS, where T cells are reactivated by CNS-resident or immigrant APCs (such as DCs, microglia and macrophages) presenting autoantigens and induce inflammation and tissue damage (42, 76). Early cohort studies showed that physical trauma does not cause or exacerbate MS (82, 83). Many researchers suggest that viral infections cause MS, for example, significantly increased immune responses to Epstein-Barr virus (EBV) were found in the serum and cerebrospinal

fluid of MS patients (84). Other environmental factors, such as chemicals, smoking and vitamin D levels, and genetic factors are also involved in the pathogenesis of MS (85).

1.5.1 Experimental autoimmune encephalomyelitis

Experimental autoimmune encephalomyelitis (EAE) is an animal model which shows pathological similarities to MS and has been widely used for studying the pathogenesis of MS and developing immunotherapies (86). One main difference between these two diseases is that EAE requires induction of immunisation while the development of MS in human is not artificial and induced by unknown autoantigens (31). EAE usually can be induced by inoculation of myelin-associated peptides in the presence of complete Freund's adjuvant (CFA) (87). In addition, there are spontaneous models of EAE and these transgenic mice carry TCRs recognising specific peptides such as the myelin oligodendrocyte glycoprotein (MOG) or MBP peptide and develop spontaneous EAE (88, 89).

1.5.2 The Tg4 mouse model

The Tg4 mouse model was established by the Wraith laboratory and more than 90% of Tg4 $CD4^+$ T cells express a transgenic TCR recognising the acetylated MBP Ac1-9 peptide. EAE in Tg4 mice can be induced by the administration of MBP Ac1-9 peptides with CFA (73). Tg4 T cells have also been applied to study peptide-induced T cell tolerance. Studies of antigen-specific immunotherapy using the Tg4 mouse model have shown that autoimmune responses in EAE can be dampened, and Tg4 $CD4^+$ T cell anergy can be induced by repetitive administration of MBP Ac 1-9 [4Y] peptides under non-immunogenic conditions (90, 91). Such peptide treatment leads to the generation of IL-10 secreting $CD4^+$ T-bet^+ $Foxp3^-$ regulatory T cells and IL-10 secreted by these Tregs contributes to the peptide-dependant protection of EAE (90, 92). These studies suggest the Tg4 TCR transgenic mouse be an appropriate animal model for studying the pathological mechanism and antigen-specific immunotherapies for MS.

1.6 T cell activation

As mentioned in section 1.3, T cell-APC interaction is a key step for initiating proliferation and differentiation of naïve T cells, known as T cell activation. T cell activation requires signal transduction from the engagement of TCR with pMHC, costimulation and cytokines.

1.6.1 TCR-pMHC interaction (signal one)

For αβ T cells, TCR α and β subunits are noncovalently associated with CD3 γε and δε dimers, and linked with CD3 ζζ dimers via disulfide bonds, forming the TCR/CD3 complex

(93). Proximal TCR signalling is briefly described in Figure 1.2. In early T cell signalling, TCRs recognise short peptides bound to MHC class I or II molecules expressed on the surface of APCs. With the assistance of CD4 or CD8 co-receptors, protein tyrosine kinase Lck is then recruited to the TCR/CD3 complex and phosphorylates immunoreceptor tyrosine-based activation motifs (ITAMs) on CD3 ζ chains (93-95). Two phosphorylated tyrosines on the ITAMs of TCR-ζ become binding sites for SH2 domains of zeta-chain-associated protein kinase 70 (ZAP-70), which further phosphorylates linker of activated T cells (LAT) and continue to transmit TCR signalling (94, 96). LAT is phosphorylated by ZAP-70 on tyrosine residues which bind the SH2 domain of adaptor protein Grb2, Gads and phospholipase PLC-γ1 (97), and these binding events assemble a LAT nucleated signalosome.

Grb2 consists of one SH2 domain and two flanking SH3 domains, which recruits Sos, a Ras activator to the membrane (98). Activated Ras induces activation of the mitogen-activated protein kinase (MAPK) cascade, which eventually activates transcription factor activator protein-1 (AP-1) (99).

The adaptor protein Gads is another member of the Grb2 family and has similar domains as Grb2. Its SH3 domain displays a different binding specificity and binds SLP-76 which is then recruited to the LAT signalosome. SLP-76 is phosphorylated by ZAP-70 and continues to recruit vav guanine nucleotide exchange factor 1 (Vav1), Nck adaptor protein (Nck) and IL-2 inducible tyrosine kinase (Itk) to the complex (98, 100). Vav1 and Nck regulate recruitment and activation of Wiskott-Aldrich syndrome protein (WASP), which interacts with actin-related protein 2/3 (Arp2/3) complex and promotes actin polymerisation (101-103). Itk not only regulates Vav1 associated actin rearrangement, but also activates PLC-γ1 (104, 105).

PLC-γ1 hydrolyses phosphatidylinositol 4,5-bisphosphate (PIP_2) to produce membrane-bound diacylglycerol (DAG) and inositol 1,4,5-trisphosphate (IP3) (106). DAG recruits protein kinase C theta (PKC-θ) and Ras guanyl nucleotide-releasing protein (RasGRP) to the membrane. The former eventually leads to activation of NF-κB in the nucleus and the latter promotes transduction of MAPK signalling pathways (107). IP3 binds IP3 receptors in the endoplasmic reticulum (ER) and induces $Ca2^{+}$ influx which leads to nuclear translocation and activation of nuclear factor of activated T cells (NFAT) (108).

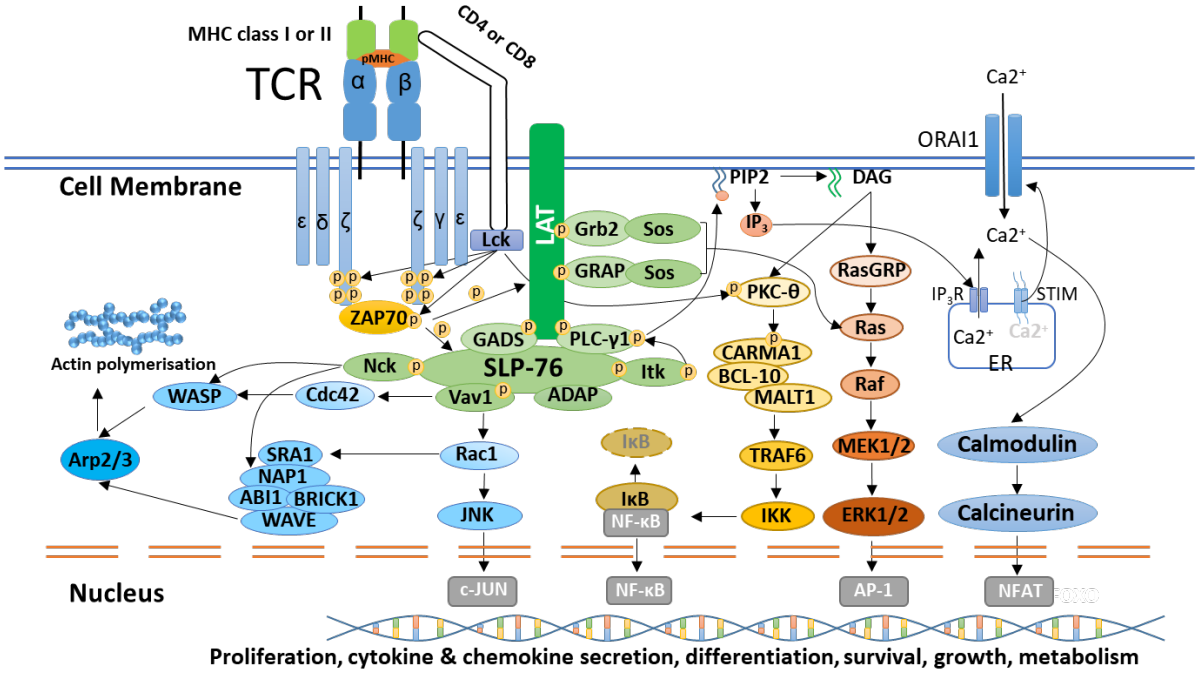

Figure 1.2 A schematic diagram of the proximal TCR signalling pathway.
Arrows indicate activation or (directions of) recruitment of signalling molecules, p in yellow circles indicate phosphorylation.

1.6.2 Costimulation (signal two)

T cell activation also requires costimulation induced by CD28 and CD80 (B7.1)/CD86 (B7.2) engagement (109). CD80 and CD86 are widely expressed on the surface of APCs and are members of the B7-CD28 superfamily (110). CD28 is constitutively expressed by $CD4^+$ and $CD8^+$ T cells (109). Upon binding, tyrosine-based signalling motifs of CD28 cytoplasmic tail are phosphorylated by protein tyrosine kinases and together with proline-rich motifs, they recruit kinases and adaptor proteins to the membrane including phosphoinositide 3-kinase (PI3K), Gads, Grb2, Itk and Lck. These signalling events eventually induce secretion of cytokines including IL-2, IL-4, IL-5, TNF-α and IFN-γ (111, 112), actin cytoskeleton remodelling, and activation of NFAT, NF-κB and AP-1 (95). CD28 deficiency or blockade of CD28 and CD80/86 interactions in mice could reduce expression of IL-2 and IL-2R (113), inhibit T cell proliferation (114) and impair Th2 responses against infections (115).

T cells require not only positive signals from costimulatory receptors to trigger immune responses, but also need negative signals from coinhibitory receptors to regulate immune responses, induce tolerance and prevent autoimmunity. Coinhibitory molecules including CTLA-4, programmed cell death protein-1 (PD-1), T-cell immunoglobulin mucin-3 (TIM-3), lymphocyte activation gene-3 (LAG-3) and T cell immunoreceptor with immunoglobulin and ITIM domains (TIGIT) have been widely studied (116).

1.6.3 Cytokines (signal three)

Signal one and two are sufficient to drive the proliferation of naïve T cells but further optimal differentiation for their effector function require a third signal from cytokines (117). As mentioned in section 1.3, differentiation of different helper subsets from $CD4^+$ naïve T cells is regulated by the cytokine environment. For $CD8^+$ T cells, IFN-α, β, γ and IL-12 play roles in regulating their expansion, survival and cytotoxic function during immune responses against infection (118, 119).

1.7 The immunological synapse

Initial formation of T cell-APC junction is regulated by engagement of TCR-pMHC, co-receptors and adhesions molecules, known as the immunological synapse (IS) (120). The formation of a stable immunological synapse is characterised by a central TCR cluster and a peripheral ring of adhesions molecules at the T cell-APC interface. Based on different spatial segregation patterns, TCR/CD3 complex and PKC-θ assemble the central supramolecular activation cluster (cSMAC), while lymphocyte function associated antigen 1 (LFA-1) and talin assemble the peripheral SMAC (pSMAC), supported by dynamic actin cytoskeleton (120-122). The formation of these supramolecular signalling complexes stabilises the IS and is important for efficient T cell activation and cytokine production (121). Tyrosine protein kinase Lck/Fyn and lipid PIP_3 are recruited to the cSMAC (121, 123, 124). The LAT nucleated signalling complex (including Grb2, Gads and SLP-76) transiently forms after TCR ligation and disappears within 3 minutes, while localisation of Zap-70 to the cSMAC remains steady for more than 30 minutes once recruited (125, 126). These observations indicate the composition of the cSMAC to be dynamic and time dependant. The role of the cSMAC at the synapse has been controversial. In a study using naive T cells, TCR-mediated tyrosine kinase signalling and accumulation of TCR and Lck were found at the periphery of the IS before the cSMAC is formed, and that the role of cSMAC was proposed to downregulate TCR signalling and mediate degradation of receptors and phosphorylated proteins (127, 128). Moreover, the cSMAC formation was found to inhibit signalling in strong agonist peptide-induced T cell activation, but enhance the stimulatory capacity of weak peptides (128, 129). However, these studies mainly focused on investigating SMAC formation after 30 minutes of T cell-APC cell coupling, thus initial signalling events within minutes after the IS formation have been less considered. Singleton *et al* have shown that within the first few minutes of T cell-ACP interactions, translocation of signalling intermediates including receptors, tyrosine kinases and lipids can be observed and are highly diverse (130). Subsequently, manipulation of localisation of LAT, one of the key components of the cSMAC revealed that transient accumulation of LAT at the centre of the IS is sufficient to promote IL-2 secretion (126). Clark *et al* proposed that the cSMAC to play two roles: the cSMAC recruits various signalling intermediates required for proximal

TCR signal transduction within the first two minutes of T cell activation, and later it selectively drives proteins like Vav1 and SLP-76 away from the cSMAC, assisted by the actin network and they continue to form smaller signalling complexes. Thus the cSMAC not only enhances early T cell activation but continues to regulate proximal TCR signalling by sequestering key signalling proteins (126). Although TCR accumulation in these two studies was consistently found at the centre of the IS at early time points, which is contradictory to that observe by Lee *et al* (127), different mouse and experimental (fixed cell conjugates vs live cell imaging) models may contribute to such inconsistency.

It should be noted that the bull's-eye structure of the cSMAC and pSMAC is mainly found in T-B cell interactions while synapses formed by T cells and DCs display a multifocal patterning without large segregation of CD3 and LFA-1, suggesting formation of the SMACs in T cell activation is restricted to specific conditions (131, 132).

1.8 Spatiotemporal organisation of T cell activation

Proximal signalling of T cell activation is initiated by ligation of TCR and pMHC, assisted by co-receptors and transduced via tyrosine phosphorylation, which eventually promotes cell proliferation, polarisation and effector function. Investigations about T cell signalling events at the IS, such as the assembly of TCR-induced signalling complexes and actin polarisation help us better understand the roles of the cSMAC and pSMAC in early T cell activation (125, 133). Many studies were conducted on 2D systems or with fixed T cell-APC conjugates using immunofluorescence to investigate localisation of signalling molecules in T cell signalling. These results provide good insights of TCR signal transduction but factors like dynamic membrane undulations and cytokine regulation have been less considered. Thus, it is of great interest to investigate distributions of signalling intermediates in T cell activation using a 3D live cell imaging systematic approach, developed by the Wuelfing laboratory. Signalling proteins can be labelled with GFP and tracked using fluorescence microscopy. Accumulation of one signalling protein within a cell is less physiologically meaningful, but localisation of two or multiple proteins at the same location and time point indicates that they are more likely to interact with each other, which often reflects their roles in signal transduction (130, 134). By applying live cell imaging on mouse TCR transgenic T cells, spatiotemporal organisation of T cell signalling proteins can be verified (134). Seven different spatiotemporal patterns (central, invagination, diffuse, lamellal, peripheral, asymmetric and distal) were defined to describe how signalling molecules distribute at the T cell-APC interface upon activation (130, 135). Criteria to identify the seven different patterns are given below (Figure 1.3). The Wuelfing laboratory has established a library of imaging data for more than 90 signalling intermediates, which were applied to study their

spatiotemporal organisation and roles in signal transduction of T cell activation (134, 135).

1.9 Thesis aims

$CD4^+$ Teffs promote both innate and adaptive immune response by secreting inflammatory cytokines such as IFN-γ, while Tregs play roles in maintaining self-tolerance and suppressing immune response mainly by secreting anti-inflammatory cytokines such as IL-10, and expressing coinhibitory ligands such as CTLA-4 (21). The mechanisms of Treg mediated immune regulation are not fully understood. Spatiotemporal organisation of proximal T cell signalling is associated with T cell function. For example, transient accumulation of LAT at the centre of the immunological synapse is associated with efficient IL-2 production (126). Naïve $CD4^+$ T cells from Tg4 TCR transgenic mice can be effectively induced into effector or regulatory phenotypes *in vitro*. As a library of substantial imaging data of Tg4 Teffs was previously established by a former lab member Helen Tunbridge, this study mainly focused on investigating spatiotemporal organisation of key signalling intermediates in Tg4 iTregs, which was then compared to that of Tg4 Teffs. The major aims of this study were to 1) generate Tg4 iTregs, 2) compare functional differences, morphological characteristics and T cell signalling of Tg4 Teffs and iTregs upon activation, 3) investigate whether manipulations of T cell activation signalling in Tg4 iTregs could alter their regulatory function.

Pattern	Example	Description
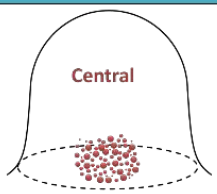	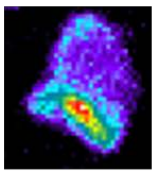	**A region with enriched accumulation at the centre of the interface, locates >20% of the interface diameter away from the edge.**
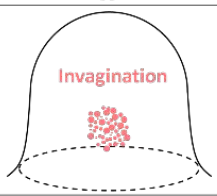	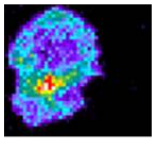	**Similar to central, but the region reaches into the cell with >1 μm from the interface.**
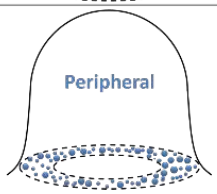	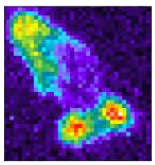	**Accumulation around the interface except the central quarter and forming a peripheral ring structure.**
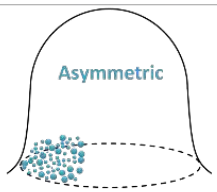	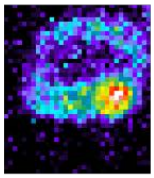	**Similar to peripheral, but the region can only be observed at one side of the interface.**
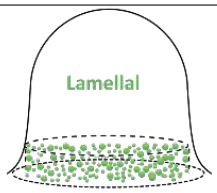	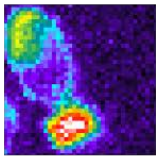	**Accumulation covering the interface, reaching into the cell with several μm and forming a lamella.**
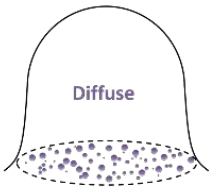	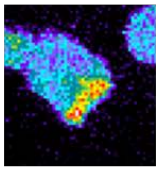	**A narrow region of accumulation with features from both central and peripheral patterns.**
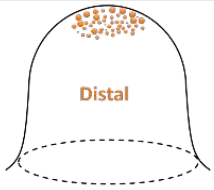	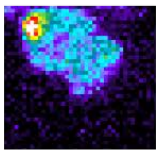	**Accumulation at the distal end of a T cell, away from the interface.**

Figure 1.3 Spatiotemporal accumulation patterns of fluorescent sensors in T cell activation

Pattern diagrams, representative images and criteria for identifying seven spatiotemporal accumulation patterns are listed. Fluorescence intensity is shown in false colour and increases from purple to red.

Chapter 2 Method

2.1 Media and reagents

2.1.1 Complete medium

RPMI 1640 Medium with L-glutamine (Gibco) with 10% fetal bovine serum (FBS) (HyClone), 50μM β-Mercaptoethanol (Gibco) and PenStrep (100 U/ml Penicillin, 100 μg/ml Streptomycin Gibco) and 50μM β-Mercaptoethanol (Gibco).

2.1.2 IL-2 complete medium

Complete medium prepared above, with 50 U/ml recombinant human (rh) IL-2 (NIH/NCI Biological Resource Branch).

2.1.3 Treg medium

Complete medium supplemented with 100 U/ml rh IL-2 and 10 ng/ml rh transforming growth factor-beta 1 (TGF-β1) (BioLegend).

2.1.4 Incomplete Phoenix cell medium

DMEM with 4.5% D-glucose, 110 mg/L sodium pyruvate and l-glutamine (Gibco), 10% FBS (Hyclone), 100 U/ml Penicillin, 100 μg/ml Streptomycin, MEM nonessential amino acids (Gibco), MEM nonessential amino acids (Gibco).

2.1.5 Complete Phoenix cell medium

Incomplete Phoenix cell medium prepared as above, with 300 μg/ml hygromycin (Invitrogen) and 1 μg/mL Diphtheria toxin (Sigma).

2.1.6 Cell separation buffer

DPBS (without calcium or magnesium) (Gibco), with 3% FBS (Hyclone) and 10 mM EDTA.

2.1.7 FACS buffer

DPBS (without calcium or magnesium) (Gibco), with 2% FBS (Hyclone) and 2 mM EDTA.

2.1.8 Antibodies

Manufacturer:	Clone:	Antibody:	Conjugated to:	Purpose:	Concentration:
eBioscience	RM4-5	Anti-mouse CD4	PerCP-Cy5.5	Staining CD4	1 µg/ml
Biolegend	53-5.8	Anti-mouse CD8b	PE/Cy7	Staining CD8	2 µg/ml
eBioscience	KJ16-133	Anti-mouse TCR Vβ 8.1/8.2	FITC	Staining TCR Vβ 8.1/8.2	2.5 µg/ml
eBioscience	eBio1D3	Anti-mouse CD19	APC	Staining CD19	1 µg/ml
Biolegend	OX-6	Anti-rat MHC II	PE	Staining MHC II	0.4 µg/ml
eBioscience	FJK-16s	Anti-mouse Foxp3	PE	Staining Foxp3	1 µg/ml
Biolegend	XMG1.2	IFN-γ	APC/Cy7	Staining IFN-γ	2 µg/ml
Biolegend	JES5-16E3	IL-10	APC	Staining IL-10	1 µg/ml
BioXcell	145-2C11	Anti-mouse CD3	-	T cell activation	1 µg/ml
BioXcell	37.51	Anti-mouse CD28	-	T cell activation	2 µg/ml
MedImmune	9D9	Anti-mouse CTLA-4	-	Blocking CTLA-4	10 µg/m
MedImmune	RMP1-14	Anti-mouse PD-1	-	Blocking-PD-1	10 µg/m

2.1.9 Imaging buffer

DPBS (without calcium or magnesium) (Gibco), with 10% (FBS) (Hyclone), 1 mM $CaCl_2$ (Sigma) and 500 µM $MgCl_2$ (Sigma).

2.1.10 Chloroquine solution

Chloroquine diphosphate (Sigma) in dH_2O (4.1 mg/mL), sterile filtered.

2.1.11 HEPES buffered saline (2x solution)

HEPES buffered saline is prepared in 500 mL (2x solution) as the following protocol:

1. Prepare a stock solution of Na_2HPO_4 dibasic (5.25 g in 500 mL of dH_2O).
2. Dissolve 8.0 g NaCl, 6.4g HEPES (sodium salt) in 10 mL of the Na_2HPO_4 stock solution.
3. Adjust pH to precisely 7.0 using NaOH or HCl. Adjust the volume to 500 mL with dH_2O.
4. Adjust the pH again to exactly 7.0.

Sterile filters are used in each step and the solution is autoclaved.

2.1.12 Paraformaldehyde solution

Paraformaldehyde (Sigma) in dH_2O (16% w/v). Dilute this solution in PBS to further prepare 4% and 1% paraformaldehyde

2.1.13 Peptides

Lyophilised MBP Ac1-9 [4K] (Ac-ASQKRPSQR-NH_2) and MBP Ac1-9 [4Y] (Ac-ASQYRPSQR-NH_2) purchased from GL Biochem, with N-terminus acetylation and C-terminus amidation. Dissolve peptides in sterile PBS at 4mg/ml and store at -20°C.

2.1.14 Fixation and permeabilisation buffers

Foxp3/transcription factor staining buffer set purchased from eBioscience. Dilute 1 part of Fixation/Permeabilisation Concentrate with 3 parts of Fixation/Permeabilisation Concentrate to prepare 1x fixation buffer. Dilute 1 part of 10x Permeabilisation Buffer with 9 parts of dH_2O to prepare 1x permeabilisation buffer.

2.1.15 Reagents for ELISA

Coating buffers:

For IFN-γ capture antibody, 0.1M Na_2CO_3 is prepared as follow: Dissolve 3.57 g $NaHCO_3$, 0.80 g Na_2CO_3 in 500 mL dH_2O, adjust pH to 7.0 with NaOH. For IL-10 capture antibody, 0.2 M Na_3PO_4 is used: Dissolve 12.49 g Na_2HPO_4, 15.47 g NaH_2PO_4 in 1 L dH_2O, adjust pH to 6.4. Buffers stored at 4°C. Both IFN- and IL-10 capture antibody were diluted 1:250 in their corresponding coating buffer.

Assay diluent:

PBS with 10% FBS, pH 7.0, freshly prepared.

Wash buffer:

PBS with 0.05% Tween-20, freshly prepared or stored at 2-8°C and used within 3 days.

Substrate solution:

Tetramethylbenzidine (TMB) substrate reagent set from BD Pharmingen, TMB and Hydrogen peroxide.

Stop solution:

1 M H_3PO_4 or H_2SO_4

2.2 Cell lines

2.2.1 Phoenix cells

Phoenix-E (ϕNX-E) cell lines were used for retrovirus transduction (136). They are a type of human embryonic kidney cell derived from 293T cells modified to produce ecotropic and amphotropic retroviruses. Cells were cultured with complete phoenix cell medium on 60 x 15mm Primaria culture dishes (BD Falcon) at 37°C with 6% CO_2, and were split twice a week (Tuesday and Friday). When splitting, medium in a dish was discarded and 1mL 0.02% EDTA was added to the dish to detach cells. Then cells were centrifuged 200g for 3 minutes and resuspended in complete phoenix cell medium. For one dish, 6 x 10^5 cells were added.

2.2.2 PL8 cells

PL8 cells were used for APCs to activated Tg4 T cells. They were generated by PEF-fusion of blast cells with M12.C3 I-A-negative B cell lymphoma, and PL8 cells were selected for their expression of MHC II molecules I-A^U (137). PL8 cells were cultured with complete medium in T25 vented tissue culture flasks at 37°C with 6% CO_2, and split 1:10 every 2 days.

2.3 Experimental Animals

2.3.1 Breeding and maintenance

All mice were bred and maintained by the animal service unit of the University of Bristol. Mice were housed in cages with unlimited supply of water and mouse chow, and paper rolls and sawdust as bedding. Breeding stocks were kept in the Bristol Veterinary School and mice between 6-12 weeks were culled for experiments.

2.3.2 Tg4 transgenic mice

Tg4 mouse model was modified to express a transgenic αβ TCR (Vα4, Vβ8.2) of a MBP Ac1-9 specific T cell hybridoma (1934.4), which originated from an encephalitogenic T cell clone (73).

2.3.3 Primary T cell isolation

Tg4 mice were culled with schedule one method. Spleens and lymph nodes were harvested from Tg4 mice and homogenised using a 5 ml syringe. Then cells were washed with 5 ml RPMI 1640 Medium (Gibco) through a 40 µm cell strainer (Falcon) and collected in a 50 ml Falcon tube, then centrifuged at 311 g, room temperature for 5 minutes. Cells were resuspended in 1 ml complete medium. To lyse red blood cells, Red Blood Cell Lysing Buffer (Sigma) was added to resuspended cells for 4 minutes and then quenched in 10 ml complete medium. Cells were then centrifuged at 311 g, room temperature for 5 mins and resuspended with lymphocytes in 10 ml complete medium.

2.3.4 Cell priming and culturing

For peptide stimulation, cells were cultured in a 24-well plate (4-5 x 10^6 per well) and primed with 10 µg/ml MBP Ac 1-9 [4K] in complete medium, rhIL-2 was added (50 U/ml) after 24 hours to induce Teffs, and cell were cultured in IL-2 complete medium.

To induce iTregs, cells were resuspened in Treg medium and cultured in a 24-well plate (3.5-4 x 10^6 per well) and primed with 10 µg/ml MBP Ac 1-9 [4K]. For anti-CD3/28 stimulation, after red blood cell lysis, cells were purified with MagniSort Mouse CD4 T cell Enrichment Kit (ebioscience) according to the MagniSort Negative Selection Protocol III. Naïve $CD4^+$ T cells were cultured in a 48-well plate (1.5 x 10^6 per well) coated with mouse anti-CD3ε (1 or 10 µg/ml) and anti-CD28 (2 µg/ml) antibodies (Bio X cell) for 48 hrs and then transferred to antibody-free wells. To induce Teffs, cells were culture with IL-2 complete medium after 24 hours. To induce iTregs, cells were cultured in daily changed Treg medium.

After initial cell priming, cells were usually cultured in relevant medium at 37°C with 6% CO_2 for five days before sorting for imaging and retroviral transduction with a sensor of interested was performed 24 hours after cell priming. Medium was changed daily and cells were split when required.

2.4 Retroviral transduction

2.4.1 Transfection of phoenix cells

The calcium phosphate transfection method was applied to introducing DNA plasmids into phoenix cells. First, 25 µl chloroquine solution (4.1 mg/ml), which inhibited lysosome-autophagosome fusion and lysosomal protein degradation (138) was added to a phoenix plate. Then the plate was kept in the incubator at 37°C with 6% CO_2 while calcium phosphate co-precipitation was being performed. One 15 ml Falcon tube was added with

0.5 ml 2 x HBS and 2 µl 1 M NaOH (tube A). Another Falcon tube was added with 428 µl sterile ddH20, 10 µl plasmid DNA and 62 µl 2M $CaCl_2$ (tube B). $CaCl_2$ solution was added drop by drop. The solution in tube B was gently added to tube A using a P1000 pipette and bubbles were generated using a pipette controller during this process. The mixed solution sat at room temperature for 1 minute and was gently added to the phoenix plate prepared without disturbing the cell monolayer. The plate was incubated at 37°C with 6% CO_2 overnight. On the next day, the plate was examined under a microscope for calcium phosphate–DNA co-precipitates and the media was exchanged with 3 mL incomplete phoenix medium. Phoenix plates were further cultured for 48 hours to produce retroviruses and used to transduce T cells.

2.4.2 Transduction of Tg4 T cells

On the following day of T cell priming, T cells and phoenix medium containing retroviruses were collected separately into 15 mL Falcon tubes and centrifuged at 311 g for 3 minutes. Supernatants from the tube of T cells were discarded and for every 1.5-2 $x10^5$ T cells, 1 ml of the phoenix medium supernatant was added for transduction. Resuspended cells were added with 8 mg/mL protamine sulphate to neutralise negative charges and enhance viral entry. Cells were added to a 24 or 48-well plate depending on cell numbers and then centrifuged at 1083 g, 32 °C, for 2 hours. Cells were resuspended in medium and cultured for four days before sorting.

2.5 Surface and intracellular staining of cells in flow cytometry

Cells were first washed with PBS (centrifuged at 311g for 3 minutes) and then stained with Zombie Aqua/NIR live/dead dye (Biolegend) diluted in PBS at 1:100 for 1 x 10^6 cells, for 20 minutes at room temperature in the dark. After another two washes, cells were resuspended in FACS buffer and stained with anti-mouse monoclonal antibodies (mAbs) for surface markers on ice for 30 minutes in the dark. After one wash with FACS buffer, cells were resuspeneded in FACS buffer ready for flow cytometry or intracellular staining.

For intracellular staining of Foxp3, Foxp3/Transcription Factor Staining Buffer Set (eBioscience) was used. After centrifugation, cells were first fixed in Fixation/Permeabilization reagent on ice for at least 30 minutes in the dark and then washed twice with Permeabilization buffer. Cells resuspended in Permeabilization buffer and stained with Fopx3 PE mAb (eBioscience) on ice for 30 minutes in the dark. After another two washes with Permeabilization buffer, cells were resuspended in FACS buffer and prepared for flow cytometry.

2.6 Suppression assay

Teffs and iTregs were prepared as described above and collected for suppression assays on the day five of culture. Intracellular Foxp3 staining was performed to confirm the percentage of $Foxp3^+$ iTregs. PL8 cells were treated with 2 µg/ml mitomycin C (Sigma) for 24 hours prior to the experiment. To set up co-cultures, naïve Tg4 $CD4^+$ T cells were purified as described above. Cells were then washed twice with PBS (centrifuged at 311g for 3 minutes). For a negative control, 2.5 x 10^5 cells were fixed in 1% PFA. The rest were resuspended in PBS and labelled with the CellTrace Violet (CTV) dye (ThermoFisher) with a working concentration of 5 µM. Cells were incubated at 37°C for 20 minutes and then quenched with equal volume of complete medium for 5 minutes at room temperature. After another 3-4 times washes with PBS, another 2.5 x 10^5 cells were fixed in 1% PFA and used as a CTV control on day 1. The other CTV^+ naïve T cells would be used as responder cells for suppression assay. Either Teffs or iTregs, CTV^+ native T cells and pre-treated PL8 cells would be co-cultured in a 48-well plate for three days. Cells were either activated with 10 µg/ml MBP Ac1-9 [4K] or plate-bound anti-CD3/28 (1/2 µg/ml) in the absence of PL8 cells. After 72 hours, cells were harvested and cell surface staining was performed to identify $CD4^+$ CTV^+ T cells. Histograms showing CTV fluorescence intensity of double positive cells were used to compare cell divisions of $CD4^+$ naïve T cells in different groups. All iTregs used in suppression assays were >75% $Foxp3^+$. To ensure the numbers of Teffs and iTregs added were the same in corresponding wells, the number of iTregs added was justified based on the percentage of $Foxp3^+$ cell. Cell samples were analysed on Acea Novocyte 3000.

2.7 Live cell imaging

After retroviral transductions, cells were continued to be cultured for another four days and sorted for GFP^+ cells. Cells were first harvested, centrifuged at 311 g for 3 minutes and resuspended in imaging buffer. GFP^+ cells were sorted with a BD Influx cell sorter (BD Bioscience). FACS sorting gate for GFP^+ cells were set as 1-1.5 (or 1/3, for ELISAs) log shift above the negative population. In parallel, 1-2 x 10^6 PL8 cells were pulsed with 10 µg/ml MBP Ac1-9 [4Y] peptide in 1ml on a 24-well plate for at least 4 hours before imaging. To perform live cell imaging, 300 µl peptide-loaded PL8 cells (around 300-600k cells) from one well were collected into a 1.5 ml Eppendorf tube. All sorted GFP^+ cells were collected into another tube. Both tubes were centrifuged at 344 g for 4 minutes. After supernatants were discarded, PL8 cells were in in 50 µl imaging buffer and T cells were resuspended in 5 µl imaging buffer (for every 10-40k cells). Depending on cell numbers, two kinds of imaging plates were either used: 348-well (35-40k T cells per well) or 1536-well (11-14k T cells per well) glass bottom MatriPlate. First, 50 µl imaging buffer was added to an empty well (not

needed in a 1536-well plate) and 5 µl of T cells were added to the bottom of the well. The plate was then set on a confocal microscope. After cells were settled, 1-3 µl of APC-containing buffer were gently added to the well, avoiding disruption of T cell distribution. Once T cells began to make contact with APCs added, imaging should begin. Acquisition configurations (detailed settings refer to Ambler *et al* (136)): a z-stacking of 21 images (1 µm each) in the fluorescent channel, 3 time points (every 20s) per minute, 1 DIC reference image taken at the mid-stack from each time point, 2 X 2 binning used to improve signal-to-noise ratio of the data, 15 minutes of acquisition. For one experiment, 46 DIC and 966 GFP z-stacks were generated and exported using Volicity software.

2.8 Analysing imaging data

Metamorph software was used to analyse imaging data. DIC images were used to identify onsets of cell coupling and 0s indicates when a stable cell couple is formed. Fluorescence images were used to identify accumulation patterns of a sensor. Pseudocolor was applied in maximum projection images and fluorescence intensity increases from purple to red. Spatiotemporal patterns (Figure 1.1) were used to analyse signalling intermediate distributions.

2.9 Enzyme-linked immunosorbent assays (ELISAs)

Supernatants were collected from cell culture by centrifugation at 311 g and stored at -20 °C or used on the day. The level of IFN-γ and IL-10 in cell culture supernatants were determined using mouse IFN-γ and IL-10 OptEIA ELISA sets from BD Biosciences with manufacturer's protocol. Briefly, Nunc-Immuno MicroWell 96-Well Plates (Thermofisher) were coated with 100 µL capture antibody diluted in coating buffer, sealed and kept at 4°C overnight. For IFN-γ ELISAs, wells were first aspirated and washed with >300 µl wash buffer for 5 times and then blocked with >200 µl assay diluent for 1 hours at room temperature. A washing step was then repeated for 5 times and 100 µL standard or samples were added and incubated at room temperature for 2 hours. Wells were again washed for 5 times added with 100 µL detection antibody and enzyme reagent and incubated for 1 hour at room temperature. A final washing step was repeated for 10 times and added with 100 µL substrate solution. The plate was incubated in the dark at room temperature for 30 minutes. Finally, 50 µL stop solution was added to each well and absorbance of each well was read at 450 and 570 nm. The final reading was obtained by subtracting absorbance at 570 nm from that at 450 nm. For IL-10 ELISAs, a same protocol was followed with fewer washes (3 times in the first and second washing step, 7 times for the last). Standard curves were generated using optical density (OD) values of sample

standards and sample concentrations were back-calculated using the linear standard curves. Duplicate or triplicate samples were applied in each experiment.

2.10 Morphological measurements

To study T cell morphology upon T cell-ACP interaction, four morphological parameters were measured using Metamorph software. These parameters were: cell depth (the length from the interface centre to the distal pole of a T cell), cell width (the width of the main cell body), interface width (the width of the contact interface) and lamellal depth (the vertical length from interface centre to the narrowest width of the lower part of a T cell). Lamellal depth would be recorded only if a visible extended lamella was observed. Its length should be >1.3 µm (Figure 2.1 A). A diagram is shown below showing the four parameters (Figure 2.2 B).

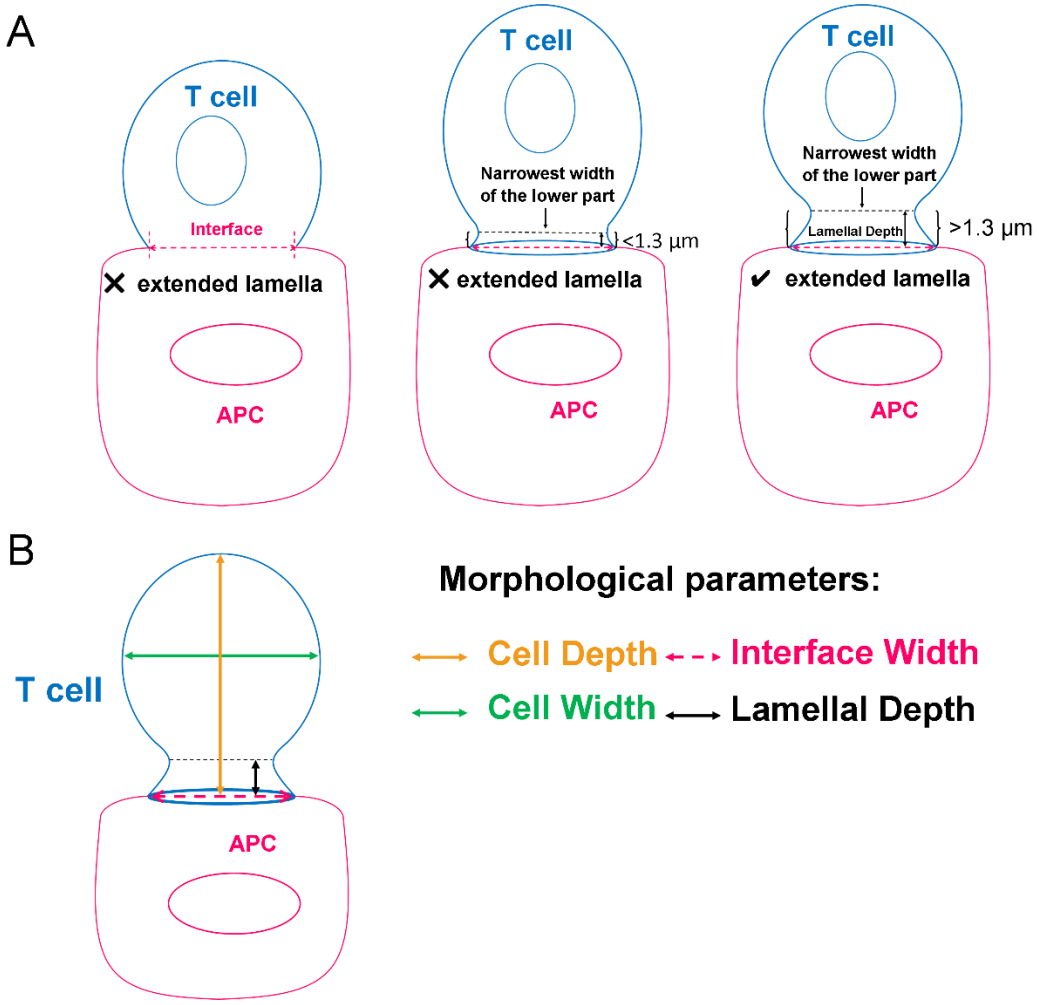

Figure 2.1 Measuring four morphological parameters upon T cell-APC interactions

Lamellal depth is be only recorded only if >1.3 µm.

2.11 Statistical analysis

Depending on the type and distribution of data, statistical significance was calculated using a Student's T-test, Analysis of Variance (ANOVA), a two proportion z-test or Chi-square test. When analysing the frequency of occurrence of spatiotemporal accumulation patterns, a two proportion z-test was applied. Proportion data were arcsine-transformed and ratio data generated in the computational analysis were log-transformed so that transformed variables could fit the normal distribution better.

Chapter 3 Model establishment and optimisation

3.1 Introduction

Due to TCR gene rearrangement, diverse TCRs which hold different affinities for peptide antigen are expressed on the surface of T cells. The TCR repertoire enables the adaptive immune system to recognise various pathogens from the environment. A well-established T cell model expressing specific TCR is commonly used to induce iTregs, so that T cell activation can be initiated and compared in the same manner using TCR-specific peptide antigens. To generate iTregs in this study, we applied the Tg4 TCR transgenic mouse model, which was previously established by the Wraith group (73). Tg4 T cells were heavily skewed to express CD4 and about 90-95% of Tg4 $CD4^+$ T cells specifically recognise MBP Ac1-9 peptides. Purified Tg4 $CD4^+$ naïve T cells can be induced into iTregs by activation with anti-CD3 and anti-CD28 (up to 95% iTregs) or MBP Ac1-9 peptides in the presence of irradiated B10.PL splenocytes (up to 75% iTregs) (139), and the former is more efficient and widely applied.

In this study, we generated Tg4 iTregs primed with anti-CD3 and anti-CD28 or stimulated by endogenous APCs presenting TCR-specific peptide in the presence of IL-2 and TGF-β. T cell signalling intermediates were labelled with GFP in Tg4 $CD4^+$ Teffs and iTregs (>75% $Foxp3^+$) for spatiotemporal distribution analysis. Live cell imaging library of Tg4 $CD4^+$ Teffs were previously established by Helen Tunbridge, and therefore we aimed to generate comparable imaging data from Tg4 iTregs in this project. Additionally, we have also compared frequencies of $Foxp3^+$ cells induced by anti-CD3/CD28 and endogenous APCs primed with TCR-specific peptide.

3.2 Chapter aims

- To induce Tg4 $Foxp3^+$ iTregs *in vitro* and perform retroviral transduction of GFP sensors on Tg4 $Foxp3^+$ iTregs
- To investigate and compare Foxp3 expression of anti-CD3/28 and MBP peptide-primed Tg4 iTregs

3.3 Purified Tg4 naïve T cells are CD4$^+$ Vβ8.2$^+$

A full stimulus of T cell activation requires signalling from MHC-TCR interaction presenting antigen peptide (signal one), costimulatory signals of CD28 and B7.1/7.2 (signal two) and cytokines released at site such as IL-1, IL-12 and type I interferons (IFNs) (signal three) (140, 141). Whereas CD4$^+$ naïve T cells activated with plate-bound anti-CD3 and anti-CD28 in the presence of TGF-β and IL-2 has been shown to be sufficient to induce Tregs, and leads to high frequencies of Foxp3 expression (over 80%) (66). In this setting, naïve CD4$^+$ T cells are required to generate iTregs. In initial experiments, Tg4 splenocytes and lymphocytes were purified with the MagniSort® Mouse CD4 Naïve T cell Enrichment Kit after red blood cell lysis. Transgenic Tg4 T cells are mostly CD4 positive and are highly responsive when primed with MBP Ac1-9 peptide (73). To validate CD4$^+$ naïve T cell population after negative selection, unpurified and purified cells prior to stimulations were stained with anti-mouse CD4, Vβ8.1/8.2, CD19, and MHC-II antibodies. Comparison between these two populations (Figure 3.1) indicates that negative selection effectively isolated CD4$^+$ Vβ8.1/8.2$^+$ population and excluded B cells and APCs such as dendritic cells and monocytes. Over 97% purified cells were CD4$^+$ Vβ8.1/8.2$^+$, twice as many as those from unpurified cells population. Less than 0.2% of B cells (CD19$^+$) and APCs (MHC-II$^+$) remained after purification. CD4$^+$ T cells were enriched and proceeded for anti-CD3/28 stimulation.

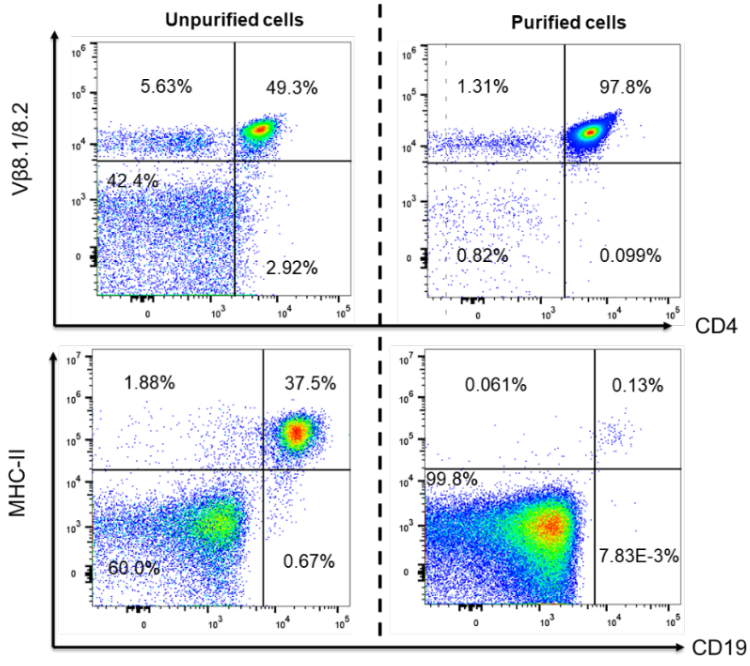

Figure 3.1 Tg4 splenocytes and lymphocytes were purified into CD4$^+$Vβ8.1/8.2$^+$T cells

Tg4 splenocytes and lymphocytes with and without negative selection were stained for CD4, CD19, Vβ8.1/8.2 and MHC-II. FACS plot shows mouse Vβ8.1/8.2 vs CD4 and CD19 vs MHC-II and four quadrant gates are drawn. The percentage of each cell population was indicated within each quadrant. Data are from one experiment.

3.4 Compared with 10 µg/ml anti-CD3, 1 µg/ml anti-CD3 leads to higher Foxp3 expression and has no significant effects on retroviral transduction

Previously described by the Wraith group (139), 1 µg/ml plate-bound anti-CD3 and 2 µg/ml anti-CD28 were used to activate $CD4^+$ naïve T cells, and with 100 U/ml IL-2 and 10ng/ml TGF-β added in complete medium to induce iTregs. They used 1 µg/ml anti-CD3 for TCR activation and in this project, we compared which concentration of anti-CD3 (1 and 10 µg/ml) would induce a higher frequency of $Foxp3^+$ iTregs (anti-CD28 concentration was the same in both conditions). Pilot experiments contained 0.1 µg/ml anti-CD3 conditions in which cells were not fully activated and failed to proliferate and differentiate (data not shown). Results (Figure 3.2) show that activating Tg4 naïve $CD4^+$ T cells with 1 µg/ml anti-CD3 led to higher Foxp3 expression than cells activated with 10 µg/ml anti-CD3 ($p<0.001$). This implies that TCR stimulus provided by 1 µg/ml anti-CD3 is enough to trigger Tg4 naïve $CD4^+$ T cell proliferation and differentiation which leads to better iTreg induction outcome.

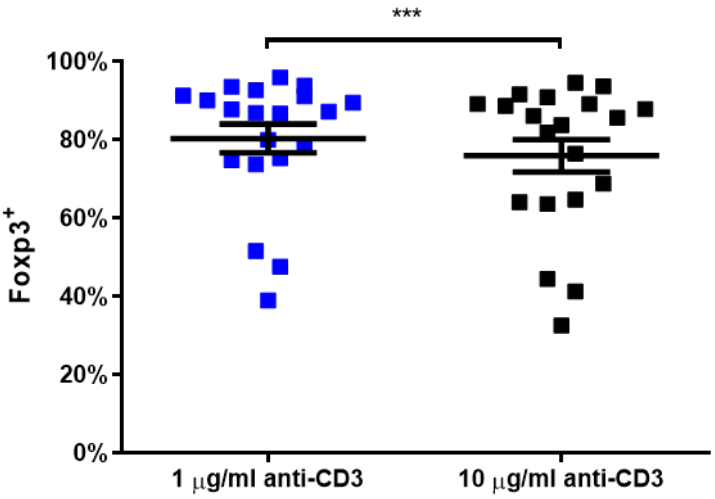

Figure 3.2 Tg4 naïve T cells primed with 1 µg/ml anti-CD3 have higher Foxp3 expression than cells treated with 10 µg/ml anti-CD3

Percentages of $Foxp3^+$ iTregs induced from Tg4 naïve $CD4^+$ T cells activated with 1 and 10 µg/ml anti-CD3 were compared. Statistical significance was calculated using paired Student's T-test with arcsine transformed data. Asterisks indicate p-value (***<0.001). A total of 20 experiments were analysed. Error bars indicate standard error of the mean.

To investigate spatiotemporal distributions of signalling molecules in Teffs and iTregs, GFP expressing T cells needs to be isolated. Prior to imaging, retroviral transduction was synchronised with Teff and iTreg induction. The transduction efficiency and percentage of GFP^+ T cells vary in experiments with different GFP-tagged signalling sensors. Therefore, we standardised our cell sorting strategy and isolated cells with high florescent signals, so that distributions of GFP-tagged molecules within T cells could be well identified in the fluorescent channel. We set a specific GFP^+ sorting gate which is 1-1.5 log shift brighter than the negative population, to identify GFP^+ cell populations with high fluorescent intensity.

TCR stimulations from anti-CD3 might have impacts on percentages of GFP^+ cells, as stronger TCR signals tend to enhance cell proliferation and influence retroviral transduction. Thus, we investigated whether activating cells using 1 or 10 µg/ml anti-CD3 would lead to different frequencies of GFP^+ cells. GFP^+ cell populations were compared using iTregs transduced with three different sensors (F-tractin-GFP, LAT-GFP and VAV1-GFP). Result (Figure 3.3) shows that there was no significant difference in percentages of GFP^+ cells between cells activated with 1 and 10 µg/ml anti-CD3. Based on the results above, we decided to use 1 µg/ml anti-CD3 to maximise Foxp3 expression in anti-CD3/28 induced Tg4 Tregs.

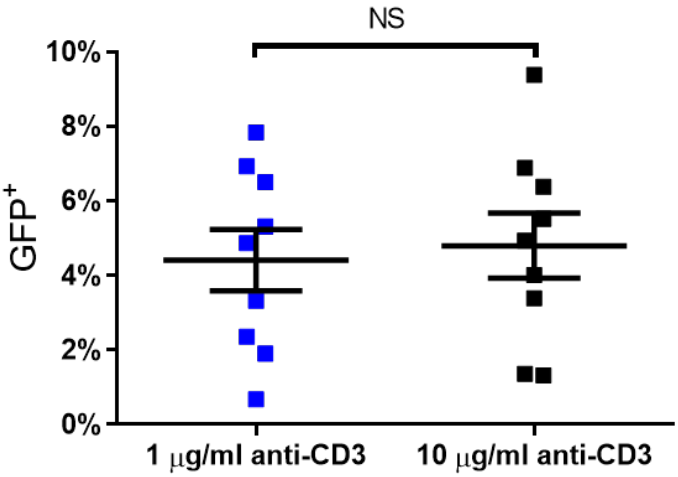

Figure 3.3 Activating Tg4 naïve T cells with 1 µg/ml and 10 µg/ml anti-CD3 have same GFP expression

GFP^+ populations of Treg-induced Tg4 naïve T cells activated with 1 and 10 µg/ml anti-CD3 were compared. Statistical significance was calculated using paired Student's T-test with arcsine transformed data. NS: not significant. A total of nine experiments were analysed. Error bars indicate standard error of the mean.

3.5 Repeated freezing and thawing of TGF-β damage Foxp3 expression

Foxp3 intracellular staining was applied to confirm Tg4 iTreg populations. iTregs used to acquire live cell imaging data were all over 75% Foxp3$^+$. In the first 10 repeated Tg4 iTregs induction experiments, Foxp3$^+$ cell population showed inconsistency in the 1 and 10 μg/ml anti-CD3 group (Figure 3.1A). Notably, the TGF-β aliquots (aliquoted in 50 μl per vial, refrozen and used continuously, noted as “normal TGF-β”) used in these 10 experiments had gone through several freeze-thaw cycles. As one of the key factors which convert CD4$^+$ naïve T cells into Foxp3 expressing iTregs (51), the potency of TGF-β is critical. We hypothesised that repeated freeze-thaw cycles would damage TGF-β activity and lower Foxp3 expression in Tg4 cells.

To verify this, we carried out another 10 experiments with fresh TGF-β aliquots, noted as “fresh TGF-β” (aliquoted in 25 μl per vial, used on the same day when T cell cultures were prepared, each aliquot was subsequently disposed), shown as Figure 3.4B. Unlike the previous experiments, Foxp3$^+$ cells treated with fresh TGF-β are more stable in both 1 and 10 μg/ml anti-CD3 group. Fluctuation of Foxp3 expression is observed in the normal TGF-β group, which could be a result of constant freeze-thaw cycles of TGF-β. Results (Figure 4.3C-D) also show that compared with cells induced with normal TGF-β, percentage of Foxp3$^+$ of cell induced with fresh TGF-β is significantly higher in the both groups ($p<0.05$). These results indicate that in the first 10 experiments, the potency of TGF-β to induce Foxp3 expressing T cells was damaged owing to repeated freeze-thaw cycles. To avoid the loss of Foxp3 expression in following experiments, we used fresh TGF-β aliquots for each Tg4 iTregs induction experiment.

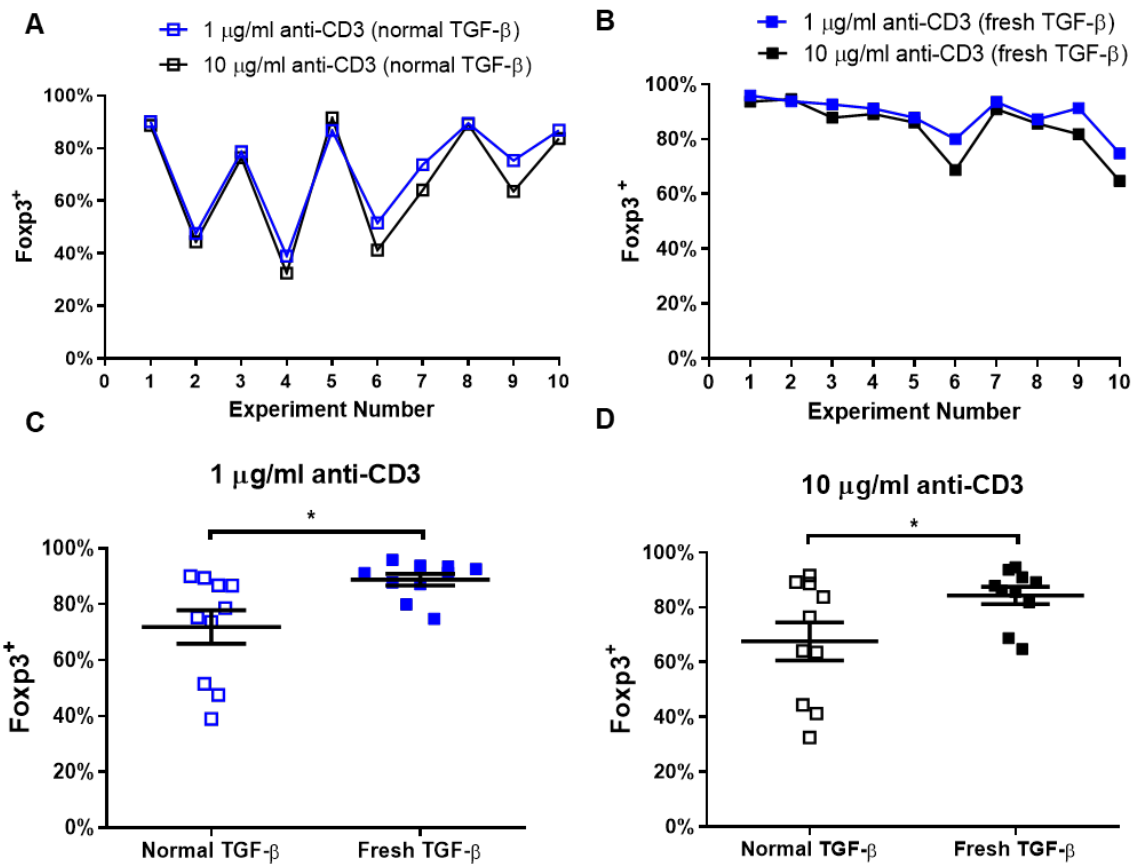

Figure 3.4 Repeated freeze-thaw cycles of TGF-β result in lower Foxp3 expression

Tg4 CD4$^+$ naïve cells were primed with plated-bound anti-CD3/28 for 48 hours and cultured in Treg medium and on day 6 of culture, cells were stained with Foxp3 antibodies. Cells were induced with normal TGF-β (aliquots went through multiple freeze-thaw cycles) or fresh TGF-β (new aliquots for each experiment). Both data from cells primed with 1 and 10 μg/ml anti-CD3 were analysed. Plot graph showing percentages of Foxp3$^+$ cells induced with **A**) normal TGF-β and **B)** fresh TGF-β. Comparing Foxp3$^+$ frequencies in cells induced with normal and fresh TGF-β primed with **C)** 1 μg/ml anti-CD3 and **D**) 10 μg/ml anti-CD3. A total of 20 experiments were used. Statistical significance was calculated using unpaired Student's T-test with arcsine transformed data. Asterisks indicate p-values (*<0.05). Error bars indicate standard error of the mean.

3.6 Priming Tg4 T cells with anti-CD3/28 leads to higher Foxp3 expression, compared with cells primed with MBP Ac1-9 peptides and APCs

During T cell recognition, $CD4^+$ or $CD8^+$ T cells bind antigenic peptides presented by MHC molecules on the surface of APCs, and once activated they continue to form an IS and eventually trigger their helper or cytotoxic functions (142). In peptide induced activation, T cells receive three activation signals from TCR-MHC interactions, co-stimulatory molecules and cytokines released by APCs (140, 141) . Tg4 transgenic TCRs recognise MBP peptides presented by APCs and initiate T cell activation, which is physiological comparable to antigen presentation *in vivo*. Previous studies have shown that $CD103^+$ lamina propria DCs in the intestine can prove antigens, retinoic acid and TGF-β to induce generation of iTregs and pTregs (59). In this project, we have induced Tg4 Teffs from RBC-lysed splenocytes and lymphocytes primed with MBP peptide (data are shown in Chapter 4). However, this might not be the most effective priming method for iTregs generation. Activating Tg4 naïve $CD4^+$ T cells with MBP Ac1-9 [4K] and irradiated APCs for iTreg induction was shown to have lower frequencies of $Foxp3^+$ cells than cells activated with anti-CD3/28 (139). Shevach and Thornton mentioned (53) that when inducing TCR transgenic Rag1 deficient mouse Tregs in the presence of DCs and anti-CD3, $Foxp3^+$ cells among induced cells only ranged from 50%-60%. With anti-CD3/28 stimulation they could generate over 90% $Foxp3^+$ cells, which is mostly applied for iTregs generation to date. They suggested this might be a result of DCs secreting pro-inflammatory cytokines such as IL-6, as IL-6 inhibits TGF-β-induced Treg differentiation and promtes generation of Th17 cells (143). Moreover, cytokines produced by APCs may also induce differentiation of other helper subsets, for example DC-derived IL-12 meditates Th1 cell development (144). Therefore, T cells activated by peptide-primed APCs receive more complete activation signals and are more comparable to cells activated *in vivo*. To investigate whether peptide activation can be applied and optimised for iTreg induction, we activated Tg4 naïve T cells with endogenous APCs primed with MBP Ac1-9 [4K], with additional IL-2 and TGF-β to generate iTregs and compared their frequencies of $Foxp3^+$ populations with those of anti-CD3/28-primed iTregs.

Tg4 splenocytes and lymphocytes were initially lysed with RBC lysis buffer and primed with MBP Ac1-9 [4K] and cultured in Treg medium for five days. Representative Foxp3 staining result shows that Tg4 naïve T cells could be induced into $CD4^+$ $Foxp3^+$ cells (Figure 3.5) in the presence of endogenous APCs presenting with MBP Ac1-9 [4K] peptides. Dominant $CD4^+$ population remained (>95%) after culturing for five days and >88% cells were $Foxp3^+$, suggesting that high frequencies of Tg4 $Foxp3^+$ cells can be induced in the present of endogenous APCs presenting MBP peptides.

A direct comparison of Foxp3 staining results shows that (Figure 3.6) the percentage of $Foxp3^+$ cells induced from anti-CD3/CD28 activated Tg4 naïve $CD4^+$ T cells was significantly higher than cells activated by MBP Ac1-9 (4K) peptide-primed endogenous APCs ($p<0.05$). This indicates that transforming purified naïve $CD4^+$ T cells into Tregs, rather than activating mixed splenocytes and lymphocytes with TCR specific peptide, leads to better iTreg generation *in vitro*. This is consistent with previous studies (53). However, the difference in frequencies of $Foxp3^+$ cells was not dramatic, as cells from both groups were all > 60% $Foxp3^+$ and their average percentage was similar (89% and 81%).

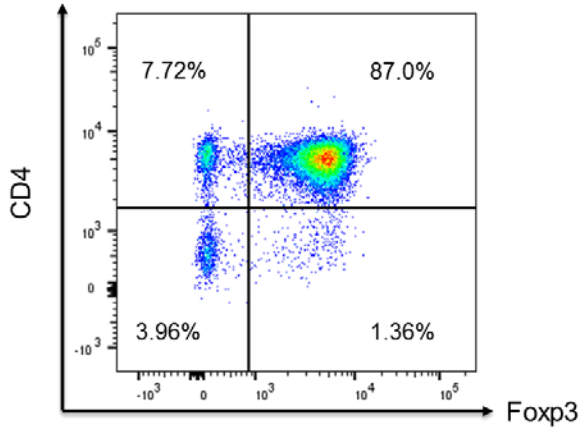

Figure 3.5 Tg4 splenocytes and lymphocytes can be induced into CD4$^+$ Foxp3$^+$ cells when activated with MBP Ac1-9 (4K) peptide and endogenous APCs.

Tg4 splenocytes and lymphocytes were harvested, primed with MBP Ac1-9 [4K] peptide and cultured for five days with IL-2 and TGF-β added, CD4 and Foxp3 staining was performed on day six. FACS plot shows CD4 vs Foxp3 and four quadrant gates are drawn. The number within each quadrant represents percentage of this population. Data are from one experiment.

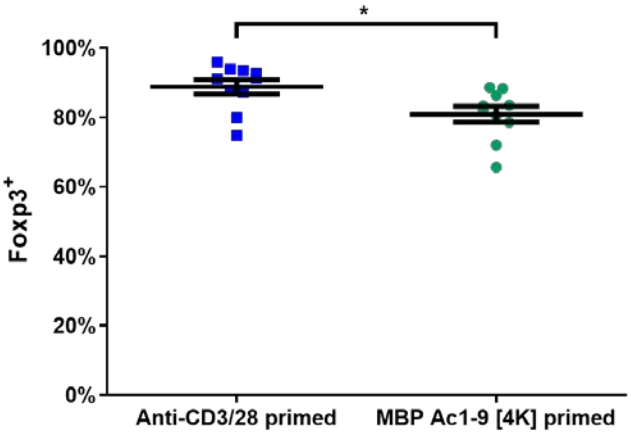

Figure 3.6 Tg4 CD4$^+$ naïve T cells activated with anti-CD3/28 have higher Foxp3 expression than cells activated with MBP Ac1-9 [4K] peptide and endogenous APCs.

Foxp3$^+$ frequencies of CD4$^+$ naïve T cells activated with antibodies (anti-CD3 and anti-CD28) and native T cells activated with MBP Ac1-9 (4K) peptide and endogenous APCs were compared on day six of culture. Cells were stained for Foxp3. Error bars indicate standard error of the mean. Statistical significance was calculated using unpaired Student's T-test with arcsine transformed data. Asterisks indicate p-values (*<0.05). A total of 20 experiments were compared and each group includes 10 independent experiments.

3.7 Tg4 Foxp3$^+$ cell populations remain after FACS sorting

To generate live cell imaging data of iTreg activation, GFP$^+$ Foxp3$^+$ T cells needed to be identified. A direct method was to first sort GFP$^+$ T cells and then validate their iTreg populations with Foxp3 intracellular staining. However, result (Figure 3.7) shows GFP fluorescence was impaired after intracellular staining. In this experiment, 11% of live cells transduced with F-tractin-GFP were GFP positive (upper plot), while after fixation and permeabilisation, less than 1% of the cells remained GFP positive (lower plot). It has been reported that the Foxp3 staining kit (eBioscience) resulted in complete loss of EYFP fluorescence, because of its insufficient fixation which failed to maintain fluorescent proteins within a cell (145). Alternatively, fixation could have destroyed the GFP fluorophore. Therefore, we were not able to directly identify Foxp3$^+$ population among live GFP$^+$ cells.

An alternative method was to perform Foxp3 intracellular staining on pre-sorted cells and assume the percentage of Foxp3$^+$ cells in pre-sorted and GFP$^+$ cells to be the same. We need to consider whether Foxp3$^+$ cell populations in FACS sorted GFP$^+$ cells would remain the same as that in pre-sorted cells. Therefore, we set up an experiment to identify Foxp3$^+$ cell populations among pre-sorted, sorted GFP$^-$ and GFP$^+$ iTregs from day 6 of culture. Investigating frequencies of Foxp3$^+$ cells in these three conditions helped us to check whether cells sorting would have impacts on percentages of Foxp3$^+$ cells. Result shows (Figure 3.8) that the major cell population in both sorted GFP$^-$ (>80%) and GFP$^+$ (>74%) cells are Foxp3$^+$, comparable with that in unsorted cells (81.1%). This indicates that fluctuations of the frequency of Foxp3$^+$ cells in pre-sorted, sorted GFP$^-$ and GFP$^+$ cells were minor. It is reasonable and practical to use Foxp3 staining results from pre-sorted samples to deduce percentages of Foxp3$^+$ cells, or iTregs in FACS sorted GFP$^+$ cells. This method to assess the percentage of iTregs was applied for all retroviral transduced iTregs, in the following chapters.

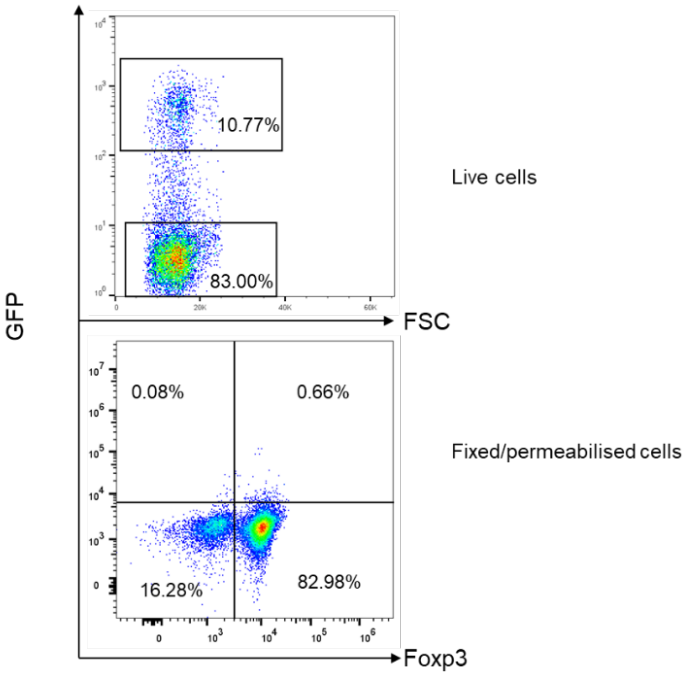

Figure 3.7 Fixation and permeabilisation lead to a loss of GFP$^+$ signals.

iTregs transduced with F-tractin-GFP were first sorted for GFP$^+$ cells (upper plot) and then identified for Foxp3+ cells after fixation and permeabilisation (lower plot). FACS plots shows forward scatter (FSC) vs GFP and Foxp3 vs GFP, two square gates were drawn indicating GFP$^+$ and GFP$^-$ cells in the upper plot, and quadrant gates are drawn in the lower plot. The percentage of each cell population was indicated within each gate. Data from one experiment were used.

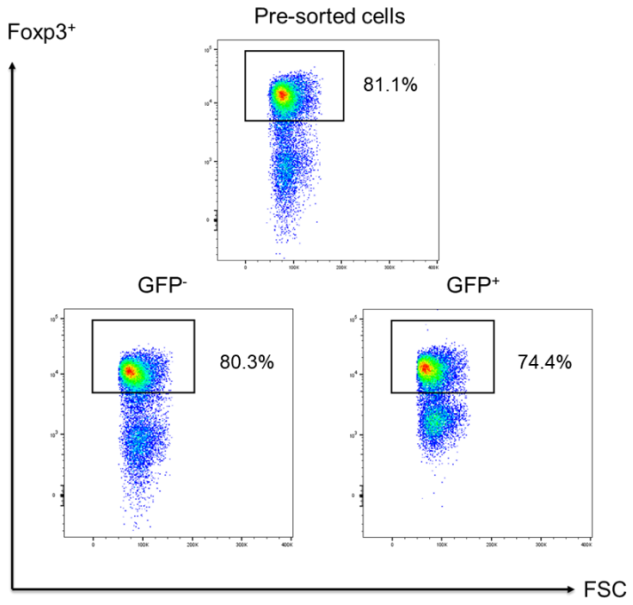

Figure 3.8 Major cell population remains Foxp3$^+$ in sorted GFP$^-$ and GFP$^+$ cells

Foxp3 expression of pre-sorted cells, GFP$^-$ and GFP$^+$ are compared. FACS plot shows Foxp3 vs forward scatter (FSC), a gate was drawn to indicate Foxp3$^+$ cells based on unstained cells, and the number indicates the percentage of the population. One experiment is shown.

3.8 Discussion

There are two main purposes in this chapter: Firstly, to induce Tg4 Foxp3$^+$ iTregs, and secondly to validate retroviral transduction with GFP-labelled signalling sensors on iTregs for further live cell imaging experiments.

Studies have demonstrated that IL-2 and TGF-β are indispensable in iTreg induction (51, 66). In terms of activating naïve T cells for iTreg differentiation, stimulating purified CD4$^+$ naïve T cells with anti-CD3 and anti-CD28 has been a common choice for their high efficacy of generating iTregs (>90% Foxp3$^+$) (53, 146). Our results show that, when comparing frequencies of Foxp3$^+$ T cells induced by 1 and 10 µg/ml anti-CD3, the former generates cells with a higher Foxp3$^+$ cell percentage, as recommended by a previous study inducing Tg4 iTregs (139). Moreover, thaw-freeze cycles have been shown to damage TGF-β activity and lower Foxp3 expression. We have optimised our anti-CD3/28-primed iTreg induction protocol. CD4$^+$ naïve T cells were stimulated with 1 µg/ml anti-CD3 and 2 µg/ml anti-CD28, then cultured in complete medium with IL-2 and TGF- β. Only fresh TGF-β aliquots which had gone through only one freeze-thaw cycles (for aliquoting stocks) were used for culturing iTregs.

Apart from iTreg induction using anti-CD3/28 antibodies, we have shown that in the same medium condition with IL-2 and TGF-β, Tg4 iTregs could be generated with TCR-specific peptide stimulation and endogenous APCs. Such activation is more physiological comparable to naïve T cell activation *in vivo*. MBP Ac1-9 [4K] peptides were added and presented by endogenous APCs to activated Tg4 naïve T cells. Day six Foxp3 staining shows that these cells were polarised to be CD4$^+$ Foxp3$^+$. In addition, for iTreg generation, activating naïve CD4$^+$ T cells with plate-bound anti-CD3/28 or in the presence of APCs and TCR-specific peptides might have different impacts on Treg phenotypes. Helios from the Ikaros transcription factor family, has been shown to be a possible marker to distinguish tTregs and pTregs (147). Thornton *et al* have observed that Helios expression was found in all tTregs, and both human and mice Treg generated *in vitro* did not express Helios. However, Verhagen and Wraith (148) have reported that iTreg priming methods could change Helios expression: Tg4 Rag-deficient CD4$^+$ splenocytes activated with MBP Ac1-9 (4K) peptide and irradiated APCs could induce Helios expressing iTregs, which was not observed in plate-bound anti-CD3 and anti-CD28 activated ones. Further study revealed that Helios$^+$ and Helios$^-$ Tregs display different suppressive abilities on autoreactive cells and TCR repertoires (149). Moreover, cells activated with anti-CD3/28 tend to have higher frequencies of iTreg populations than cells activated in the presence of APCs, this was consistently observed in this project and previous studies (53, 139). One possible factor contributing to the relatively low Foxp3 induction in the presence of APCs is IL-6 expression

at the activation site. IL-6 can be found in antigen-stimulated PBMCs and secreted by various cell types such as B cells, T cells, monocytes, fibroblasts and tumour cells (150). IL-6 and TGF-β together have been shown to drive naïve T cells to become Th17 cells and inhibit TGF-β-induced Foxp3 expression (143). Th17 cells play opposite roles against Tregs by secreting pro-inflammatory cytokines such as IL-17, IL-21 and GM-CSF to promote inflammatory responses (151). Differentiations of Tregs and Th17 cells are both regulated by TGF-β and a balance between these two cell types can be shifted by cytokines as IL-2 correspondingly inhibits Th17 differentiation (152, 153). It is likely that purified $CD4^+$ T cells in antibody activation have less IL-6 in the culture because of fewer cell types. Therefore, identifying the Th17 cell population or level of IL-6 in antibody and peptide activated Tregs might help us to understand how Foxp3 expression is regulated by activation methods.

Foxp3 staining on of iTregs on day 6 of culture was performed to verify iTres populations. An initial FACS staining experiment identifying $Foxp3^+$ GFP^+ cells have failed owing to the loss of GFP fluorescence after cell fixation and permeabilisation. This was very likely caused by the insufficient fixation of the Foxp3 staining kit (eBioscience) (145). In addition, the fluorescent protein used in this experiment, the F-tractin-GFP, is not a membrane associated protein and more likely to diffuse from cells after permeabilisation. Therefore, we used an alternative approach: To determine the percentage of iTreg cell populations in pre-sorted cells and assume it to be the same as that in GFP^+ cells. Intracellular staining shows that approximate iTreg frequencies were found in pre-sorted, sorted GFP^- and GFP^+ cells, which supports our assumption. In this project, most iTregs generated with both anti-CD3/28 and MBP peptides priming raged from 60% to 90%, and cells used for iTregs imaging were mainly >75% $Foxp3^+$. The threshold was set mainly owing to minor fluctuations of iTreg induction rates and therefore, these up to 25% systemic errors needed to be considered. Overinterpretations of differences found when comparing iTreg and Teff spatiotemporal distribution patterns should be avoid.

In summary, with optimised iTreg induction protocol, we have generated Tg4 $Foxp3^+$ iTregs *in vitro* and performed initial retroviral transduction experiments with three signalling sensors (F-tractin-GFP, LAT-GFP and Vav1-GFP) on Tg4 iTregs. Further functional assays, morphological studies and spatiotemporal patterning analysis in iTregs and Teffs would be conducted in the next chapter. The frequency of $Foxp3^+$ cells activated with anti-CD3/28 was significantly higher than that of cells activated by MBP Ac1-9 [4K] peptide and endogenous APCs. We would further compare these iTregs in terms of their morphology and spatiotemporal distribution patterns of LAT-GFP, TCR-ζ-GFP and F-tractin-GFP during T cell activation.

Chapter 4 Tg4 Teffs and iTregs: different cell functions, morphological characteristics and signalling intermediate distributions

4.1 Introduction

As the differentiation protocol of Tg4 iTregs with high Foxp3 frequency was established, we could then investigate their biological characteristics, in comparison to Tg4 Teffs. There are three aspects in this project that we are interested in: immunological cell functions, morphological features and distributions of key signalling molecules in T cell activation.

First, cell functional assays were applied to study and compare how Teffs and iTregs could impact $CD4^+$ naïve T cell proliferation. Based on cytokine profiles, lineage-specific transcription factors and immunological functions, $CD4^+$ T helper (Th) cells are mainly divided into several subsets: Th1, Th2, Th9, Th17, Tfh cells and Tregs (21). Tregs suppress immune responses and prevent autoimmunity. When co-cultured, $CD4^+$ $CD25^+$ Tregs are capable of suppressing $CD4^+CD25^-$ T cell proliferation in the presence of APCs or soluble anti-CD3 or both, and inhibit IL-2 production of $CD4^+CD25^-$ T cells. In the Tg4 model, when activated with MBP Ac1-9 peptide and irradiated APCs, Tg4 iTregs suppress naïve $CD4^+$ T cell proliferation (139).

However, these studies focused on investigating Treg-induced suppression in co-culturing conditions where activated responder T cells are mixed with Tregs with certain ratios, while parallel assessments of the effect of adding Teffs were usually missing. Therefore, we performed T cell suppression assays by co-culturing CTV labelled naïve Tg4 T cells with Tg4 Teffs or iTregs, to investigate their impacts on naïve $CD4^+$ T cell proliferation. In MBP Ac1-9 triggered T cell activation, Th1 response is the dominant effector pathway in Tg4 $CD4^+$ T cells and they are capable to secrete IFN-γ (154). Thus, we mainly characterised and compared Tg4 Th1 cells in Teffs with $Foxp3^+$ iTregs.

T cell functions are usually related with their cytokine profiles. As one of the signature cytokines of Th1 cells, IFN-γ induces activation of macrophages, stimulates IgG production of B cells and promote cytotoxic T cell differentiation in defence against microbial infections (155). In contrast, IL-10 is an immunoregulatory cytokine expressed by different cell types such as macrophages, DCs, Th1, Th2, Tr1 and NK cells (156). It has been found to naturally suppress inflammatory reactions in skin and IL-10 knockout mice develop chronic

enterocolitis (157, 158). IL-10 has been related with Treg mediated immune suppression (159) and both $Foxp3^+$ and $Foxp3^-$ Tregs are capable of secreting cytokine IL-10 (68, 160, 161). To further compare functions of Tg4 Teffs and iTregs during T cell activation, we investigated their expression and secretion of these two distinct cytokines, IFN-γ and IL-10 by utilising intracellular cytokine staining and ELISAs.

Secondly, with defined morphological parameters, we assessed and compared cell shapes of Teffs and iTregs during their activation. Dynamic morphological changes of T cells during antigen recognition were observed in early studies (162, 163). Interaction of T cells and antigen-presenting B cells was found to undergo three stages (contact, recognition and stabilisation), which could last > 20 minutes (163). First, a T cell starts to explore around a B cell (contact) and then move towards the B cell and covers a part of its surface (recognition). In the third stage (stabilisation), the T cell partially retracts from the B cell and forms a round shape. After a cell couple is stable, the T cell will not seek to interact with other B cells. Rounder T cell shape has been found to be positively related with increasing intracellular Ca^{2+} concentration (162, 163). When forming a stable conjunction with DCs, naive $CD4^+$ T cells were found to become flattened and went through either elongated-flattened or round-flattened morphological changes during the IS formation (164). Compared with elongated-flattened $CD4^+$ T cells, higher level of $Ca2^+$ signalling, increased accumulation of TCR-signalling molecule and F-actin were found in the IS of round-flattened $CD4^+$ T cells (164). This indicates the former might lead to less effective T cell activation and weaker immune response. To evaluate and compare morphological changes in Tg4 Teffs and iTregs, we defined an extended lamella region and four morphological parameters (interface width, cell width, lamella depth and cell depth), described in chapter 2. Between Teffs and iTreg, we compared their relative interface width (the ratio of interface width to cell width), relative lamella depth (the ratio of lamella depth to cell depth) and overall cell shape (the ratio of lamella depth to interface width). A wider interface is indicative of a stable T cell-APC interaction which physically promotes binding of TCR-pMHC, co-receptors and adhesion molecules and improves activation. A longer lamella indicates a more elongated shape of a T cell, which is associated with weaker T cell activation (164). Thirdly, cells with an extended lamella region or a high ratio of lamella depth to interface width likely to show a slender cell shape, as it has a long lamella or narrow interface or both and forms a less stable and compressed cell couple. Clark *et al* have shown that within the first two minutes of T cell activation, recruitment of proximal T cell signalling intermediates (such as LAT and SLP-76) is critical for efficient T cell activation (126). Dynamic morphological changes of T cells within these two minutes are likely to play roles in T cell activation. Therefore, in this study we measured and compared morphological parameters within the first two minutes of Teff and iTreg activation.

Finally, it is of great interest to investigate how key signalling molecules during T cell activation localise in Tg4 Teffs and iTregs, as previous studies show that diverse spatiotemporal patterning of signalling intermediates are closely associated with T cell activation (130, 134). Moreover, diminishing F-actin structures impaired activation of key components of T cell activation and calcium signalling (165), and manipulation of LAT localisation alters T cell signalling and effector functions (126). In this chapter, we selectively investigated and compared spatiotemporal distributions of five key signalling intermediates (LAT, TCR ζ chain, PKC-θ, Vav1 and F-actin) during early activation of Tg4 Teffs and iTregs.

As one of the key component of the cSMAC, LAT associates with key molecules to transduce and amplify proximal TCR signalling. LAT nucleates a signalling complex by not only binding signalling proteins such as Grb2, PLC-γ1, and Gads via their SH2 domain, but also associating crucial molecules for T cell activation like Cbl, SOS, Vav1 and SLP-76 (97, 166, 167). Rapid LAT signalosome assembly is associated with dynamic actin network after TCR triggering, and actin mediated cytoskeleton assists initiation and maintenance of TCR-pMHC interactions (168). F-actin accumulation has been found to contribute T cell morphological changes and stabilise the IS formation (164), and its polymerisation and redistribution at the distal SMAC (dSMAC) and pSMAC at the IS drive TCR microcluster towards the cSMAC (169). In summary, we would track and compare localisation of these five different but related signalling molecules (LAT, TCR ζ chain, PKC-θ, Vav1 and F-actin) during Teff and iTreg activation and investigate their roles in effector and regulatory functions.

The seven distinct spatiotemporal patterns defined hold different roles in T cell activation (134). Representing the cSMAC, the central accumulation at the interface is related with proximal TCR-induced signalling including CD3, TCR-ζ, CD28, Lck, ZAP-70 and LAT, which initiate early T cell activation (121, 130, 134). The invagination pattern is preliminarily regarded as a reduced central pattern, as T cell invagination removes receptors like CD2 from the centre of the interface and mediates resetting of proximal T cell signalling (170). The peripheral pattern represents the pSMAC which covers the periphery of the IS interface and is enriched with actin accumulation (121, 134, 171). The asymmetric pattern shows an individual smaller protrusion near the interface, driven by actin (134). A transient lamellal signalling network supported by a deep actin matrix represents the lamellal pattern, which was prominently found in key activation regulators such as SLP-76 (135). Lamellal signalling intermediates covering the entire interface localise similarly with actin, and such lamellal distributions are related with signal modulation and amplification (134, 135). The

diffuse pattern covers the entire interface and localises near the membrane showing both central and peripheral features, which currently needs more functional studies to define their biological roles (134). The six patterns above describe accumulation at the interface while the last pattern, the distal pattern denotes proteins moving away from the interface to the distal pole during T cell activation, and disrupting the formation of this distal pole complex impairs cytokine secretion (172). Therefore, spatiotemporal organisation of signalling intermediates in early T cell activation could be quantitatively analysed and compared with the seven patterns. In addition, large-scale imaging data of sensors of interest (in this project, LAT-GFP) could be analysed in parallel by a recently established computational approach, as an automated alternative (173).

4.2 Chapter aims

- To assess and compare suppressive abilities and cytokine production of IFN-γ and IL-10 of Tg4 Teffs and iTregs.
- To measure and compare morphological parameters of Tg4 Teffs and iTregs within the first two minutes of T cell activation.
- To acquire and compare live cell imaging data of five key signalling intermediates (LAT, TCR ζ, PKC-θ, Vav1 and F-actin) of Tg4 Teffs and iTregs in early T cell activation.

A table is shown below denoting symbols used in this chapter for different cell types

Table 4.1 Symbols and patterns denoting cell types or conditions in chapter 4

Cell type	Symbol
Teffs (MBP Ac1-9 [4K] primed)	▲
Teffs (anti-CD3/28 primed)	◆
iTregs (MBP Ac1-9 [4K] primed)	●
iTregs (anti-CD3/28 primed)	■

4.3 Tg4 Teffs and iTregs suppress Tg4 naïve $CD4^+$ T cell proliferation in the presence of APCs

To characterise Tg4 iTregs and Teffs, we first studied and compared their immunological features including suppressive functions and cytokine production (IFN-γ and IL-10).

iTregs are capable of suppressing activation and proliferation of $CD4^+$ T cells (174). To assess their suppressive ability on T cell activation and proliferation, we set up suppression assays by co-culturing responder Tg4 naïve T cells with Teffs or iTregs, and CTV labelling was used to track cell proliferation. iTregs used for suppression assays were anti-CD3/28-primed and >75% $Foxp3^+$ and Teffs were primed with MBP Ac1-9 [4K] and they were cultured in relevant medium for five days in advance. We defined control and experimental wells and the first experiment was prepared as the following settings: In a control well, CTV labelled Tg4 naïve $CD4^+$ T cells were co-cultured with PL8 cells (as APCs) and primed with MBP Ac1-9 [4K], 1:0.25 ratio (8×10^5 naïve T cells and 2×10^5 PL8 cells). In the experimental wells, with same cells added as in a control well, Tg4 $CD4^+$ Teffs or iTregs were added, with 1:0.25:0.25 ratio (8×10^5 naïve T cells, 2×10^5 PL8 cells and 2×10^5 Teffs or iTregs). All cells were cultured for 72 hours before analysis. In addition, 2.5×10^5 naïve $CD4^+$ T cells labelled with CTV were fixed on day one to indicate fluorescent intensity of naive T cells which did not divide. CTV fluorescent signals were compared among all live $CD4^+$ cells. Results show that (Figure 4.1 A) in the control well (peaks in orange), naïve T cells proliferated and divided for at least five times. About 3% of CTV^+ cells went through five cell divisions and less than 2% of the cells did not divide. Unexpectedly, in both experimental wells, suppression on cell proliferation was observed. In the well with Teffs (Figure 4.1 A, peaks in red), only 0.2% of CTV^+ cells divided five times and 15% of them did not divide. In the well with iTregs (Figure 4.1 A, peaks in green), 0.1% of the CTV^+ cells divided five times and 18% of them did not divide. These observations indicate that both Teffs and iTregs suppressed naïve T cell proliferation when co-cultured with APCs presenting the MBP Ac1-9 peptide.

Next, we increased ratio of Teffs/iTregs to responder cells (from 1:0.25 to 1:1) to investigate how this would impact the suppression. In this setting, CTV^+ naïve cells in all wells were titrated down to 5×10^5. In the control well, the same amount of PL8 cells (5×10^5) were added. In the experimental wells, PL8 cells and Teffs or iTregs were added with equal number of cells (5×10^5) to corresponding wells (1:1 ratio). Results (Figure 4.2 B) show that in the control well (peaks in orange), naïve T cells proliferated but fewer cell divisions were observed: 6% of CTV^+ cells went through three cell divisions and 28% did not divide. In the well with Teffs (Figure 4.2 B, peaks in red), only 3% of CTV^+ cells divided and 97% of the

cells remained undivided. Only one clear peak was observed and hardly any cells divided for more than once. In the well with iTregs (Figure 4.2 B, peaks in green), 12% of the CTV^+ cells divided and 87% of them remained undivided. It was undistinguishable whether these cells divided for more than once but very unlikely.

These results show that in conditions with different cell ratios, Teffs and iTregs showed a comparable ability to suppress naïve $CD4^+$ T cell proliferation in the presence of PL8 cells with MBP Ac1-9 [4K] added in the culture. When comparing CTV^+ cell proliferation across these two experiments, suppression was prominently enhanced by increasing the ratio of Teffs or iTregs to responder cells (from 1:0.25 to 1:1), suggesting suppression on naïve T cells was positively associated with the proportion of Teffs or iTregs in the co-culture. However, increasing the ratio of PL8 cells to responder cells also enhanced the suppression (peaks in orange, Figure 4.2), though not as effective. It was unclear whether this observation was experimental variance, as there were the only two experiments where the suppression induced with different ratios of PL8 cells to responder cells could be compared. If not, it might indicate that a low ratio of PL8 cells to naïve $CD4^+$ T cells (0.25:1) is sufficient to promote cell proliferation, while a higher ratio of PL8 cells to naïve $CD4^+$ T cells (1:1) could inversely inhibit their proliferation. Although treated with mitomycin C, nutrient deprivation of PL8 cells, as B lymphoma cells, might still exist before their apoptosis.

A

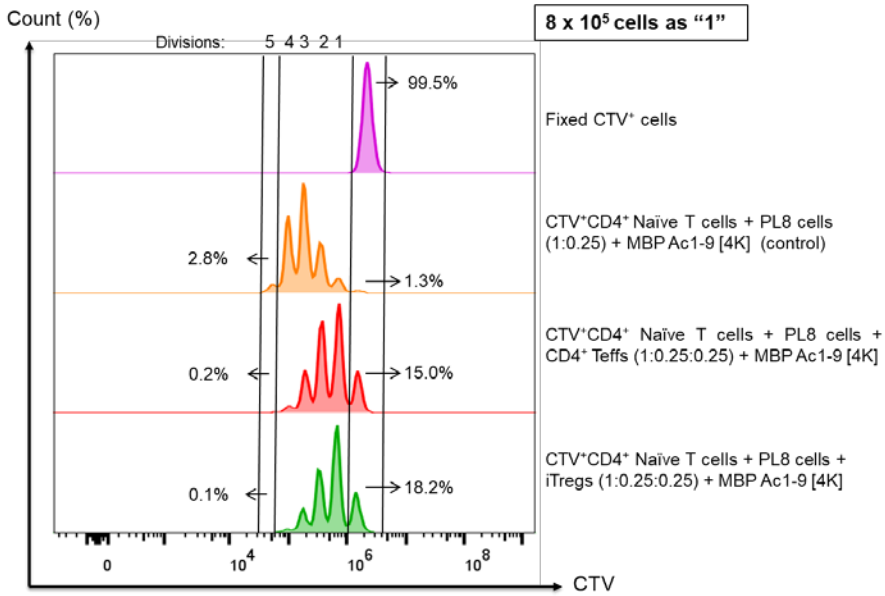

B

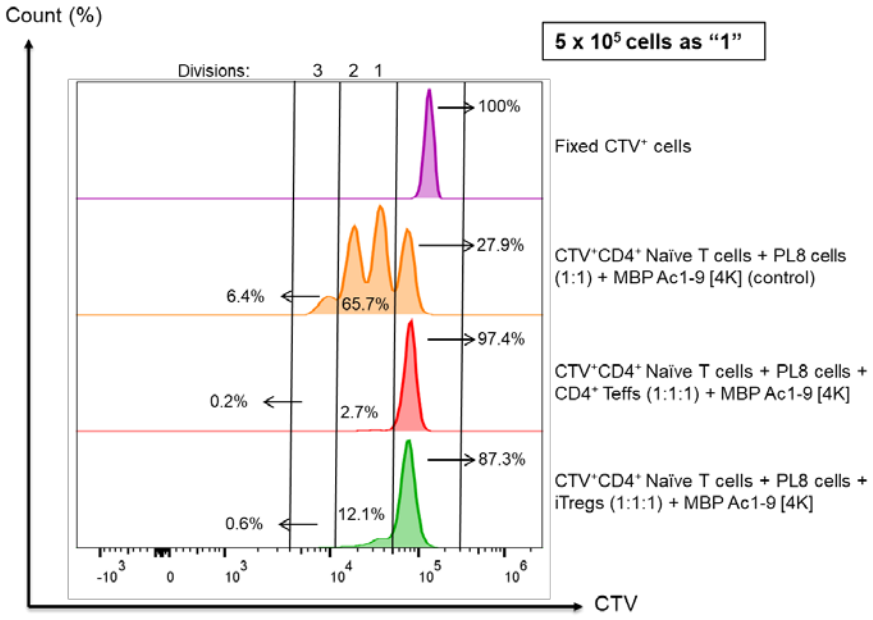

Figure 4.1 Teffs and iTregs suppress naïve CD4$^+$ T cell proliferation in the presence of APCs.

CTV labelled native CD4$^+$ T cells were co-cultured with Teffs or iTregs and activated by MBP Ac1-9 [4K] peptide. FACS staining were performed after 72 hours of culture to identify live CD4$^+$CTV$^+$ population. **A and B)** Histograms showing CTV cell population in four conditions with cell numbers and ratios indicated. Divisions indicate times that CTV$^+$ cells had divided, Cell types, numbers and ratios are indicated on the right of each row. Each histogram represents one experiment.

4.4 Clone 4 $CD8^+$ Teffs suppress Tg4 naïve $CD4^+$ T cell proliferation in the presence of APCs

Results above show that when activated by MBP Ac1-9 [4K]-primed PL8 cells, both Tg4 Teffs and iTregs suppressed Tg4 naïve $CD4^+$ T cell proliferation. The suppression induced by Teffs and iTregs raised a question: did the existence of a second T cell population contribute to the suppression observed or Teffs and iTregs both suppress proliferation of naïve T cells? The suppression observed might be owing to a competition for nutrients and cytokines such as amino acids and IL-2, in a well with three cell types. To investigate this, we replaced $CD4^+$ Teffs with $CD8^+$ Teffs from a different transgenic mouse model, the Clone 4 model. Clone 4 mice are transgenic for a TCR that recognises an MHC class I H-$2K^d$ restricted influenza hemagglutinin (HA) peptide (175).

In this experiment, same numbers of $CD4^+$ CTV^+ naïve T cells and PL8 cells were added to all wells, 5 x 10^5 each, 1:1 ratio. Two sets of ratios were adjusted in the experimental wells. In wells with iTregs, either 1 x 10^5 or 5 x 10^5 iTregs were added. The ratios of $CD4^+$ CTV^+ naïve T cells to PL8 cells to iTregs were set to be 1:1:0.2 and 1:1:1 in wells with iTregs. Same number of cells and ratios were applied in wells with Clone 4 $CD8^+$ T cells, but HA peptide was not added. As Clone 4 $CD8^+$ cells were expected to hold a low affinity for the MBP Ac1-9 peptide, they were unlikely to be activated by PL8 cells, thus to keep them proliferating, supplementary IL-2 was added.

Results show that in the control well (Figure 4.2, peaks in orange), CTV^+CD4^+ T cells went through up to five cell divisions with six clear peaks. About 14% of them divided five times and 5.2% did not. In the well with 1 x 10^5 $CD4^+$ iTregs (Figure 4.2, peaks in light green, 1:1:0.2 ratio), five clear peaks were identified. About 6% of $CD4^+$ CTV^+ T cells divided for at least four times and 26% of them did not divide. Suppression was still found in this well as when compared with the control well, more cells remained undivided and barely any cells divided for five times. In a well with 5 x 10^5 iTregs (Figure 4.2, peaks in dark green, 1:1:1 ratio), only two clear CTV^+ peaks were detected and about 13% of $CD4^+$ CTV^+ cells underwent one cell division. Most $CD4^+$ CTV^+ cells, about 87% did not divide. These results combined show that the level of suppression was related with the number of iTregs in the co-culturing well. More iTregs led to stronger suppression on $CD4^+$ naïve T cell proliferation.

Similar results were found upon addition of Clone 4 $CD8^+$ Teffs, as a control for suppressive Treg functions. In the well with 1 x 10^5 $CD8^+$ Teffs (Figure 4.2, peaks in light blue, 1:1:0.2 ratio), $CD4^+$ CTV^+ cells underwent only one cell division (16%), with two clear CTV^+ peaks found. In the well with 5 x 10^5 $CD8^+$ Teffs (Figure 4.2 peaks in dark blue, 1:1:1 ratio), more

CD4$^+$ CTV$^+$ cells remained undivided (91%) and the rest only divided for once. Together with the two experiments above, these results indicate that suppression on Tg4 CD4$^+$ naïve T cell proliferation can be induced by co-culturing them with Tg4 CD4$^+$ Teffs, Tg4 iTregs or Clone 4 CD8$^+$ Teffs in the presence of PL8 cells presenting the MBP peptide. Therefore, this suppression observed might not be specifically induced by one certain type of T cells we used here, but by a combination of PL8 cells and an additional Teff/iTreg population. However, it was uncertain if the mechanisms of such suppression induced by these three different cells were the same. We shall further discuss this in chapter discussion.

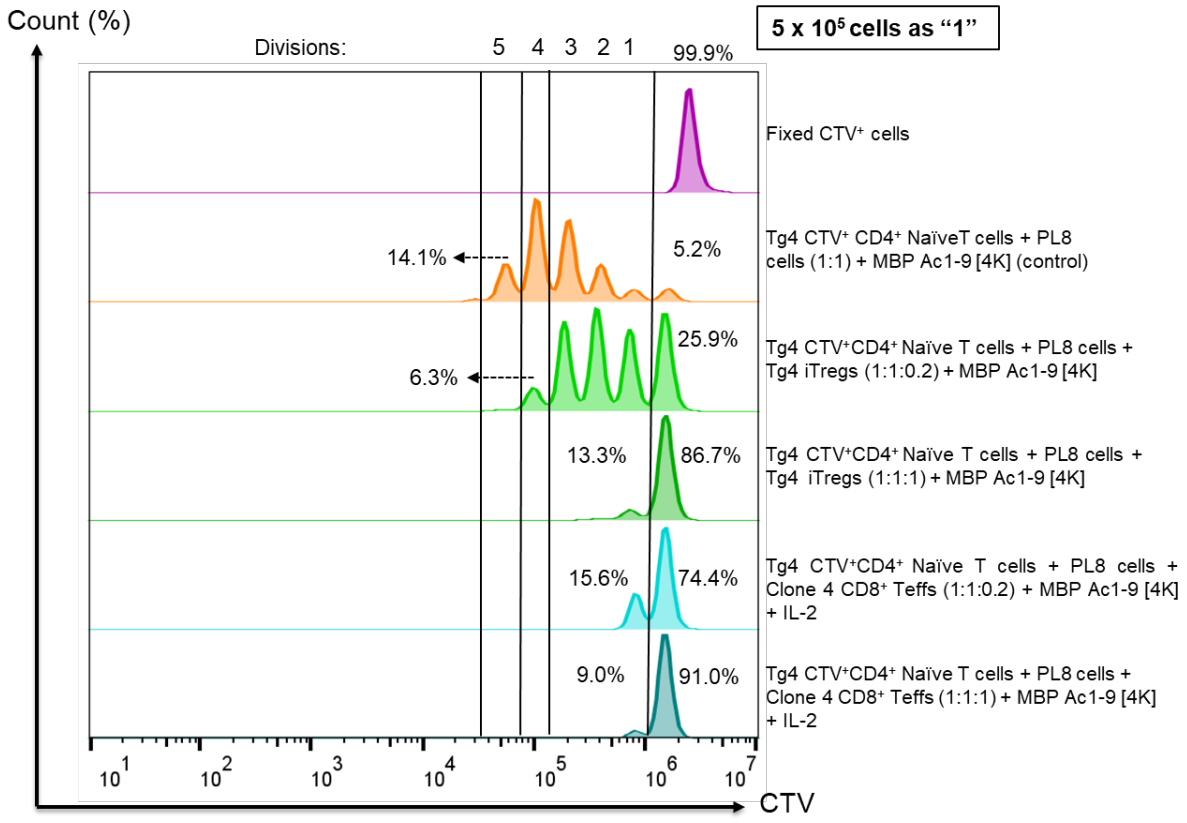

Figure 4.2 Clone 4 Teffs suppress Tg4 CD4$^+$ naïve T cell proliferation in the presence of APCs.

Tg4 native CD4$^+$CTV$^+$T cells were co-cultured with Tg4 iTregs or Clone4 CD8$^+$ Teffs and activated by MBP Ac1-9 [4K] peptide for 72 hours. FACS staining was performed to identify live CD4$^+$CTV$^+$ population. Histograms show CTV cell population in six conditions. Divisions indicate times that CTV$^+$ cells had divided. Cell types, numbers and ratios are indicated on the right of each row. IL-2 was added to activate Clone 4 CD8$^+$ Teffs. Data from one experiment are shown.

4.5 Tg4 naïve T cells primed with anti-CD3/28 are not suppressed by Tg4 iTregs

Simplified co-culturing conditions could help to investigate this suppression better. To validate this idea, we changed the activation method for the naïve T cells in wells by replacing PL8 cells with anti-CD3/28 antibodies. Thus, we could study whether suppression observed above was associated with the presence of APCs. We set up two repeated independent experiments without PL8 cells and MBP peptide and used anti-CD3/28 to provide TCR activation and co-stimulatory signals. Other conditons remained the same as above except that IL-2 was no longer added to wells containing Clone 4 $CD8^+$ Teffs.

In the first experiment, four clear CTV^+ peaks were found in the control well (Fgiure 4.3 A, peaks in orange) indicating CTV^+ cells underwent up to three divisions. Less than 2% of the cells divided four times and 20% of them remained undivided. In a well with 1 x 10^5 Tg4 Teffs (Figure 4.3 A, peaks in pink, 1:0.2 ratio), CTV^+ cells had undergone up to four cell divisions. About 16% of the cells divided four times and 9% of them did not divide. In the other well with 1 x 10^5 Tg4 Teffs (Figure 4.3 A, peaks in red, 1:1 ratio), 18% of CTV^+ cells have divided for four times and lest than 2% of them did not divide. In both wells with Tg4 $CD4^+$ Teffs, CTV^+ naïve T cells went through the same number of cell divisions and no suppression was observed. Moreover, the proliferation rate of CTV^+ cells co-cultured with Tg4 $CD4^+$ Teffs was increased because more of them had divided for four times and fewer of them remained undivided, compare to the control well.

Similar observations were found in wells with Tg4 iTregs and Clone 4 $CD8^+$ Teffs. In the well with 1 x 10^5 Tg4 iTregs (Figure 4.3 A, peaks in light green, 1:0.2 ratio), 13% of CTV^+ cells underwent four cell divisions and 13% of them did not divide. In the well with 5 x 10^5 Tg4 iTregs (Figure 4.3 A, peaks in green, 1:1 ratio), 18% of CTV^+ cells underwent four cell divisions and only 2.9% of them remained undivided. In the well with 1 x 10^5 Clone 4 $CD8^+$ Teffs (Figure 4.3 A, peaks in light blue, 1:0.2 ratio), 12% of CTV^+ cells underwent four cell divisions and 13% of them did not divide. More CTV^+ cell (32%) had undergone four cell divisions in the well with 5 x 10^5 Clone 4 $CD8^+$ Teffs (Figure 4.3 A, peaks in blue, 1:1 ratio) and less than 4% of them remained undivided. No suppression on the proliferation of CTV^+ cells in all these wells was observed. In contrast, their proliferation was enhanced in all wells with Tg4 $CD4^+$ Teffs, Tg4 iTregs or Clone 4 $CD8^+$ Teffs because more CTV^+ cells divided four times (>11%), compared with the control (1.4%). Possibly, additional Teffs or iTregs activated by anti-CD3/28 (without MHC restriction) contributed to the pool of IL-2, which promoted better proliferation of naïve T cells.

In the second repeated experiment (Figure 4.3 B), similar results were observed. In the control well (Figure 4.3 B, peaks in orange), about 3% of CTV^+ cells had undergone five cell divisions and 8% of them did not divide. In this epxeriment, CTV^+ peaks in experimental wells with Tg4 $CD4^+$ Teffs, Tg4 iTregs and Clone 4 $CD8^+$ Teffs displayed similar patterns. CTV^+ cells in both control and experimental wells had undergone at least five cell divsions. Again, no suppression was found.

In summary, results combined show that when activaed with anti-CD3/28, Tg4 naïve $CD4^+$ T cell proliferation was not suppresed by iTregs, $CD4^+$ or $CD8^+$ Teffs. Tg4 $CD4^+$ naïve T cells activated by anti-CD3/28 underwent up to four or five cell divsions when PL8 cells were absent. Suppression was found in all wells co-culturing Tg4 $CD4^+$ naïve T cells with Tg4 $CD4^+$ Teffs, iTregs or Clone 4 $CD8^+$ Teffs in the presence of MBP peptide-primed PL8 cells. Higher ratio of PL8 cells might partially suppress naïve T cell prolifeartion. Our results suggest that interactions between Tg4 $CD4^+$ Teffs, iTregs or Clone 4 $CD8^+$ Teffs with PL8 cells evidently suppress Tg4 $CD4^+$ naïve T cell proliferation. The presence of PL8 cells is critical for the suppression to occur but the mechnism of suppression in each condition might be different, we would further discuss this in the discussion section of this chapter.

A

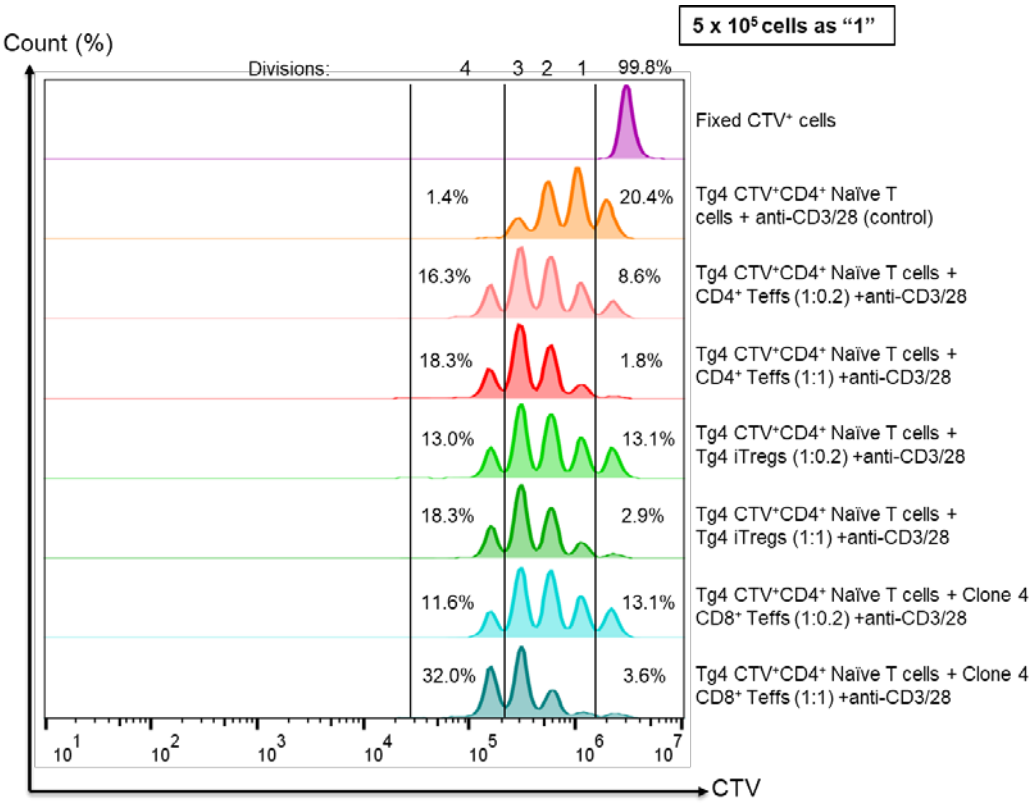
5 x 10⁵ cells as "1"
Count (%)
Divisions: 4 3 2 1 99.8%
Fixed CTV⁺ cells
1.4% 20.4%
Tg4 CTV⁺CD4⁺ Naïve T cells + anti-CD3/28 (control)
16.3% 8.6%
Tg4 CTV⁺CD4⁺ Naïve T cells + CD4⁺ Teffs (1:0.2) +anti-CD3/28
18.3% 1.8%
Tg4 CTV⁺CD4⁺ Naïve T cells + CD4⁺ Teffs (1:1) +anti-CD3/28
13.0% 13.1%
Tg4 CTV⁺CD4⁺ Naïve T cells + Tg4 iTregs (1:0.2) +anti-CD3/28
18.3% 2.9%
Tg4 CTV⁺CD4⁺ Naïve T cells + Tg4 iTregs (1:1) +anti-CD3/28
11.6% 13.1%
Tg4 CTV⁺CD4⁺ Naïve T cells + Clone 4 CD8⁺ Teffs (1:0.2) +anti-CD3/28
32.0% 3.6%
Tg4 CTV⁺CD4⁺ Naïve T cells + Clone 4 CD8⁺ Teffs (1:1) +anti-CD3/28
10¹ 10² 10³ 10⁴ 10⁵ 10⁶ 10⁷
CTV

B

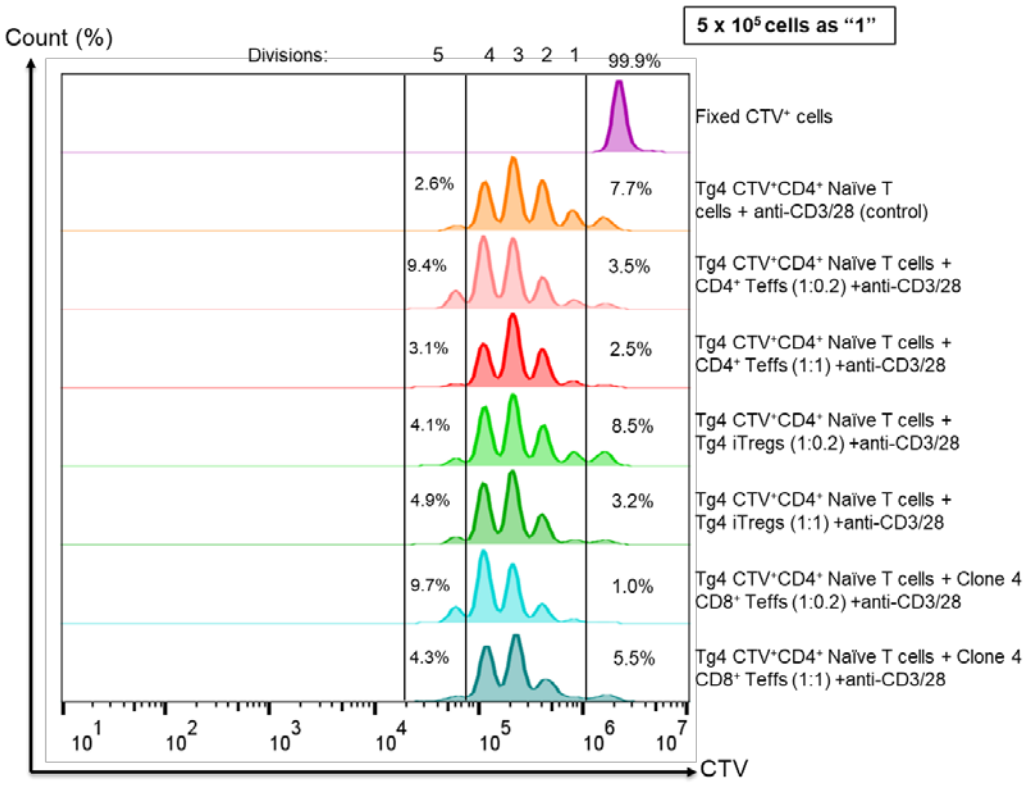
5 x 10⁵ cells as "1"
Count (%)
Divisions: 5 4 3 2 1 99.9%
Fixed CTV⁺ cells
2.6% 7.7%
Tg4 CTV⁺CD4⁺ Naïve T cells + anti-CD3/28 (control)
9.4% 3.5%
Tg4 CTV⁺CD4⁺ Naïve T cells + CD4⁺ Teffs (1:0.2) +anti-CD3/28
3.1% 2.5%
Tg4 CTV⁺CD4⁺ Naïve T cells + CD4⁺ Teffs (1:1) +anti-CD3/28
4.1% 8.5%
Tg4 CTV⁺CD4⁺ Naïve T cells + Tg4 iTregs (1:0.2) +anti-CD3/28
4.9% 3.2%
Tg4 CTV⁺CD4⁺ Naïve T cells + Tg4 iTregs (1:1) +anti-CD3/28
9.7% 1.0%
Tg4 CTV⁺CD4⁺ Naïve T cells + Clone 4 CD8⁺ Teffs (1:0.2) +anti-CD3/28
4.3% 5.5%
Tg4 CTV⁺CD4⁺ Naïve T cells + Clone 4 CD8⁺ Teffs (1:1) +anti-CD3/28
10¹ 10² 10³ 10⁴ 10⁵ 10⁶ 10⁷
CTV

Figure 4.3 When activated with anti-CD3/28, Tg4 $CD4^+$ naïve T cell proliferation was not suppressed by Tg4 $CD4^+$ Teffs, iTregs or Clone 4 $CD8^+$ Teffs.

Tg4 native $CD4^+CTV^+$T cells were co-cultured with Tg4 iTregs or Clone4 $CD8^+$ Teffs and activated by anti-CD3/28 for 72 hours. FACS staining was applied to identify live $CD4^+CTV^+$ population. **A and B)** Histograms show CTV cell population in eight conditions. Divisions indicate times that CTV^+ cells had divided. Cell types, numbers and ratios are indicated on the right of each row. Data from two experiment are shown.

4.6 Tg4 Teffs secrete more IFN-γ and iTregs tend to maintain IL-10 secretion during their development

Since suppression assays were not be able to distinguish and compare functional impacts of Tg4 Teffs and iTregs on Tg4 naive T cells, we then studied their cytokine profiles to further inverstigate funtional differences of Tg4 Teffs and iTregs. As mentioned previsouly in section 4.1, IFN-γ is critical in inducing immune response against pathogens while IL-10 is a key immuesuppressive molecule. Therefore, to assess their effector and suppresive fucntion, we studied IFN-γ and IL-10 secretion in Teffs and iTregs.

The combination of phorbol myristate acetate (PMA) and ionomycin is an effective method to promote cytokine secretion by T cells, as PMA specifically activates the PKC signalling pathway and ionomycin increases $Ca2^{+}$ influx (176). Thus here we used PMA/ionomyin to stimulate Tg4 Teffs and iTregs and study their cytokine secretion. Teffs and iTregs on day 6 of culturing were harversted and restimulated with 100ng/ml PMA and 1ug/ml Ionomycin for 1 hour. GolgiStop (BD Bioscience) was then added to the culture to block protein transport and increase cytokine accumulation. Intracellular staining was applied to identify IFN-γ and IL-10 production after another 3 hours of incubation. For experiments done at early stage of this project, iTregs were mainly induced with anti-CD3/28 activation. MBP Ac1-9 [4K]-primed Teffs and anti-CD3/28-primed iTregs (>74% $Foxp3^{+}$) were inititaly used for cytokine staining experiments. Results (Figure 4.4) show that frequences of IFN-γ^{+} or IL-10^{+} Teffs and iTregs on day 6 of culture were not significantly different. The mean percentage of IFN-γ^{+} Teffs (Figure 4.4 A) was 8% and iTregs was 5%. Freqencues of IL-10^{+} Teffs and iTregs were even lower (Figure 4.4 B). The mean freqence of $IL10^{+}$ Teffs was less than 1% and that of iTregs was less than 0.5%. This indicates that PMA and Inomycin restimulated Teffs and iTregs on day 6 of culture, barely secreted IL-10. The levels of IFN-γ secretion of Teffs and iTregs were slightly higher. These data imply that after five days of culture, PMA and Inomycin restimulated Teffs and iTregs showed a weak ability to secrete cytokines. Therefore, we then inverstigated how the production of these cytokines changed during Teff and iTreg differetiation after initial cell priming.

We had switched from the anti-CD3/28 to MBP peptide priming method to induce iTregs during the project. MBP peptide-primed iTregs were more comparable with Teffs which were primed with the same method, and more comparable to pTreg ELISAs were perfomred on MBP peptide-primed T cells, except for one experiment in IFN-γ ELISAs using data from anti-CD3/28-primed iTregs (Figure 4.4 C). Its secretion pattern was not different from the peptide-primed iTregs so this set of data was also plotted. After cells were peptide or antibody-primed on day 1, we collected cell culture supernatants from Teff or iTreg-

inducing conditions and performed IFN-γ and IL-10 ELISAs on samples from five days of culture (Day 2-6). Foxp3 intracellular staining was performed on day 6 to identify Treg population and iTregs used in IFN-γ ELISAs were >64% $Foxp3^+$, in IL-10 ELISAs were >63% $Foxp3^+$. Results (Figure 4.4 C) show that IFN-γ was dectected in both Teff and iTreg-inducing condtions. The amounts of IFN-γ dectected over the five days in Teff-inducing conditions were significantly higher ($p<0.05$) than those in iTreg-inducing conditions. When comparing IFN-γ concentrations on individual days, significantly higher levels of IFN-γ ($p<0.01$) were detected in Teff-inducing conditions on day 3 and 4 of culture, compared to that in iTreg-inducing conditions. Mean concentrations of IFN-γ detected in Teff-inducing conditions on days 4-6 were higher than that in iTreg-inducing conditions, but the differences were not significant. In addition, IL-10 secretion was also detected in both Teff and iTreg-inducing conditions (Figure 4.4 D). However, no significant differences were found when comparing daily or overall IL-10 production of the two conditions. More IL-10 was detected in Teff-inducing conditions on day 2, 3 and 4 while more was found in iTreg-inducing conditions on Day 6. These indicate that during five days of culture, IL-10 was transiently released into cell culture in both conditions, and iTreg-inducing cells tended to secrete more sustained but relatively low amounts of IL-10 from day 4.

IFN-γ and IL-10 secretion increased from day 2, peaked on day 3 of culture and decreased afterwards in both conditons. It should be noted that cell medium was exchanged on daily base and most cells were split 1:2 on day 3-6. This could contibute to the peak accmulation of IFN-γ and IL-10 on day 3 and relatively low cytokine serection after day 3.

Low levels of IL-10 were detected during Teff and iTreg development, and restimulation using PMA and inomycin did not enhance IL-10 production. It was previsouly shown that antigen-specific iTregs were able to produce IL-10 when co-cultured with peptide-pulsed DCs for 18 hours (177). Therefore, we restimulated Teffs or iTreg (>62% $Foxp3^+$) from day 5 of culture with mitomycin C treated PL8 cells and MBP peptides to investigate their ability to produce IL-10 upon restimulation (Figure 4.4 E). The result shows that restimulated iTregs produced slightly more IL-10 than Teffs, but the difference was not significant.

In summary, these results show that when restimulated with PMA and ionomycin on day 6 of culture, low levels of INF-γ were detected in Teffs and Tregs. IL-10 secretion was hardly found in either conditon. ELISAs show that IFN-γ and IL-10 were both detected during the development of Teffs and iTregs and more IFN-γ production was found in the former. In additon, iTregs showed a trend to maintain IL-10 production at later stages of their development and produce more IL-10 when restimulated with MBP peptide and PL8 cells.

These data suggest that Tg4 iTregs produce less IFN-γ but hold a better ability to produce more IL-10 than Teffs.

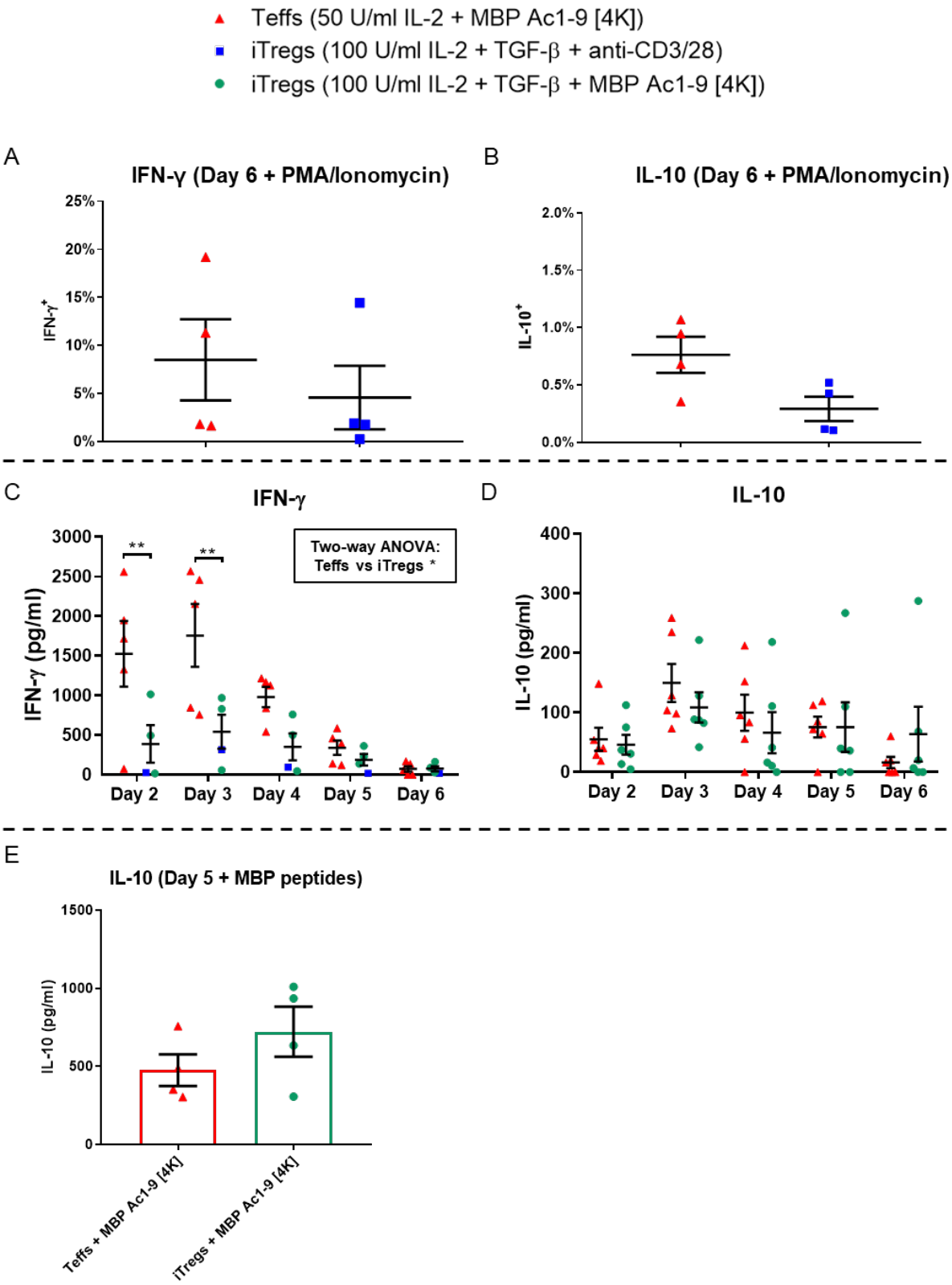
Teffs (50 U/ml IL-2 + MBP Ac1-9 [4K])
iTregs (100 U/ml IL-2 + TGF-β + anti-CD3/28)
iTregs (100 U/ml IL-2 + TGF-β + MBP Ac1-9 [4K])
A
IFN-γ (Day 6 + PMA/Ionomycin)
IFN-γ+
25%
20%
15%
10%
5%
0%
B
IL-10 (Day 6 + PMA/Ionomycin)
IL-10+
2.0%
1.5%
1.0%
0.5%
0.0%
C
IFN-γ
IFN-γ (pg/ml)
3000
2500
2000
1500
1000
500
0
**
**
Two-way ANOVA:
Teffs vs iTregs *
Day 2
Day 3
Day 4
Day 5
Day 6
D
IL-10
IL-10 (pg/ml)
400
300
200
100
0
Day 2
Day 3
Day 4
Day 5
Day 6
E
IL-10 (Day 5 + MBP peptides)
IL-10 (pg/ml)
1500
1000
500
0
Teffs + MBP Ac1-9 [4K]
iTregs + MBP Ac1-9 [4K]

Figure 4.4 Less IFN-γ secretion was detected during iTreg development.

Intracellular cytokine staining and ELISA were performed to assess IFN-γ and IL-10 production of Teffs and iTregs. Teffs and iTregs on day 6 of culture were restimulated with PMA and Ionomycin for 1 hour and then treated with GolgiStop protein transport inhibitor for 3 hours before cytokine staining. Intracellular cytokine staining showing **A)** IFN-γ^+ and **B)** IL-10^+ cell populations of Teffs and iTregs on day 6 of culture. Data from four experiments were arcsine-transformed and statistical significance was calculated using paired Student's T-test. Cell culture supernatants used for ELISAs were daily collected from cell culture of Teffs and iTregs for five days (day 2 to 6 of culture). ELISAs showing **C)** IFN-γ and **D)** IL-10 detected in Teff and iTreg-inducing cell culture from day 2 to 6. Data from five experiments were used for IFN-γ ELISAs and six for IL-10 ELISAs. Teffs and iTregs from day 5 of culture were restimulated with mitomycin C treated PL8 cells and MBP peptides and cell culture supernatants were collected for **E)** Determining IL-10 secretion by restimulated Teffs and iTregs on day 5. Statistical significance was calculated using **C-D)** Two-way ANOVA and **E)** paired Student's T-test. Asterisks indicates p-values (*<0.05, **<0.01). Error bars indicate standard error of the mean.

In addition, to identify how cytokine secretion was correlated with Foxp3 expression, we performed intracellular staining on another sets of cells to examine Foxp3$^+$ cell population during Teff and iTreg development. Result shows (Figure 4.5) that the percentage of Foxp3$^+$ T cells in iTreg-inducing conditions was significantly higher than that in Teff-inducing conditions ($p<0.0001$), from day 3 to 6 of culture. With additional TGF-β and higher concentration of IL-2, naïve T cells were effectively transformed into Foxp3$^+$ iTregs from day 3 and Foxp3$^+$ cell population gradually increased afterwards. The frequency of Foxp3$^+$ iTregs peaked on day 5. Foxp3$^+$ cell population was hardly detected in Teff-inducing conditions in any day of culture. This indicates that the cell types in Teff and iTreg-inducing conditions were different from day 3 to 6 of culture, which should be noted when comparing their cytokine secretion.

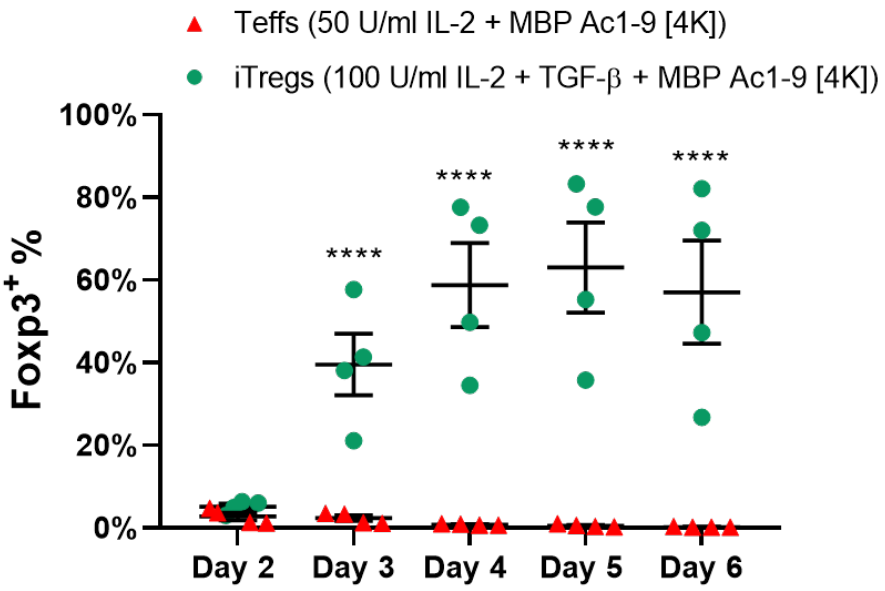

Figure 4.5 TGF-β and a higher concentration of IL-2 significantly induced Foxp3$^+$ iTregs.

Purified lymphocytes and splenocytes were primed with MBP Ac1-9 [4K] and induced into Teffs (50 U/ml IL-2) and iTregs (100 U/ml IL-2 and 10 ng/ml TGF-β) for five days. Cell samples were collected, fixed and stained for Foxp3 antibody on each day. Data from four experiments were analysed. Statistical significance was calculated with arcsine transformed data using Two-way ANOVA. Asterisks indicated p-values (****<0.0001). Error bars indicate standard error of the mean.

As IFN-γ secretion was mainly detected on day 3 and 4, we next performed cytokine staining on Teff and iTreg-inducing T cells from these days to identify IFN-γ producing cell populations. Protocol was followed as described earlier in this section. Cells were stained with CD4, Foxp3 and IFN-γ antibodies to separate Foxp3$^-$ IFN-γ$^+$ Teffs and Foxp3$^+$ IFN-γ$^+$ iTregs. Result (Figure 4.6 A) shows that frequencies of Foxp3$^-$ IFN-γ$^+$ Teffs and Foxp3$^+$ IFN-γ$^+$ iTregs on day 3 and 4 of culture were not significantly different and were both around 100%. This suggests that Teffs and iTreg on day 3 and 4 of culture are prominent producers of IFN-γ and highly activated. To assess the expression level of IFN-γ within IFN-γ$^+$ T cell populations, the median fluorescence intensity (MFI) of IFN-γ+ populations was compared. Result (Figure 4.6 B) shows that both Foxp3$^-$ Teffs and Foxp3$^+$ iTregs had higher level of IFN-γ expression on day 3 but the MFI of IFN-γ$^+$ cells among these two groups on day 3 and 4 was not significantly different.

Together, we have investigated IFN-γ and IL-10 expression during Teff and iTreg developments (day 2 to 6 of culture). IFN-γ expression was mainly detected in Teff and iTreg-inducing conditions on day 2 to 4, and IL-10 expression was mainly found on day 3 and 4 (but with relatively low concentration). Both cytokines were barely detected on day 5 and 6. More IFN-γ was detected during the development of Teffs, compared to that of iTregs but iTregs displayed a trend of maintaining IL-10 secretion during their development. This suggests these mature iTregs will be more suppressive once reactivated. Intracellular cytokine staining assays showed that Foxp3$^-$ Teffs and Foxp3$^+$ iTregs on day 3 and 4 were genuine sources of IFN-γ. In addition, restimulation with PMA and Ionomycin was not able to enhance IFN-γ and IL-10 expression in Teffs and iTregs on day 6.

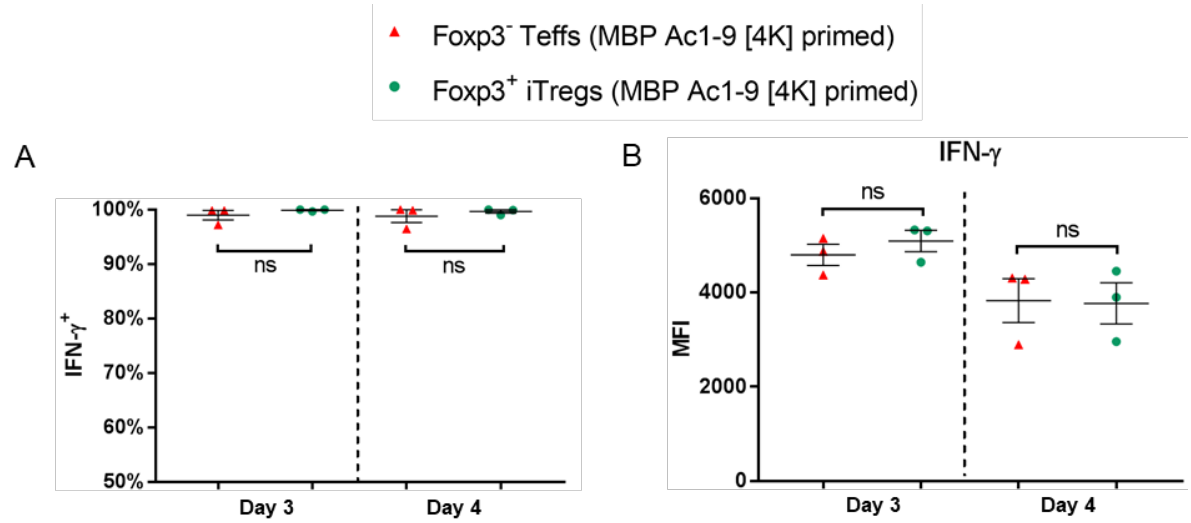

Figure 4.6 Teffs and iTregs were prominent producers of IFN-γ on day 3 and 4 of culture.

Intracellular cytokine staining was performed to assess IFN-γ expression of Teffs and iTregs on day 3 and 4 of culture. Teffs and iTregs on day 3 of culture were restimulated with PMA and Ionomycin for 1 hour and then treated with GolgiStop protein transport inhibitor for 3 hours. Cells were stained with CD4, Foxp3 and IFN-γ to identify $Foxp3^{-}IFN\text{-}\gamma^{+}$ Teffs and $Foxp3^{+}IFN\text{-}\gamma^{+}$ iTregs. **A)** Comparing percentages of $IFN\text{-}\gamma^{+}$ cells between $Foxp3^{-}$ Teffs and $Foxp3^{+}$ iTregs from day 3 of culture. **B)** Comparing MFIs of $IFN\text{-}\gamma^{+}$ cells of $Foxp3^{-}$ Teffs and $Foxp3^{+}$ iTregs from day 3 of culture. Data were from three experiments and statistical significance was calculated using paired Student's T-test, ns, not significant. Error bars indicate standard error of the mean.

4.7 Tg4 iTregs form a less stable IS in early T cell activation

To quantify cell shape changes during early T cell activation, we defined three morphological ratios based on measurements of four parameters (described section 2.10): the ratio of interface width to cell width, lamella depth to cell depth and lamella depth to interface width. These three ratios could quantify the level of widening and extension of a cell. Live cell imaging was performed to record T cell-APC interactions between Tg4 T cells transduced with GFP-sensors and peptide-primed PL8 cells, as APCs. PL8 cells were pulsed with MBP Ac1-9 [4Y] for at least 4 hours before imaging. Morphological measurements were done on DIC images. We have measured the four parameters in both MBP Ac1-9 [4K] and anti-CD3/28-primed Teffs and iTregs (transduced with LAT-GFP) for the first two minutes after a stable cell couple was formed.

Representative imaging data showing measurements of four morphological parameters are aligned in Figure 4.7 A. A T cell was identified whether they formed an extended lamella, otherwise its lamella depth was recorded as “0”. In MBP Ac1-9 [4K]-primed T cells (Figure 4.7 B), iTregs displayed a narrower interface when forming IS across the first two minutes, compared with Teffs ($p<0.001$). Significant differences were found at the 0s ($p<0.05$), 20s ($p<0.01$) and 120s ($p<0.05$) time point. When comparing the ratios of lamella depth vs cell depth (Figure 4.7 C), iTregs tended to have a longer lamella (higher mean ratios) than Teffs but no significant differences were observed at each time or over the two minutes. The ratio of lamella depth over interface width of iTregs was significantly higher than that of Teffs over the two minutes (Figure 4.7 D, $p<0.0001$), suggesting that iTregs form a thinner and longer cell shapes within this period. Significant differences were observed at the 0s ($p<0.0001$), 20s ($p<0.0001$) and 60s ($p<0.01$) time point, reflecting a narrower interface and longer lamella in iTregs.

The lamella depth was only measured if an extended lamella was observed during these two minutes, therefore we counted numbers of cells couples with and without an extended lamella and compared their percentages. Result shows (Figure 4.7 E) that at the early time points (0s and 20s), more iTreg cell couples formed an extended lamella than Teffs ($p<0.01$). These results suggest that when MBP Ac1-9 [4K]-primed iTregs interact with PL8 cells, their interfaces of contact are not spreading as wide as that of MBP Ac1-9 [4K]-primed Teffs, and they displayed a more extended slender cell shape and formed more lamella regions in the first 20 seconds. This might lead to a less stable synapse formation and subsequently, less effective T cell activation.

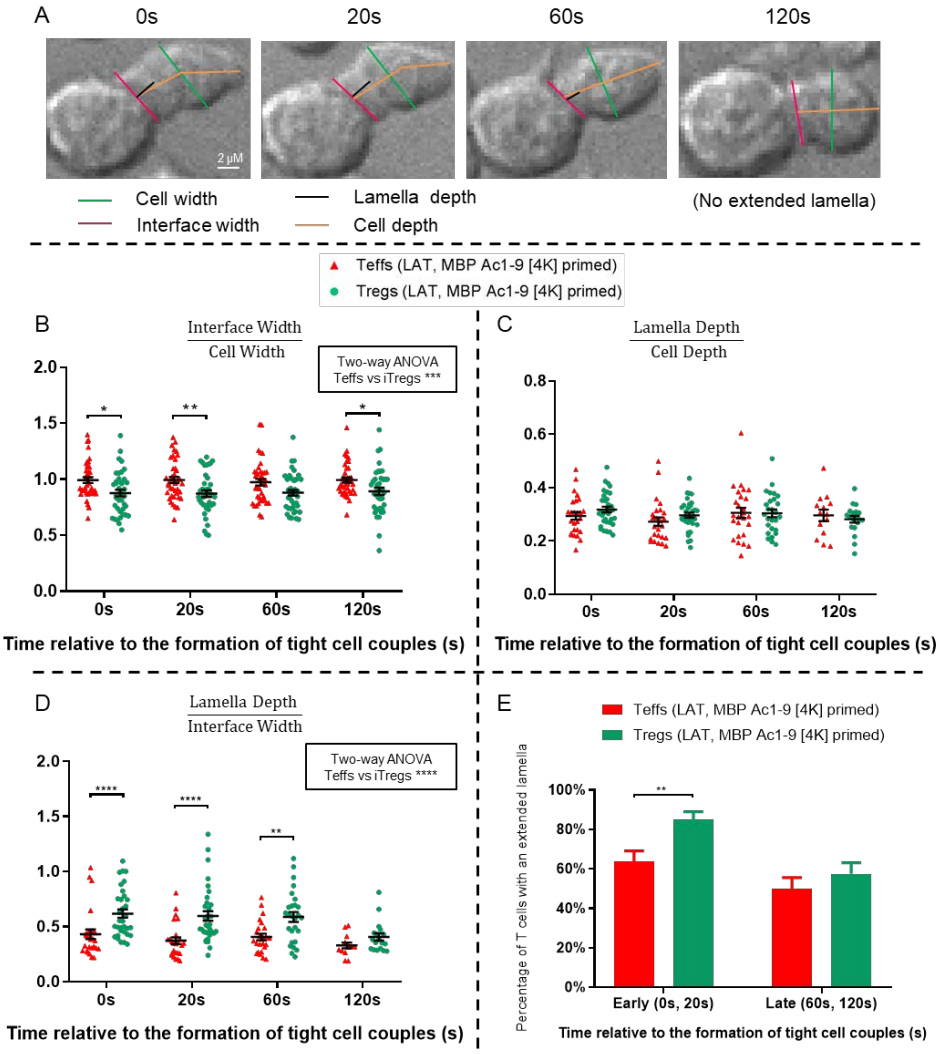

Figure 4.7 MBP Ac1-9 [4K]-primed iTregs display a narrower immune synapse interface, more slender cell shape and form more extended lamellae compared to MBP Ac1-9 [4K]-primed Teff† in early T cell activation.

LAT-GFP transduced MBP Ac1-9 [4K]-primed Teffs and iTregs interacted with MBP Ac1-9 [4Y]-primed PL8 cells and were imaged every 20 seconds for 15 minutes. Morphological parameters were measured within the first two minutes of T cell activation, 0s indicates the time when a tight cell couple was formed. **A)** Representative DIC images showing measurements of four morphological parameters. Comparing the ratios of **B)** interface width to cell width, **C)** lamella depth to cell depth, **D)** lamella depth to interface width between Teffs and iTregs. **E)** Comparing percentages of Teffs and iTregs formed an extended lamella region. **B-E)** 40 cells from four experiments for Teffs and 40 cells from two experiments for iTregs were analysed. **B-C)** Statistical significance was calculated with log-transformed data using Two-way ANOVA. **E)** Statistical significance was calculated using Chi-square test. Asterisks indicate p-values (*<0.05, **<0.01, ***<0.001, ****<0.0001). Error bars indicate standard error of the mean.

† LAT-GFP imaging data of Tg4 MBP peptide-primed Teffs were generated by former PhD student Helen Tunbridge.

Same analysis and comparisons were performed in anti-CD3/28-primed T cells. No significant differences were found when comparing the ratios of interface width to cell width, and lamella depth to cell depth between Teffs and iTregs (Figure 4.8 A and B). Compared to Teffs, iTregs had an overall higher ratio of lamella depth over interface width ($p<0.05$), indicating their shapes were more extended (Figure 4.8 C), but no significant differences were observed at individual time points. Figure 4.8 D shows that more anti-CD3/28-primed iTreg cell couples formed an extended lamella at late time points (60s and 120s, $p<0.01$), compared to anti-CD3/28-primed Teffs. These suggest that in anti-CD3/28-primed cells, iTregs form more extended lamellae and tended to have a more slender cell shape over the first two minutes of T cell activation which might be a sign of less stable T cell-APC interactions.

In summary, we have measured and compared morphological parameters during the first two minutes of Tg4 Teff and iTreg activation with different priming conditions. iTregs displayed a more elongated and slender cell shape when forming an IS with APCs, compared with Teffs. In addition, more extended lamellae near the IS were observed in iTregs. This indicates that iTreg form a less stable IS which might lead to less effective T cell activation. The level of differences varied when comparing within MBP peptide and anti-CD3/28-primed cells, but their trends remained consistent.

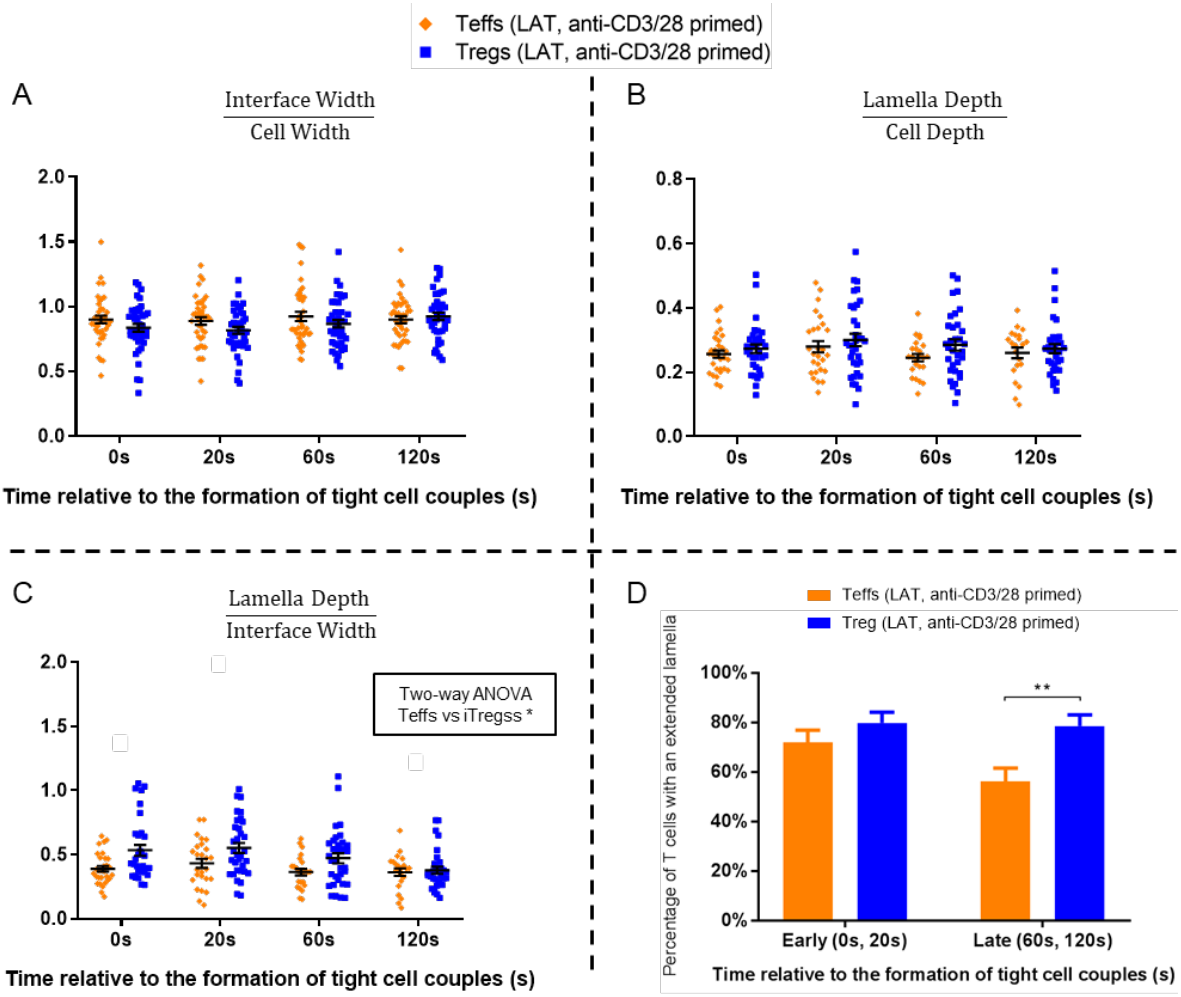

Figure 4.8 Anti-CD3/28 iTregs tend to form a more slender cell shape and more extended lamellae than anti-CD3/28-primed Teffs in early T cell activation.

LAT-GFP transduced anti-CD3/28-primed Teffs and iTregs interacted with MBP Ac1-9 [4Y]-primed PL8 cells and were imaged every 20 seconds for 15 minutes. Morphological parameters were measured within the first two minutes of T cell activation, 0s indicates the time when a tight cell couple was formed. Comparing the ratios of **A)** interface width to cell width, **B)** lamella depth to cell depth, **C)** lamella depth to interface width between Teffs and iTregs. **D)** Comparing percentages of Teffs and iTregs with an extended lamella region. 40 cells from two experiments for Teffs and 41 cells from four experiments for iTregs were analysed. **A-C)** Statistical significance was calculated using Two-way ANOVA. **D)** Statistical significance was calculated using Chi-square test. Asterisks indicate p-values (*<0.05, **<0.01). Error bars indicate standard error of the mean.

4.8 LAT overall and central accumulation at the IS of Tg4 iTregs are diminished

Tg4 Teffs and iTregs have shown different cytokine profiles during their development and cell shape changes when activated. Next we studied and compared spatiotemporal organisation of key signalling intermediates during early T cell activation of Teffs and iTregs. First several minutes of T cell activation are accompanied by various events such as changes of calcium signalling and cell shapes, transport of surface receptors, cytoskeleton, signalling intermediates, and transcriptional factors (130, 134, 163, 178). As a transmembrane adaptor protein, LAT plays indispensable roles in proximal signal transduction during T cell activation. Followed by pMHC-TCR-induced activation, LAT is phosphorylated by ZAP-70 on tyrosine residues which bind the SH2 domain of Grb2, Gads and PLC-γ1 (97). The formation and function of LAT-nucleated multiple signalling complexes is summarised in section 1.6.1. LAT deficiency in Jurkat cells leads to impaired intracellular calcium signalling, defective phosphorylation of PLC-γ1, Vav and SLP-76 and reduced activation of AP-1 and NFAT, which can all be restored by reconstitution of LAT (179, 180).

The roles of LAT localisation in T cell activation have been controversial. Early study revealed that localisation of LAT into the glycolipid-enriched microdomains (GEMs) by palmitoylation was required for T cell activation (181, 182). However, following studies showed that LAT localisation to the lipid raft is not essential for T cell activation and development, while targeting LAT to the plasma membrane is sufficient for its function in T cells (183-185). To investigate LAT localisation and better understand how LAT spatiotemporal distributions contributes to its signal transduction upon T cell activation, we have previously constructed a LAT-GFP fusion protein to visualise and track LAT localisation during T cell activation, using TCR transgenic 5C.C7 T cells (130). Upon peptide triggered TCR activation, LAT and other associated signalling intermediates such as ZAP-70, PKC-θ, Itk, PLC-γ, Rac and Rho localised at the centre of the T cell-APC interface or the cSMAC (130). Clustered by thousands of molecules, supramolecular signalling complexes play important roles in innate antiviral responses (186), inflammation (187), cell death regulation (188) and cancer cell survival (189). By applying fluorescence microscopy, extensive studies of composition and functions of supramolecular signalling complexes have been conducted (190, 191). To better explore cSMAC function, Clark *et al* investigated and systematically manipulated localisation of three key adaptor proteins of the cSMAC including LAT, SLP-76 and Grb2 under different T cell activation conditions (126). They found that when fully activated, LAT was efficiently recruited to the interface in the first two minutes of cell coupling and displayed a preference for central accumulation.

Attenuation of T cell activation signalling by costimulation blockade and IL2-inducible T-cell kinase (ITK) knockout both led to diminished LAT central accumulation and their combination prominently impaired LAT accumulation at the interface (126). Moreover, costimulation blockade and Itk deficiency or both combined significantly reduced the level of IL-2 mRNA. Diminished central LAT accumulation at the interface upon such attenuated activation conditions could be restored or even exceedingly enhanced, by fusing LAT with additional Vav1 SH2SH3SH2 or PKC-θ V3 protein interaction domain respectively. The former also enhanced IL-2 mRNA production (126).

These data together indicate that LAT central localisation at the T cell-APC interface upon TCR-pMHC mediated activation contributes to the formation of cSMAC and effector function of T cells. It is still unknown how LAT localises at the IS of iTregs upon activation and whether this will have effect on iTreg function. To track and observe LAT localisation in Tg4 T cells, we first investigated LAT-GFP spatiotemporal distributions in early T cell activation of Tg4 Teffs and iTregs, with two priming methods (MBP peptides and anti-CD3/28). LAT-GFP transduced iTregs were >73% Foxp3^{+}.

Representative still images in Figure 4.9 shows LAT-GFP distributions in Teffs and iTregs in the first two minutes of T cell activation, under the confocal microscope. Images from the DIC and GFP channel are shown.

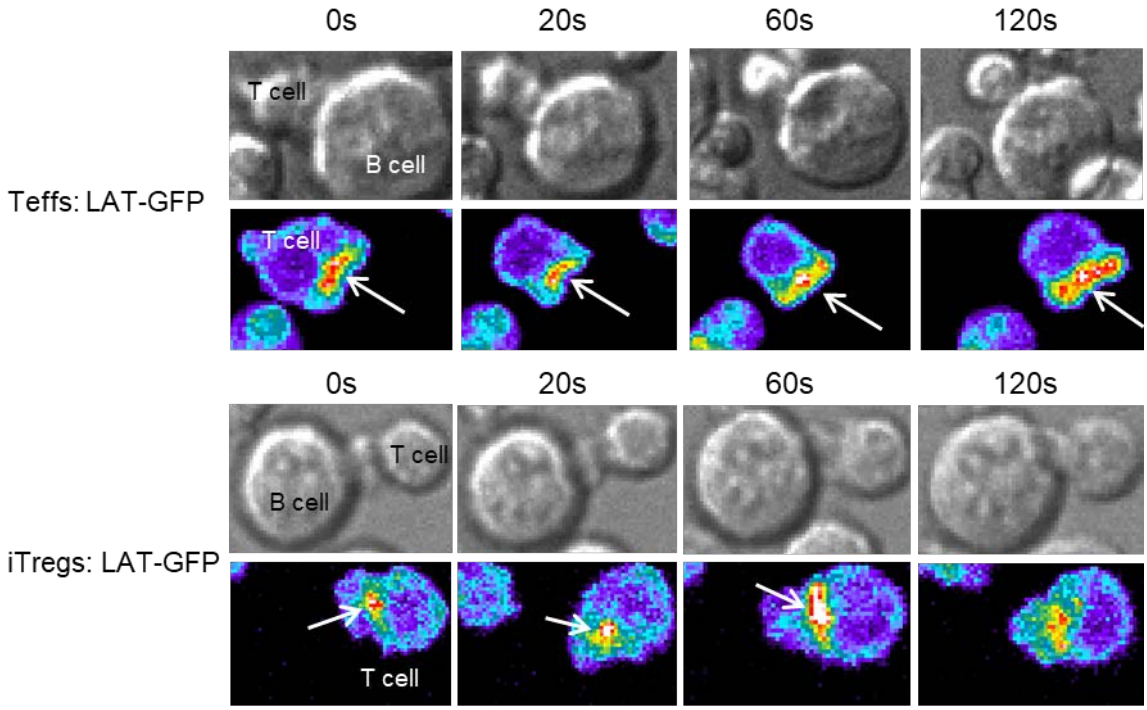

Figure 4.9 Representative live cell images showing LAT-GFP distributions in Tg4 Teffs and iTregs in the first two minutes of T cell activation (0s, 20s, 60s and 120s time points).

Top: DIC images from four time points. Bottom: matching top-down maximum projections of three-dimensional LAT-GFP fluorescent images (intensity is encoded in pseudocolour and increases from purple to red). Time is given in seconds relative to the formation of a tight cell couple and arrows denote accumulation of the sensor.

In MBP Ac1-9 [4K]-primed Teffs (Figure 4.10 A), started with low accumulation at the -40s and -20s time point, LAT-GFP overall accumulation increased from the -20s time point. The percentage of cells showing LAT-GFP accumulation peaked at the 40s time point with 63% of cell couples showed accumulation at the interface. The accumulation decreased steadily after the peak, reaching the lowest point at the 300s time point (23%). For MBP peptide-primed Teffs, the dominant spatiotemporal accumulation pattern was the central pattern. At the 0s, 20s and 40s time point, respectively 31%, 42% and 35% of Teffs showed LAT-GFP central accumulation.

In MBP Ac1-9 [4K]-primed iTregs (Figure 4.10 B), LAT-GFP accumulation peaked at the 60s time point with 31% of iTregs showed accumulation at the interface and decreased afterwards. The distal pattern was observed to be dominant (29% at 0s) before the 20s time point, while the invagination was dominant after the 20s time point (18% at 20s). The statistical comparison (Figure 4.10 E, first row) shows that LAT-GFP overall accumulation in MBP Ac1-9 [4K]-primed iTregs was significantly lower than that of Teffs at eight time points ($p<0.05$, 0s-100s, 180s and 420s). As statistical tests were conducted for 12 times (12 time points) for each comparison, pure chances of incorrectly rejecting the null hypotheses increased. Therefore, the Bonferroni correction was applied to adjust p-values. P-values below 0.05 are indicated with asterisks. Asterisks in black indicates that observed differences remain significant with the Bonferroni correction ($p<0.004$). Asterisks in blue indicates that observed differences are no longer significant with the Bonferroni correction ($0.004<p<0.05$). At the 20s and 40s time point, observed differences were still significant after the Bonferroni correction ($p<0.001$). Together, these results suggest that during early T cell activation, MBP Ac1-9 [4K]-primed iTreg display impaired overall LAT accumulation at the interface, compared to Teffs with the same priming method.

LAT-GFP overall accumulation at the interface in anti-CD3/28-primed Teffs (Figure 4.10 C) peaked at the 80s time point (76% of Teffs showing LAT-GFP accumulation at the IS). No major reduction of accumulation was found afterward, as more than 60% of cells showing LAT-GFP accumulation at the interface from the 80s-420s time point. Before the 80s time point, LAT-GFP showed mainly central and invagination accumulation while the diffused pattern was more dominant after the 120s time point.

Overall LAT-GFP accumulation of anti-CD3/28-primed iTregs (Figure 4.10 D) peaked at the 120s with 52% of iTregs showing LAT-GFP accumulation at the IS, which was the latest peak of accumulation across the four conditions. The accumulation decreased afterwards. Consistent with the differences found in the MBP Ac1-9 [4K]-primed T cells, anti-CD3/28-primed iTregs displayed lower LAT-GFP overall accumulation at the 0s-100, 180s and 420s

time points (Figure 4.10 E, second row). Significant differences were still observed at the 0s, 40s, 80s, 100s and 420s time points with the Bonferroni correction ($p<0.004$). These observations indicate that during early T cell activation, overall LAT accumulation in ani-CD3/28 primed iTreg is diminished, compared with anti-CD3/28-primed Teffs.

Comparisons of these four data sets suggest that LAT overall accumulation in iTregs to be diminished, compared with Teffs in both MBP Ac1-9 [4K] and anti-CD3/CD28 primed conditions. Therefore, signal transduction in LAT nucleated protein complexes in early iTreg activation is likely to be impaired, which leads to less efficient T cell activation.

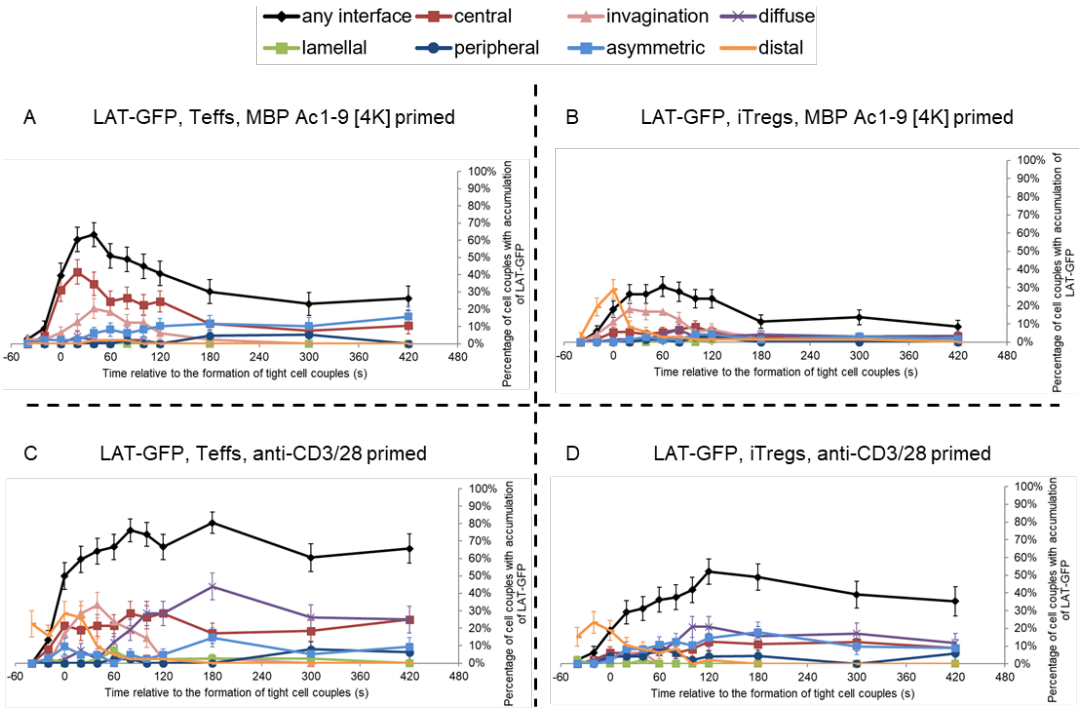

E Statistical comparisons of any interface accumulation

Time (s)	-40	-20	0	20	40	60	80	100	120	180	300	420
Teffs (4K) vs iTregs(4K)	0.78	0.83	0.02	0.0004	0.0001	0.04	0.03	0.03	0.08	0.02	0.33	0.04
			*	***	***	*	*	*		*		*
Teffs (anti-CD3/28) vs iTregs (anti-CD3/28)	0.84	0.49	0.004	0.007	0.004	0.008	0.0005	0.004	0.23	0.005	0.09	0.03
			**	**	**	**	***	**		**		*
Teffs (4K) vs Teffs (anti-CD3/28)	0.92	0.79	0.44	0.90	0.91	0.20	0.01	0.01	0.02	1.1E-05	0.002	0.002
							*	*	*	****	**	**
iTregs (4K) vs iTregs (anti-CD3/28)	0.86	0.76	0.89	0.90	0.71	0.66	0.36	0.07	0.003	1.8E-05	0.005	0.003
									**	****	**	**

Figure 4.10 Overall LAT accumulation at the IS are diminished in both MBP Ac1-9 [4K] and anti-CD3/28-primed iTregs†, compared with Teffs††.

LAT-GFP transduced Teffs and iTregs were activated by MBP Ac1-9 [4Y]-primed PL8 cells and imaged every 20 seconds for 15 minutes. DIC and GFP images were analysed to identify formations of a tight cell couple (0s) and spatiotemporal distribution patterns of LAT-GFP for 12 time points in **A)** MBP Ac1-9 [4K]-primed Teffs (49 cell couples analysed, four experiments), **B)** MBP Ac1-9 [4K]-primed iTregs (72 cell couples analysed, two experiments), **C)** anti-CD3/28-primed Teffs (42 cell couples analysed, two experiments), **D)** anti-CD3/28-primed iTregs (48 cell couples analysed, four experiments), **E)** Comparisons of LAT-GFP accumulation between different cell types at the IS using a two proportion z-test. Numerals and asterisks indicate p-values, and asterisk colours indicate whether differences remain significant with the Bonferroni correction (0.004<*<0.05, 0.004<**<0.01, 0.001<**<0.004, 0.0001<***<0.001, ****<0.0001). Error bars indicate standard error of the mean.

† LAT-GFP imaging data of Tg4 iTregs were jointly analysed (MBP peptide-primed) and analysed (anti-CD3/28-primed) by Christoph Wuelfing.

†† LAT-GFP imaging data of Tg4 MBP peptide-primed Teffs were generated and analysed by former PhD student Helen Tunbridge, data of anti-CD3/28-primed Teffs were analysed by Christoph Wuelfing.

Spatiotemporal accumulation of GFP-sensors can be classified into seven defined accumulation patterns: central, invagination, diffuse, lamellal, peripheral, asymmetric and distal accumulation and such patterns of signalling molecules were found to be highly diverse (130, 135). T cell activation and functions are related with spatiotemporal organisation of signalling intermediates. Singleton *et al* have shown that knocking out the gene of tyrosine kinase, IL-2 inducible T cell kinase (Itk) in mice could change the spatiotemporal localisation of 14 signalling intermediates (including TCR and LAT) involved in T cell activation (192). Targeting cell division cycle 42 (Cdc42), one of the central accumulation impaired proteins, to the centre of the T cell-APC interface restored actin accumulation in the Itk knockout T cells. Therefore, it is of interest to investigate LAT accumulation patterns in Tg4 T cells.

Central, invagination and distal accumulation patterns of LAT-GFP were main dominant patterns found in Teffs and iTregs (Figure 4.10 A-D). LAT central accumulation is associated with efficient T cell activation and IL-2 production (126), while specific roles of LAT invagination accumulation is yet to be discussed. Invagination accumulation pattern localises at the centre of the interface and reaches μm deep into a T cell, possibly removes receptors such as CD2 away from the centre of the interface in T cell activation and reset proximal T cell signalling (170). Therefore, invagination accumulation is considered to be a diminished central accumulation and indicative of protein transporting away from the cSMAC. As both the central and invagination pattern describe sensor accumulation near the centre of the interface, we tentatively consider the invagination pattern to be a diminished central pattern. The difference between the central and invagination is that the latter is >1 μm away from the interface and reaches deep into a T cell (130). We first compared both patterns together between Teffs and iTregs and then compare each pattern separately.

In MBP Ac1-9 [4K]-primed Teffs and iTregs, the former showed significantly more LAT-GFP central + invagination accumulation compared at seven time points ($p<0.05$, 0s-120s) (Figure 4.11 A). With the Bonferroni correction, significant differences were observed at the 20s ($p<0.004$) and 40s ($p<0.001$) time points. Consistently, when comparing only central accumulation, Teffs displayed more central LAT-GFP accumulation than iTregs (Figure 4.11 B) at similar time points ($p<0.05$, 0s-80s and 120s). Differences were still significant at three time points ($p<0.001$, 0s, 20s and 40s) with the Bonferroni correction. No significant differences were found when comparing LAT-GFP invagination accumulation of Teffs and iTregs (Figure 4.11 C). Only a few iTregs showed LAT-GFP central accumulation as the percentages of these cells were lower than 10% across all time points, while the percentage of iTregs with LAT-GFP invagination accumulation was similar to that in Teffs. Together, these results show that MBP Ac1-9 [4K]-primed Teffs display more LAT-GFP central

accumulation in the first two minutes of T cell-APC interaction, compared to in MBP Ac1-9 [4K]-primed iTregs. Proximal LAT-mediated signal transduction is likely to be impaired in iTregs owing to a reduction of LAT central localisation.

In anti-CD3/28-primed T cells, percentage of cells showing central + invagination LAT-GFP accumulation together were significantly lower in iTregs, compared with Teffs at six time points (Figure 4.11 D, 0s-100s). These differences all remained significant with the Bonferroni correction ($p<0.004$). When comparing only the LAT-GFP central accumulation of Teffs and iTregs (Figure 4.11 E), significant differences were found at the 40s, 80s and 100s time point but these were no longer significant with the Bonferroni correction ($0.004<p<0.05$). However, when comparing the invagination pattern, Teffs show more LAT-GFP invagination accumulation than iTregs at six time points (Figure 4.11, 0s-100s, $p<0.05$). Differences at the 40s and 60s time point remained significant with the Bonferroni correction ($p<0.004$). These comparisons show that in anti-CD3/28-primed Teffs, more central and invagination accumulation of LAT-GFP at the interface was found near the centre of the IS within the first 100 seconds of T cell activation, compared to anti-CD3/28-primed iTregs. Differences were mainly found when comparing their invagination accumulation pattern within the same time period. Consistent with the observations found in peptide-primed T cells, LAT localisation near the centre of the interface is also diminished in anti-CD3/28-primed iTregs which impairs proximal LAT signalling in early T cell activation.

One of the key questions mentioned previously is whether different ways of priming Tg4 naïve T cells (peptide vs antibody), will change how Teffs and iTregs behave. To investigate this in the aspect of spatiotemporal organisation, we compared LAT-GFP distributions within MBP peptide and anti-CD3/28 prime Teffs and iTregs. In Teffs, (Figure 4.10 A and C), the percentage of anti-CD3/28-primed Teffs showing LAT-GFP overall accumulation was significantly higher at six time points (Figure 4.10 E, third row, $p<0.05$, 80s-420s), and such differences were still significant at the 180s, 300s and 400s time point with the Bonferroni correction ($p<0.004$), compared to MBP Ac1-9 [4K]-primed Teffs. Moreover, the peak of LAT-GFP accumulation was delayed by 40 seconds in anti-CD3/28-primed Teffs. LAT-GFP was more likely to remained at the interface in anti-CD3/28-primed Teffs after this peak.

When jointly compared, LAT-GFP central + invagination accumulation of MBP peptide and anti-CD3/28-primed Teffs displayed similar patterning (Figure 4.11 A and D). In both priming condition, percentage of Teffs with central + invagination accumulation peaked at the 40s time point and gradually decreased afterwards. However, MBP peptide-primed Teffs showed more central localisation preference for LAT-GFP, particularly in the first two minutes of cell coupling (Figure 4.10 A). LAT-GFP central accumulation pattern was

dominant in MBP peptide-primed Teffs in the first two minutes, and the percentage of peptide-primed Teffs with such accumulation peaked at the 40s (42%). In contrast, both LAT-GFP central and invagination accumulation patterns were found to be dominant during this period in anti-CD3/28-primed Teffs (Figure 4.11 C). In addition, LAT-GFP diffuse accumulation pattern was more dominant after the 120s time point.

When comparing the iTreg data sets, more LAT-GFP overall accumulation in anti-CD3/28-primed iTregs (Figure 4.10 B and D) were found and differences were significant at four time points (Figure 4.10 E, fourth row, $p<0.01$, 120s-420s), and were still significant except at the 300s time point with the Bonferroni correction. The peak of LAT-GFP accumulation was delayed by one minute in anti-CD3/28-primed iTregs and after reaching the peak at the 120s time point, LAT-GFP accumulation also sustained at the interface. Percentage of iTregs showing any accumulation pattern of LAT-GFP in both priming conditions was relatively low (<20%) at all time points. A dominant LAT-GFP invagination pattern was found in MBP peptide-primed iTregs in the first 80s of cell coupling.

These comparisons show that in early activation of MBP peptide and anti-CD3/28-primed Tg4 T cells, more LAT-GFP overall accumulation was found in anti-CD3/28-primed T cells, particularly at later time points (after 120 seconds). The central LAT-GFP accumulation observed in anti-CD3/28-primed Teffs was not as dominant as it was in MBP peptide-primed Teffs. Together these results indicate that, in MBP peptide-primed T cells, LAT is more likely to be recruited to the centre of the interface within the first minute after the synapse is formed, and later be removed from the interface. While in early activation of anti-CD3/28-primed T cells, LAT localisation at the interface is delayed and more likely to maintain at the interface after the first two minutes of cell coupling. As the cSMAC regulates effective recruitment of large number of signalling proteins to the interface centre in the first two minutes of cell coupling (55), it is possible that this inefficient transport and clearance of LAT at the interface during anti-CD3/28-primed T cell activation, could hinder cSMAC formation and disrupt the regulation of signalling intermediates localisation in proximal T cell signalling. In other word, T cell activation in anti-CD3/28-primed cells might be less effective.

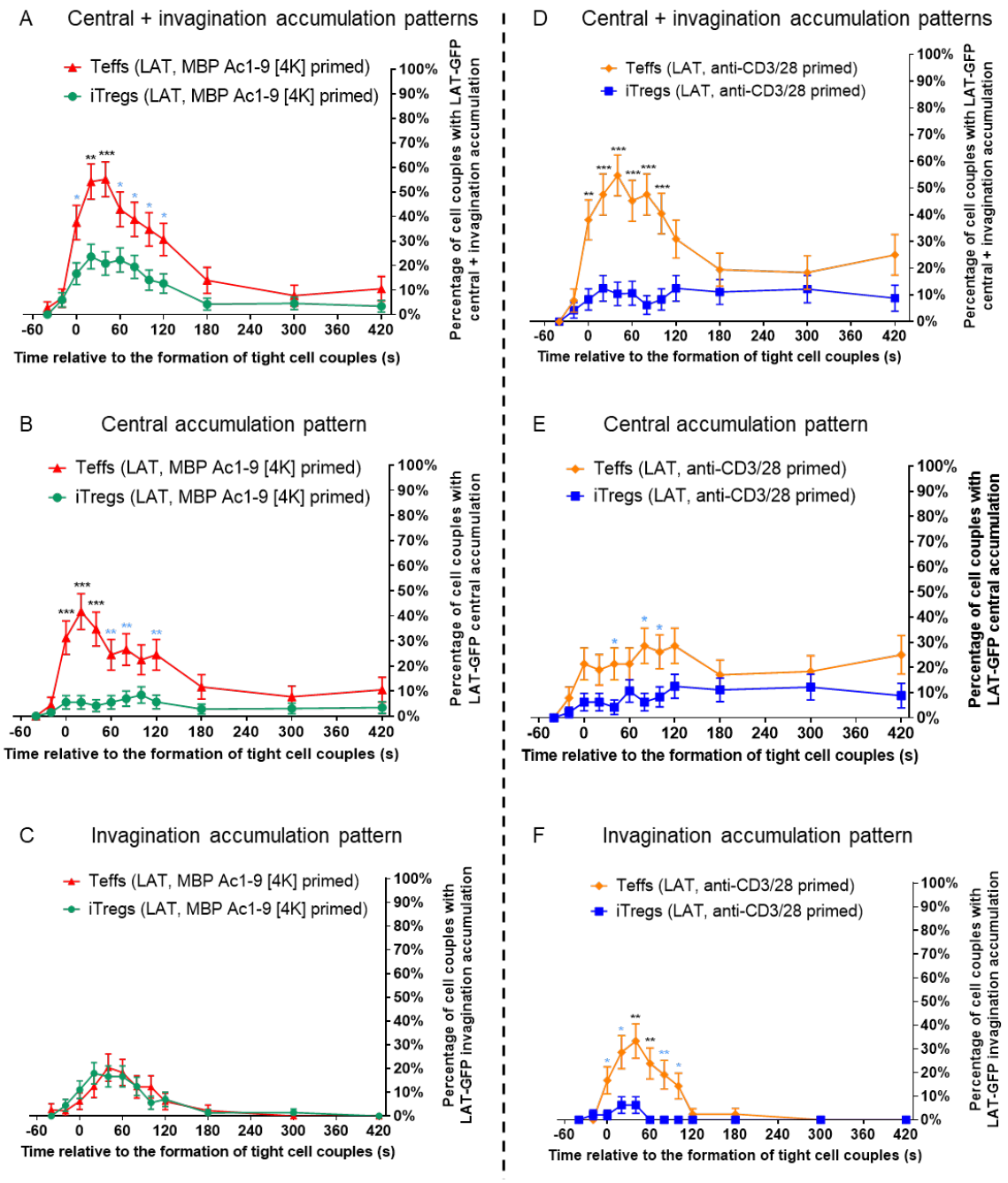

Figure 4.11 LAT-GFP central accumulation at the IS in MBP Ac1-9 [4K]-primed iTregs and invagination accumulation in anti-CD3/28-primed iTregs are diminished.

Direct comparisons of percentages of cell couples with LAT-GFP central + invagination, central and invagination spatiotemporal patterns in MBP AC1-9 [4K]-primed **A-C**) and anti-CD3/28-primed **D-F**) Teffs and iTregs. **A-C)** MBP Ac1-9 [4K]-primed Teffs: 49 cell couples, four experiments, MBP Ac1-9 [4K]-primed iTregs: 72 cell couples two experiments, **D-F)** anti-CD3/28-primed Teffs: 42 cell couples, two experiments, anti-CD3/28-primed iTregs: 48 cell couples, four experiments. A two proportion z-test was applied to calculate statistical significance. Asterisks indicate p-values and colours indicate whether differences remain significant with the Bonferroni correction (0.004<*<0.05, 0.004<**<0.01, 0.001<**<0.004, ***<0.001). Error bars indicate standard error of the mean.

The distal accumulation pattern was mainly found to be dominant before the formation of tight cell couples in iTregs (Figure 4.10 B and D). As the distal pattern describes localisation of a sensor at the distal end of a T cell, away from the interface, which is excluded from "any interface" accumulation patterns. Thus, we compared distal accumulation patterns within MBP peptide and anti-CD3/28-primed Teffs and iTregs.

Percentages of MBP Ac1-9 [4K]-primed iTregs with distal LAT-GFP accumulation was significantly higher at the -20s and 0s time point, compared with Teffs (Figure 4.12 A, $p<0.01$) and the difference was only significant at the 0s time point with the Bonferroni correction ($p<0.001$). No significant differences were found between anti-CD3/28-primed Teffs and iTregs (Figure 4.12 B). Then we compared the distal accumulation between same cell types with a different priming method (peptide vs antibody). Anti-CD3/28-primed Teffs show more distal accumulation of LAT-GFP, compared with Teffs primed with MBP Ac1-9 [4K], at four time points (Figure 4.12 C, $p<0.05$). The differences remained significant at the 0s and 20s time point with the Bonferroni correction ($p<0.001$). Significant difference was only found at the 0s time point when comparing the LAT-GFP distal accumulation between the two type of iTregs (Figure 4.12 D, $p<0.05$), which was not significant with the Bonferroni correction. The distal pattern of LAT-GFP was mainly observed before the 60s time point in three out of four cell types and barely observed in MBP Ac1-9 [4K]-primed Teffs.

These comparisons indicate that before the formation of the IS in early activation, some LAT-GFP molecules are transiently recruited towards the distal end in MBP peptide-primed iTregs and anti-CD3/28-primed Teffs/iTregs. They diffuse away from the site after tight cell coupling. Recruitment of LAT-GFP to the interface centre in MBP peptide-primed Teffs is not disrupted as that in the other three cell types. Therefore, distal localisation in MBP peptide-primed iTregs and anti-CD3/28-primed Teffs/iTreg appears to slow down LAT transition to the centre and possibly reduces the total amounts of LAT at the interface centre upon the IS formation. This might partially contribute to the reduced LAT central localisation found in iTregs and anti-CD3/28-primed Teffs. These observations also suggest that anti-CD3/28 primed T cells are likely to activate less efficiently.

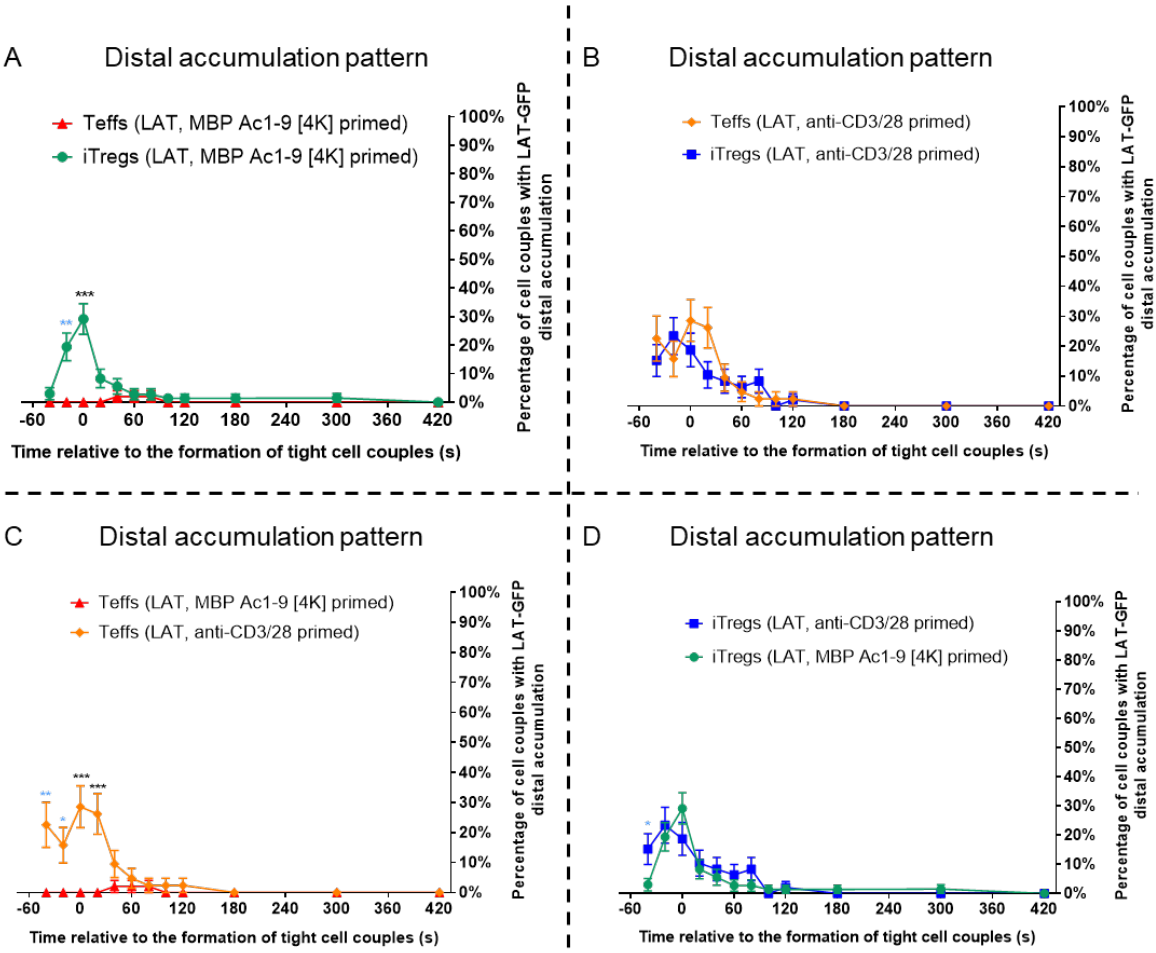

Figure 4.12 Distal LAT-GFP accumulation was observed in MBP Ac1-9 [4K]-primed iTregs, anti-CD3/28-primed Teffs and iTregs at early time points.

Direct comparisons of percentages of cell couples showing LAT-GFP accumulation in MBP AC1-9 [4K] and anti-CD3/28-primed Teffs and iTregs. Comparing LAT-GFP distal accumulation between **A)** MBP Ac1-9 [4K]-primed Teffs and iTregs **B)** anti-CD3/28-primed Teffs and iTregs, **C)** MBP Ac1-9 [4K] and anti-CD3/28-primed Teffs and **D)** MBP Ac1-9 [4K] and anti-CD3/28-primed iTregs. MBP Ac1-9 [4K] Teffs: 49 cell couples, four experiments, MBP Ac1-9 [4K]-primed iTregs: 72 cell couples, two experiments, anti-CD3/28-primed Teffs: 42 cell couples, two experiments, anti-CD3/28-primed iTregs: 48 cell couples, four experiments. A two proportion z-test was applied to calculate statistical significance. Asterisks indicate p-values and colours indicate whether differences remain significant with the Bonferroni correction (0.004<*<0.05, 0.004<**<0.01, <0.001**<0.004, ***<0.001). Error bars indicate standard error of the mean.

4.9 Computational analyses show reduced LAT overall and central accumulation at the IS of Tg4 iTregs

Manually identifying spatiotemporal patterns of various GFP-sensors potentially allows biases to occur. First, localisation which shows ambiguous features of more than one pattern does occur. Secondly when analysing imaging data, knowing a cell type and sensor subconsciously affects how we identify the patterns. Blind scoring is a good way to reduce these biases, and part of our analysis on morphological data has been processed in this way. Nevertheless, a general and automated approach could help to assess interface accumulation better in our study. Previously, with the help from the Computational Biology Department from Carnegie Mellon University, we have developed a large-scale computational approach (173). For a given GFP-labelled sensor imaging data set, coordinates and time points indicating onsets of each cell couple were manually identified with a mid-plane DIC image. This DIC image and GFP images of 12 time points (including all 21 z stacks) relative to the formation of tight cell couples could be used to generate a three-dimensional (3D) model map. Fluorescent images were segmented and shape-normalised into a standardised semi-spheroid cell shape displaying sensor distributions within a T cell.

Representative fluorescent 3D images of Teffs and iTregs transduced with LAT-GFP are displayed below (Figure 4.13 A). From top to bottom, slices of images from five time points (0s, 60s, 120s, 180s and 300s) relative to the synapse formation are shown. Image slices close to the middle plane across these five time points reveal that after the IS was formed, LAT-GFP in Teffs and iTregs mainly localised near the T cell-APC interface.

Utilising GFP images of 21 z stacks from all 12 time points, two 3D model maps displaying relative probabilities of LAT-GFP accumulation during Teff/iTreg-APC interactions were generated (Figure 4.13 B, upper row in each panel). Relative fluorescence values were scaled to a fraction of total fluorescence of the sensor, which indicate average probabilities of enrichment, across all time points. To compare LAT-GFP distributions near the IS formed by Teffs and iTregs, we defined a region contains the highest 10% of fluorescent 3D pixels as an approximation of the IS (173) (Figure 4.13 B, lower row in each panel). Relative enrichment of each sensor of all 12 time points could be extracted from the 3D models. Sensor enrichment describes a ratio of the amount of the sensor in a defined region to the average amount in the entire cell, across all time points (173). Result (Figure 4.13 C) shows in MBP Ac1-9 [4K]-primed Teffs, LAT-GFP mean enrichment was the lowest at the -20s time point, gradually increased over time and reached its peak at the 420s point. While in the MBP Ac1-9 [4K]-primed iTregs, the enrichment of LAT-GFP also started increasing from

the -20s time point but reached the peak at the 40s time point and maintained with a minor reduction afterwards. Statistical analysis shows that upon Teff activation, LAT-GFP enrichment at the synapse was significantly higher at five time points ($p<0.05$, 80s, 120s-420s), compared to iTregs. Mean enrichment of LAT-GFP in the Teff condition at the other seven time points was also higher than that in iTregs but not significant. With the Bonferroni correction, significant differences were only found at the 420s time points ($p<0.001$).

In summary, MBP Ac1-9 [4K]-primed Teffs show more LAT accumulation at the IS, when compared with MBP Ac1-9 [4K]-primed iTregs and such differences are more prominent after the first minute of cell coupling. This again suggests that the total amount of LAT transported to the synapse in iTregs to be reduced which is mostly consistent with the observations in section 4.8.

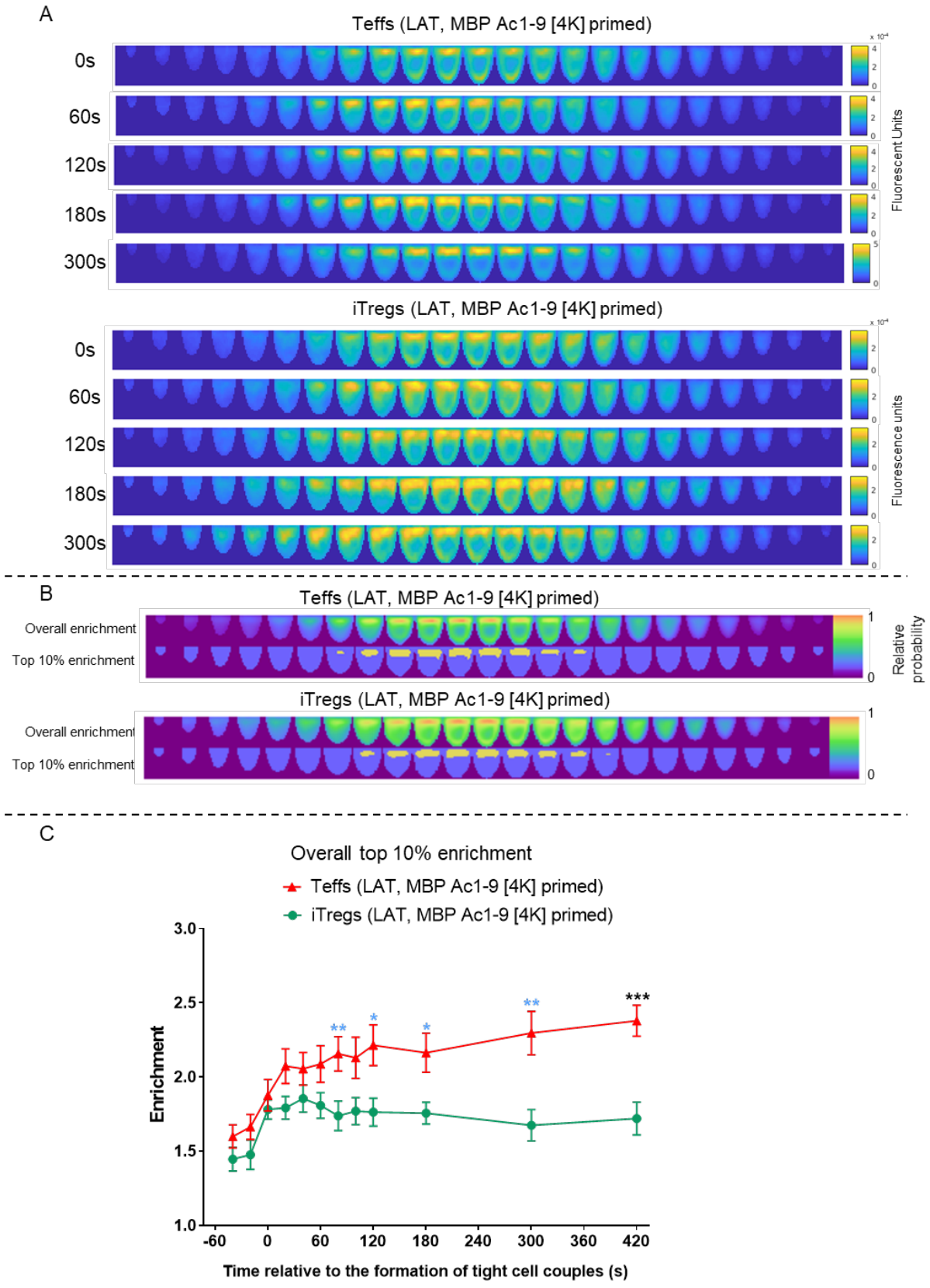
A
Teffs (LAT, MBP Ac1-9 [4K] primed)
0s
60s
120s
180s
300s
Fluorescent Units
iTregs (LAT, MBP Ac1-9 [4K] primed)
0s
60s
120s
180s
300s
Fluorescence units
B
Teffs (LAT, MBP Ac1-9 [4K] primed)
Overall enrichment
Top 10% enrichment
Relative probability
iTregs (LAT, MBP Ac1-9 [4K] primed)
Overall enrichment
Top 10% enrichment
C
Overall top 10% enrichment
Teffs (LAT, MBP Ac1-9 [4K] primed)
iTregs (LAT, MBP Ac1-9 [4K] primed)
Enrichment
3.0
2.5
2.0
1.5
1.0
-60
0
60
120
180
240
300
360
420
Time relative to the formation of tight cell couples (s)
**
*
*
**
***

Figure 4.13 Computational model maps indicate that MBP Ac1-9 [4K]-primed iTregs show diminished LAT-GFP accumulation in the defined IS region.

Computational 3D model maps were generated by analysing DIC and GFP images with coordinates and time points indicating onsets of cell couples. T cells are rotated with the IS facing upward. Slices are placed left to right indicating their z positions relative to the middle plane. False-colour scales are applied to indicate relative fluorescence intensity.

A) Representative single image slices of 3D models showing average LAT-GFP distributions in MBP Ac1-9 [4K]-primed Teffs and iTregs when activated. Time points relative to the formation of cell couples are listed vertically and false colour scales indicate relative fluorescence. **B)** Computational 3D model maps showing average probabilities of LAT-GFP distributions in the whole cell (overall enrichment) and defined IS region (top 10% enrichment) during the activation of MBP Ac1-9 [4K]-primed Teffs and iTregs. False-colour scales indicate relative probability. **C)** Comparing LAT-GFP enrichment in the defined IS region (top 10% enrichment) during the activation of MBP Ac1-9 [4K]-primed Teffs and iTregs. Images are aligned from left to right indicating their z positions relative to the middle plane. Teffs: 28 cell couples, four experiments, iTregs: 28 cell coupes, two experiments. Log-transformed ratio data (enrichment) were analysed with unpaired Student's test to calculate statistical significance. Asterisks indicate p-values and colours indicate whether differences remain significant with the Bonferroni correction (0.004<*<0.05, 0.004<**<0.01, ***<0.001). Error bars indicate standard error of the mean.

As compared with Teffs, LAT-GFP central accumulation during iTreg activation was found to be diminished (Figure 4.11 B), we further investigated whether this could also be found in the 3D models. We defined a “central core” region with a cylindrical shape near the IS, shown below (Figure 4.14 A). A standardised cell shape is a semi-ellipsoid and rotated so that the interface of contact is facing upward. We set the relative radius of the interface to be “1”, and the relative radius and height (depth into the cell) of the cylinder to be “0.5”. This is an approximated central region of the IS. Two 3D model maps were generated to show average LAT-GFP enrichment in the whole cell (Figure 4.14 B, upper row) or central region of the IS in MBP peptide-primed Teffs and iTregs (Figure 4.14 B, lower row). LAT-GFP enrichment in the central region in both Teff and iTreg was observed (Figure 4.14 C), as enrichment mainly concentrated in their middle planes. LAT-GFP central accumulation in Teffs started low at the -20s time point and increased over time. It peaked at the 300s time point. In iTregs, LAT-GFP central enrichment was the lowest at the -20s time point and peaked at the 40s time point, but slowly decreased afterwards. At all 12 time points, the mean enrichment of LAT-GFP within the central core of Teffs was higher than that of iTregs and the differences were significant at five time points ($p<0.05$, 120s, 180s, 300s and 420s). However, no significant differences were found with the Bonferroni correction ($p>0.004$).

These results suggest that in early T cell activation, LAT accumulation in the central region of the IS in MBP peptide-primed iTregs is diminished, particularly after the first minute of activation, compared to Teffs.

Computational 3D model analysis offered us an automated and systemic approach to compare GFP-labelled protein distributions in Teffs and iTregs in T cell activation. All GFP images of a protein of interest could be inputted to visualise its enrichment at any of or all 12 time points. Combined results above, after the first minute of the IS formation, LAT-GFP in MBP primed Teffs displayed more overall and central accumulation at the IS than that in iTregs. Notably, time points where significant differences were found in LAT-GFP datasets were not identical between our manual scoring and computational analysis (Figure 4.10 E and 13 C). The former identified differences mainly before the 120s time point while the latter identified differences after the 60s time point. In addition, the trends of LAT-GFP accumulation showed by these two approaches were partly diverse, as LAT-GFP accumulation identified in the manual scoring system usually peaked around or before the 60s time point and decreased afterwards, while such accumulation identified in the computational analysis system sustained after the 60s time point. As the computational analysis approach is still under development, it has limitations. Diverse spatiotemporal distribution patterns cannot be fully recognised by the computational analysis. Central and invagination accumulation patterns which describe different localisation conditions of the

cSMAC associated proteins are indistinguishable by the computational analysis system at present. Moreover, the computational system includes and analyses vesicular LAT accumulation, which is removed by manual pattern analysis. In addition, at the current stage, fewer cell couples can be recognised and analysed by the programme (e.g. for LAT-GFP accumulation, 28 of 48 cell couple of Teffs were recognised by the computer), which limits the utilisation of our current datasets. Therefore, manual identification of spatiotemporal patterns of senor distributions is a well-defined reliable approach, and combined with supplementary automated computational models, we could further quantify and investigate diverse spatiotemporal distributions of different signalling intermediates in T cell signalling in a comprehensive context. Because of the superior ability to distinguish closely related patterns at the centre of the interface, we will use manual pattern classification as a main approach to assess accumulation of other sensors at the interface for the remainder of this thesis.

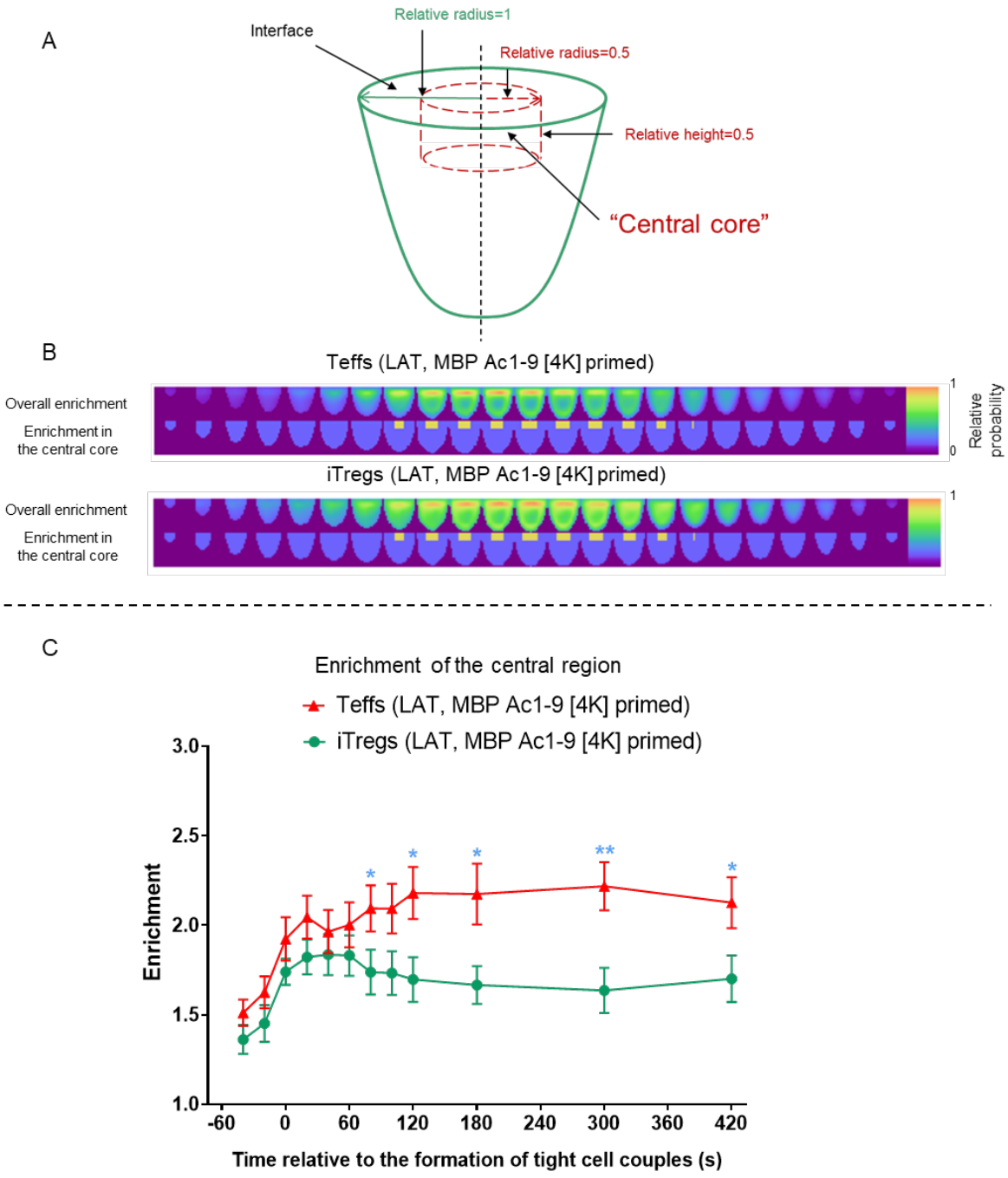
A
Interface
Relative radius=1
Relative radius=0.5
Relative height=0.5
"Central core"
B
Teffs (LAT, MBP Ac1-9 [4K] primed)
Overall enrichment
Enrichment in the central core
1
0
Relative probability
iTregs (LAT, MBP Ac1-9 [4K] primed)
Overall enrichment
Enrichment in the central core
1
C
Enrichment of the central region
Teffs (LAT, MBP Ac1-9 [4K] primed)
iTregs (LAT, MBP Ac1-9 [4K] primed)
Enrichment
3.0
2.5
2.0
1.5
1.0
-60
0
60
120
180
240
300
360
420
Time relative to the formation of tight cell couples (s)

Figure 4.14 MBP Ac1-9 [4K]-primed iTregs show diminished central LAT-GFP accumulation in the defined IS region, compared to Teffs.

A central core region was defined in 3D computational models to compare LAT-GFP central accumulation at the IS bewteen MBP Ac1-9 [4K]-primed Teffs and iTregs. **A)** A diagram showing the definition of the "central core", an approximated cylinder near the interface. The interface is regarded as a circle with a relative radius of "1" and the relative radius and height of the cylinder is "0.5". **B)** Computational 3D model maps showing average probabilities of LAT-GFP distribution in the whole cell (overall enrichment) and defined central core region during the activation of MBP Ac1-9 [4K]-primed Teffs and iTregs. False colour scales indicate relative probability. **C)** Comparing LAT-GFP accumulation in the central core during the activation of MBP Ac1-9 [4K]-primed Teffs and iTregs. Images are aligned from left to right indicating their z positions relative to the middle plane. Teffs: 28 cell couples, four experiments, iTregs: 28 cell coupes, two experiments. Ratios (enrichment) were log-transformed and analysed with unpaired Student's test to calculate statistical significance. Asterisks indicate p-values and colours indicate whether differences remain significant with the Bonferroni correction (0.004<*<0.05, 0.004<**<0.01). Error bars indicate standard error of the mean.

4.10 TCR-ζ accumulation at the IS of Tg4 iTregs is diminished but increased at the distal pole

As LAT signalling was most likely to be impaired owing the diminished LAT central localisation in iTregs, we next investigated whether LAT associated signal transductions were also defective. The engagement of TCR and pMHC of TCR-MHC is a key step to initiate T cell activation. It is commonly acknowledged that proximal TCR signalling to be the upstream of LAT recruitment at single molecular level. However, this is not the case from the perspective of supramolecular signalling complexes. LAT nucleated signalosome is the upstream of TCR central clustering at the interface, as we discuss below.

Similar to LAT, a TCR-ζ-GFP fusion protein was generated to study its roles at the IS (193). In a previous study by Singleton *et al*, upon pMHC-TCR induced T cell activation, TCR-ζ in 5C.C7 TCR transgenic T cells was efficiently recruited, mostly from the distal pole of the cell, to the centre of the T cell-APC interface, at the beginning of tight cell coupling (0s) (130). Interestingly, LAT started to localise at the centre of the interface before the synapse was steadily formed and central LAT-GFP accumulation peaked at the 0s time point (126). After the peak, LAT central accumulation diminished and reached its lowest point at the 120s time point while TCR-ζ continued to localise at the interface centre after the 60s time point, and still showed relatively a high level of central clustering after the 300s time point. Together these data suggest that at the supramolecular level, LAT central clustering at the interface subsequently promotes TCR-ζ central clustering at the cSMAC of the interface. Consistently, we have shown in the last section that LAT accumulation in Tg4 Teffs showed a similar pattern of accumulation with pronounced central clustering around the 20s time point (Figure 4.10-11). In brief, initial proximal TCR signalling is required for LAT activation and recruitment but the assembly of LAT signalosome in the cSMAC promotes downstream TCR central clustering.

Investigation of TCR-ζ localisation at the IS of Tg4 T cells will provide ideas to study its roles in the cSMAC and relation with the upstream LAT signalosome. Same as described earlier, we transduced Tg4 T cells with TCR-ζ-GFP and compared its accumulation patterning in Teffs and iTreg upon activation. In this dataset, Teffs were all primed with MBP peptides, while iTreg were MBP peptide and anti-CD3/28-primed. iTregs transduced with TCR-ζ-GFP were >75% Foxp3^{+}.

Representative images of TCR-ζ-GFP accumulation in Teffs and iTregs in the first two minutes of T cell activation are shown below (Figure 4.15). Images are from the DIC and GFP channel.

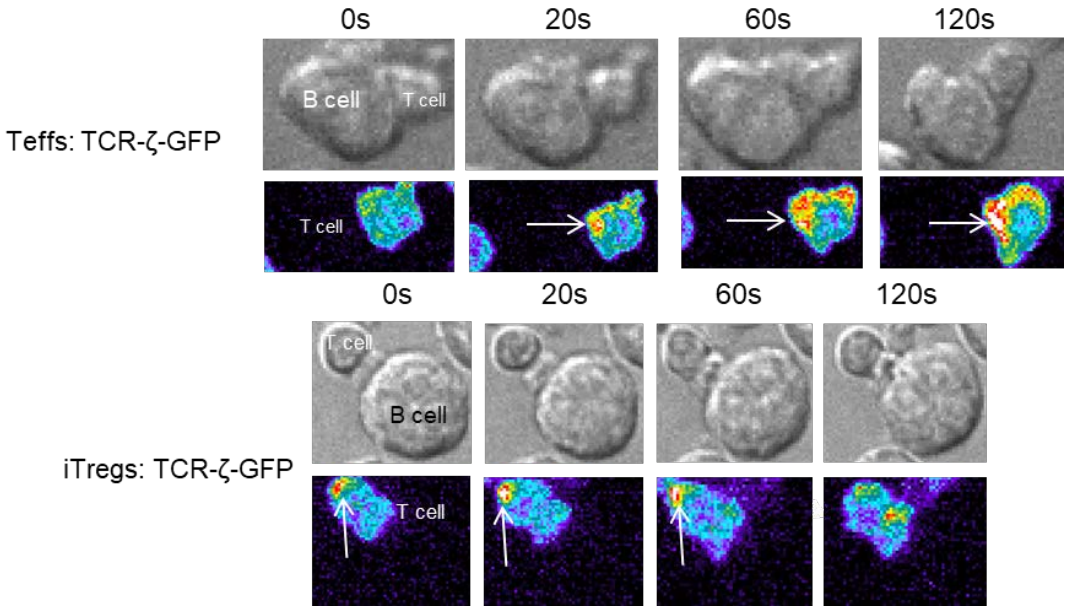

Figure 4.15 Representative live cell images of Tg4 Teffs and iTregs transduced with TCR-ζ-GFP from four time points in early T cell activation.

Top: DIC images from four time points. Bottom: matching top-down maximum projections of three-dimensional TCR-ζ-GFP fluorescent images (intensity is encoded in pseudocolour and increases from purple to red). Time is given in seconds relative to the formation of a tight cell couple and arrows show accumulation of the sensor.

In MBP Ac1-9 [4K]-primed Teffs (Figure 4.16 A), TCR-ζ-GFP accumulation peaked at the 60s time point with 58% Teffs showing accumulation at the IS. After the first minute of cell coupling, TCR-ζ-GFP showed sustained accumulation at the interface for six minutes and the 69% of Teffs showing TCR-ζ-GFP accumulation at the last time point (420s) showing an increasing trend of accumulation. Such pattern was not observed in MBP Ac1-9 [4K]-primed iTregs (Figure 4.16 B). TCR-ζ-GFP accumulation only peaked once at the 40s time point with 55% of iTregs showing accumulation and decreased afterwards. This showed that in MBP peptide-primed Teffs, TCR-ζ-GFP was recruited to the interface in the first minute after the IS formation and remained for sustained TCR signalling transduction in the next six minutes. On the contrary, in MBP peptide-primed iTregs, although TCR-ζ-GFP was being driven to the interface at early time points, such accumulation was not retained at the interface and gradually diminished after the 80s time point. A direct comparison (Figure 4.16 D, upper row) between MBP Ac1-9 [4K]-primed Teffs and iTregs showed that Teffs displayed significantly more TCR-ζ-GFP accumulation at later time points ($p<0.05$, 100s-420s). However, iTregs showed more TCR-ζ-GFP accumulation at the -20s and 0s time point ($p<0.05$). Differences remained significant at the 180s and 420s time points with the Bonferroni corrections ($p<0.004$). This may indicate that after the first 80s of cell coupling, more TCR-ζ molecules are recruited to the IS in Teff activation, compared with iTregs.

Among all accumulation patterns, no dominate accumulation patterns of TCR-ζ-GFP at the interface were observed in MBP Ac1-9 [4K]-primed Teffs (Figure 4.16 A) as several patterns were found at multiple time points. TCR-ζ-GFP central accumulation of the IS of Teffs showed an increasing trend after the 180s time point and peaked at the last time point with 38% of cell showing TCR-ζ-GFP central accumulation. TCR-ζ-GFP peripheral and asymmetric accumulation were mostly observed in Teffs at early time points and gradually diminished after the 120s time point. While in MBP peptide-primed iTregs (Figure 4.16 B), TCR-ζ-GFP peripheral accumulation was mainly observed, as the percentage of cells with TCR-ζ-GFP peripheral accumulation at the interface was dominant at six time points (-20s-80s) and peaked at the 20s time point (41%).

When comparing TCR-ζ-GFP central accumulation between MBP peptide-primed Teffs and iTregs (Figure 4.16 E), the mean percentage of Teffs showing such accumulation was continuously higher after two minutes of cell coupling. The difference was only significant at the 420s time points, but prominent ($p<0.001$). Apart from localising at the interface, TCR-ζ-GFP also showed distal accumulation in MBP peptide-primed iTregs (Figure 4.16 B). Distal TCR-ζ-GFP accumulation in these iTregs also showed an increasing trend from the 120s time point. Percentage of in MBP peptide-primed iTregs with distal accumulation peaked at the -20s (40%) and 420s (45%) time point. While in Teffs (Figure 4.16 A), low distal TCR-ζ-

GFP accumulation was observed before the 60s time point (<30% cells showing distal accumulation) and barely detected afterwards. A direct comparison of TCR-ζ-GFP distal accumulation (Figure 4.16 F) showed TCR-ζ-GFP distal accumulation was significantly higher in MBP Ac1-9 [4K]-primed iTregs at eight time points ($p<0.05$, 0s, 60s-420s), compared with Teffs. Differences were still significant at four time points (60s, 180s, 300s and 420s) with the Bonferroni correction.

Together, these results show that in early T cell activation, TCR-ζ overall and central accumulation in MBP Ac1-9 [4K]-primed iTregs are diminished, particularly after two minutes of cell coupling. Upon activation, TCR-ζ-GFP was recruited to the periphery of the synapse in MBP Ac1-9 [4K]-primed Teffs and iTregs at early time points (within the first minute of cell coupling). In Teffs, TCR-ζ-GFP then stabilised at the interface after the 120s time point and showed an increasing trend of central TCR-ζ-GFP accumulation and distal TCR-ζ-GFP accumulation was only observed before the 60s time point with low percentage of cells displaying such pattern. This sustained accumulation of TCR clusters at the interface indicates that a stable cSMAC at the IS begin to form after the first two minutes of cell coupling in early Teff activation. While in iTregs, TCR-ζ-GFP accumulation at the interface was not persistent and diminished after the 40s time point, and more TCR-ζ-GFP molecules localised at the distal end of the cell during iTreg activation. Scarcely detectable central accumulation across all time points and increased distal accumulation of TCR-ζ-GFP after the first minute of cell coupling suggest that the transport of TCRs to the interface is inefficient and TCRs are prematurely cleared from the interface and barely released from the distal pole. Therefore, the cSMAC is not properly formed in early iTreg activation which would attenuate downstream tyrosine kinase signalling cascades and lead to defective T cell activation.

In addition, we also investigated TCR-ζ-GFP spatiotemporal accumulation patterns in early activation of anti-CD3/28-primed iTregs (Figure 4.16 C). TCR-ζ-GFP overall accumulation at the interface of anti-CD3/28-primed iTregs was relatively low across all time points, and it peaked at the 100s time point with 36% of the cells showing TCR-ζ-GFP accumulation and decreased afterwards. TCR-ζ-GFP diffuse accumulation was dominant at six time points (40s-180s) but the percentage of cells showing such accumulation was <20% across all time points. However, prominent distal TCR-ζ-GFP accumulation was observed before the 60s and at the 420s time point. Distal accumulation of TCR-ζ-GFP peaked at the 0s time point with 56% iTregs showing such accumulation and decreased afterward untill the 180s time point. The percentage of iTregs with distal TCR-ζ-GFP accumulation started to increase again from the 180s time point and showed an ascending trend till the last time point. When comparing these two types of iTregs, the percentage of cells with TCR-ζ-GFP

overall accumulation was higher in MBP peptide-primed iTregs at six time points ($p<0.01$, -40s-40s, 420s). Differences remained significant with the Bonferroni correction at five time points ($p<0.004$, -40s-40s).

Combined with the result above, these observations indicate that in early iTreg activation, more TCR-ζ-GFP accumulation was found at the interface in MBP Ac1-9 [4K]-primed iTreg at early time points (before the 40s time point). In MBP peptide-primed iTregs, TCR-ζ-GFP also transported to the interface more efficiently, as the peak of TCR-ζ-GFP overall accumulation was delayed for 60 seconds in anti-CD3/28-primed iTregs. Peripheral TCR-ζ-GFP accumulation was hardly found anti-CD3/28-primed iTregs but both types of iTregs displayed similar distal TCR-ζ-GFP accumulation patterning which peaked at early time points and showed an increasing trend at late time points. These suggest that in early T cell activation, fewer TCR-ζ subunits are recruited to the interface of anti-CD3/28-primed iTregs activation, and the translocation of TCRs to the synapse is less effective, compared to that in MBP peptide-primed iTregs. Thus, during early IS formation, the recruitment of TCR-CD3 complexes to the interface in anti-CD3/28-primed iTreg and cSMAC formation is likely to be more defective than that in MBP peptide-primed iTregs. Thus, anti-CD3/28 priming partially reduces the ability to transport TCRs to the interface in iTregs. These data are consistent with those observed in LAT accumulation analyses, which suggest that anti-CD3/28 priming tends to generate T cells which activate less efficiently. In summary, both iTregs display impaired TCR localisation at the interface of the IS, which would diminish TCR signal transduction and T cell activation in iTregs.

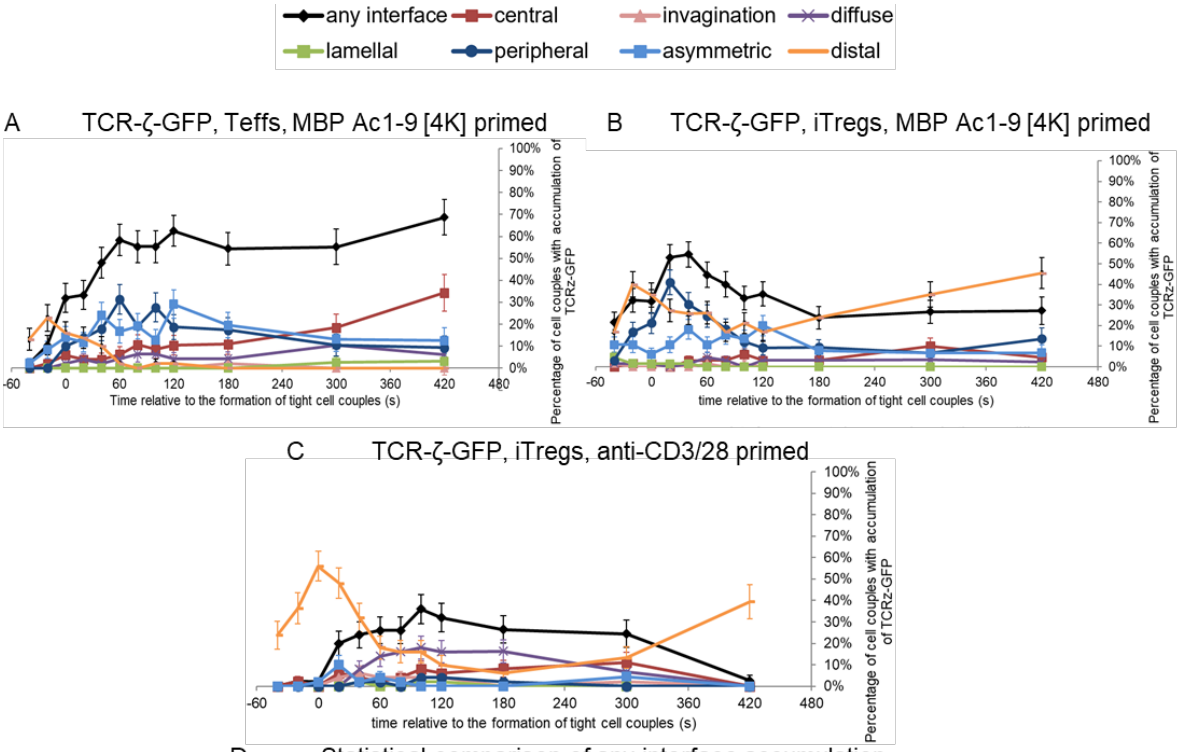

D Statistical comparison of any interface accumulation

Time (s)	-40	-20	0	20	40	60	80	100	120	180	300	420
Teffs (4K) vs iTregs (4K)	0.008	0.01	0.86	0.05	0.61	0.21	0.16	0.03	0.008	0.002	0.009	0.0008
	**	*						*	**	**	**	***
iTregs (4K) vs iTregs (anti-CD3/28)	0.003	0.003	0.0001	0.0006	0.002	0.06	0.17	0.92	0.86	0.91	0.97	0.006
	**	***	***	***	**							**

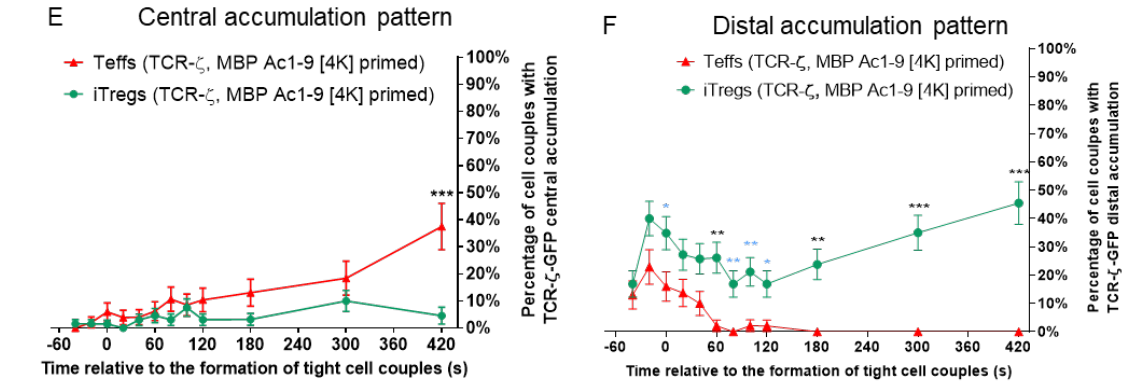

Figure 4.16 TCR-ζ-GFP accumulation in MBP Ac1-9 [4K]-primed iTregs[†] is diminished at the IS but increases at the distal pole, compared to Teffs[††].

TCR-ζ-GFP transduced Teffs and iTregs were activated by MBP Ac1-9 [4Y]-primed PL8 cells and imaged every 20 seconds for 15 minutes. DIC and GFP images were analysed to identify formations of tight cell couples and investigate spatiotemporal distribution patterns of TCR-ζ-GFP of **A)** MBP Ac1-9 [4K]-primed Teffs (51 cell couples, four experiments), **B)** MBP Ac1-9 [4K]-primed iTregs (66 cell couples, three experiments), **C)** anti-CD3/28-primed iTregs (50 cell couples analysed, three experiments). **D)** Statistical comparisons of TCR-ζ-GFP accumulation at the IS of difference cells using a two proportion z-test. Comparing **E)** central and **F)** distal TCR-ζ-GFP accumulation between MBP Ac-19 [4K]-primed Teffs and iTregs. Numerals and asterisks indicate p-values and asterisk colours indicate whether differences remain significant with the Bonferroni correction (0.004<*<0.05, 0.004<**<0.01, 0.001<**<0.004, ***<0.001). Error bars indicate standard error of the mean.

[†] TCR-ζ-GFP imaging data of Tg4 iTregs were generated and analysed (MBP peptide-primed) by former lab member Silvia Cirillo, data of anti-CD3/28-primed iTregs were analysed by Christoph Wuelfing.

[††] TCR-ζ-GFP imaging data of Tg4 MBP peptide-primed Teffs were generated and analysed by former PhD student Helen Tunbridge.

4.11 PKC-θ accumulation at the IS increases in Tg4 iTreg showing more diffuse and lamellal patterning

Diminished spatiotemporal distributions of LAT and TCR-ζ were identified above and we further investigate the downstream of LAT signalosome. Apart from the TCR-CD3 complex, the protein kinase C-theta (PKC-θ) is another central element of the cSMAC and translocation of PKC-θ to the immune synapse is associated with T cell activation and proliferation (121, 122). In early T cell activation, PLC-γ1 cleaves PIP_2 and generates a second messenger, DAG, which binds the C1 domains of PKC-θ and meditates its translocation to the IS (194). In addition, Lck directly phosphorylates PKC-θ, which also recruits it to the membrane (195). GCK-like kinase (GLK, or MAP4K3) activated by SLP-76, further phosphorylates and activates PKC-θ (196), which subsequently leads to activation of NF-κB, AP-1 and NFAT (197-199).

However, roles of PKC-θ in Tregs function seem to be more elusive. PKC-θ is important in Treg development *in vivo*, as PKC-θ knockout mice have a significantly reduced number of tTregs and pTregs, but PKC-θ deficient Tregs are as potent as wild-type Tregs in suppressive functions (200). In a model using planar bilayers with ICAM-1 and anti-CD3 antibodies to form the IS with Teffs and Tregs (201), PKC-θ was sequestered in the distal pole of Tregs and the level of PKC-θ recruitment to the IS was significantly lowered, compared to Teffs. Moreover, PKC-θ was found to negatively regulate a feedback loop and reduce suppressive functions of Tregs which could be enhanced by PKC-θ blockade (201). While *in vitro*, PKC-θ mediates inhibition of iTreg differentiation via an AKT-Foxo1/3A pathway, and using PKC-θ inhibitors or knocking out PKC-θ enhances iTreg differentiation (202). These results together suggest that PKC-θ mediates immune response by shifting a balance between Teff and Treg responses (202, 203).

In the previous study by Singleton *et al* (130), PKC-θ-GFP displays a strong preference for central accumulation at the IS in 5C.C7 and DO11.10 TCR transgenic T cells, and substantial phosphorylation of PKC-θ observed in these T cells validates its activation at the cSMAC. Therefore, to further study and compare PKC-θ localisation at the interface in both Teffs and iTregs, we next transduced Tg4 Teffs and iTregs with PKC-θ-GFP to investigate its spatiotemporal distributions during their activation. These T cells were all MBP peptide-primed and iTregs transduced with PKC-θ-GFP were >75% $Foxp3^+$. Representative images from the DIC and GFP channel of PKC-θ-GFP accumulation in Teffs and iTregs in the first two minutes of T cell activation are listed below (Figure 4.17).

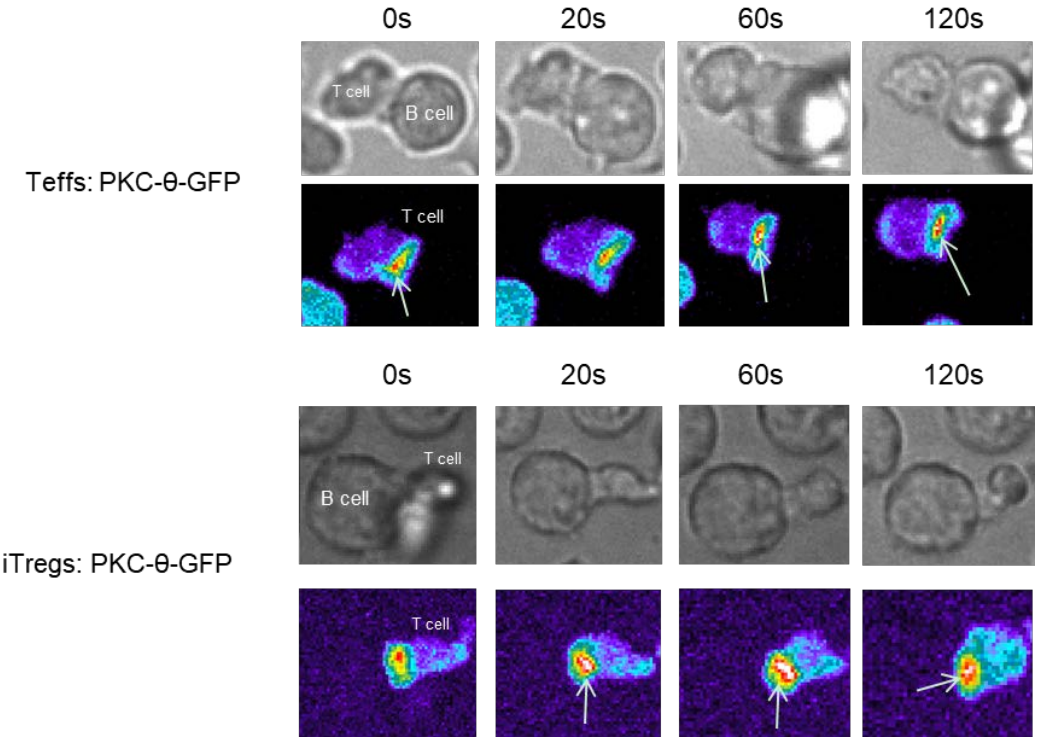

Figure 4.17 Representative live cell images showing PKC-θ-GFP accumulation in Tg4 Teffs and iTregs from four time points (0s-120s) in early T cell activation.

Top: DIC images from four time points. Bottom: matching top-down maximum projections of three-dimensional PKC-θ-GFP fluorescent images (intensity is encoded in pseudocolour and increases from purple to red). Time is given in seconds relative to the formation of a tight cell couple and arrows show accumulation of the sensor.

In MBP Ac1-9 [4K]-primed Teffs (Figure 4.18 A), PKC-θ-GFP started to accumulate at the IS from the -40s time point (13% of cell showing accumulation) and the percentage of Teffs showing accumulation peaked at the 0s time point (61%). The percentage gradually decreased afterwards. This indicates that in Teffs, PKC-θ-GFP was initially recruited to the interface and then driven away from the IS right after a stable IS was formed. The dominant accumulation pattern of PKC-θ-GFP was the central pattern. PKC-θ-GFP accumulation at the centre of the interface peaked at the 0s time point with 26% of Teffs displaying such accumulation.

Unlike what we found in the sensors above, PKC-θ-GFP accumulation at the IS in iTregs was enhanced across all time points observed, compared with Teffs. In MBP Ac1-9 [4K]-primed iTregs (Figure 4.18 B), about 47% of iTreg cell couples showed PKC-θ-GFP accumulation at the IS at the -40s time point and the percentage peaked at the 20s time point (74%). The accumulation remained at the interface for several minutes and 68% of iTregs at the last time point still showed PKC-θ-GFP accumulation at the IS. PKC-θ-GFP localisation at the IS during iTreg activation displayed mixed accumulation patterns (central,

diffuse and lamellal patterns were mainly found) and no dominate patterns were identified. A statistical comparison (Figure 4.18 C) shows that PKC-θ-GFP displayed significantly more accumulation at the IS in iTregs at seven time points ($p< 0.05$, -40s, -20s, 80s, 100s, 180s, 300s and 420s), compared to that in Teffs. With the Bonferroni correction, significant differences remained at three time points ($p<0.001$, -40s, -20s and 420s). This indicates that overall accumulation of PKC-θ at the IS of iTregs is increased, in comparison to Teffs.

As the central localisation of PKC-θ at the immune synapse is one of the key components of the cSMAC, we compared PKC-θ-GFP central accumulation during Teff and iTreg activation. MBP Ac1-9 [4K]-primed Teffs and iTregs (Figure 4.18 D) showed comparable central PKC-θ-GFP accumulation and iTregs only showed more central patterning at the 420s time point ($p<0.05$). This was not significant with the Bonferroni correction. In addition, among other patterns of PKC-θ-GFP accumulation in Teffs and iTregs, significant differences could be found when comparing their diffuse and lamellal patterns. In general, the mean percentage of iTregs showing PKC-θ-GFP diffuse and lamellal patterning at the IS were higher than that of Teffs at all 12 time points (Figure 4.18 E and F). PKC-θ-GFP showed more diffuse accumulation (Figure 4.18 E) at the IS at five time points ($p<0.05$, -20s, 40s, 60s, 80s and 120s), and differences remained significant at the 60s, 80s, and 120s time points after the Bonferroni correction ($p<0.004$). When comparing the their lamellal accumulation pattern of PKC-θ-GFP (Figure 4.18 F), more accumulation could be found in iTregs at seven time points ($p<0.05$, -40s-60s, 420s). Differences found at the -40s and 0s remained significant with the Bonferroni correction ($p<0.004$). Thus, iTregs showed more diverse accumulation patterns of PKC-θ-GFP than Teffs.

Together, these results show that the overall accumulation of PKC-θ at the IS in MBP Ac1-9 [4K]-primed iTregs was enhanced in early activation, compared to that in Teffs with the same priming method. This was particularly prominent before the 0s and at the 420s time point. At most time points, the levels of PKC-θ overall accumulation in Teffs and iTregs are comparable. These results are contradictory to those in the previous study by Zanin-Zhorov *et al*, where they found PKC-θ was sequestered away from the IS of human Tregs by investigating T cell-APC conjugates on planar bilayers (201). However, more diverse accumulation patterns (central, diffuse and lamellal) of PKC-θ were observed in early iTreg activation, which suggests that iTregs are less likely to focus PKC-θ accumulation to the centre, compared to Teffs. Therefore, PKC-θ localisation at the IS of iTregs does not show a pronounced preference for central clustering, which is observed in Teffs.

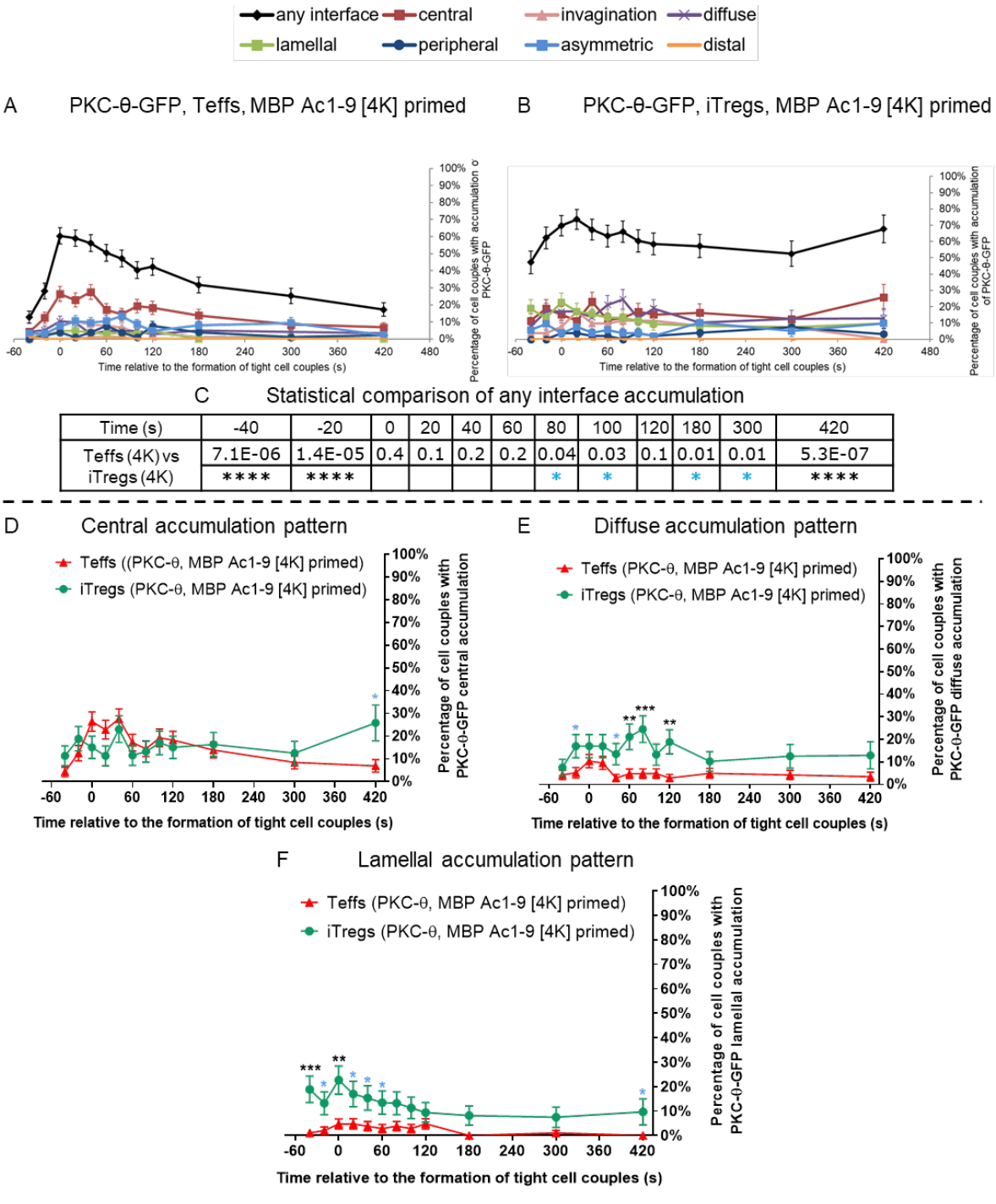

Time (s)	-40	-20	0	20	40	60	80	100	120	180	300	420
Teffs (4K) vs iTregs (4K)	7.1E-06	1.4E-05	0.4	0.1	0.2	0.2	0.04	0.03	0.1	0.01	0.01	5.3E-07
	****	****					*	*		*	*	****

Figure 4.18 More PKC-θ-GFP molecules accumulate at the IS of iTregs[†].

Live cell imaging was performed on cell interactions of PKC-θ-GFP transduced MBP Ac1-9 [4K]-primed Teffs or iTregs and MBP Ac1-9 [4Y]-primed PL8 cells. Spatiotemporal distribution patterns of PKC-θ-GFP of **A)** MBP Ac1-9 [4K]-primed Teffs (106 cell couples, six experiments) and **B)** MBP Ac1-9 [4K]-primed iTregs (53 cell couples, four experiments) were analysed and compared. **C)** Statistical comparisons of PKC-θ-GFP accumulation at the IS of difference cells using a two proportion z-test. Direct comparisons of PKC-θ-GFP **D)** central, **E)** diffuse, and **F)** lamellal accumulation at the IS of Teffs and iTregs using a two proportion z-test. Numerals and asterisks indicate p-values and asterisk colours indicate whether differences remain significant with the Bonferroni correction (0.004<*<0.05, 0.004<**<0.01, 0.001<**<0.004, 0.0001<***<0.001, ****<0.0001). Error bars indicate standard error of the mean.

[†] PKC-θ-GFP imaging data of Tg4 Teffs were generated and analysed by former PhD student Helen Tunbridge and lab member Silvia Cirillo. PKC-θ-GFP imaging data of Tg4 iTregs were generated and analysed by Silvia Cirillo.

4.12 Vav1 accumulation is enhanced at the IS of anti-CD3/28-primed Tg4 iTregs

In pMHC-TCR induced early T cell activation, SLP-76 is recruited to the LAT signalosome and phosphorylated SLP-76 continues to transport Vav1, a guanine nucleotide exchange factor (GEF) for Rho family, to the IS by binding the SH2 domain of Vav1 (204). The localisation of Vav-1 to the IS requires the presence of its SH2 and $SH3_B$ domain, and mutations of these domains completely (SH2) or partially ($SH3_B$) reduced the transport of Vav1 to the IS and impaired Vav1 phosphorylation (204). Vav1 plays crucial roles in T cell activation as it is required for TCR-induced intracellular Ca^{2+} influx, activates phosphoinositide 3-kinases (PI3K), and regulate activation of extracellular signal-regulated kinase (ERK) MAP kinases, transcriptional factor NF-κB and NAFT (204-208). Moreover, defective antigen-receptor clustering, actin polymerisation and reorganisation, LFA-1 mediated adhesion and cell polarisation observed in Vav1 deficient T cells suggest Vav-1 to be an important regulator of actin cytoskeleton in T cell activation (209, 210).

Previously, Roybal *et al* used a Vav1-GFP fusion protein (made by Victor Tybulewicz) to investigate Vav1 spatiotemporal distributions upon peptide-induced T cell activation in 5C.C7 T cells (134). Vav1 showed mainly lamellal and peripheral localisation which could be regulated by modest interference with actin network (165). Transient early accumulation in the cSMAC was also observed. In this project, we further studied and compared Vav1-GFP spatiotemporal localisation at the IS MBP Ac1-9 [4K]-primed Teffs and anti-CD3/28-primed iTregs, however, imaging data of anti-CD3/28-primed Teffs and MBP Ac1-9 [4K]-primed iTregs transduced with Vav1-GFP were not acquired. iTregs transduced with Vav1-GFP were >74% $Foxp3^+$. Representative images displaying Vav1-GFP accumulation in Teffs and iTregs in the first two minutes of T cell activation are shown below (Figure 4.19).

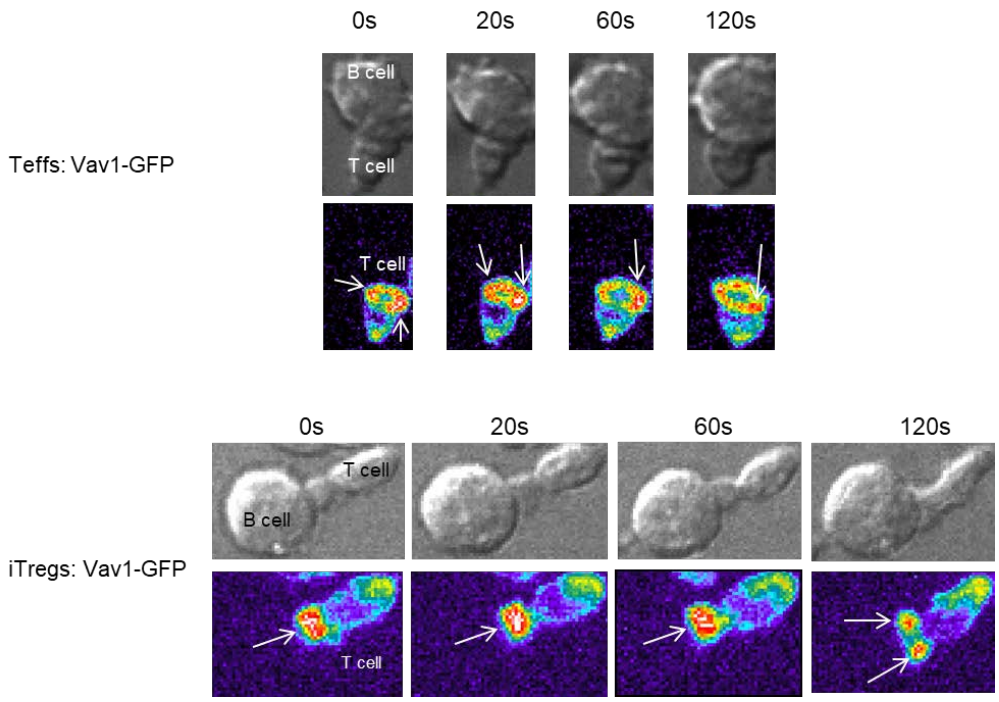

Figure 4.19 Representative live cell images of Tg4 Teffs and iTregs transduced with Vav1-GFP from four time points in early T cell activation.

Top: DIC images from four time points. Bottom: matching top-down maximum projections of three-dimensional Vav1-GFP fluorescent images (intensity is encoded in pseudocolour and increases from purple to red). Time is given in seconds relative to the formation of a tight cell couple and arrows show accumulation of the sensor.

In MBP Ac1-9 [4K]-primed Teffs (Figure 4.20 A), Vav1-GFP started to accumulate at the IS from the first time point and peaked at the 0s (49% of cells showing accumulation) time points. The accumulation remained stable at the IS with a slight fluctuation between the 40s and 100s time point. Vav1-GFP accumulation slowly decreased from the 100s time point to the last, 420s time point (still with 38% of cells showing accumulation). The peripheral and asymmetric patterns were two main patterns observed. In contrast, in anti-CD3/28-primed iTregs (Figure 4.20 B), Vav1-GFP overall accumulation maintained a relative high level of accumulation from the 0s to 180s time point, as more than 67% of cells showing accumulation at all these eight time points, and the percentage of cells showing accumulation gradually decreased afterwards. Vav1-GFP showed mainly peripheral and lamellal patterning in anti-CD3/28-primed iTregs.

A statistical comparison of overall Vav1-GFP accumulation shows (Figure 4.20 C) that anti-CD3/28-primed iTregs showed more Vav-1-GFP accumulation at seven time points (20s-180s), compared with MBP Ac1-9 [4K]-primed Teffs. All these differences remained significant with the Bonferroni correction suggesting the differences to be prominent. However, results in section 4.14 and 4.10 indicate that the method of cell priming (MBP

peptide and anti-CD3/28) could have impacts on spatiotemporal distribution of signalling molecules. Although significant differences were found when comparing percentages of cells showing accumulation of a same sensor (LAT-GFP and TCR-ζ-GFP) in peptide and antibody primed iTregs (Figure 4.10 E, 4.16 D), such differences were mostly observed within a period of time points and were not found intensively across most time points. Thus it is possible that partial enhanced Vav1-GFP accumulation would still be observed in MBP peptide-primed iTregs. In summary, these results suggest that Vav1 localisation at the anti-CD3/28-primed iTregs is upregulated, compared to MBP Ac1-9 [4K]-primed Teffs, but it is uncertain whether similar results would still be observed when comparing Teffs and iTregs which are primed in the same way, either with MBP Ac1-9 [4K] or anti-CD3/28.

A Vav1-GFP, Teffs, MBP Ac1-9 [4K] primed

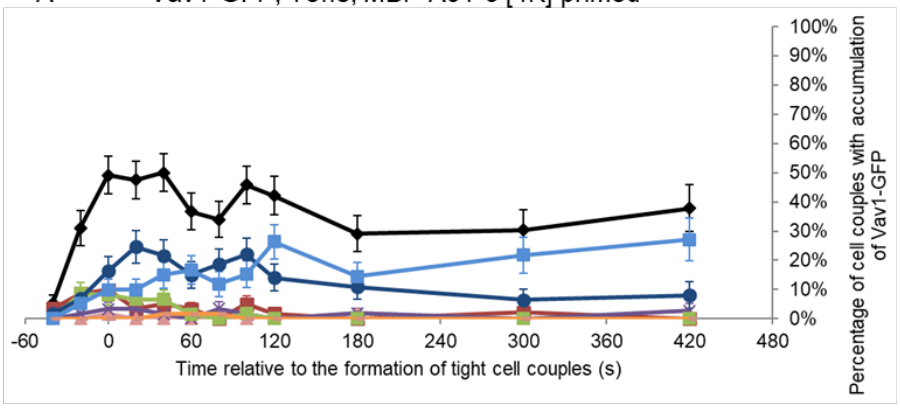

B Vav1-GFP, iTregs, anti-CD3/28 primed

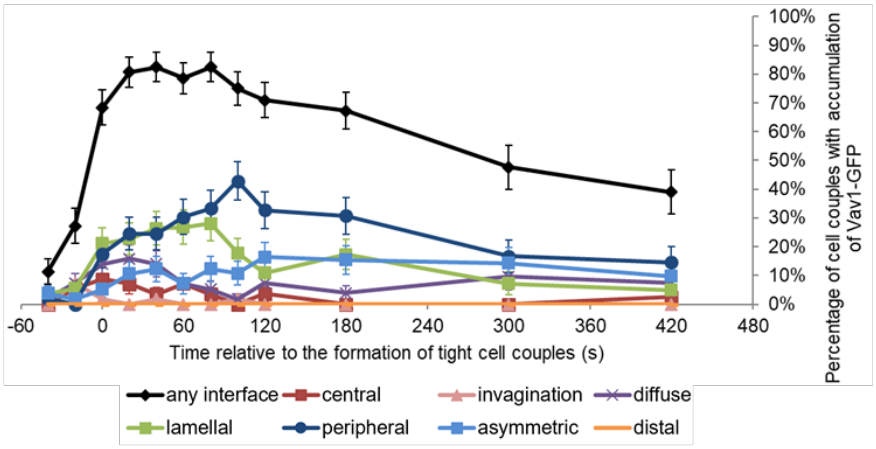

C Statistical comparison of any interface accumulation

Time (s)	-40	-20	0	20	40	60	80	100	120	180	300	420
P-value	0.40	0.82	0.05	0.0004	0.0005	1.3E-05	3.3E-07	0.003	0.004	0.0002	0.15	0.90
				***	***	****	****	**	**	***		

Figure 4.20 Anti-CD3/28-primed iTregs[†] display more Vav1-GFP accumulation at the IS, compared to MBP Ac1-9 [4K]-primed Teffs[††].

Vav1-GFP transduced MBP Ac1-9 [4K]-primed Teffs or anti-CD3/28-primed iTregs were activated with MBP Ac1-9 [4Y]-primed PL8 cells and image for 15 minutes. Spatiotemporal distribution patterns of Vav1-GFP of **A)** MBP Ac1-9 [4K]-primed Teffs (61 cell couples, seven experiments) and **B)** anti-CD3/28-primed iTregs (57 cell couples, two experiments) analysed and compared. **C)** Comparing Vav1-GFP overall accumulation at the IS between MBP Ac1-9 [4K]-primed Teffs and anti-CD3/28-primed iTregs with a two proportion z-test. Numerals and asterisks indicate p-values and all differences observed remained significant with the Bonferroni correction (0.001<**<0.004, 0.0001<***<0.001, ****<0.0001). Error bars indicate standard error of the mean.

[†] Vav1-GFP imaging data of Tg4 iTregs were analysed by Christoph Wuelfing.

[††] Vav1-GFP imaging data of Tg4 Teffs were generated and analysed by former PhD student Helen.

4.13 F-actin accumulation at the IS of Tg4 iTregs is delayed

Together these results above show that the IS formation and LAT nucleated signalling complexes are impaired in Tg4 iTregs. As morphological data suggest that T cell spreading and cell coupling in iTregs are also defective, we speculate the cytoskeleton network which drives T cell spreading to be also impaired. In leukocytes, actin filaments (F-actin, the polymerised form of actin) regulate membrane plasticity which generates force to drive cell movements (211). Triggered by TCR-pMHC engagement, rapid accumulation and dynamic remodelling of F-actin have been observed at the interface (171, 212). F-actin polymerisation at the T cell-APC interface forms a lamellipodium structure which increases the area of contact during the IS formation (102). Intact actin dynamics are required for the formation of a mature IS, central TCR-pMHC accumulation at the interface and efficient T cell proliferation (171). Moreover, a F-actin-rich peripheral ring has been widely observed at the IS (p-SMAC) and plays key roles in stabilising the interface, Ca^{2+} signalling and centralisation of proximal signalling complexes (168, 213, 214). At the IS of $CD8^{+}$ T cells, the peripheral F-actin ring formed upon contact is essential for initiating lytic granule secretion for killing (215). Disruption of F-actin cytoskeleton inhibits the formation of TCR microclusters, TCR-induced calcium signalling and IFN-γ production (214, 216), and depletion of actin dynamic regulators also impairs cytoskeletal rearrangement, T cell activation, proliferation and cytokine secretion (217, 218).

As mentioned in the last section, Vav1 regulates F-actin accumulation at the IS and most likely by catalysing the GDP/GTP exchange on cell division control protein 42 homolog (Cdc42) and Ras-related C3 botulinum toxin substrate 1 (Rac1), small GTPases of the Rho family (102, 207). Localised and activated Cdc42 binds Wiskott-Aldrich syndrome protein (WASP) (219), while Rac1 further activates WASP-family verprolin-homologous protein-2 (WAVE2) (101). Both WASP and WAVE2 interact with Arp2/3 complex and induce actin polymerisation (101, 102). Vav1 also directly binds haematopoietic-cell-specific protein-1(HS1) which stabilise F-actin accumulation at the IS (220). Moreover, the interaction of Vav1 and dynamin-2 (DNM2) is required for T cell activation, as DNM2 regulates actin reorganisation and modulates Vav1-mediated signalling events (221).

Therefore, by controlling cell motility, stabilising T cell-APC conjugates and the IS formation, F-actin network regulates T cell activation, and regulation of F-actin polarisation in T cells is mediated by downstream TCR signalling cascades. It is of great interest to investigate how F-actin accumulation at the synapse interacts with the LAT signalosome.

F-tractin-GFP binds F-actin, as a reporter to visualise dynamic actin network at the IS in T cell activation (222). We have previously constructed a F-tractin-GFP protein to investigate

F-actin localisation and enrichment during early T cell activation in 5C.C7 cells (134). F-actin was found to drive transient lamellal signalling organisation which is important for efficient T cell activation. In addition, by using a drug which disrupts F-actin structure, we showed that modest interference of actin dynamics could alter lamellal signalling localisation, impair activation of lamellal signalling molecules and calcium signalling (165). Finally, in this chapter, we performed live cell imaging on Tg4 Teffs and iTregs transduced with F-tractin-GFP to study and compare spatiotemporal localisation of F-tractin-GFP during their activation. F-tractin-GFP transduced iTreg were > 75% Foxp3^{+}. Representative images of Teffs and iTregs transduced with F-tractin-GFP in the first two minutes of T cell activation are shown below (Figure 4.19)

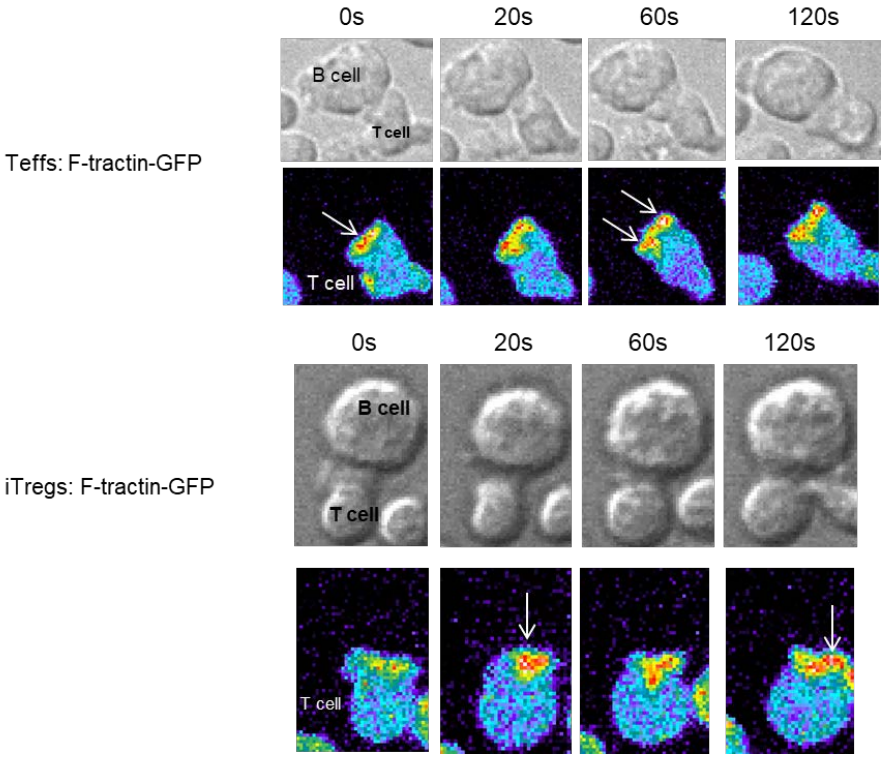

Figure 4.21 Representative live cell images of Tg4 Teffs and iTregs transduced with F-tractin-GFP from four time points in early T cell activation.

Top: DIC images from four time points. Bottom: matching top-down maximum projections of three-dimensional F-tractin-GFP fluorescent images (intensity is encoded in pseudocolour and increases from purple to red). Time is given in seconds relative to the formation of a tight cell couple and arrows show accumulation of the sensor.

In MBP Ac1-9 [4K]-primed Teffs (Figure 4.22 A), F-tractin-GFP accumulation at the synapse was observed from the -40s time point with 40% of cell showing accumulation and the percentage peaked at the 40s time points (100%). F-tractin-GFP steadily maintained at the interface till the last time point (94%). F-tractin-GFP mainly displayed peripheral, diffuse and

lamellal patterning in MBP peptide-primed Teffs before the 120s time point, and peripheral, and diffuse F-tracin-GFP accumulations were mainly observed afterwards. In MBP Ac1-9 [4K]-primed iTregs (Figure 4.22 B), F-tractin-GFP accumulation at the IS also gradually increased from the -40s time point with 37% of iTregs showing this accumulation, but the percentage peaked later at the 120s time point (76%). F-tractin-GFP accumulation at the interface remained stable till the last time point. The peripheral accumulation pattern was dominant in MBP peptide-primed iTregs at nine time points (20s to 420s). Similar observations were found in anti-CD3/28-primed iTregs (Figure 4.22 C): overall F-tractin-GFP accumulation peaked at the 180s time point (81% of the cells showing F-tractin-GFP accumulation) and was stable afterwards. Across all time points recorded, peripheral, asymmetric and diffuse F-tractin-GFP accumulation were mainly observed in anti-CD3/28-primed iTregs.

In a direct comparison (Figure 4.22 D, upper row), more cells displayed overall F-tractin-GFP accumulation in MBP Ac1-9 [4K]-primed Teffs at six time points (0s-100s), compared to MBP Ac1-9 [4K]-primed iTregs ($p<0.05$). All these differences were significant with the Bonferroni correction ($p<0.004$), suggesting diminished accumulation of F-tractin-GFP at these time points. In addition, the peak of F-tractin-GFP accumulation (120s) in MBP peptide-primed iTregs was delayed, compared with Teffs (40s). These data together suggest that before the IS formation in early T cell activation, F-actin is recruited to the interface in MBP peptide-primed Teffs and iTregs but iTregs starts to show significantly reduced F-actin accumulation at the interface after the formation of a stable IS. The restored F-tractin-GFP accumulation in iTregs after the 120s time point indicates that F-actin accumulation in early iTreg activation is delayed, possibly owing to the inefficient recruitment of F-actin to the IS. Such diminished and delayed F-actin accumulation in iTregs is consistent with their weaker ability to form a mature synapse observed in section 4.7. As F-actin serves as a scaffold in the formation of the IS and TCR microclusters, defective F-actin cytoskeleton contributes to impaired T cell spreading and proximal signal transduction in early iTreg activation.

When comparing F-tractin overall accumulation in MBP Ac 1-9 [4K] and anti-CD3/28-primed iTregs (Figure 4.22 D lower row), only one significant difference was found at the -20s time point ($p<0.05$). It was not significant with the Bonferroni correction ($p>0.004$). This indicates that F-tractin-GFP accumulation at the IS in MBP peptide-primed and anti-CD3/28-primed iTreg activation is similar. The differences found when comparing two types of iTregs (peptide and anti-CD3/28-primed) transduced with a same sensor are variable (LAT/TCR-ζ/F-tractin-GFP), suggesting the impacts of different priming methods of iTregs might be sensor-dependant.

A F-tractin-GFP, Teffs, MBP Ac1-9 [4K] primed

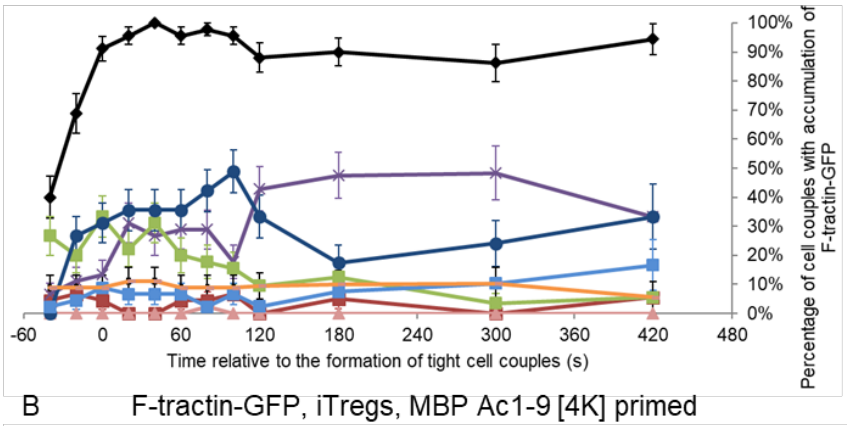

B F-tractin-GFP, iTregs, MBP Ac1-9 [4K] primed

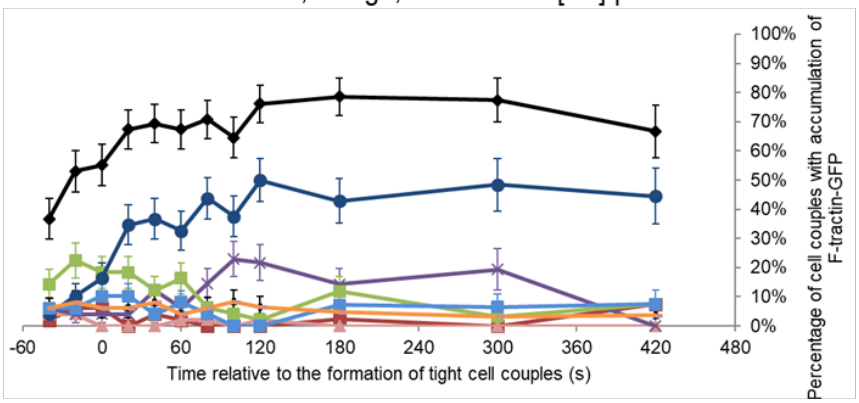

C F-tractin-GFP, iTregs, anti-CD3/28 primed

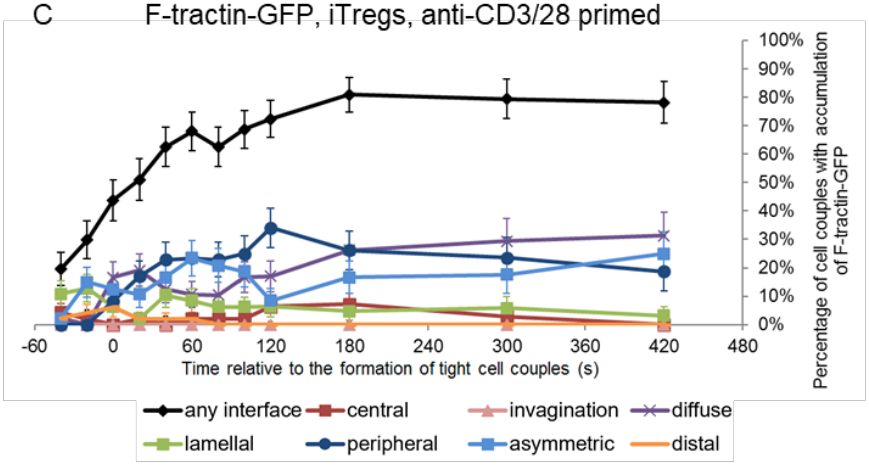

D Statistical comparison of any interface accumulation

Time (s)	-40	-20	0	20	40	60	80	100	120	180	300	420
Teffs (4K) vs iTregs(4K)	0.91	0.17	0.0002	0.001	0.0002	0.001	0.001	0.0006	0.24	0.27	0.59	0.07
			***	**	***	**	**	***				
iTregs (4K) vs iTregs (anti-CD3/28)	0.10	0.04	0.36	0.16	0.62	0.89	0.52	0.83	0.86	1.0	0.91	0.49
		*										

Figure 4.22 F-tractin-GFP distribution during MBP Ac1-9 [4K]-primed iTreg activation is delayed[†].

Live cell imaging was performed on F-tractin-GFP transduced MBP Ac1-9 [4K]-primed Teffs/iTregs and anti-CD3/28-primed iTregs activated with MBP Ac1-9 [4Y]-primed PL8 cells, for 15 minutes. F-tractin-GFP distribution patterns of **A)** MBP Ac1-9 [4K]-primed Teffs (three experiments, 45 cell couples), **B)** MBP Ac1-9 [4K]-primed iTregs (five experiment, 49 cell couples), **C)** anti-CD3/28-primed iTregs (three experiments, 48 cells). **D)** Direct comparisons of F-tractin-GFP accumulation in different cells using **a** two proportion z-test. Numerals and asterisks indicate p-values and asterisk colours indicate whether differences remain significant with the Bonferroni correction (0.004<*<0.05, 0.001<**<0.004, ***<0.001). Error bars indicate standard error of the mean.

[†] F-tractin-GFP imaging data of Tg4 Teffs and iTregs were generated and analysed by former lab member Silvia Cirillo, and F-tractin-GFP imaging data of anti-CD3/28-primed Tg4 iTregs were analysed by Christoph Wuelfing.

4.14 Discussion

In this chapter, we have investigated immunological functions (suppression on T cell proliferation, IFN-γ and IL-10 secretion), morphological characteristics and spatiotemporal distributions of five important and related signalling molecules (LAT, TCR-ζ, PKC-θ Vav1 and F-actin) in early TCR-pMHC induced Tg4 Teff and iTreg activation.

4.14.1 Suppressions from Tg4 Teffs, iTregs and Clone 4 Teffs are different

We hypothesised that Tg4 iTregs would be able to suppress Tg4 naïve $CD4^+$ T cells proliferation and Tg4 Teffs which mainly consist of Th1 cells (154), should not. Upon cell-cell contact, purified $CD4^+CD25^+$ Tregs can suppress $CD4^+CD25^-$ T cell proliferation and block IL-2 production when activated by anti-CD3 or APCs or both (174, 223). Tg4 iTregs also showed suppression on naïve $CD4^+$ T cell proliferation when activated with MBP Ac1-9 peptide and irradiated APCs (139). Such immunosuppressive activity with minimum antigen specificity of iTregs distinguishes from other $CD4^+$ helper subsets (21). Therefore, in this project, we measured and compared the level of suppression induced by both Tg4 Teffs and iTregs.

When activated by MBP Ac1-9 [4K], Tg4 anti-CD3/28-primed iTregs and MBP Ac1-9 [4K]-primed Teffs showed a comparable suppressive ability to inhibit Tg4 naïve $CD4^+$ T cell proliferation, and higher ratios of Teffs/iTregs to naïve $CD4^+$ T cells were related with stronger suppression. Similar results were found in control experiments measuring suppression of Clone 4 $CD8^+$ Teffs on Tg4 naïve T cells. However, such suppression was not observed when cells were activated with plate-bound anti-CD3/28 instead of PL8 cells and MBP peptide, suggesting interactions between Tg4 Teffs, iTregs, or Clone 4 Teffs and PL8 cells play key roles in inducing suppression on Tg4 naïve T cell proliferation.

The existence of PL8 cells, might partially contribute to suppression observed. It is curious that higher ratios of PL8 cells to responder cells partially enhanced suppression, though this could be a result of variability from only one set experiments. PL8 cells die a few days after treated with mitomycin C, however, as B lymphoma cells, they might deprive nutrients of the culture before their apoptosis. Adding additional Teff or iTregs might enhance such process. Tg4 Teffs or iTregs may also compete for MBP peptides with the Tg4 naïve T cells as they all form the same pMHC-TCR interaction, while this does not apply to Clone 4 cells. It is also suspected that IL-2 consumption by activated $CD4^+$ or $CD8^+$ cells in the culture might partially lead to the suppression. The trimeric IL-2R consists of three chains, CD25 (IL-2Rα), CD122 (IL-2Rβ) and CD132 (IL-2Rγ) (224). Naïve $CD4^+$ T cells do not express expression CD25 and express low levels of CD122 and CD132, while upon TCR activation, CD25 is highly expressed by $CD4^+$ and $CD8^+$ T cells (225). Tregs suppress T cell proliferation by

inhibiting IL-2 production (174). With a high level of CD25, Tregs also compete with naive $CD4^+$ T cells for IL-2, and IL-2 and TCR signals promote IL-10 production in Tregs (226). Tg4 $CD4^+$ Teffs and Clone $CD8^+$ Teffs had been continuously cultured with exogenous IL-2 and likely express high levels of IL-2R. Therefore, their high affinity for binding IL-2 might contribute to the suppression of Tg4 naïve T cells. However, additional IL-2 added in wells with Clone 4 $CD8^+$ Teffs might be sufficient for the naïve T cells to overcome this. Moreover, interactions of PL8 cells and Clone 4 T cells should be considered. PL8 cells were generated by fusing blast cells with M12 C3 cells which originated from BALB/c B lymphoma cells expressing $H\text{-}2^d$ MHC (137, 227). Clone 4 T cells originated from B10.D2 mice and were homozygous for $H\text{-}2^d$ (175). However, Clone 4 TCRs were specifically selected to recognise HA peptides presented by MHC class I $H\text{-}2K^d$, and such selection would also apply to MHC class I of PL8 cells. Therefore, PL8 cells should not be able to activate CL4 cells in the presence of MBP peptides which are not agonist peptides for their TCRs. A control condition containing PL8 cells, Clone 4 T cells and MBP peptides without additional IL-2 should better clarify this argument.

One possible explanation for not detecting suppression in plate-bound anti-CD3/28 activated cells might be that the TCR stimulation was too strong. Suppression was hardly found in conditions activated by plate-bound anti-CD3 (174). Shevach suggested that when T cells bound anti-CD3 attached to a plate, they receive a continuous potent signal which allows cells to overcome Treg-induced suppression (228). Even when induced by lower concentrations of anti-CD3, this resistance to suppression remains. Moreover, the use of anti-CD28 in addition to soluble anti-CD3 and irradiated accessory cells is not recommended, as stronger costimulation hinders Treg-mediated suppression by enhancing IL-2 production (228). Additional anti-CD28 or exogenous IL-2 abrogates $CD4^+$ $CD25^+$ Treg suppression on $CD4^+CD25^-$ T cells when activated by anti-CD3 or peptide-primed APCs (223). In this project, the level of costimulation from 2 µg/ml anti-CD28 has not been assessed. Some anti-CD3/28 activated $CD4^+$ naïve T cells showed even enhanced proliferation in the presence of Teffs/iTregs, indicating that they might have received more IL-2 produced by activated Teffs/iTregs. Therefore, these data suggest that using plate-bound anti-CD3 and additional anti-CD28 to obtain suppression in this assay to be difficult.

Overall, the *in vitro* iTreg suppression applied in this study has several defects. The direct cell to cell contact of iTregs and naive T cells were not monitored. Experimental controls and repeated experiments were neither sufficient to draw clear conclusions. Cells activated by plate-bound anti-CD3/28 were likely to overcome Treg suppression owing to the continuous stimulation. Further adjustments are required to better assess the suppressive capabilities of iTregs. For example, using irradiated endogenous Tg4 accessory cells or

anti-CD3 only should be more appropriate to activate Tg4 naïve cells in the presence of Tg4 iTregs or Teffs. To verify whether the suppression is induced via cell to cell contact or cytokines, a membrane previously described (229) which allows soluble molecules but not cells to penetrate, could be added to wells.

4.14.2 Tg4 iTregs secrete less IFN-γ and potentially more IL-10

Cytokines produced by different subsets of T cells are linked with their functions. As mentioned, IFN-γ is a signature cytokine produced by Th1 cells for effector functions and induces innate and T cell response (21). Activating Tg4 naïve T cells *in vitro* with MBP peptides triggers a dominant Th1 response (154). This was observed in our Teff-inducing conditions as high concentrations of IFN-γ were detected 24 hours after MBP priming. Lower levels of IFN-γ were detected in iTreg-inducing conditions and intracellular cytokine staining also confirmed that both Tg4 Teffs and iTregs secrete IFN-γ. The levels of IFN-γ in the two conditions were significantly different on day 2 and 3. The ratio of $Foxp3^+$ to $Foxp3^-$ cells gradually increased from day 2-5 indicates the transformation of iTregs from naive $CD4^+$ T cells. On day 2, most cells in iTreg-inducing conditions did not express Foxp3. Therefore, it might be that Th1 cells in iTreg-inducing conditions still contributed to the main production of IFN-γ at early stages of iTreg induction. These Th1 cells eventually either died out or transformed into iTregs. On day 3, about 40% of the cells were $Foxp3^+$ in iTreg-inducing condition. The different levels of IFN-γ detected on this day could be owing to a weaker capability of iTregs to produce IFN-γ, and these Tg4 iTregs likely maintained some Th1 phenotypes. This could be an intrinsic feature of Tg4 T cells. IFN-γ production of Tregs has been associated with their regulatory function. A lower suppressive capacity of $CD4^+CD25^+$ Treg against collagen-induced arthritis (CIA) was previously found in IFN-γ receptor (IFN-γR) deficient mice, suggesting IFN-γ could mediate Treg-induced suppression (230). Besides, restimulation of alloantigens *in vivo* led to a transient increase of IFN-γ mRNA in alloantigen-reactive $CD4^+CD25^+$ Tregs, and neutralisation of IFN-γ upon adoptive transfer of Tregs abrogated their immunoregulatory function (231). $CD4^+CD25^+Foxp3^+$ Tregs isolated from spleens and lymph nodes do not express IFN-γ, but IFN-γ and T-bet expression can be detected in after culturing them with IL-12 for 72 hours (232). This suggests the plasticity of Teffs and Tregs could be regulated via an epigenetic mechanism. Moreover, IFN-γ production of stable $Foxp3^+$ iTregs also helps to prevent experimental GVHD (233). Possibly, rapid and transient production of IFN-γ inhibits immune response by inducing apoptosis of naïve and Th2 cells, as they express both IFN-γR1 and IFN-γR2 and are more sensitive (234). In summary, IFN-γ detected during Tg4 iTreg development is secreted by both Th1 cells and iTregs which hold a weaker IFN-γ-secreting ability. These iTregs likely maintain partial Th1 phenotypes.

A relatively low amount of IL-10 has been detected during the generation of both Tg4 Teffs and iTregs, particularly on day 3 of induction. IL-10 can be secreted by a wide range of cells such as DCs, macrophages, mast cells, NK cells, eosinophils, neutrophils, B cells, $CD8^+$ T cells and several subsets of $CD4^+$ T cells including Th1, Th2, Th17, $Foxp3^-$ (Tr1) and $Foxp3^+$ Tregs (reviewed by Ng *et al* (156)). Tg4 Th1 cells could be induced to secrete IL-10 by chronic repeated intranasal administration of MBP peptides *in vivo* (92). A subsequent study revealed that Th2-derived IL-4 could promote IL-10 production by these Th1 cells, and IL-4 blockade could inhibit their IL-10 expression (235). Also, high antigen dose and IL-12 can promote IL-10 production by Th1 cells (236). Possibly, transient IL-10 production by Teffs was owing to a relatively high concentration of MBP-peptides and IL-12 released by PL8 cells in cell culture. When Tg4 Teffs from day 5 of culture were reactivated, they produced IL-10. As mixed splenocytes and lymphocytes were used for cell priming, direct sources of the transient IL-10 production on day 3 were uncertain. Using markers in addition to Foxp3 for other T cells subsets (such as T-bet for Th1, GATA3 for Th2 and ROR-γt for Th17 (21)) and accessory cells alongside with IL-10 staining would be a possible solution. During the generation of Tg4 iTregs, the percentage of $Foxp3^+$ cells in iTreg-inducing conditions peaked on day 5 and Tg4 iTregs showed a trend to sustain IL-10 production on day 5 and 6. They secreted slightly but not significantly more IL-10 when restimulated on day 5. These observations combined indicate that Tg4 $Foxp3^+$ iTregs tend to produce more IL-10 than Tg4 Teffs. Further IL-10 staining or IL-10 mRNA determination would help to assess the production of IL-10 by Tg4 Teffs and iTregs.

4.14.3 Defective IS formation is associated with delayed F-actin accumulation in Tg4 iTregs

There are three different stages of interactions between T and antigen-presenting B cells: contact, recognition and stabilisation (163). The initial two minutes of activation of Tg4 T cells mostly fall into the contact and recognition phases, where dynamic morphological changes and increased $Ca2^+$ influx occur. At these early stages in antigen presentation to B cells, T cells increase their interface of contact, pulling the cell body towards and engulf a proportion of the APC. During these early phases, LAT transduced Tg4 iTregs show a reduced contact length and are more likely to form an extended lamella, compared to Teffs. In the first two minutes of activation, the interface of contact in Tg4 iTregs does not spread as wide that in Teffs. It should be noted that F-actin accumulation at the IS of iTregs is also significantly reduced within the two minutes of activation. These data suggest that defective T cell spreading of iTregs at the synapse is associated with delayed actin polymerisation. Moreover, iTregs also display a more elongated cell shape within these two minutes and they formed more extended lamellae at early time points (0s and 20s). Proximal T cell activation signals subsequently induce actin polymerisation at the interface, which increases

the area of contact and stabilises IS formation (102). Defective F-actin-dependant scaffolds impair the formation of proximal TCR microclusters and more elongated cell shapes are indicative of less efficient T cell activation (164, 214). Thus, compared to that of Teffs, morphological features of iTregs in the first two minutes of T cell activation suggest that the IS formation of iTregs are defective, which most likely are associated with diminished F-actin polarisation within this period.

4.14.4 Impaired assembly of LAT supramolecular complexes contributes to less efficient activation of Tg4 iTregs

Proximal T cell activation signalling is triggered by TCR-pMHC engagement with the assistance of CD4 or CD8 co-receptor and cytokine signals, which subsequently recruits the tyrosine kinase Lck to phosphorylate ITAMs of TCR-ζ chains. When phosphorylated, ITAMs bind ZAP-70 which continues to phosphorylate LAT and promotes the formation of LAT nucleated supramolecular signalling complexes (94). As a signalling hub, LAT binds Grb2, Gad, and PLC-γ 1 and eventually drives more signalling intermediates including Sos1, SLP-76, Nck and Vav to the LAT signalosome via multivalent interactions, and further leads to F-actin polarisation, Ca^{2+} influx and activation of transcriptional factors such as AP-1, NF-κB and NFAT. These signalling events, together with signals from costimulatory and cytokine receptors, eventually induce T cell proliferation, cell migration, cytokine secretion and effector functions (185, 237).

As defective IS formation has been observed in Tg4 iTregs, likely, proximal TCR signal transduction is also impaired. To investigate and compare TCR-induced signal transduction in early activation of Tg4 Teffs and iTregs, we have acquired and analysed live cell imaging data of five GFP-tagged signalling intermediates (LAT, TCR-ζ, PKC-θ, Vav1 and F-tractin) during the first few minutes of activation. Spatiotemporal pattern analyses show that Tg4 iTregs display impaired spatiotemporal distributions of LAT, TCR ζ, F-actin in early T cell activation but increased overall PKC-θ accumulation at the T cell-APC interface. When analysing spatiotemporal organisation of signalling intermediates of the cSMAC in these several minutes, two different time-dependent roles played by the cSMAC needed to be considered (126). In the first 60-120 seconds of T cell activation, the cSMAC efficiently induces central clustering of various signalling intermediates including LAT, Grb2, SLP-76, PKC-θ (126, 130, 135). After the 120s time point, many of these molecules withdraw from the cSMAC and some (such as SLP-76, Vav1, PIP_2 and Itk) intensively spread around the IS forming actin-associated lamellal complexes (126, 134, 135). In addition, rapid translocation of NFAT and NF-κB to the nucleus also occurs after the 60s or 120s time point, which indicates that rapid accumulation of proximal signalling intermediates at early time

points are sufficient to activate these transcriptional factors and promote further T cell activation (130, 135).

Spatiotemporal localisation of LAT in this study consistently reflects the time-dependent roles played by the cSMAC. In the first 60-120 seconds of Tg4 Teff activation, LAT rapidly accumulates at the centre of the T cell-APC interface and simultaneously induces clustering of PKC-θ, Vav1 and TCR-ζ, and F-actin polymerisation at the IS. After the first two minutes of activation, LAT localisation at the IS gradually diminishes, as well as that of PKC-θ and Vav1. While TCR-ζ accumulation remains at the interface with an increasing trend of central clustering and F-actin accumulation remains at a high level at the IS. They continue to stabilise the mature IS. This cSMAC-regulated spatiotemporal organisation in early activation is impaired in Tg4 iTregs. Overall accumulation of LAT and F-actin are significantly reduced at the IS of iTregs in the first two minutes and TCR-ζ clustering at the immune synapse is also attenuated, particularly after the 120s time point. These data illustrate that in iTregs, diminished LAT accumulation fails to rapidly assemble LAT signalosome, subsequently upsets actin polymerisation and TCR central clustering at the IS. This interaction is bi-directional, as Roybal *et al* showed that in costimulation blocked 5C.C7 T cells, enhancing actin polarisation restores LAT central clustering (173). Together, morphological studies and spatiotemporal pattern analyses of proximal signalling intermediates indicate that early T cell activation and IS formation are defective in iTregs. It is unclear why PKC-θ accumulation in iTregs is increased with diverse accumulation patterns and its roles in Treg function is complicated (200, 201). Moreover, the fact that PKC-θ is not directly recruited to the cSMAC by LAT signalosome, but CD28 (238) may partially explain why its localisation in iTreg activation is more intact.

As early activation signalling events are defective in iTregs, translocation and activation of transcriptional factors including NFAT and NF-κB at the downstream are likely to be affected. Compared to Teffs, iTregs secrete less IFN-γ upon activation, which could be partially associated with attenuated activation of NFAT, as NFAT also induces IFN-γ production in $CD4^+$ T cells (239).

In conclusion, in early TCR-induced activation of Tg4 iTregs, defective assembly of LAT signalosome subsequently results in impaired proximal TCR clustering and F-actin polarisation at the IS. These diminished signalling events together contribute to less efficient activation of iTregs, with unstable IS formation and a weakened ability to produce IFN-γ. It is of interest to investigate whether enhancement or restoration of LAT localisation could change proximal T cell signalling in iTregs and alter how iTregs behave. We attempt to answer this question in the rest of the thesis.

Chapter 5 Dual CTLA-4 and PD-1 blockade inhibits development but improves activation of MBP peptide-primed Tg4 iTregs

5.1 Introduction

Tg4 iTregs display a reduced ability to secrete IFN-γ and forming a mature IS, which is associated with their defective proximal T cell signalling events. Therefore, the enhancement of these events could promote better iTreg activation and subsequently affect their function. Another key element required for T cell activation apart from TCR signalling is costimulation, which is negatively regulated by coinhibitory (or checkpoint) receptors (116). As Tregs express several coinhibitory molecules including CTLA-4, PD-1, TIGIT and LAG3, blocking their coinhibitory pathways should enhance activation of iTregs. CTLA-4 and PD-1 have been extensively studied for their therapeutic potentials in autoimmunity and cancer (240-243). In this chapter, we investigated the roles of CTLA-4 and PD-1 in iTreg cell development, activation and function.

CTLA-4 is a homolog of CD28 but with a much higher affinity for binding CD80 and CD86 expressed on APCs by a factor of 50-2000-fold (244). Resting T cells do not express CTLA-4 and can be induced by activation, but Tregs constitutively express CTLA-4 (245, 246). Unlike CD28, binding of CTLA-4 and CD80/86 does not induce costimulatory signals, thus by competing with CD28 for binding sites, CTLA-4 negatively regulates T cell activation (244). CTLA-4 induced inhibition of T cells could be regulated by the strength of TCR stimulation. Reviewed by Buchbinder *et al* (247), upon weak TCR stimulation, CD28 predominantly binds CD80/86 and enhances IL-2 production, cell proliferation and survival. While upon strong TCR stimulation, CTLA-4 competes with CD28 as its expression on the cell surface is upregulated, which inhibits T cell activation. Other studies suggest that CTLA-4 could also induce direct inhibition by antagonising TCR-mediated signals and increasing T cell motility to reduce the efficiency of TCR-pMHC engagement (248, 249). Takahashi *et al* showed that blockade of CTLA-4 *in vivo* and *in vitro* impairs the suppressive function of Treg in mice, thus the expression of CTLA-4 contributes to Tregs mediated immune suppression and self-tolerance (246). Moreover, specific deletion of CTLA-4 in Foxp3$^+$ Tregs lead to systemic lymphoproliferation and fatal autoimmune disease which indicates CTLA-4 is required by naturally occurring Tregs for their immune regulatory function (250). A recent study shows that CTLA-4 expressed by Tregs can directly capture CD80 and CD86 from migratory DCs via a process of trans-endocytosis, which may contribute to Treg-mediated suppression (50).

PD-1 is a member of the B7-CD28 family and binds its ligand PD-L1 and PD-L2 to inhibit T cell proliferation and cytokine production (251, 252). Activated T cells, B cells and myeloid cells express PD-1 and PD-L1 is constitutively expressed by T cells, B cells, macrophages and DCs(251, 253). While PD-L2 is more restrictedly expressed in DCs, macrophages and some resting peritoneal B1 cells (254). Upon T cell-ACP interactions, PD-1 ligation induces phosphorylation of its immunoreceptor tyrosine-based switch motif (ITSM) and immunoreceptor tyrosine-based inhibitory motif (ITIM), which recruit phosphatases including SHP-1 and SHP-2 (255). These phosphatases induce dephosphorylate signalling molecules and antagonise TCR and CD28 triggered activation signalling (e.g ZAP-70, PI3K and Ras signalling pathways), thus inhibit T cell activation (256). PD-L1 also plays a key role in iTreg development and cell function. PD-L1 deficient APCs show an impaired ability to induce $Foxp3^+$ iTregs, and PD-L1-coated beads maintain Foxp3 expression and enhance iTreg-mediated immune suppression on Teffs (257, 258).

Early studies showed that blocking CTLA-4 and PD-1 pathway enhances anti-tumour immune responses respectively (259, 260). Monoclonal antibodies (mAbs) targeting CTLA-4, PD-1 and PD-L1 have been intensively studied for their immunotherapeutic potentials and some have been approved for treating different types of cancers including melanoma, lung cancer, breast cancer and B-cell lymphoma (243). Moreover, both anti-CTLA-4 and anti-PD-1 antibodies have been shown to effectively induce deletion of Tregs in the tumour microenvironment in mouse models (261, 262). While Sharma *et al* showed two mAbs for CTLA-4, ipilimumab and tremelimumab do not delete Tregs in human cancers (263).

How CTLA-4 and PD-1 directly regulate development and suppressive function of Tregs is not fully understood. In this section, we aim to investigate their roles in the induction and activation of Tg4 iTregs. Thus, we first treated Tg4 naive T cells with anti-CTLA-4 or anti-PD-1 or both mAbs during their induction to become iTregs. Frequencies of $Foxp3^+$ cells in controls and mAb-treated conditions were examined from day 2-6 of culture. Moreover, IFN-γ and IL-10 ELISAs were applied to monitor changes of cytokine production in each condition during iTreg induction. To study whether the dual blockade could change how iTregs behave, we blocked CTLA-4 and PD-1 pathways during the first several minutes of iTreg activation and live cell imaging was performed. Morphological parameters and LAT localisation of anti-CTLA-4/PD-1 blocked iTregs were analysed to assess the effects of the dual blockade on T cell morphology and impaired spatiotemporal distributions of LAT in early iTreg activation. Experiments were conducted mainly on MBP peptide-primed iTregs but additional data were acquired using anti-CD3/28-primed iTreg as supplements.

5.2 Chapter aims

- To treat naïve Tg4 T cells with anti-CTLA-4 or anti-PD-1 or both mAbs during induction of iTregs and assess their Foxp3 expression from day 2-6 of culture.
- To assess the impacts of anti-CTLA-4, anti-PD-1, and both mAbs on IFN-γ and IL-10 production during iTreg induction.
- To conduct live cell imaging on LAT-GFP transduced iTreg treated with dual blockade of CTLA-4 and PD-1, and compare their morphological parameters and LAT-GFP spatiotemporal distributions to that of untreated Teffs and iTregs.

A table is shown below indicating symbols used in this chapter for different conditions.

Table 2 Symbols and patterns denoting cell types or conditions in chapter 5

Condition	Symbol
Teffs (MBP Ac1-9 [4K] primed)	▲
Teffs (anti-CD3/28 primed)	◆
iTregs (MBP Ac1-9 [4K] primed)	●
iTregs (MBP Ac1-9 [4K] primed) + anti-CTLA-4	△
iTregs (MBP Ac1-9 [4K] primed) + anti-PD-1	○
iTregs (MBP Ac1-9 [4K] primed) + anti-CTLA-4/PD-1	□
iTregs (anti-CD3/28 primed)	■
iTregs (anti-CD3/28 primed) + anti-CTLA-4	△
iTregs (anti-CD3/28 primed) + anti-PD-1	○
iTregs (anti-CD3/28 primed) + anti-CTLA-4/PD-1	□

5.3 Dual blockade of CTLA-4 and PD-1 inhibits Tg4 iTreg development

First, we investigated the roles of CTLA-4 and PD-1 in Tg4 iTreg development by blocking CTLA-4 or PD-1 or both using mAbs during iTreg induction. Tg4 naïve T cells were primed with MBP Ac1-9 [4K] and endogenous APCs as described above. Cells were cultured in Treg-inducing medium containing IL-2 and TGF-β for five days. Additional anti-CTLA-4 or anti-PD-1 or both blocking mAbs were added into experimental groups from day 1 with a final concentration of 10 μg/ml. Cell medium was exchanged daily with supplemental mAbs and cells were split when required, usually on day 3. To track the differentiation of iTregs, cell samples were collected on a daily base from day 2 and stained for Foxp3 to identify iTreg populations in each condition.

Figure 5.1 A summarises frequencies of $Foxp3^+$ cells in each condition from day 2-6 of culture. Consistently, the percentage of $Foxp3^+$ cells in each condition gradually increased from day 3 and peaked on day 5. This pattern was consistently observed in all four repeated experiments. The percentage of $Foxp3^+$ cells in the control condition where no blocking mAbs were added, was the highest among the four conditions from day 3 to 6. Treating iTreg-inducing cells with anti-CTLA-4 or anti-PD-1 or both continuously reduced the frequency of $Foxp3^+$ cells from day 3-6 and using both mAbs led to a most remarkable reduction. On day 6, the percentage of $Foxp3^+$ cells decreased by an average of 11% (anti-CTLA-4), 14% (anti-PD-1) and 24% (anti-CTLA-4/PD-1) respectively. In the condition treated with both anti-CTLA-4/PD-1, the percentage of $Foxp3^+$ cells was the lowest on those four days. The inhibition induced by these mAbs were cumulative. Multiple comparisons using Two-way ANOVA show that no significant differences were identified when comparing the percentages of $Foxp3^+$ cells among all conditions. However, by normalising the frequencies of $Foxp3^+$ cells in treatment groups to control groups from day 3-6, differences observed were prominent (Figure 5.1 B). Blockade of CTLA-4, PD-1 and both significantly reduced the frequency of $Foxp3^+$ cells ($p<0.05$). Anti-PD-1 showed slightly better inhibition of Foxp3 expression than anti-CTLA-4. Additional data from experiments where iTregs-inducing cells were treated with and without both mAbs for five days were compared. These cells were only stained for Foxp3 on day 6. A direct comparison (Figure 5.1 C) shows that the percentages of $Foxp3^+$ cells in iTreg-inducing cells treated with anti-CTLA-4/PD-1 on day 6 were significantly reduced by an average of 20%, compared to untreated iTreg-inducing cells ($p<0.0001$).

These results indicate that during the induction of Tg4 iTregs primed with MBP peptide, blocking both CTLA-4 and PD-1 downregulates the proportion of $Foxp3^+$ cell in these cells

and therefore inhibit iTreg development. Blocking CTLA-4 or PD-1 alone moderately inhibits iTreg development and using both mAbs leads to a most significant reduction of Foxp3$^+$ populations. Foxp3$^+$ T cells were mainly identified from day 3 of culture, which suggests that naïve T cells need about 24 hours of priming to express Foxp3. Therefore, CTLA-4 and PD-1 co-inhibitory pathways play important roles in maintaining Foxp3 expression during iTreg development.

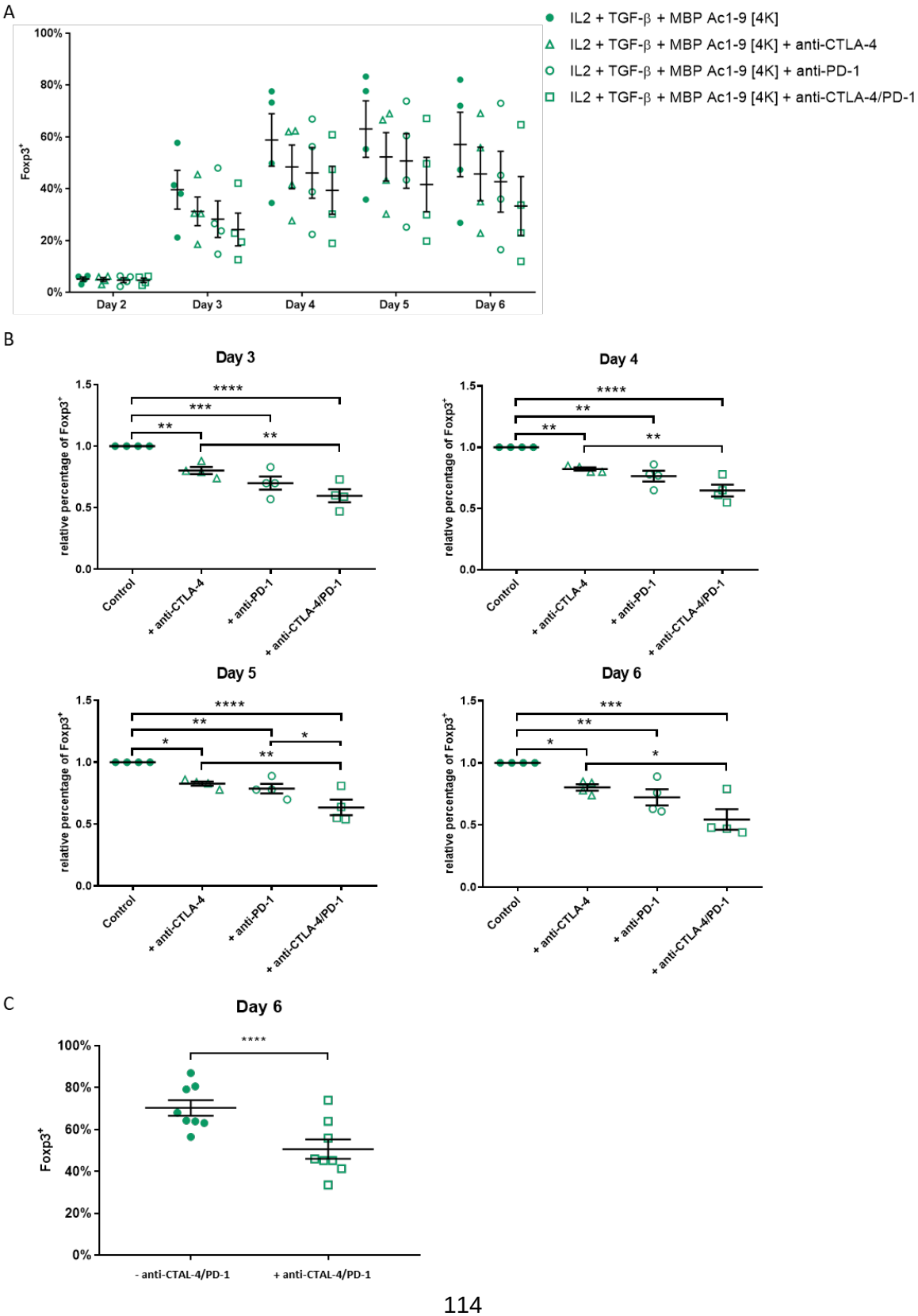

Figure 5.1 Dual CTLA-4 and PD-1 blockade inhibits induction of Foxp3$^+$ iTregs.

iTreg-inducing cells were treated with anti-CTLA-4 or anti-PD-1 or both mAbs with a final concentration of 10 µg/ml and were cultured for five days. Cell samples were collected daily from day 2-6 of culture for identifying Foxp3$^+$ cell populations. Data of untreated iTreg-inducing cells refer to Figure 4.5. **A)** A summary plot graph of percentages of Foxp3$^+$ cells from four conditions from day 2-6, data are from four experiments, **B)** The relative percentages of Foxp3$^+$ cells from four conditions on day 3-6, cells without treatments were used as controls for normalisation, data are four experiments, **C)** Comparing the percentages of Foxp3$^+$ cells of untreated and anti-CTLA-4/PD-1 daily treated iTregs on day 6, data are from eight experiments. Proportions were arcsine transformed or normalised to control, and statistical significance was calculated using **A)** Two-way ANOVA, **B)** One-way ANOVA, **C)** paired Student's T-test. Asterisks indicates p-values (*<0.05, **<0.01, ***<0.001, ****<0.0001) and error bars indicate standard error of the mean.

5.4 Dual blockade of CTLA-4 and PD-1 slightly enhances IFN-γ and IL-10 production during Tg4 Teff and iTreg development

As we have shown in the last chapter that Tg4 iTregs are less capable to produce IFN-γ and tend to maintain IL-10 secretion during their induction, we further investigated whether IFN-γ and IL-10 secretion during iTreg development could be altered by CTLA-4 and PD-1 blockades. In addition, we applied the same treatments on Teff-inducing cells (cultured with less IL-2 and no TGF-β). A series of cell supernatants were collected daily from cell cultures and ELISAs were performed to assess IFN-γ and IL-10 production during the five days of culture. Data from a total of five experiments were plotted (Figure 5.2) and three of these experiments did not contain conditions treated with only anti-CTLA-4 or anti-PD-1.

IFN-γ ELISAs show that during the induction of Teffs (Figure 5.2 A), increased IFN-γ production were found in cells treated with anti-CTLA-4 or anti-PD1 or both mAbs, mainly on day 2, 4 and 5. Among all conditions, the amounts of IFN-γ detected peaked on day 3 and a combination of blocking CTLA-4 and PD-1 had best outcomes in enhancing IFN-γ secretion, which significantly increased IFN-γ secretion of Teffs on day 4 ($p<0.05$). IFN-γ secretion detected was relatively low on day 5 and 6.

Different observations were found in iTreg-inducing conditions (Figure 5.2 B and C), as blocking CTLA-4 or PD-1 or both during iTreg development only slightly increased IFN-γ production, compared to that of untreated iTregs. As single antibody treatments using anti-CTLA-4 or anti-PD-1 were only performed in two paired experiments, we analysed two separate graphs showing data from all paired experiments to reduce experimental variability. IFN-γ secretion detected also peaked on day 3 and 4 in all iTreg-inducing conditions and was barely detected on day 6. Blocking PD-1 and blocking both CTLA-4 and PD-1, tended to enhance IFN-γ secretion better than blocking CTLA-4 in iTreg-inducing cell cultures on day 3 and 4 (Figure 5.2 B). Overall, IFN-γ secretion by iTreg was barely affected by the blockades.

To summarise, these data suggest that blocking both CTLA-4 and PD-1 mostly enhances IFN-γ production during Tg4 Teff development. Stronger enhancement of IFN-γ secretion in Teff-inducing conditions was observed suggesting Teffs are more responsive to the blockades than iTregs, regarding IFN-γ secretion. Moreover, in iTreg-inducing conditions, enhanced IFN-γ secretion might not only contributed by iTregs, as the blockades downregulated the proportions of these cells during iTreg induction (shown in Figure 5.1). It is likely that this slightly increased IFN-γ secretion was owing to reduced $Foxp3^+$ and

increased Teff cell populations, as we have shown in section 4.6 that Tg4 Foxp3^{+} iTregs secrete less IFN-γ, compared to Teffs.

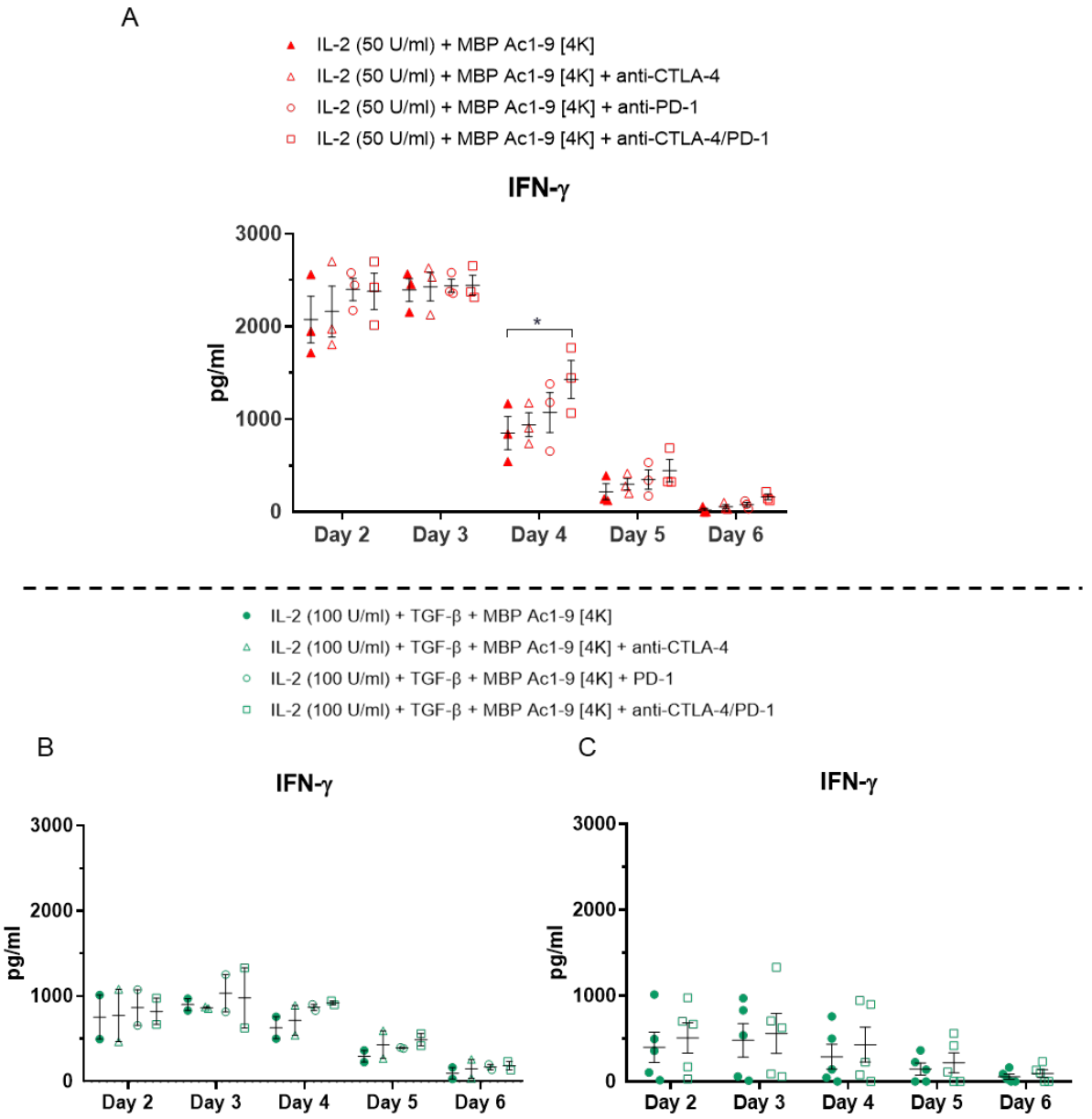

Figure 5.2 Blocking CTLA-4 and PD-1 during the induction of Teffs and iTregs slightly increases IFN-γ production.

ELISAs were performed on daily collected supernatants from cell cultures of **A)** Teff and **B and C)** iTreg-inducing cells treated with anti-CTLA-4, anti-PD-1 or both, to assess IFN-γ production. Data from a total of five experiments are used. To show all paired experiments, the number of repeated experiments in each condition is different: three in **A)**, two in **B)** and five in **C)**. Statistical significance was calculated using Two-way ANOVA. Asterisks indicate p-values (*<0.05) and error bars indicate standard error of the mean.

As shown in section 4.6, IL-10 secretion was relatively low during both Tg4 Teff and iTreg development. In addition, using a combination of anti-CTLA-4/PD-1 had a better effect on enhancing IFN-γ secretion, so we applied IL-10 ELISAs to investigate whether this combination with both mAbs would alter IL-10 production during Teff and iTreg development. Data are from a total of five experiments and two experiments did not contain conditions of Teff-inducing cells treated with anti-CTLA-4/PD-1.

Again, results from IL-10 ELISAs show that blocking both CTLA-4 and PD-1 slightly enhanced IL-10 secretion during Tg4 Teff and iTreg induction (Figure 5.3 A). In untreated and anti-CTLA-4/PD-1 treated Teff-inducing conditions, IL-10 was mainly detected on day 3-5. Blocking both CTLA-4 and PD-1 during Teff-induction slightly increased the amounts of IL-10 on day 3-5. For untreated iTreg-inducing conditions, IL-10 secretion detected was relatively low and dual mAb treatment slightly enhanced IL-10 secretion of iTreg-inducing cells on day 3-6. Although no significant differences were identified when comparing any two of these conditions, this is likely owing to the variability of experiments and trends of enhancement could be found on day 3-5. Together these results suggest that blocking both CTLA-4 and PD-1 shows a trend of enhancing IL-10 production during Tg4 Teff and iTreg development.

However, as low levels of IL-10 production were observed during the induction of both types of cells, dual mAb treatment might have a limited effect on IL-10 secretion during their development. We have shown in section 4.6 that activating mature Teffs and iTregs on day 5 of culture could induce IL-10 secretion. Therefore, we restimulated untreated Teffs and iTregs on day 5 of culture using MBP Ac1-9 [4K] peptides and mitomycin C treated PL8 cells and measured the amounts of IL-10 released after 18 hours. Additional anti-CTLA-4/PD-1 mAbs were added into parallel conditions as treatment groups. Figure 5.3 B shows that blocking CTLA-4 and PD-1 for 18 hours in restimulated Teffs and iTregs had little effects on their IL-10 secretion. This dual mAb treatment marginally downregulated IL-10 secretion in restimulated iTregs, but the difference was not significant.

In summary, dual CTLA-4 and PD-1 blockade slightly promotes both IFN-γ and IL-10 production detected during induction of Tg4 Teffs and iTregs. Blocking CTLA-4 and PD-1 during the activation of mature Teffs and iTregs does not affect their IL-10 secretion.

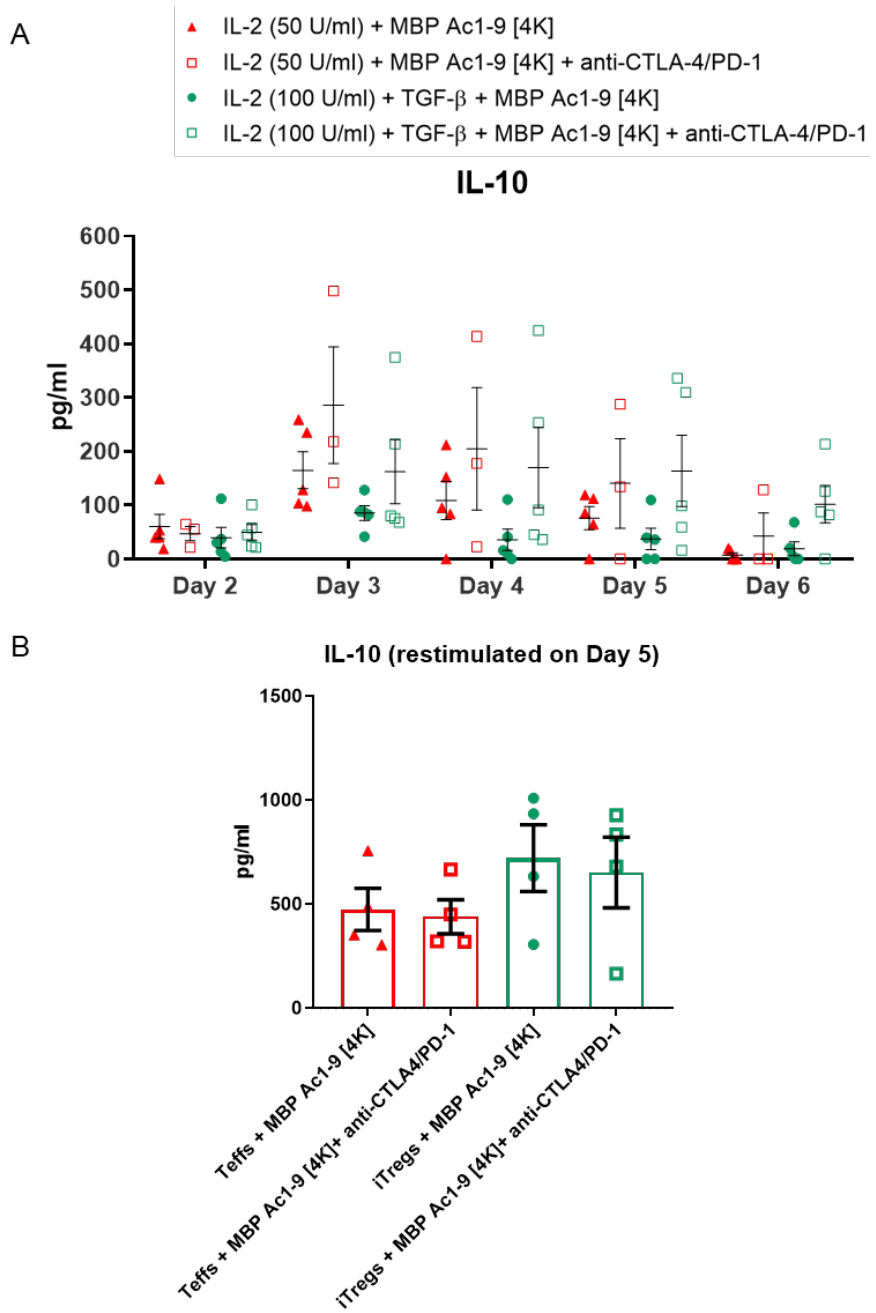

Figure 5.3 Blocking CTLA-4 and PD-1 slightly increases IL-10 production during Teff and iTreg generation but has no impacts on IL-10 production of restimulated Teffs and iTregs.

Cells supernatants from conditions of Teff and iTreg-inducing cells treated with anti-CTLA-4, anti-PD-1 or both for five days were collected and used for **A)** IL-10 ELISAs, data are from a total of five experiments. Anti-CTLA-4/PD-1 mAbs were added to restimulated Teffs and iTregs (>62% Foxp3^{+}) from day 5 of culture and cells were incubated for 18 hours. Supernatants were then collected and **B)** IL-10 ELISAs were performed, data are from five experiments. Statistical significance was calculated using **A)** Two-way and **B)** One-way ANOVA, and error bars indicate standard error of the mean.

5.5 Blocking CTLA-4 and PD-1 during T cell activation helps to stablise the IS formation in Tg4 MBP peptide-primed iTregs

Morphological comparisons in section 4.7 show that Tg4 iTregs form a less stable IS during the first two minutes of T cell activation. In this chapter, we further investigated whether blocking both CTLA-4 and PD-1 would affect the IS formation upon Tg4 iTreg activation, induced by MBP Ac1-9 [4Y] peptide-primed PL8 cells. Before live cell imaging, we resuspended Tg4 iTregs in imaging buffer with anti-CTLA-4/PD-1, both in a final concentration of 10 µg/ml. To be consistent with iTregs analysed in section 4.7, LAT-GFP transduced iTregs were used (>75% Foxp3^{+}). DIC images were used for measuring morphological parameters. The three morphological ratios during the first two minutes of activation of Tg4 Teffs, iTregs and iTregs treated with anti-CTLA-4/PD-1 were compared. We first analysed experiments using MBP Ac1-9 [4K]-primed cells.

As previously observed in MBP peptide-primed T cells from section 4.7, Teffs formed a wider interface in the first two minutes of activation. In the group comparison, the ratio of interface width to cell width (Figure 5.4 A) of Teffs was significantly higher than that of iTregs at the 0s, 20s and 120s time points ($p<0.05$). The differences were prominent at the 0s and 20s time point ($p<0.01$). The result shows that the ratio of interface width to cell width of iTregs treated with ant-CTLA-4/PD-1 during their activation was higher than that of iTregs without treatments at all four time points ($p<0.05$), and the difference was highly significant at the 60s and 120s ($p<0.0001$) time point. While there were no significant differences observed when comparing this ratio of iTregs treated with anti-CTLA-4/PD-1 to that of Teffs, at all four time points. At the 60s and 120s time point, the mean ratio of interface width to cell width of iTregs treated with ant-CTLA-4/PD-1 was even higher than that of Teffs. These comparisons show that blocking both CTLA-4 and PD-1 during the first two minutes of MBP peptide-primed iTreg activation, significantly extended the interface of the IS, particularly at late time points. The dual mAb treated iTregs spread their cell membranes as Teffs did, during the first two minutes of cell coupling, which might be related with more stable synapse formation.

When comparing the ratios of lamella depth to cell depth among these three conditions, no significant differences were found at any time point (Figure 5.4 B), suggesting the dual mAb treatment does not change the length of the extended lamellae in MBP peptide-primed T cells.

The ratio of lamella depth to interface describes overall shapes of T cells during cell coupling. As shown in section 4.7, MBP peptide-primed iTregs showed a significantly higher

ratio of lamella depth to interface at the 0s ($p<0.0001$), 20s ($p<0.0001$) and 60s ($p<0.05$) time point, compared to Teffs (Figure 5.4 C). This ratio of iTregs treated with anti-CTLA-4/PD-1 was significantly lower than that of untreated iTreg at the 0s ($p<0.05$) time point. When comparing this ratio of anti-CTLA-4/PD-1 treated iTregs with that of Teffs, one significant difference was observed at the 20s time point ($p<0.01$). The dual mAb treatment ether eliminated or diminished the differences observed when comparing this ratio between Teffs and iTregs in the first minute of activation. These show that when treated with anti-CTLA-4/PD-1, MBP peptide-primed iTreg showed a more flattened or less elongated cell shape near the IS in the first minute of activation. This indicates that blocking CTLA-4/PD-1 might induce the formation of tighter cell couples during the activation of MBP peptide-primed iTregs.

In section 4.7, more MBP peptide-primed iTregs were found to form an extended lamella at early time points (0s and 20s) of activation, therefore, we investigated whether the dual mAb treatment would affect this. The result (Figure 5.4 D) shows that in MBP peptide-primed cells, no significant differences were found when comparing the frequency of cells with an extended lamella in iTregs treated with anti-CTLA-4/PD-1 and without. This frequency of iTregs with the treatment was still significantly higher than that in Teffs ($p<0.05$) at early time points, but the level of significance was lowered. This shows that blocking CTLA-4 and PD-1 during the activation of MBP peptide-primed iTregs, partially reduced the formation of an extended lamella in the first twenty seconds of cell coupling.

These results together suggest that the CTLA-4 and PD-1 dual blockade during the first two minutes of MBP peptide-primed iTreg activation helps to stabilise the IS and pulling the T cell, as well as the nucleus closer to the interface by extending the interface of the IS and partially shortening their extended lamellae. This help to form a more stable IS and enhances TCR-induced activation signalling.

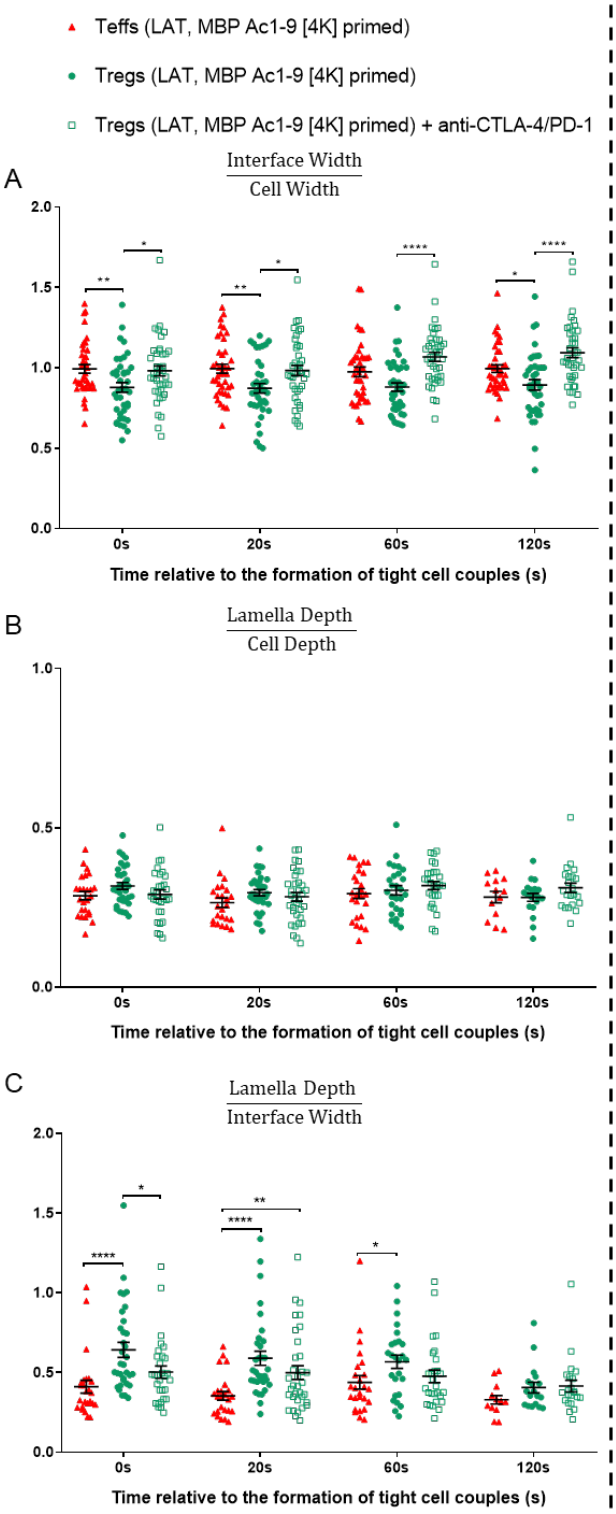
Teffs (LAT, MBP Ac1-9 [4K] primed)
Tregs (LAT, MBP Ac1-9 [4K] primed)
Tregs (LAT, MBP Ac1-9 [4K] primed) + anti-CTLA-4/PD-1
A
Interface Width / Cell Width
Time relative to the formation of tight cell couples (s)
B
Lamella Depth / Cell Depth
Time relative to the formation of tight cell couples (s)
C
Lamella Depth / Interface Width
Time relative to the formation of tight cell couples (s)
0s
20s
60s
120s

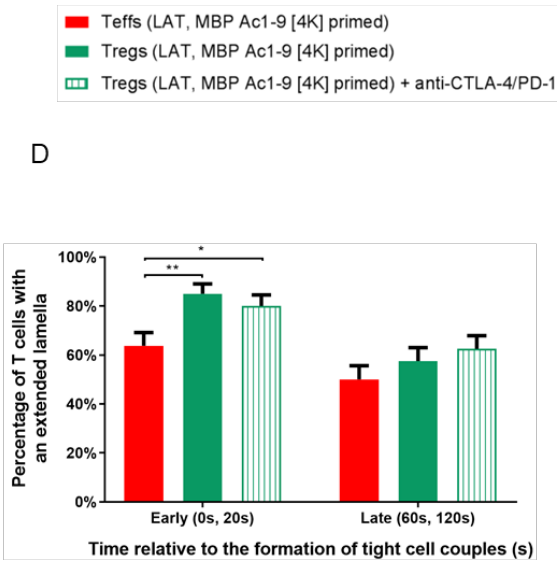
Teffs (LAT, MBP Ac1-9 [4K] primed)
Tregs (LAT, MBP Ac1-9 [4K] primed)
Tregs (LAT, MBP Ac1-9 [4K] primed) + anti-CTLA-4/PD-1
D
Percentage of T cells with an extended lamella
Early (0s, 20s)
Late (60s, 120s)
Time relative to the formation of tight cell couples (s)

Figure 5.4 The dual anti-CTLA-4/PD-1 blockade widens the interfaces of the IS and reduces the formation of extended lamellae during the activation of MBP Ac1-9 [4K]-primed iTregs.

LAT-GFP transduced MBP Ac1-9 [4K]-primed iTregs were activated with MBP Ac1-9 [4Y]-primed PL8 cells, with 10 µg/ml anti-CTLA-4/PD-1 mAbs and were imaged for 15 minutes. Four morphological parameters were measured within the first two minutes of activation and 0s indicates the time when a tight cell couple was formed. Data from untreated Teffs and iTregs refers to Figure 4.7. Comparing the ratios of **A)** interface width to cell width, **B)** lamella depth to cell depth, **C)** lamella depth to interface width of Teffs, untreated and anti-CTLA-4/PD-1 treated iTregs during the first two minutes of activation. **D)** Comparing the percentages of Teffs, untreated and anti-CTLA-4/PD-1 treated iTregs with an extended lamella region. 40 cell couples from two experiments for anti-CTLA-4/PD-1 treated iTregs were analysed. Statistical significance of log-transformed data was calculated using **A)** Two-way ANOVA or **B-C)** mixed-effect model as some values are not recorded for cells without an extended lamella. **D)** Statistical significance was calculated using Chi-square test. Asterisks indicate p-values (*<0.05, **<0.01, ****<0.0001). Error bars indicate standard error of the mean.

5.6 Blocking CTLA-4 and PD-1 partially increase overall and central LAT accumulation in MBP peptide-primed iTreg activation

Finally, we investigated whether CTLA-4 and PD-1 dual blockades would have effects on LAT accumulation at the IS during iTreg activation. MBP Ac-1-9 [4K]-primed iTregs transduced with LAT-GFP were blocked with anti-CTLA-4/PD-1 and live images were acquired. Anti-CTLA-4/PD-1 treated LAT-GFP transduced iTregs were >75% $Foxp3^{+}$. Spatiotemporal distributions of LAT-GFP in this condition were analysed and compared with data from MBP peptide-primed iTregs and Teffs.

Representative images show LAT-GFP accumulation during the activation of iTregs treated with anti-CTLA-4/PD-1 (Figure 5.5). We referred LAT-GFP imaging data from MBP peptide-primed Teffs and iTregs described in section 4.8, and compared them with data acquired from iTregs treated with anti-CTLA-4/PD-1. When CTLA-4 and PD-1 were blocked in MBP peptide-primed iTregs (Figure 5.6 C), LAT-GFP gradually accumulated at the interface and the accumulation peaked at the 0s time point with 42% of iTregs showing LAT-GFP accumulation at the IS. Afterwards, LAT-GFP accumulation remained relatively stable at the IS with minor fluctuations till the last time point, with 30% of iTregs treated with anti-CTLA-4/PD-1 showing LAT-GFP accumulation. In terms of accumulation patterns observed at the IS, LAT-GFP showed mainly central and invagination patterning in the first two minutes of activation in iTregs treated with anti-CTLA-4/PD-1. In addition, a few iTregs with the treatment displayed LAT-GFP asymmetric and diffuse accumulation patterns, but not dominantly. Upon activation, LAT-GFP also accumulated at the distal pole of iTregs treated with anti-CTLA-4/PD-1, as LAT-GFP distal accumulation increased rapidly from the -40s time point and peak at the 0s time points, with 38% of the cells showing distal LAT-GFP accumulation. Distal LAT-GFP accumulation swiftly diminished in the first minute of activation but >10% of the cells still showed such accumulation from the 60s to 180s time point.

Among MBP peptide-primed T cells, LAT-GFP overall accumulation at the interface of iTregs with the dual mAb treatment was compared with that of Teffs and iTregs. The peak of LAT-GFP accumulation in dual mAb treated iTregs appeared one minute earlier than that in iTregs without the treatment. Statistical analysis shows that the percentage of anti-CTLA-4/PD-1 treated iTregs with LAT-GFP overall accumulation at the IS was significantly higher than that of untreated iTregs at the 0s, 300s and 420s time points (Figure 5.6 D, the second row). When compared to Teffs, this percentage was significantly lower at the 20s and 40s time points (Figure 5.6 D, the third row). However, all these differences were no longer significant with the Bonferroni correction ($0.004<p<0.05$). Notably, fewer differences were

identified when comparing LAT-GFP overall accumulation in iTregs treated with anti-CTLA-4/PD-1 and Teffs (at two time points), than those found when comparing the accumulation in iTregs and Teffs (Figure 5.6 D, the first row, at eight time points). These results and comparisons indicate that blocking CTLA-4 and PD-1 during the activation of MBP primed iTregs partially restores the LAT overall accumulation at the IS, showing an earlier peak of accumulation.

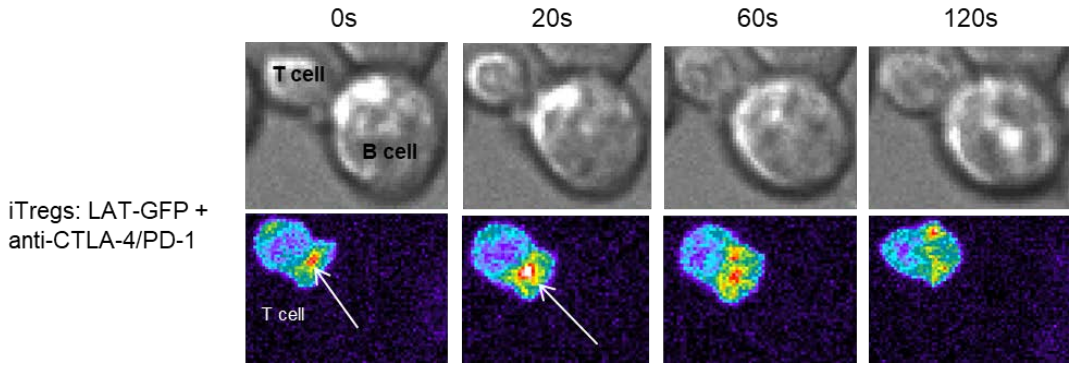

Figure 5.5 Representative live cell images showing LAT-GFP distribution in Tg4 iTregs in the first two minutes of T cell activation (0s, 20s, 60s and 120s time points), when CTLA-4 and PD-1 were blocked.

Top: DIC images from four time points. Bottom: matching top-down maximum projections of three-dimensional LAT-GFP fluorescent images (intensity is encoded in pseudocolour and increases from purple to red). Time is given in seconds relative to the formation of a tight cell couple and arrows denote accumulation of the sensor

A LAT-GFP, Teffs, MBP Ac1-9 [4K] primed

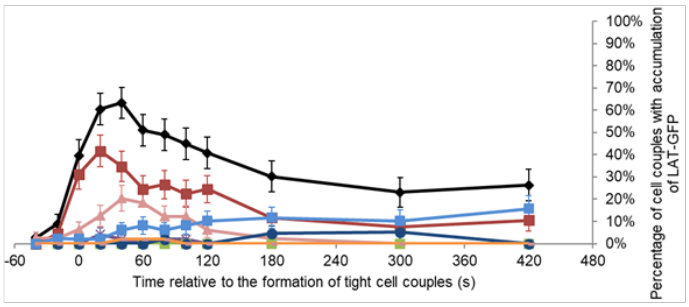

B LAT-GFP, Tregs, MBP Ac1-9 [4K] primed

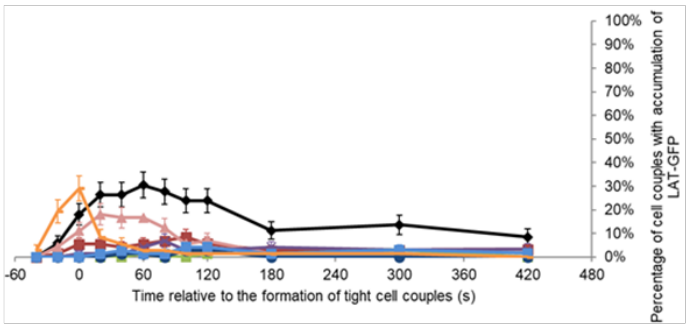

C LAT-GFP, Tregs + anti-CTLA-4/PD-1, MBP Ac1-9 [4K] primed

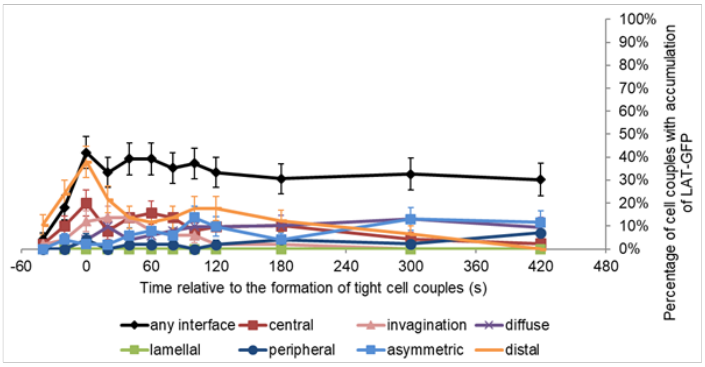

D Statistical comparison of any interface accumulation

Time (s)	-40	-20	0	20	40	60	80	100	120	180	300	420
Teffs vs Tregs	0.78	0.83	0.02	0.0004	0.0001	0.04	0.03	0.03	0.08	0.02	0.33	0.04
			*	***	***	*	*	*		*		*
Tregs vs Tregs + anti-CTLA-4/PD-1	0.34	0.080	0.0070	0.53	0.19	0.42	0.49	0.16	0.35	0.16	0.030	0.0098
			**								*	**
Teffs vs Tregs + anti-CTLA-4/PD-1	0.84	0.32	0.97	0.01	0.03	0.32	0.24	0.57	0.57	0.85	0.46	0.89
				*	*							

Figure 5.6 When CTLA-4 and PD-1 are blocked, overall LAT-GFP accumulation at the IS in early activation of MBP Ac1-9 [4K]-primed iTregs is increased.

LAT-GFP transduced MBP Ac1-9 [4K]-primed iTregs were activated by MBP Ac1-9 [4Y]-primed PL8 cells with a combined blockade of CTLA-4 and PD-1, and imaged for 15 minutes. Live cell images were analysed to identify the 0s time point when the IS was formed. Data from MBP Ac1-9 [4K]-primed **A)** Teffs and **B)** iTregs refer to Figure 4.10. **C)** Spatiotemporal distribution patterns of LAT-GFP for 12 time points in MBP Ac1-9 [4K]-primed iTregs blocked with anti-CTLA-4/PD-1 (48 cell couples analysed, two experiments). **D)** Comparisons of LAT-GFP accumulation among different cell types at the IS using a two proportion z-test. Numerals and asterisks indicate p-values, and asterisk colours denote whether differences remain significant with the Bonferroni correction (0.004<*<0.05, 0.004<**<0.01, 0.001<**<0.004, ***<0.001). Error bars indicate standard error of the mean.

We then investigated whether the dual blockade of CTLA-4 and PD-1 could change LAT central and invagination accumulation at the interface during MBP peptide-primed iTreg activation. During the activation of iTregs and anti-CTLA-4/PD-1 treated iTregs, no significant differences were found when comparing the percentages of iTregs with either LAT-GFP central or invagination accumulation at the interface (Figure 5.7 B). In both conditions, LAT-GFP central + invagination accumulation peaked at early time points (0s and 40s) and diminished afterwards. This percentage of Teffs was still higher than that of iTreg treated with anti-CTLA-4/PD-1 at most time points (0s-420s) and the differences were significant at the 20s, 40s, 100s and 120s time points (Figure 5.7 C). The difference was only significant at the 20s time point with the Bonferroni correction. When comparing this percentage between iTregs and Teffs, more differences were found (Figure 5.7 A). Therefore, when CTLA-4 and PD-1 are blocked, the amounts of LAT central and invagination accumulation at the interface during the early activation of MBP Ac1-9 [4K]-primed iTregs are almost unaffected.

When comparing only the central accumulation pattern, the percentage of iTregs blocked with anti-CTLA-4/PD-1 showing LAT-GFP central accumulation at the interface was higher than that of untreated iTregs at nine time points (Figure 5.8 B, -40s-80s, 120s and 180s). However, the difference was only significant at the 0s time point and was not with the Bonferroni correction ($0.004<p<0.05$). Teffs again showed more LAT-GFP central accumulation at most time points (0s-420s) and the percentage of Teffs showing central accumulation was significantly higher than that in iTregs treated with anti-CTLA-4/PD-1 at the 20s and 40s time point (Figure 5.8 C). The difference remained significant at the 20s time point with the Bonferroni correction ($p<0.001$). Thus, the dual CTLA-4 and PD-1 blockade slightly increases LAT central accumulation during MBP peptide-primed iTreg activation.

LAT-GFP invagination accumulation at the interface in iTegs treated with anti-CTLA-4/PD-1 was comparable to that in Teffs and iTregs, with fewer cells showing this accumulation from the 20s-80s time points (Figure 5.8 E-F). The invagination accumulation of LAT-GFP peaked at an early time point (20s or 40s) and gradually diminished after the peak, in all three cells types. No significant differences were identified when comparing this accumulation pattern between any two of the three conditions.

In summary, blocking CTLA-4 and PD-1 during early activation of MBP Ac1-9 [4K]-primed iTregs, partially increases LAT overall and central accumulation at the IS. These results are consistent with that from the morphological analysis in section 5.5, as they both indicate that

early activation of iTregs is enhanced when CTLA-4 and PD-1 coinhibitory pathways are blocked, showing more stable IS formation and partially enhanced LAT signalling.

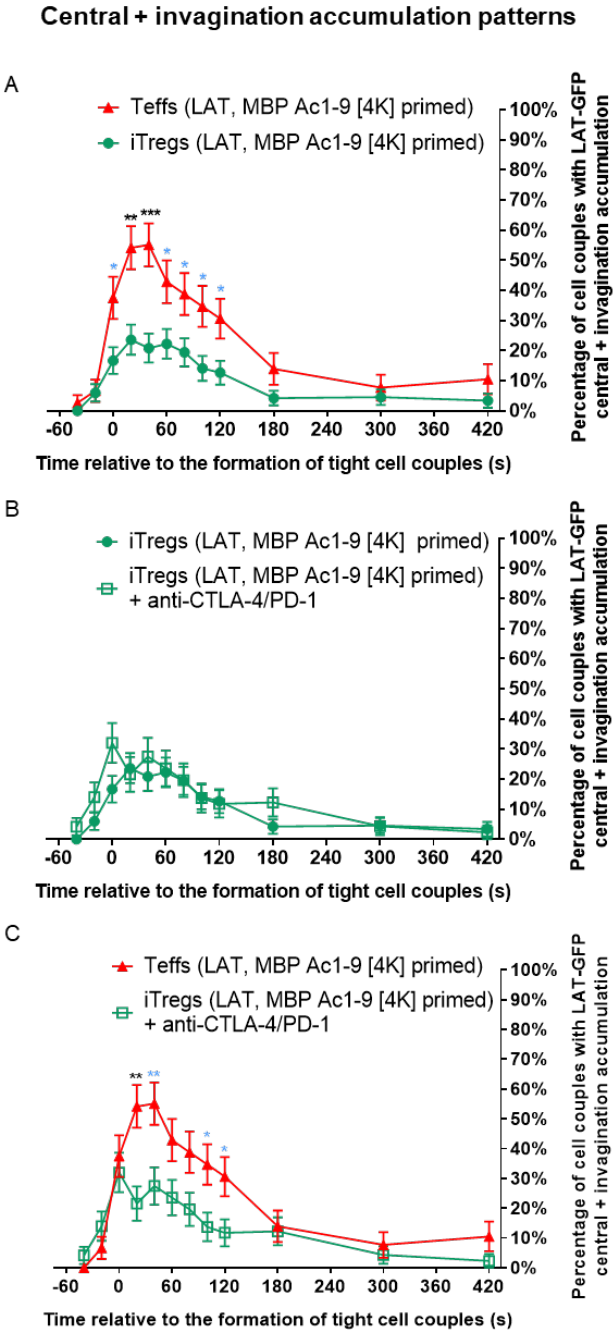

Figure 5.7 The percentage of iTregs with LAT-GFP central + invagination accumulation at the IS are comparable in untreated and CTLA-4/PD-1 blocked MBP Ac1-9 [4K]-primed iTregs.

LAT-GFP central + invagination patterning during T cell activation is compared between MBP Ac1-9 [4K]-primed **A)** Teffs and iTregs, **B)** iTregs and anti-CTLA-4/PD-1 treated iTregs, and **C)** Teffs and anti-CTLA-4/PD-1 treated iTregs. Data of Teffs and untreated iTreg refer to Figure 4.11 and 48 cell couples from two experiments for iTregs treated with anti-CTLA-4/PD-1 were analysed. A two proportion z-test was used to calculate statistical significance. Asterisks indicate p-values and colours indicate whether differences remain significant with the Bonferroni correction (0.004<*<0.05, 0.004<**<0.01, 0.001<**<0.004, ***<0.001). Error bars indicate standard error of the mean.

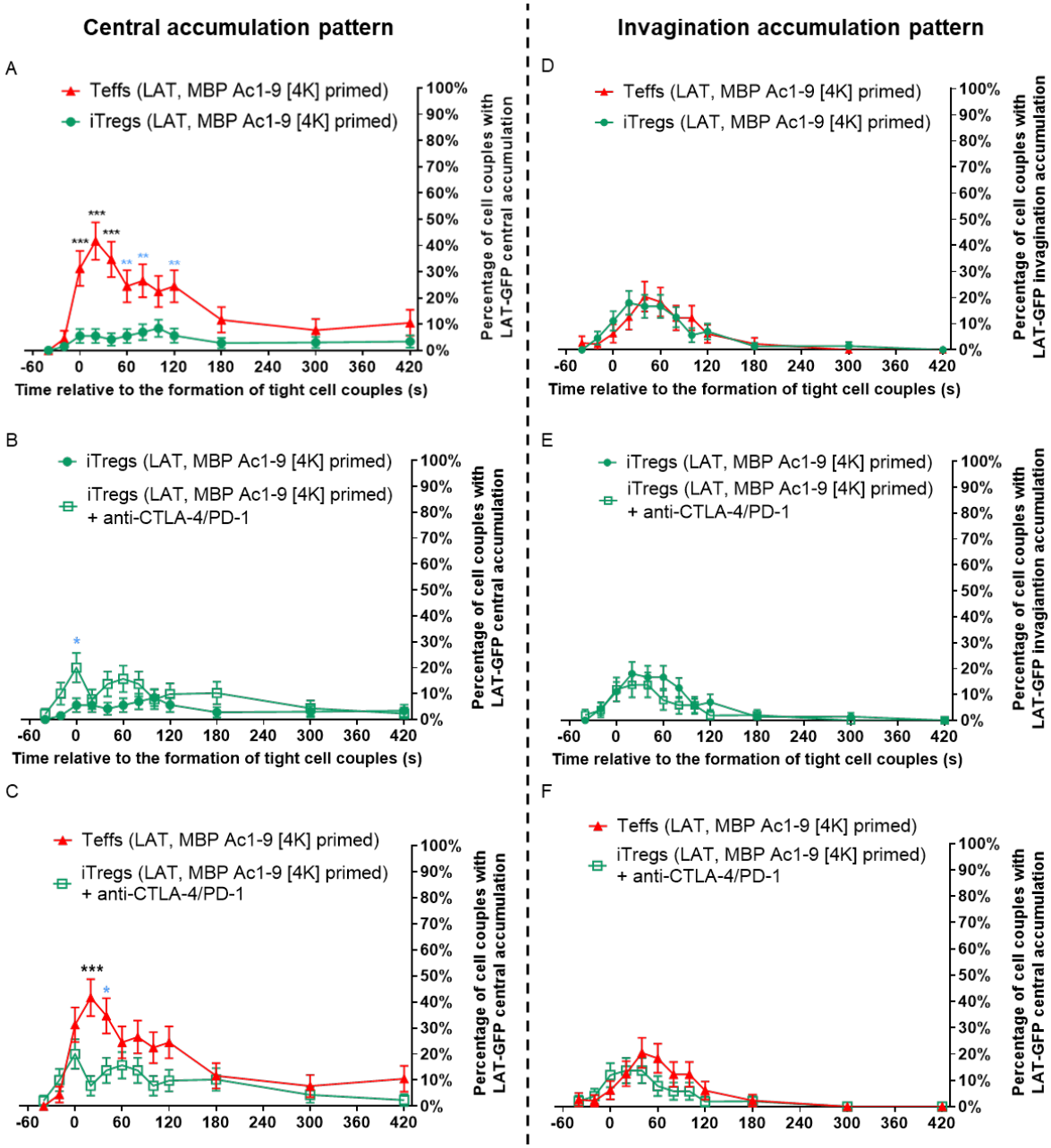

Figure 5.8 Blocking CTLA-4/PD-1 enhances LAT-GFP central accumulation during MBP Ac1-9 [primed] iTreg activation.

Comparing LAT-GFP **A-C)** central and **D-F)** invagination accumulation during the activation of MBP Ac1-9 [4K]-primed Teffs, iTregs and CTLA-4/PD-1 blocked iTregs. Data of Teffs and untreated iTregs refer to Figure 4.11 and 48 cell couples from two experiments for iTregs treated with anti-CTLA-4/PD-1 were analysed. Statistical significance was calculated with a two proportion z-test. Asterisks indicate p-values and colours indicate whether differences remain significant with the Bonferroni correction (0.004<*<0.05, 0.004<**<0.01, ***<0.001). Error bars indicate standard error of the mean.

5.7 Computational analyses show increased LAT accumulation at the IS of anti-CTLA-4/PD-1 treated iTregs

With the assistance of the 3D computational model, we built another 3D model map showing relative probabilities of LAT-GFP accumulation in MBP peptide-primed iTreg activation when blocked with anti-CTLA-4 and PD-1. We first compared the LAT-GFP enrichment at the defined IS region which shows the top 10% of the fluorescence of the three conditions. As shown previously in section 4.9, LAT-GFP enrichment at the IS of Teffs was higher than that of iTregs without the dual mAb treatment across all 12 time points (Figure 5.9 A). Significant differences were found at five time points, though none remained significant with the Bonferroni correction. When blocked with anti-CTLA-4/PD-1, higher levels of LAT-GFP enrichment at the IS of iTregs during their activation were also found at all 12 time points, compared to that of iTregs without the treatment (Figure 5.9 B), though a significant difference was only observed at the -40s time point. When compared to that of Teffs (Figure 5.9 C), less LAT-GFP enrichment was observed at the IS of iTregs treated with anti-CTLA-4/PD-1 at most time points (60s to 420s), but the difference was only significant at the 420s time point ($p<0.01$). These observations together show that the level of differences of LAT-GFP enrichment observed during the activation of Teffs and iTregs was lowered, when CTLA-4/PD-1 pathways were blocked in iTregs. This suggests that blocking CTLA-4/PD-1 during iTreg activation help to transport LAT to the IS.

LAT-GFP enrichment in the centre of the IS of Teffs was higher than that of iTregs at all 12 time points and significant differences were found at five time points, which were not significant with the Bonferroni correction (Figure 5.9 D). Blocking CTLA-4/PD-1 did not enhance LAT-GFP central accumulation at the interface in iTregs, as iTregs with and without the treatment showed comparable LAT-GFP enrichment in the central region during activation (Figure 5.9 E). It is notable that the level of differences was increased when comparing LAT-GFP enrichment in the central region of the IS of Teffs and iTregs with the dual mAb treatment (Figure 5.9 F). Significant differences were found at more time points (20s, 60s-420s) and were prominent at the 120s, 180s and 420s ($p<0.004$). Therefore, blocking CTLA-4/PD-1 results in a slight reduction of LAT accumulation in the central core of the IS during iTreg activation.

In summary, computational analysis shows that blocking CTLA-4 and PD-1 pathways during MBP peptide-primed iTreg activation enhances LAT accumulation at the IS but slightly downregulates LAT accumulation in the central core of the IS. These are partially consistent with the observations from the spatiotemporal distribution analysis in section 5.6. An increased overall LAT accumulation at the IS of CTLA-4 and PD-1 blocked iTregs is

detected by both spatiotemporal patterning and computational analysis but decreased LAT accumulation in the central core is found by the latter, though the reduction is mild. However, the computational system detects fewer cells couples and does not distinguish LAT-GFP central and invagination accumulation, which are both detected in the central core. This might explain the inconsistency. In general, both spatiotemporal pattern-based and computational analysis show that the impacts of CTLA-4/PD-1 blockades on central + invagination accumulation of LAT during MBP peptide iTreg activation is minor and the former identifies partially enhanced LAT central accumulation induced by the dual blockade.

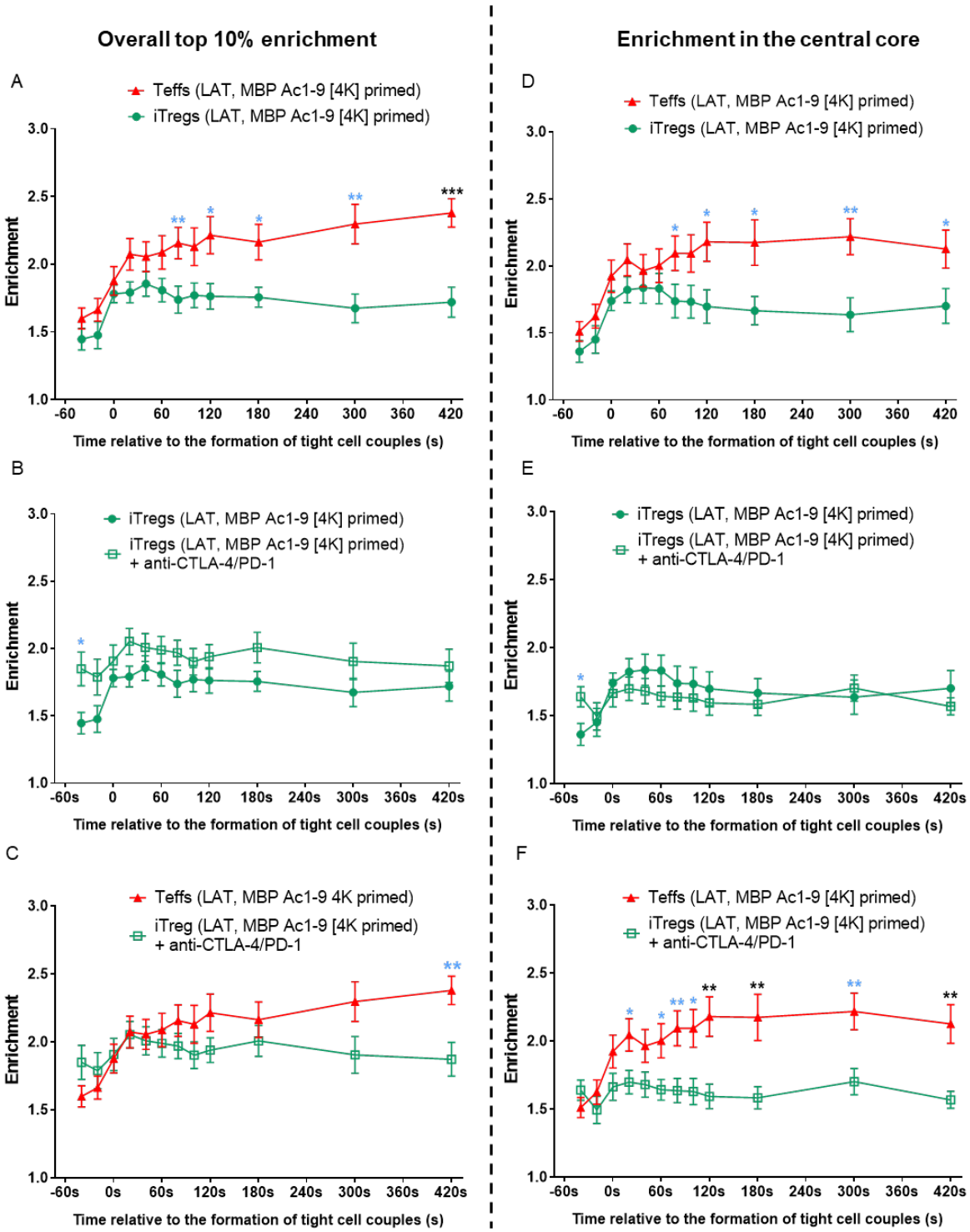
Overall top 10% enrichment
Enrichment in the central core
A
B
C
D
E
F
Teffs (LAT, MBP Ac1-9 [4K] primed)
iTregs (LAT, MBP Ac1-9 [4K] primed)
iTregs (LAT, MBP Ac1-9 [4K] primed) + anti-CTLA-4/PD-1
Teffs (LAT, MBP Ac1-9 4K primed)
iTreg (LAT, MBP Ac1-9 [4K primed) + anti-CTLA-4/PD-1
Enrichment
Time relative to the formation of tight cell couples (s)

Figure 5.9 Computational analysis show that anti-CTLA-4/PD-1 enhances overall LAT-GFP accumulation during the activation of MBP Ac1-9 [4K]-primed iTregs.

LAT-GFP accumulation in anti-CTLA-4/PD-1 treated iTregs were computationally analysed and 3D model maps were generated. Comparing LAT-GFP enrichment in the defined IS region (top 10% enrichment) during the activation of MBP Ac1-9 [4K]-primed **A)** Teffs and iTregs, **B)** iTregs and anti-CTLA-4/PD-1 treated iTregs, **C)** Teffs and anti-CTLA-4/PD-1 treated iTregs. Comparing LAT-GFP enrichment in the central core of the IS during the activation of MBP Ac1-9 [4K]-primed **D)** Teffs and iTregs, **E)** iTregs and anti-CTLA-4/PD-1 treated iTregs, **F)** Teffs and anti-CTLA-4/PD-1 treated iTregs. Data of Teffs and iTregs refer to Figure 4.13 and 4.14, and 26 cell couples from two experiments for anti-CTLA-4/PD-1 treated iTregs were analysed. Log-transformed data were analysed with unpaired Student's T-test to calculate statistical significance. Asterisks indicate p-values and colours indicate whether differences remain significant with the Bonferroni correction (0.004<*<0.05, 0.004<**<0.01, *<0.004). Error bars indicate standard error of the mean.

5.8 Anti-CD3/28-primed iTregs show complex phenotypes in response to CTLA-4 and PD-1 blockades during activation

As shown in chapter 4, MBP peptide-primed and anti-CD3/28-primed iTregs have some differences in spatiotemporal patterns of LAT-GFP and TCR-ζ-GFP, which indicates that their proximal T cell signalling events are not entirely the same. To verify whether blocking CTLA-4 and PD-1 has the same effects on both types of iTregs, we repeated some imaging experiments using anti-CD3/28-primed, LAT-GFP transduced iTregs (>75% $Foxp3^+$). Moreover, we included additional data from treatments using single blockades (only anti-CTLA-4 or anti-PD-1) to investigate their impacts during iTreg activation.

However, blockades of CTLA-4, PD-1 and both induced fairly complicated responses of anti-CD3/28-primed iTregs. In brief, morphological analyses in the first two minutes of activation (Figure 5.10) show that blocking either CTLA-4, PD-1 or both, widens the interface of contact but results in the formation of longer extended lamellae and more elongated cell shapes of anti-CD3/28-primed iTregs. As wider interfaces and shorter lamellae are signs for stable IS formation, it is difficult to judge whether these treated ant-CD3/28-primed iTregs were forming stable or labile cell couples.

Moreover, anti-CTLA-4, anti-PD-1 and their combination regulate the spatiotemporal organisation of LAT differently in the first several minutes of anti-CD3/28-primed iTreg activation (Figure 5.11-13). Anti-CTLA-4 enhanced both LAT overall and central accumulation, while anti-PD-1 affected neither. Blocking both CTLA-4 and PD-1 in early anti-CD3/28-primed iTreg activation significantly reduced LAT overall accumulation and barely changed LAT central accumulation (untreated iTregs shows low LAT central accumulation in the first place). Although blocking CTLA-4 alone promotes anti-CD3/28-primed iTreg activation, dual CTLA-4 and PD-1 blockade has the opposite effect. Therefore, anti-CD3/28-primed iTreg have continuously shown phenotypes that are different to that of MBP peptide-primed iTregs.

The rest of this section show figures describing observations that we have summarised above. It should be noted that currently, we are not able to fully explain the mechanisms of these results, as parallel experiments (i.e. blocking CTLA-4 and PD-1 separately) were not conducted on MBP peptide-primed iTregs.

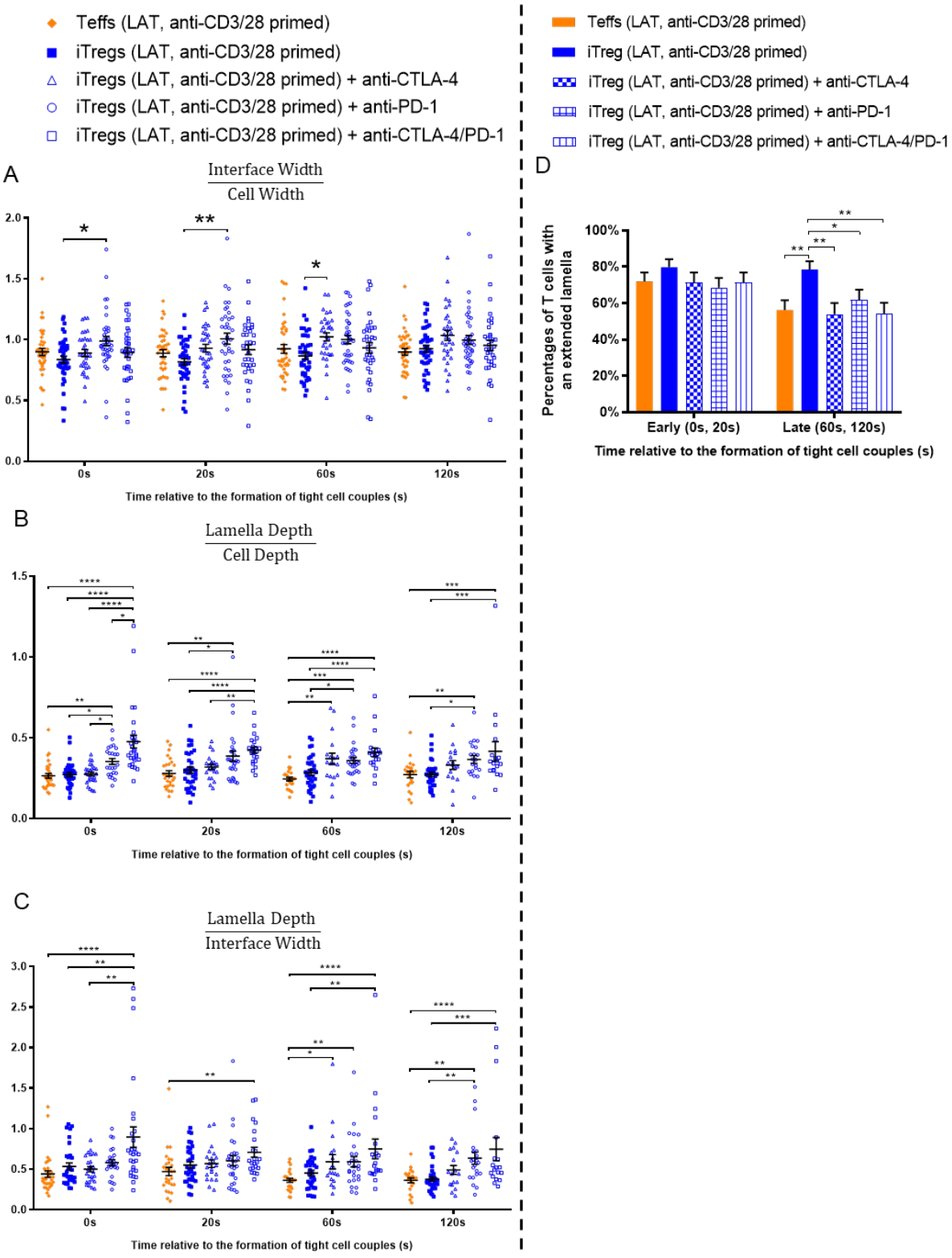
Teffs (LAT, anti-CD3/28 primed)
iTregs (LAT, anti-CD3/28 primed)
iTregs (LAT, anti-CD3/28 primed) + anti-CTLA-4
iTregs (LAT, anti-CD3/28 primed) + anti-PD-1
iTregs (LAT, anti-CD3/28 primed) + anti-CTLA-4/PD-1
A
Interface Width / Cell Width
Time relative to the formation of tight cell couples (s)
B
Lamella Depth / Cell Depth
Time relative to the formation of tight cell couples (s)
C
Lamella Depth / Interface Width
Time relative to the formation of tight cell couples (s)
0s
20s
60s
120s
Teffs (LAT, anti-CD3/28 primed)
iTreg (LAT, anti-CD3/28 primed)
iTreg (LAT, anti-CD3/28 primed) + anti-CTLA-4
iTreg (LAT, anti-CD3/28 primed) + anti-PD-1
iTreg (LAT, anti-CD3/28 primed) + anti-CTLA-4/PD-1
D
Percentages of T cells with an extended lamella
Early (0s, 20s)
Late (60s, 120s)
Time relative to the formation of tight cell couples (s)

Figure 5.10 T cell morphological analysis of anti-CD3/28-primed Teffs, iTregs, iTregs treated with anti-CTLA-4, anti-PD-1 and both mAbs, during the first two minute of activation.

LAT-GFP labelled anti-CD3/28-primed iTregs were activated with MBP Ac1-9 [4Y]-primed PL8 cells, with 10 µg/ml anti-CTLA-4, anti-PD-1 or both mAbs and were imaged for 15 minutes. Four morphological parameters were measured within the first two minutes of activation and 0s indicates the time when a tight cell couple was formed. Data from untreated Teffs and iTregs refers to Figure 4.8. Comparing the ratios of **A)** interface width to cell width, **B)** lamella depth to cell depth, **C)** lamella depth to interface width of Teffs, untreated, anti-CTLA-4, anti-PD-1 and anti-CTLA-4/PD-1 treated iTregs during the first two minutes of activation. **D)** Comparing the percentages of Teffs, untreated, anti-CTLA-4, anti-PD-1 and anti-CTLA-4/PD-1 treated iTregs with an extended lamella. Cell couples of iTregs analysed: 33 from two experiments (anti-CTLA-4), 38 from two experiments (anti-PD-1) and 35 from two experiments (anti-CTLA-4/PD-1). Statistical significance of log-transformed data was calculated using **A)** Two-way ANOVA or **B-C)** mixed-effect model as zero values were not analysed for cells without an extended lamella. **D)** Statistical significance was calculated using Chi-square test. Asterisks indicate p-values (*<0.05, **<0.01, ***<0.001, ****<0.0001). Error bars indicate standard error of the mean.

A LAT-GFP, Teffs, anti-CD3/28 primed

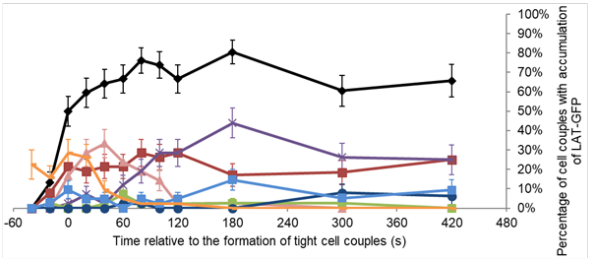

B LAT-GFP, iTregs, anti-CD3/28 primed

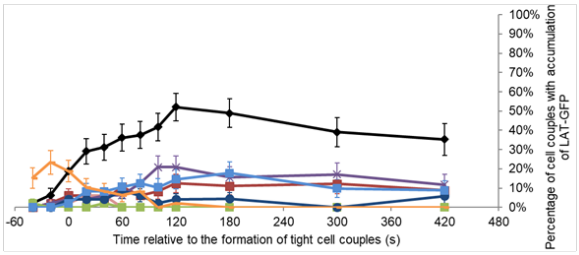

C LAT-GFP, iTregs + anti-CTLA-4, anti-CD3/28 primed

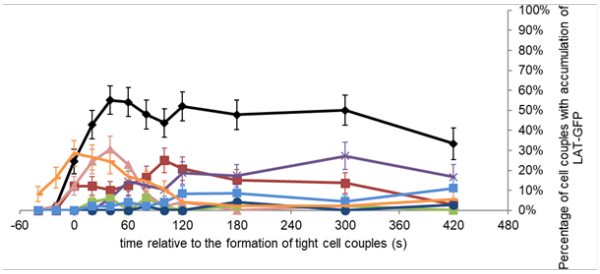

D LAT-GFP, iTregs + anti-PD-1, anti-CD3/28 primed

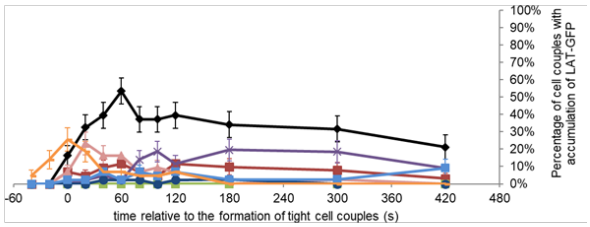

E LAT-GFP, iTregs + anti-CTLA-4/PD-1, anti-CD3/28 primed

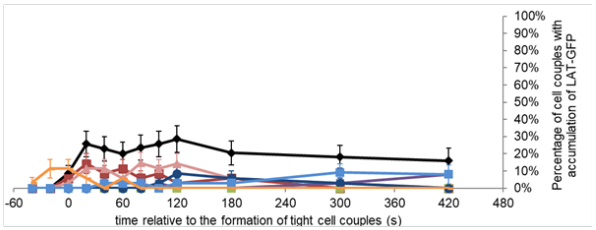

F Statistical comparison of any interface accumulation

Time (s)	-40	-20	0	20	40	60	80	100	120	180	300	420
Teffs vs iTregs	0.84	0.49	0.004	0.007	0.004	0.008	0.0005	0.004	0.23	0.005	0.09	0.03
			**	**	**	**	***	**		**		*
iTregs vs iTregs + anti-CTLA-4	1	0.6	0.7	0.2	0.03	0.1	0.4	1	0.8	0.9	0.4	0.9
					*							
Teffs vs iTregs + anti-CTLA-4	-	0.1	0.02	0.2	0.5	0.3	0.01	0.008	0.2	0.003	0.5	0.02
			*				*	**		**		*
iTregs vs Tregs + anti-PD-1	1	0.3	1	0.9	0.5	0.2	0.9	0.8	0.3	0.2	0.6	0.32
Teffs vs iTregs + anti-PD-1	-	0.05	0.002	0.02	0.04	0.3	0.0007	0.001	0.02	5.9E-05	0.02	0.0008
		*	**	*	*		***	**	*	****	*	***
iTregs vs iTregs + anti-CTLA-4/PD-1	0.85	0.35	0.32	0.92	0.55	0.18	0.27	0.20	0.06	0.02	0.09	0.18
										*		
Teffs vs iTregs + anti-CTLA-4/PD-1	-	0.08	0.0003	0.006	0.007	0.0001	1.4E-05	7E-05	0.002	7.7E-07	0.0007	0.0005
			***	**	**	***	****	****	**	****	***	***

Figure 5.11 Blocking CTLA-4 enhances, but blocking both CTLA-4 and PD-1 reduces LAT-GFP overall accumulation at the IS during the activation of anti-CD3/28-primed iTregs.

LAT-GFP transduced anti-CD3/28-primed iTregs were activated by MBP Ac1-9 [4Y]-primed PL8 cells, and blocked with anti-CTLA-4, anti-PD-1 or both mAbs. Cells were imaged using spinning disk confocal microscopy for 15 minutes. DIC and GFP images were analysed to identify T cell-APC cell interactions. LAT-GFP spatiotemporal accumulation data of **A)** Teffs and **B)** iTregs refer to Figure 4.10. Spatiotemporal distribution patterns of LAT-GFP during the activation of **C)** anti-CTLA-4 treated anti-CD3/28-primed iTregs, (33 cell couples from two experiments), **D)** anti-PD-1 treated anti-CD3/28-primed iTregs (38 cell couples from two experiments), **E)** anti-CTLA-4/PD-1 treated anti-CD3/28-primed iTregs (35 cell couples analysed from two experiments. **F)** Comparisons of LAT-GFP overall accumulation at the IS among different cell types using a two proportion z-test. Numerals and asterisks indicate p-values, and asterisk colours indicate whether differences remain significant with the Bonferroni correction (0.004<*<0.05, 0.004<**<0.01, 0.001<**<0.004, ***<0.001, ****<0.0001). Error bars indicate standard error of the mean.

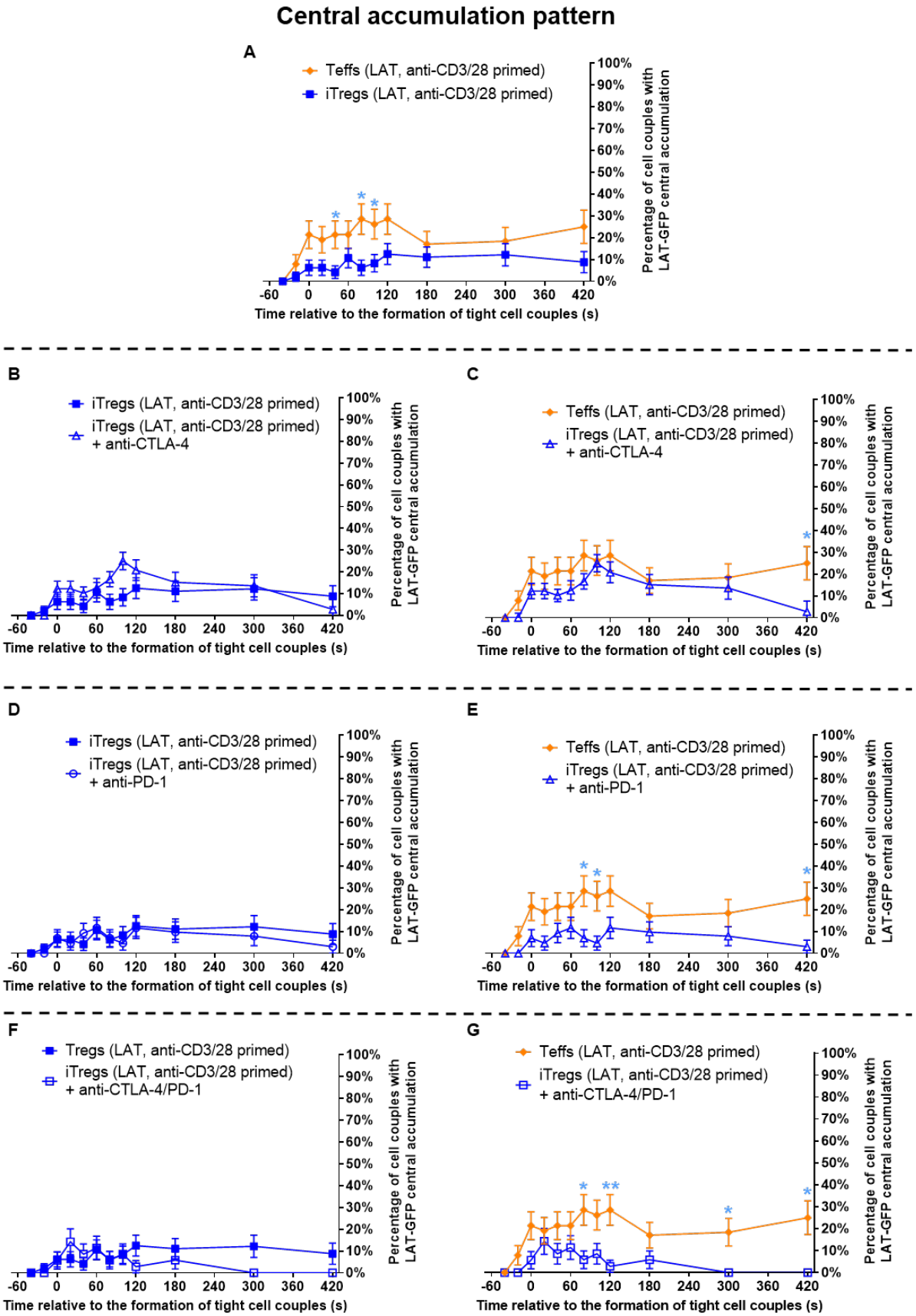
Central accumulation pattern
A
Teffs (LAT, anti-CD3/28 primed)
iTregs (LAT, anti-CD3/28 primed)
Percentage of cell couples with LAT-GFP central accumulation
Time relative to the formation of tight cell couples (s)
B
iTregs (LAT, anti-CD3/28 primed)
iTregs (LAT, anti-CD3/28 primed) + anti-CTLA-4
C
Teffs (LAT, anti-CD3/28 primed)
iTregs (LAT, anti-CD3/28 primed) + anti-CTLA-4
D
iTregs (LAT, anti-CD3/28 primed)
iTregs (LAT, anti-CD3/28 primed) + anti-PD-1
E
Teffs (LAT, anti-CD3/28 primed)
iTregs (LAT, anti-CD3/28 primed) + anti-PD-1
F
Tregs (LAT, anti-CD3/28 primed)
iTregs (LAT, anti-CD3/28 primed) + anti-CTLA-4/PD-1
G
Teffs (LAT, anti-CD3/28 primed)
iTregs (LAT, anti-CD3/28 primed) + anti-CTLA-4/PD-1

Figure 5.12 Blocking CTLA-4 enhances LAT-GFP central accumulation at the IS during the activation of anti-CD3/28-primed iTregs.

LAT-GFP central accumulation at the interface is compared between anti-CD3/28-primed **A)** Teffs and iTregs, **B)** iTregs and anti-CTLA-4 treated iTregs, **C)** Teffs and anti-CTLA-4 treated iTregs, **D)** iTregs and anti-PD-1 treated iTregs, **E)** Teffs and anti-PD-1 treated iTregs, **F)** iTregs and anti-CTLA-4/PD-1 treated iTregs and **G)** Teffs and anti-CTLA-4/PD-1 treated iTregs. Data of Teffs and untreated iTreg refer to Figure 4.11, 33 cell couples from two experiments for iTregs treated with anti-CTLA-4, 38 cell couples from two experiments for iTregs treated with anti-PD-1 and 35 cell couples from two experiments for iTregs treated with anti-CTLA-4/PD-1 were analysed. A two proportion z-test was used to calculate statistical significance. Asterisks indicate p-values and differences observed were not significant with the Bonferroni correction ($0.004<*<0.05$, $0.004<**<0.01$). Error bars indicate standard error of the mean.

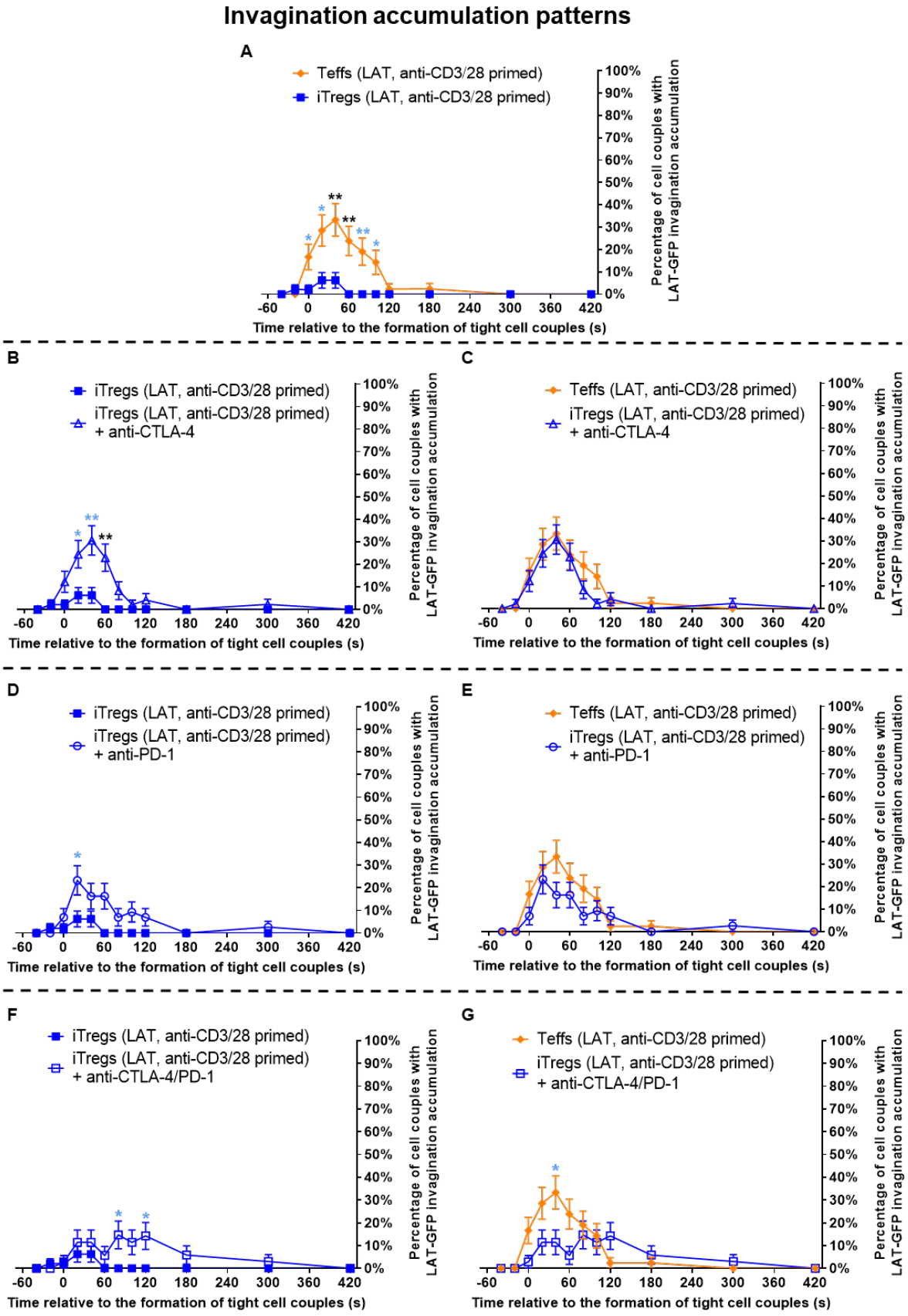
Invagination accumulation patterns
A
Teffs (LAT, anti-CD3/28 primed)
iTregs (LAT, anti-CD3/28 primed)
Percentage of cell couples with LAT-GFP invagination accumulation
Time relative to the formation of tight cell couples (s)
B
iTregs (LAT, anti-CD3/28 primed)
iTregs (LAT, anti-CD3/28 primed) + anti-CTLA-4
C
Teffs (LAT, anti-CD3/28 primed)
iTregs (LAT, anti-CD3/28 primed) + anti-CTLA-4
D
iTregs (LAT, anti-CD3/28 primed)
iTregs (LAT, anti-CD3/28 primed) + anti-PD-1
E
Teffs (LAT, anti-CD3/28 primed)
iTregs (LAT, anti-CD3/28 primed) + anti-PD-1
F
iTregs (LAT, anti-CD3/28 primed)
iTregs (LAT, anti-CD3/28 primed) + anti-CTLA-4/PD-1
G
Teffs (LAT, anti-CD3/28 primed)
iTregs (LAT, anti-CD3/28 primed) + anti-CTLA-4/PD-1

Figure 5.13 Blocking CTLA-4 restores LAT-GFP invagination accumulation at the IS during the activation of anti-CD3/28-primed iTregs.

Comparisons of LAT-GFP invagination accumulation at the interface between anti-CD3/28-primed **A)** Teffs and iTregs, **B)** iTregs and anti-CTLA-4 treated iTregs, **C)** Teffs and anti-CTLA-4 treated iTregs, **D)** iTregs and anti-PD-1 treated iTregs, **E)** Teffs and anti-PD-1 treated iTregs, **F)** iTregs and anti-CTLA-4/PD-1 treated iTregs and **G)** Teffs and anti-CTLA-4/PD-1 treated iTregs. Data of Teffs and untreated iTreg refer to Figure 4.11, 33 cell couples from two experiments for iTregs treated with anti-CTLA-4, 38 cell couples from two experiments for iTregs treated with anti-PD-1 and 35 cell couples from two experiments for iTregs treated with anti-CTLA-4/PD-1 were analysed. At two proportion z-test was used to calculate statistical significance. Asterisks indicate p-values and differences observed were not significant with the Bonferroni correction (0.004<*<0.05, 0.004<**<0.01, **<0.004). Error bars indicate standard error of the mean.

5.9 Discussion

In summary, dual CTLA-4 and PD-1 blockade inhibits generation of Tg4 Foxp3$^+$ iTregs and slightly enhances IFN-γ and IL-10 secretion during Teff and iTreg development. Blocking both CTLA-4 and PD-1 also improves iTreg activation and enhances LAT overall accumulation at the T cell-APC interface. These results were acquired using MBP peptide-primed cells. Anti-CD3/28-primed iTregs treated with anti-CTLA-4, anti-PD-1 and both mAbs display complex and elusive phenotypes in early activation, which are different to that of MBP peptide-primed iTregs. However, peptide-primed iTregs are more physiologically relevant to naturally occurring Tregs while antibody-primed iTregs do not receive cytokine signals and direct regulation from APCs upon cell priming, and they show different phenotypes (discussed in section 3.8). Therefore, we mainly address the research questions in this chapter based on data generated using peptide-primed Teffs and iTregs.

5.9.1 CLTA-4 and PD-1 play roles in Treg differentiation and regulatory function

Tregs express CTLA-4, PD-1 and PD-L-1 which play roles in Treg-mediated suppression and tolerance (247). Blocking CTLA-4, PD-1 or both coinhibitory pathways significantly downregulates induction of Tg4 Foxp3$^+$ iTregs, which could be observed on day 3 to 6 of culture. The effects are cumulative as the combination of both mAbs most significantly reduces the frequency of Tg4 Foxp3$^+$ iTregs.

CTLA-4 contributes to self-tolerance maintained by Tregs and CTLA-4 deficiency impairs their suppressive function (246, 250). However, *in vivo* studies show that CTLA-4 blockade enhances proliferation of Foxp3$^+$ Tregs in mice and human (264, 265). Moreover, previous work by Verhagen *et a*l shows that CTLA-4KO Tg4 mice are resistant to induction of EAE, owing to an increased number of Foxp3$^+$ Tregs in the thymus and spleen (266). Later the same group found that CTLA-4 is expressed in the thymus of Tg4 T cells, and deletion of CTLA-4 skews thymocytes towards a Foxp3$^+$ Treg phenotype by modulating TCR repertoire (267). These results suggest that CTLA-4 regulates the development of tTregs and control their expansion in the periphery. A subsequent study shows that deficiency of CTLA-4 impairs Tg4 Foxp3$^+$ iTreg differentiation (268), which is consistent with our results. CTLA-4 likely plays different roles in regulating the development of naturally occurring and extrathymically induced Tregs (268). PD-1-PD-L1 pathway regulates Treg-mediated suppression and peripheral tolerance. PD-1 expression on Tregs inhibits PD-1L$^+$ CD8$^+$ T cell proliferation during infection and PD-L1 promotes conversion and maintenance of iTregs (258, 269). PD-1 blockade significantly reduces the suppressive activity of Tregs (258). Tumour-infiltrating Tregs also express high levels of both CTLA-4 and PD-1, which contribute to Treg-mediated suppression in the tumour microenvironment (270). A recent

study shows that the combination of anti-CTLA-4 and anti-PD-1 also additively reduces the frequencies of Tregs, and promotes the expansion of $CD4^+$ and $CD8^+$ Teffs in a murine tumour (271). In summary, CTLA-4 and PD-1 are key modulators of the immunosuppressive function of Tregs and blocking their corresponding coinhibitory pathways impairs the induction of iTregs.

5.9.2 Dual blockade of CTLA-4 and PD-1 enhances cytokine secretion by promoting T cell activation

Blocking both CTLA-4 and PD-1 during the induction of Tg4 Teffs and iTregs tends to promote cytokine production detected in cell cultures. The enhancement is more obvious on IFN-γ production by Teff-inducing cells. Moreover, iTreg-inducing cells treated with the dual blockade secreted more IL-10 at later stages of induction (day 5 and 6). As described in chapter 4, Tg4 iTregs hold a weaker ability to secrete IFN-γ but are potentially more capable of secreting IL-10, while Teffs secrete both cytokines with a slightly weaker ability to maintain IL-10 production at later stages of induction. Our results suggest that blocking both CTLA-4 and PD-1 coinhibitory pathways promotes T cell activation (possibly by enhancing CD28 costimulation) in initial priming of Teffs and iTregs, which is likely to enhance their intrinsic cytokine-secreting abilities. In other words, when these two coinhibitory pathways are blocked, Teffs and iTregs potentially secrete more IFN-γ and IL-10 respectively. However, it should be noted that anti-CTLA-4, anti-PD-1 and their combination reduce frequencies of $Foxp3^+$ cells during iTreg induction. Therefore, it is unclear whether increased IL-10 production induced by blockades was purely owing to an increasing ratio of Teffs to iTregs in iTreg-inducing conditions. Ideally, staining these cells for Foxp3, T-bet, IFN-γ and IL-10 together would help to address this question. Moreover, investigating CTLA-4 and PD-1 expression on Tg4 Teffs and iTregs would also be useful for assessing direct impacts of the blockades on these cells.

5.9.3 Blocking both CTLA-4 and PD-1 improves iTreg activation and partially restores LAT overall accumulation

Morphological analyses show that in the first two minutes of activation, anti-CTLA-4/PD-1 treated iTregs formed a wider interface of contact, compared to untreated iTregs. These results suggest that anti-CTLA-4/PD-1 dual blockade helps to stabilise the IS formation of iTregs and enhances activation. However, the continuous extension of the T cell-APC interface is not required at later stages of activation. In T-B cell interactions, after the contact length of the interface and $Ca2^+$ signalling reach their peak level, T cells enter a stabilisation phase and partially retracts from the B cell, which causes cell rounding (163). During interactions of T cells with B cells or DCs, stable conjunctions and effective T cell activation are correlated with a round cell shape (163, 164). The relative interface width of

anti-CTLA-4/PD-1 treated iTregs was even wider than that of Teffs at late time points (60s and 120s), suggesting that that the dual blockade of CTLA-4 and PD-1 might excessively extend that interface of contact and might prevent cell rounding. Their activation might not be as efficient as that of Teffs.

Spatiotemporal patterning analyses also indicate that iTreg activation is improved by blocking CTLA-4 and PD-1 during activation. Dual blockade of CTLA-4 and PD-1 partially increases LAT overall accumulation at the interface upon iTreg activation. However, impaired LAT central accumulation at the interface is only slightly enhanced by the dual blockade, suggesting the dual blockade has limited effects on the cSMAC assembly. Clark *et al* have shown that cSMAC associated signalling intermediates such as LAT, Grb2 and SLP-76, are rapidly recruited to the centre of the interface in early T cell activation and transient LAT accumulation at the interface centre is associated with efficient IL-2 production (126). Moreover, costimulation blockade also impairs LAT overall and central accumulation and downregulates IL-2 secretion (126). CTLA-4 and PD-1 both downregulate CD28 induced costimulation and inhibit T cell proliferation and survival (247, 256). Most likely, inefficient iTreg activation partially contributes to their expression of CTLA-4 and PD-1. Therefore, blocking CTLA-4 and PD-1 enhances costimulation and partially improves proximal T cell signalling in iTreg activation.

To understand the respective roles of CTLA-4 and PD-1 play in iTreg activation, the same imaging experiments will need to be conducted on MBP peptide-primed iTregs treated with only CTLA-4 or PD-1. Although data acquired using anti-CD3/28-primed iTregs suggest that impacts of anti-CTLA-4, anti-PD-1 and their combination on iTreg activation are different, it is uncertain whether the same results would be observed in MBP peptide-primed iTregs.

Chapter 6 Enhanced LAT localisation at the T cell-APC interface stabilises IS formation and tends to regulate IL-10 and IFN-γ secretion of iTregs

6.1 Introduction

The formation of the IS provides a fundamental scaffold for sustained TCR engagement with pMHC and signal transduction for T cell activation (120). During such process, polarisation and clustering of various signalling intermediates including receptors, kinases, adaptor proteins and cytoskeletal compartments are highly diverse in time and space (130). Segregation of these molecules into spatial domains, the supramolecular activation clusters, are required for efficient T cell activation (121). Supramolecular complexes consist of thousands of molecules which closely interact with each other. Upon TCR-induced activation, phosphorylated LAT nucleates a multiple signalling complex including Grb2, PLC-γ1, Gads, Sos1, and SLP-76 (185), forming the LAT signalosome, as part of the central supramolecular activation cluster (cSMAC). When recruited by LAT to the membrane, Grb2 binds Sos1 and together can form a 2:1 complex, which cross-links LAT molecules and induces oligomerisation of LAT (272). For protein-protein interactions, the number of bindng motifs is critical and we refer that as the valence (126). For example, Gads can bind two tyrosine-containing motifs of LAT via its SH2 domain, thus the valence of LAT for Gads can range from 0 to 2 (185). Therefore multivalent protein interactions contribute to LAT clustering and allow the formation of supramolecular complexes.

Upon full stimulus conditions, LAT shows a distinct preference for central localisation at the T cell-APC interface in the first two minutes of activation in 5C.C7 T cells (126), as well as in Tg4 Teffs in this project. Attenuation of T cell activation can be achieved by costimulation blockade or Itk-deficiency, which leads to diminished tyrosine phosphorylation and partial loss of the valence in the LAT signalosome (126). This subsequently reduces LAT central localisation at the interface and IL-2 production. The V3 domain of PKC-θ contains a proline-rich motif which associates with CD28 and is required for the localisation of PKC-θ to the cSMAC (238). Therefore, by fusing LAT with the protein domain PKC-θ V3 (LAT V3) or Vav1 SH3SH2SH3 (LAT Vav, which also increases the number of protein-binding motifs), Clark *et al* increased LAT valence and restored LAT centrality upon attenuated activation conditions (126). However, fusion with the PKC-θ V3 domain excessively sustained LAT central accumulation at the interface, which did not enhance IL-2 mRNA production and moderately impaired recruitment of Grb2, Lck and Vav1 to the interface under full T cell stimulation. While fusion of LAT with Vav1 SH3SH2SH3 domain substantially reconstituted

LAT localisation and consistently enhanced the amount of IL-2 mRNA under attenuated activation conditions. These data suggest that forcing LAT central localisation at the interface to a correct extent, not immoderately, improves IL-2 secretion when T cell stimulation is attenuated.

In this study, we have observed defective formation of the IS, impaired LAT central localisation and a weakened ability to secrete IFN-γ in Tg4 iTregs under full stimulus conditions. Such phenotypes of iTreg are reminiscent to that of Teffs under attenuated T cell stimulation. However, polarisation of Teffs and Tregs from naive $CD4^+$ T cells is regulated at the level of transcription (273) and acute modification of the proximal T cell signalling is unlikely to change their lineage. As increasing LAT valence enhances its central localisation, we hypothesise that by fusing LAT with PKC-θ V3 or Vav1 SH3SH2SH3 domain, impaired LAT central accumulation can be restored in Tg4 iTregs. Essentially, this raises a question: will restoration of central LAT localisation polarise iTregs to show more Teff-like phenotypes or simply enhance iTreg effector function owing to improved proximal signalling? To answer this question, we transduced iTregs with the fusion protein LAT V3-GFP or LAT Vav-GFP, performed live-cell imaging and ELISAs on these iTregs. Then we investigated the impacts of these fusion proteins on T cell morphology, LAT polarisation and cytokine production of IFN-γ and IL-10 upon activation of iTregs.

6.2 Chapter aims

- To measure morphological parameters in the first two minutes of activation of LAT V3-GFP and LAT Vav-GFP expressing iTregs and compare the relative interface width, lamella depth, overall cell shape and frequencies of forming an extended lamella among LAT-GFP transduced Teffs and iTregs, LAT V3-GFP and LAT Vav-GFP transduced iTregs during this period.
- To investigate the spatiotemporal organisation of LAT V3-GFP and LAT Vav-GFP in iTregs and compare these to LAT-GFP accumulation in iTregs and Teffs in early activation.
- To assess IFN-γ and IL-10 secretion of LAT-GFP, LAT V3-GFP and LAT Vav-GFP expressing iTregs after 18 hours of T cell activation by ELISAs.

A table is shown below denoting main symbols used in this chapter for different cell types

Table 6.1 Symbols denoting cell types in chapter 6

Cell type	Symbol
Teffs (MBP Ac1-9 [4K] primed, LAT)	▲
Teffs (anti-CD3/28 primed, LAT)	◆
iTregs (MBP Ac1-9 [4K] primed, LAT)	●
iTregs (anti-CD3/28 primed, LAT)	■
iTregs (MBP Ac1-9 [4K] primed, LAT V3)	✖
iTregs (anti-CD3/28 primed, LAT V3)	✕
iTregs (MBP Ac1-9 [4K] primed, LAT Vav)	▽

6.3 LAT V3 and LAT Vav widen the T cell-APC interface and shorten the elongated cell shape of iTregs in early activation

First, we investigated whether the expression of LAT V3 and LAT Vav in Tg4 iTregs would change the shape of iTregs in the first two minutes of iTreg activation. Live cell imaging was performed on LAT V3-GFP or LAT Vav-GFP expressing iTregs and morphological parameters were measured. We compared the three defined ratios (the relative interface width, relative lamella depth and overall cell shape) of LAT-GFP expressing Teffs and iTregs transduced with LAT-GFP, LAT V3-GFP or LAT Vav-GFP to each other, during the first two minutes of activation. A wider T cell-APC interface increases the contact area for interactions of proximal receptors and ligands, which likely induces stronger signal transduction. Moreover, T cells with no or a shorter extended lamella often form a round-flattened shape upon activation which is associated with effective T cell activation (164). Thus comparing the three morphological ratios of the four types of cells allow us to assess the level of their activation. Cells were MBP peptide-primed and data of LAT-GFP transduced Teffs and iTregs are from Figure 4.7, section 4.7.

To recapitulate, in LAT-GFP expressing cells, Teffs showed a significantly wider interface than that of iTregs at the 0s, 20s and 120s time point ($p<0.05$, Figure 6.1 A). LAT V3-GFP expressing iTregs had a significantly higher ratio of interface width to cell width, compared

to that of LAT-GFP expressing iTregs at the 60s and 120s time point ($p<0.01$). Moreover, no differences were found when comparing this ratio of LAT V3-GFP expressing iTregs to that of LAT-GFP expressing Teffs at all four time points. These data together indicate that LAT V3 expression in iTregs widens the interface of the synapse during the first two minutes of activation. While in LAT-Vav-GFP expressing iTregs, the relative interface width was less altered. No significant differences were found when comparing the ratios of interface depth to cell depth of LAT-GFP and LAT Vav-GFP expressing iTregs at all four time points, thus their relative interface width was comparable. LAT-GFP expressing Teffs showed a significantly wider interface than that of LAT Vav-GFP expressing iTregs only at the 120s time point ($p<0.01$). These data show that the interface width of iTregs expressing LAT Vav-GFP is slightly extended, compared to that of LAT-GFP expressing iTregs. In general, in the first 20 seconds of activation, expression of LAT V3-GFP and LAT Vav-GFP widens the interface of iTregs, and their interface width is more comparable to that in LAT-GFP expressing Teffs. Moreover, LAT V3-GFP expressing iTregs also displayed a significantly higher ratio of interface width to cell width than that of LAT Vav-GFP expressing iTreg at the 60s ($p<0.001$) and 120s time points ($p<0.01$). Thus, LAT V3 is continuously widening the interface throughout the first two minutes of activation.

The relative lamella depth of LAT-GFP expressing Teffs and iTregs was comparable across all four time points (Figure 6.1 B). In LAT V3-GFP expressing iTregs, the ratio of lamella depth to cell depth was significantly decreased across all time points, compared to that of LAT-GFP expressing iTregs ($p<0.05$). The difference was prominent at the 0s time point ($p<0.0001$). Moreover, this ratio of LAT V3-GFP expressing iTregs was lower than that of LAT-GFP expressing Teffs at all four time, though the differences were not significant. These results suggest that the extend lamella of LAT V3-GFP expressing iTregs during the first two minutes of activation is shortened and its depth is more comparable to that of LAT-GFP expressing Teffs. Although this ratio of LAT Vav-GFP expressing iTregs was lower than that of LAT-GFP expressing iTregs at the 0s time point, no significant differences were observed at all four time points. Again at the 60s time point, the relative lamella depth of LAT Vav-GFP expressing iTregs was also significantly longer than that of LAT V3 expressing iTregs ($p<0.05$). Therefore, the expression of LAT Vav in iTregs only slightly reduces the depth of extended lamellae, while the expression of LAT V3 continuously shortens the lamellae in the first two minutes of iTreg activation. However, the depth of extended lamellae in LAT Vav-GFP expressing iTregs was more comparable to that in LAT-GFP expressing Teffs. Therefore, the reduction of lamella depth induced by LAT V3 seems to shape iTregs to be more morphologically similar to Teffs.

Then we compare the overall cell shapes of these cells. LAT-GFP expressing showed a more slender cell shape than LAT-GFP expressing Teffs in the first minute of activation ($p<0.0001$ at 0s and 20s, $p<0.01$ at 60s, Figure 6.1 C). In LAT V3-GFP expressing iTregs, the ratio of lamella depth to interface width was significantly lower than that of LAT-GFP expressing iTregs at the 0s, 20s and 60s time point ($p<0.01$). Again, when comparing this ratio of LAT-GFP expressing Teffs and LAT V3-GFP expressing iTregs, no significant differences at all four time points. These together show that the expression of LAT V3 reduces the ratio of lamella depth to interface width in iTregs, and the overall cell shape of LAT V3 expressing iTregs is more similar to that of LAT-GFP expressing Teffs. LAT Vav-GFP expressing iTregs showed a reduced ratio of lamella depth to interface width at the 0s and 20s time point, compared to that of LAT-GFP expressing iTregs. No significant differences were observed when comparing this ratio of these two types of cells. However, LAT Vav-GFP expressing iTregs had the highest ratio of lamella depth to interface width at the 120s time point, and it was significantly higher than that of LAT-GFP expressing Teffs at the 20s ($p<0.01$) and 120s time point ($p<0.05$). Again at the 60s, LAT Vav-GFP expressing iTregs showed a significantly higher ratio than that of LAT V3-GFP expressing iTregs ($p<0.05$). These comparisons indicate that the expression of LAT Vav in iTregs reduces the ratio of lamella to interface width in the first 20 seconds of activation. The slender cell shape of LAT Vav-GFP expressing iTregs at the 120 second was mainly owing to their relatively narrow interface at that time point (Figure 6.1 A). Teffs still showed the most compressed cell shape among the four types of cells but LAT V3 and LAT Vav (to a lesser extent) partially changed the slender cell shape of iTregs, making it more comparable to that of Teffs.

Finally, we investigated whether the frequencies of iTregs forming an extended lamella was affected by the expression of LAT V3 and LAT Vav in the two minutes of activation. As described in section 4.7, at early time points of activation (0s and 20s), more LAT-GFP expressing iTregs formed an extended lamella than LAT-GFP expressing Teffs ($p<0.01$, Figure 6.1 D). The percentage of LAT V3-expressing iTregs forming an extended lamella was not significantly different to that of LAT-GFP expressing Teffs and iTregs in the two minutes. While in LAT Vav-GFP iTregs, the percentage of cells forming an extended lamella was significantly lower than that of LAT-GFP expressing iTregs at early time points. This percentage of LAT Vav-GFP expressing iTregs was the lowest at late time points (60s and 120s), compared to that of the other three cells. It was also significantly lower than that of LAT V3-GFP expressing iTregs at late time points. These comparisons suggest that the expression of LAT Vav in iTregs reduces the frequency of iTregs to form an extended lamella during the first two minutes of activation, which is likely to improve the IS formation and activation signalling. While the expression of LAT V3 is not as effective.

In brief, the expression of LAT V3 in iTregs widens the T cell-APC interface in the first two minutes of iTreg activation. Moreover, the extended lamella of LAT V3-GFP expressing iTregs was significantly shortened, when comparing to that of LAT-GFP expressing iTregs in the first minute of activation. Therefore, the main body of LAT V3-GFP expressing iTregs is more flattened and shortened, which is more similar to that of LAT-GFP expressing Teffs. LAT-V3 expression in Tg4 iTregs help to form a more stable IS with a wider interface and shorter extended lamella, compared to that of LAT-GFP expressing iTreg. This is likely to enhance T cell signalling throughout the first two minutes of activation.

LAT Vav expression in iTregs extends the interface and reduces the depth of extended lamellae in the first 20 seconds of activation. Thus, the overall cell shape of LAT Vav-GFP expressing iTregs is more comparable to that of LAT-GFP expressing Teffs at early time points. The expression of LAT Vav in iTregs also reduces the formation of extended lamellae within this period of time, which contributes to the formation of more tight cell couples. Therefore, T cell activation of LAT Vav-GFP expressing iTregs at early time points (0s and 20s) is likely to be enhanced, compared to that of LAT-GFP expressing iTregs. Notably, morphological differences between LAT-GFP expressing Teffs and iTregs were mainly found to be significant at early time points. Such differences were mostly not significant when comparing the morphological parameters of LAT Vav-GFP expressing iTregs and LAT-GFP expressing Teffs. Therefore, both of the expression of LAT V3 and LAT Vav in iTregs improve the IS formation by widening the T cell-APC interface and shortening the elongated cell shape of iTregs. iTregs transduced with either of the two fusion proteins are more morphological comparable to LAT-GFP expressing Teffs. However, such alterations in LAT V3 expressing iTreg sustains throughout the first two minutes of activation, which is seemingly excessive, while LAT Vav mainly changes the cell shape of iTregs in the first 20 seconds of activation. It is worth considering how the modification of LAT V3 and LAT Vav will affect iTreg activation and what phenotypes they drive iTregs to show. To address this question, spatiotemporal patterning analyses and cytokine production assays were applied on LAT V3 and LAT Vav expressing iTregs in the following sections.

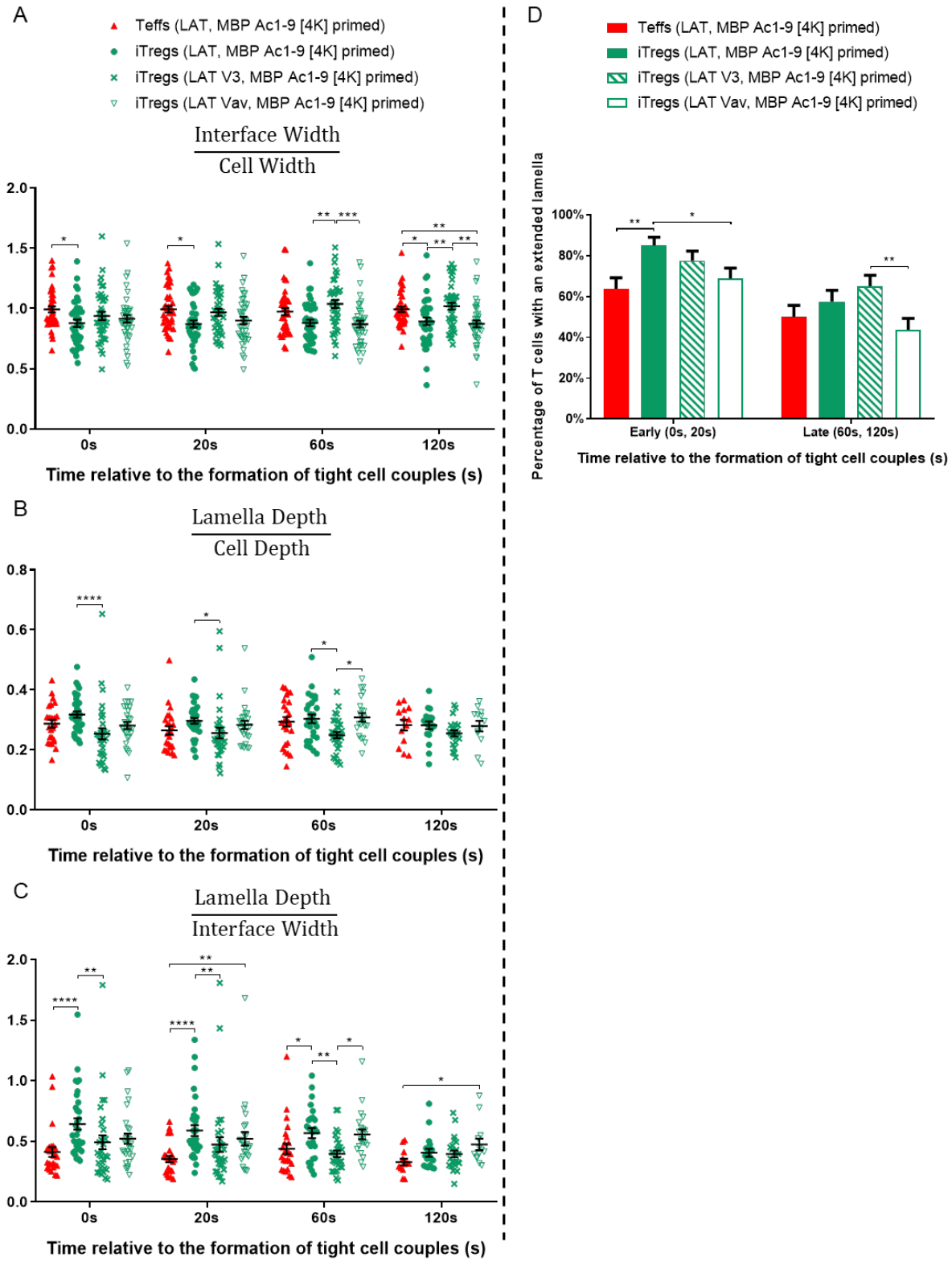
A
Teffs (LAT, MBP Ac1-9 [4K] primed)
iTregs (LAT, MBP Ac1-9 [4K] primed)
iTregs (LAT V3, MBP Ac1-9 [4K] primed)
iTregs (LAT Vav, MBP Ac1-9 [4K] primed)
Interface Width
Cell Width
2.0
1.5
1.0
0.5
0.0
0s
20s
60s
120s
Time relative to the formation of tight cell couples (s)
B
Lamella Depth
Cell Depth
0.8
0.6
0.4
0.2
0.0
0s
20s
60s
120s
Time relative to the formation of tight cell couples (s)
C
Lamella Depth
Interface Width
2.0
1.5
1.0
0.5
0.0
0s
20s
60s
120s
Time relative to the formation of tight cell couples (s)
D
Teffs (LAT, MBP Ac1-9 [4K] primed)
iTregs (LAT, MBP Ac1-9 [4K] primed)
iTregs (LAT V3, MBP Ac1-9 [4K] primed)
iTregs (LAT Vav, MBP Ac1-9 [4K] primed)
Percentage of T cells with an extended lamella
100%
80%
60%
40%
20%
0%
Early (0s, 20s)
Late (60s, 120s)
Time relative to the formation of tight cell couples (s)

Figure 6.1 The expression of LAT V3-GFP and LAT Vav-GFP in MBP Ac1-9 [4K]-primed iTregs widen the interface of the IS and shorten the cell shape of iTregs in early activation.

LAT V3-GFP transduced MBP Ac1-9 [4K]-primed iTregs were activated with MBP Ac1-9 [4Y]-primed PL8 cells were imaged for 15 minutes using confocal microscopy. Four morphological parameters were measured within the first two minutes of activation and 0s indicates when a tight cell couple was formed. Comparing the ratios of **A)** interface width to cell width, **B)** lamella depth to cell depth, **C)** lamella depth to interface width of LAT-GFP expressing Teffs, LAT-GFP, LAT V3-GFP, and LAT Vav-GFP expressing iTregs during the first two minutes of activation. **D)** Comparing the percentages of LAT-GFP expressing Teffs, LAT-GFP, LAT V3-GFP, and LAT Vav-GFP expressing iTregs with an extended lamella in early activation. Data of LAT-GFP transduced Teffs (40 cell couples of four experiments) and iTregs (40 cell couples of two experiments) refers to Figure 4.7. 40 cell couples from four experiments for LAT V3-GFP and two experiments for LAT Vav were analysed. Statistical significance of log-transformed data was calculated using **A)** Two-way ANOVA or **B-C)** mixed-effect model as some values are not recorded for cells without an extended lamella. **D)** Statistical significance was calculated using Chi-square test. Asterisks indicate p-values (*<0.05, **<0.01, ***<0.001, ****<0.0001). Error bars indicate standard error of the mean.

6.4 Fusing LAT with the PKC-θ V3 domain strongly enhances LAT localisation at the interface and partially restores LAT central accumulation in MBP peptide-primed iTregs

We have shown that LAT overall and central accumulation at the interface are defective in both MBP peptide and anti-CD3/28-primed iTregs upon activation in chapter 4. As the morphological phenotypes of MBP peptide-primed iTregs are altered by the expression of LAT V3, it is of great interest to investigate the spatiotemporal accumulation patterns of LAT V3 in MBP peptide-primed iTreg activation. Therefore, we analysed LAT V3-GFP accumulation during the activation of MBP Ac1-9 [4K]-primed iTregs with the acquired live-cell imaging data. LAT V3-GFP transduced iTregs were >75% Foxp3^{+}. Figure 6.2 shows representative images of LAT V3-GFP expressing iTregs in the first two minutes of T cell activation in the DIC and GFP channel.

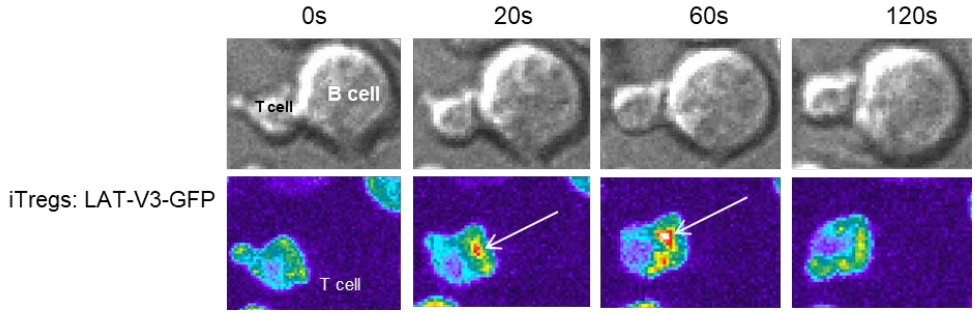

Figure 6.2 Representative live cell images of Tg4 iTregs transduced with LAT V3-GFP from four time points in early T cell activation.

Top: DIC images from four time points. Bottom: matching top-down maximum projections of three-dimensional LAT V3-GFP fluorescent images (intensity is encoded in pseudocolour and increases from purple to red). Time is given in seconds relative to the formation of a tight cell couple and arrows show accumulation of the sensor.

The spatiotemporal accumulation of LAT V3-GFP during early activation of MBP Ac1-9 [4K]-primed iTregs was analysed and compared to that of LAT-GFP Teffs and iTregs with the same priming and activating condition (Figure 6.3). Data of LAT-GFP accumulation in MBP peptide-primed Teffs and iTregs refer to Figure 4.10. In iTregs, the overall accumulation of LAT V3-GFP in iTregs gradually increased from the -20s time point and peaked at the 40s time point with 80% of iTregs showing accumulation (Figure 6.3 C). This high level of LAT V3-GFP accumulation remained at the interface afterwards and was observed in 68% of iTregs at the last time point. Among different patterns found at the interface, the diffuse accumulation pattern of LAT V3-GFP was dominant at all time points and peaked at the 120s time point with 40% of iTregs showing this pattern. While LAT-GFP diffuse accumulation was barely observed in neither Teffs nor iTregs. Central LAT V3-GFP accumulation was found mainly in the first two minutes of activation. The accumulation of LAT V3-GFP at the distal pole was found at early time points and peaked at the -20s time point with formed with 25% of iTreg showing such accumulation. The distal patterning of LAT V3-GFP diminished afterwards, which is similar to what observed in the distal LAT-GFP accumulation in iTregs.

In the direct comparison, the percentage of iTregs with LAT V3-GFP accumulation at the interface during iTreg activation was higher than that of LAT-GFP overall accumulation at all 12 time points. (Figure 6.3 D, the second row). The enhancement was extremely prominent as highly significant differences were found at all time points ($p<0.0001$). Moreover, this percentage was also higher than the that of Teffs showing overall LAT-GFP accumulation at all time points. The differences were significant at all time points except for 0s to 40s ($p<0.01$), and they remained significant with the Bonferroni correction at the -20s, 100s-420s time point ($p<0.004$). To summarise, the high level of LAT V3-GFP localisation at the interface indicates that fusing LAT to the PKC-θ V3 domain strongly increases LAT overall accumulation at the IS in early activation of Tg4 MBP peptide-primed iTregs. The extent of enhancement is outstanding as the upregulated accumulation of LAT V3 at the interface sustained for at least six minutes after the peak of accumulation, whilst LAT localisation at the IS in both Teffs and iTregs diminished after the peak in the first few minutes of activation. Such enhancement is likely to reinforce LAT clustering at the cSMAC. It is unclear how the inefficient clearance of LAT V3 molecules at the interface would affect the cSMAC and LAT related signal transduction at later time points.

A

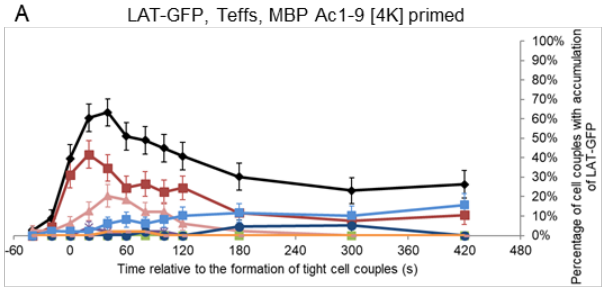

B

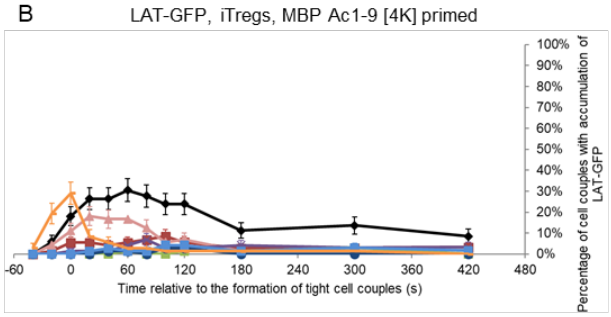

C

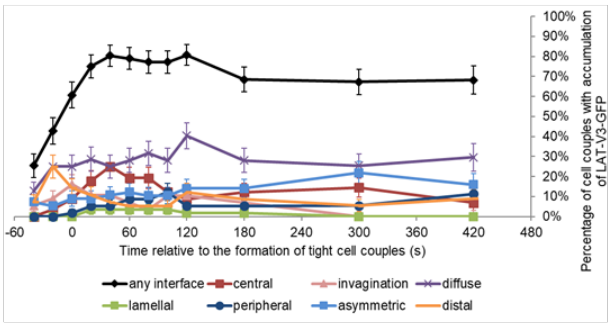

D Statistical comparison of any interface accumulation

Time (s)	-40	-20	0	20	40	60	80	100	120	180	300	420
Teffs (LAT) vs iTregs (LAT)	0.78	0.83	0.02	0.0004	0.0001	0.04	0.03	0.03	0.08	0.02	0.33	0.04
			*	***	***	*	*	*		*		*
iTregs (LAT) vs iTregs (LAT V3)	4.6E-05	3.4E-06	1.7E-06	1.3E-07	4.1E-09	1.3E-07	6.8E-08	6.8E-09	5.4E-10	9.0E-11	4.5e-09	9.5E-10
	****	****	****	****	****	****	****	****	****	****	****	****
Teffs (LAT) vs iTregs (LAT V3)	0.008	0.0004	0.05	0.17	0.08	0.005	0.005	0.001	5.8E-05	0.0003	6E-05	0.0004
	**	***				**	**	**	****	***	****	***

Figure 6.3 LAT V3-GFP displays prominent accumulation at the IS during early activation of MBP Ac1-9 [4K]-primed iTregs

LAT V3-GFP transduced MBP Ac1-9 [4K]-primed iTregs were activated by MBP Ac1-9 [4Y]-primed PL8 cells and imaged using spinning disk confocal microscopy for 15 minutes. DIC and GFP images were analysed to determine formations of a tight cell couple (0s). Data of LAT-GFP accumulation in MBP Ac1-9 [4K]-primed **A)** Teffs (n=49, four experiments) and **B)** iTregs (n=72, two experiments) refer to Figure 4.10. **C)** Spatiotemporal distribution patterns of LAT V3-GFP for 12 time points in MBP Ac1-9 [4K]-primed iTregs (n=57, four experiments). **D)** Comparing the percentages of cells with LAT-GFP or LAT V3-GFP accumulation at the interface during the activation of corresponding cell types using a two proportion z-test. Numerals and asterisks indicate p-values, and asterisk colours denote whether differences remain significant with the Bonferroni correction (0.01<*<0.05, 0.004<**<0.01, 0.001<**<0.004, 0.0001<***<0.001, ****<0.0001). Error bars indicate standard error of the mean.

Next, we compared the central or invagination patterning of LAT V3-GFP in MBP peptide-primed iTregs with that of LAT-GFP in Teffs and iTregs in early activation (Figure 6.4). As shown in Figure 4.10 of section 4.8, the percentage of Teffs showing either central or invagination accumulation of LAT-GFP was higher than that of iTregs from the 0s to 420s time point. Significant differences were found at seven time points ($p<0.05$, 0s-120s) and the differences remained significant at the 20s and 40s time point with the Bonferroni correction ($p<0.004$). Figure 6.4 B shows that the percentage of iTregs with LAT V3-GFP central + invagination accumulation was higher than that with LAT-GFP central + invagination accumulation across all time points. However, a significant difference was only found at the 180s time point, but it was not significant with the Bonferroni correction ($0.004<p<0.05$). The percentage of Teffs with LAT-GFP central + invagination accumulation was higher than that of iTregs with LAT V3-GFP central + invagination accumulation in the first 180 seconds of activation (Figure 6.4 C). The differences were only significant at the 20s time point but did not remain significant with the Bonferroni correction ($0.004<p<0.05$). These comparisons indicate that in early MBP peptide-primed iTreg activation, LAT accumulation near the centre of the interface is upregulated by the fusing LAT to the PKC-θ V3 domain, although the defective accumulation is not fully restored.

Then we separately compared the central and invagination accumulation of LAT V3-GFP and LAT-GFP in these conditions. The LAT-GFP central accumulation in iTregs was low and less than 10% of the cells showing such accumulation at all time points (Figure 6.5 A). Teffs showed more central LAT-GFP accumulation than iTregs at 11 out of 12 time points, and the percentage of Teffs with LAT-GFP central patterning was significantly higher than that of iTreg from the 0s to 120s time point ($p<0.01$). LAT V3-GFP showed more central accumulation than that of LAT-GFP in iTregs, mainly from the 20s to 80s, 180s and 300s time point (Figure 6.5 B). Significant differences were found at the 40s ($p<0.004$) and 60s ($0.01<p<0.05$). Teffs still showed more central LAT-GFP accumulation than LAT V3-GFP central accumulation in iTregs, mainly in the first two minutes of activation. The percentage of Teffs with central LAT-GFP accumulation was significantly higher than that of iTreg with central LAT V3-GFP accumulation at the 20s ($p<0.004$) and 40s ($0.01<p<0.05$) time point (Figure 6.5 C). These analyses show that fusion of LAT with the PKC-θ V3 domain partially restores its central accumulation during early activation of MBP peptide-primed iTregs.

The invagination accumulation of LAT-GFP in MBP peptide-primed Teffs and iTregs was similar at all time points (Figure 6.5 D). The percentage of iTregs with LAT V3-GFP invagination accumulation was also comparable to that of Teffs or iTregs showing LAT-GFP invagination patterning across all time points (Figure 6.5 E and F). No significant differences

were observed in both comparisons. Thus, fusion with PKC-θ V3 domain does not affect LAT invagination accumulation in iTregs.

In addition, fusion of PKC-θ V3 strongly increases diffuse accumulation of LAT in MBP peptide-primed iTregs. Initially, LAT-GFP did not show much diffuse accumulation in either MBP peptide-primed Teffs or iTregs in early activation (Figure 6.6 A). It was notable that LAT V3-GFP showed significantly more diffuse accumulation than that of LAT-GFP in Teffs and iTregs (Figure 6.6 B and C). Highly significant differences were observed in both comparisons at almost all time points (-20s-420s). These results indicate that a fair number of LAT molecules, which are driven to the interface by the additional PKC-θ V3 domain, diffuse at the entire interface during the first few minutes of activation.

Together, these observations indicate that fusing LAT with the PKC-θ V3 domain strikingly enhances LAT overall accumulation at the T cell-APC interface and partially restores impaired LAT central localisation in the early activation of Tg4 MBP peptide-primed iTregs. Also, diffuse LAT accumulation in iTregs is strongly enhanced by fusing it with PKC-θ V3, to a greater extent than that observed in Teffs. By increasing the valence of LAT, the PKC-θ V3 domain drives more LAT molecules to the interface which provide more docking sites for downstream signalling proteins (such as Grab2, Gads and PLCγ-1), thus enhances LAT signalosome-mediated early T cell signalling.

In Teffs, LAT-GFP overall accumulation at the interface gradually diminished after the peak of accumulation and remained at a low level after the 120s time point. While in iTregs, LAT V3-GFP overall accumulation peaked at the 40s time point and such accumulation largely remained at the interface for at least six minutes, showing a mixed patterning of accumulation. However, sustained localisation of LAT at the interface might not be necessary for T cell function. Clark *et al* (126) showed that upon full and attenuated T cell activation, LAT V3 displayed sustained localisation with a strong central preference at the interface in 5C.C7 T cells, but the amount of IL-2 mRNA was not affected. Therefore, it is of interest to investigate how the expression of LAT V3 would change functions of iTregs. Moreover, the enhanced overall accumulation of LAT V3 at the interface consistently matches the morphological phenotypes of LAT V3 expressing iTregs observed in the first two minutes of activation (Figure 6.1). Thus, fusing LAT with the PKC-θ V3 domain increases LAT localisation at the interface to a great extent and simultaneously enhances T cell-APC conjunctions of Tg4 MBP peptide-primed iTregs in early activation. As LAT central localisation is only partially restored by the fusion of PKC-θ V3 domain in the first two minutes of activation, the enhancement on signal transduction regulated by the cSMAC is likely to be limited.

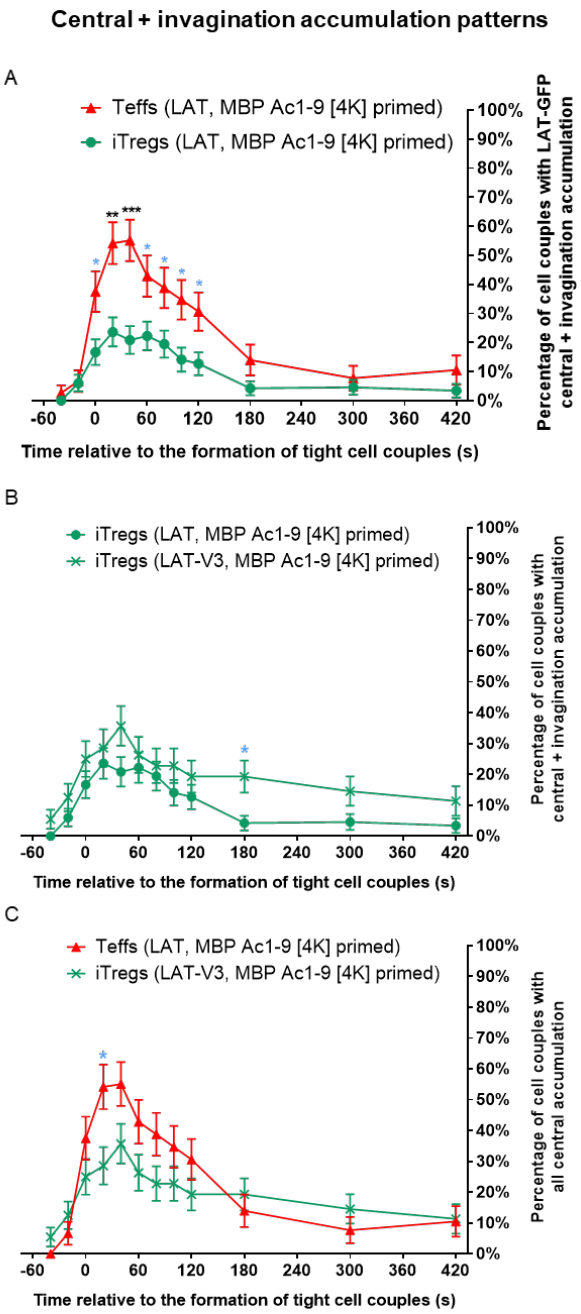

Figure 6.4 In early activation of MBP Ac1-9 [4K]-primed iTregs, the total amount of central and invagination accumulation of LAT V3-GFP at the interface is increased, compared to that of LAT-GFP.

In early activation of MBP peptide-primed T cells, the percentages of cells with central + invagination accumulation of **A)** LAT-GFP in Teffs and iTregs, **B)** LAT-GFP and LAT V3-GFP in iTregs and **C)** LAT-GFP in Teffs and LAT V3-GFP in iTregs were compared. Data of LAT-GFP transduced Teffs (n=49, four experiments) and iTregs (n=72, two experiments) refer to Figure 4.11, and 57 cell couples of LAT V3-GFP expressing iTregs from four experiments were analysed. A two proportion z-test was used to calculate statistical significance. Asterisks indicate p-values and colours indicate whether differences remain significant with the Bonferroni correction (0.01<*<0.05, 0.004<**<0.01, 0.001<**<0.004, ***<0.001). Error bars indicate standard error of the mean.

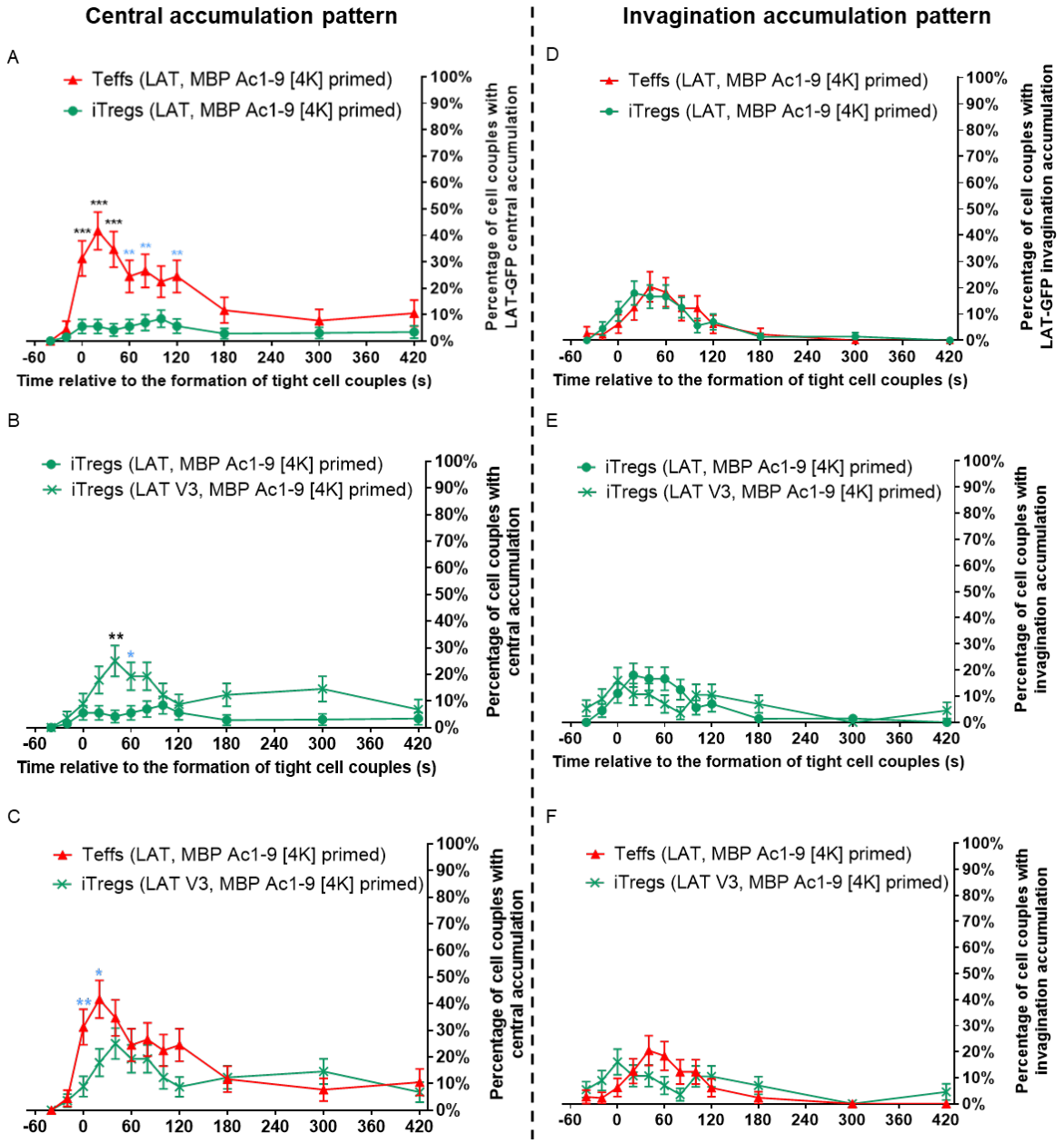

Figure 6.5 More LAT V3-GFP central accumulation is found at the interface in early activation of MBP peptide-primed iTregs, compared to that of LAT-GFP.

In early activation of MBP peptide-primed T cells, comparing the percentages of cells showing central patterning of **A)** LAT-GFP in Teffs and iTregs, **B)** LAT-GFP and LAT V3-GFP in iTregs and **C)** LAT-GFP in Teffs and LAT V3-GFP in iTregs, and the percentages of cells showing invagination patterning of **D)** LAT-GFP in Teffs and iTregs, **E)** LAT-GFP and LAT V3-GFP in iTregs and **F)** LAT-GFP in Teffs and LAT V3-GFP in iTregs. Data of LAT-GFP transduced Teffs (n=49, four experiments) and iTregs (n=72, two experiments) refer to Figure 4.11, and 57 cell couples of LAT V3-GFP expressing iTregs from four experiments were analysed. Statistical significance was calculated with a two proportion z-test. Asterisks indicate p-values and colours indicate whether differences remain significant with the Bonferroni correction (0.01<*<0.05, 0.004<**<0.01, 0.001<**<0.004, ***<0.001). Error bars indicate standard error of the mean.

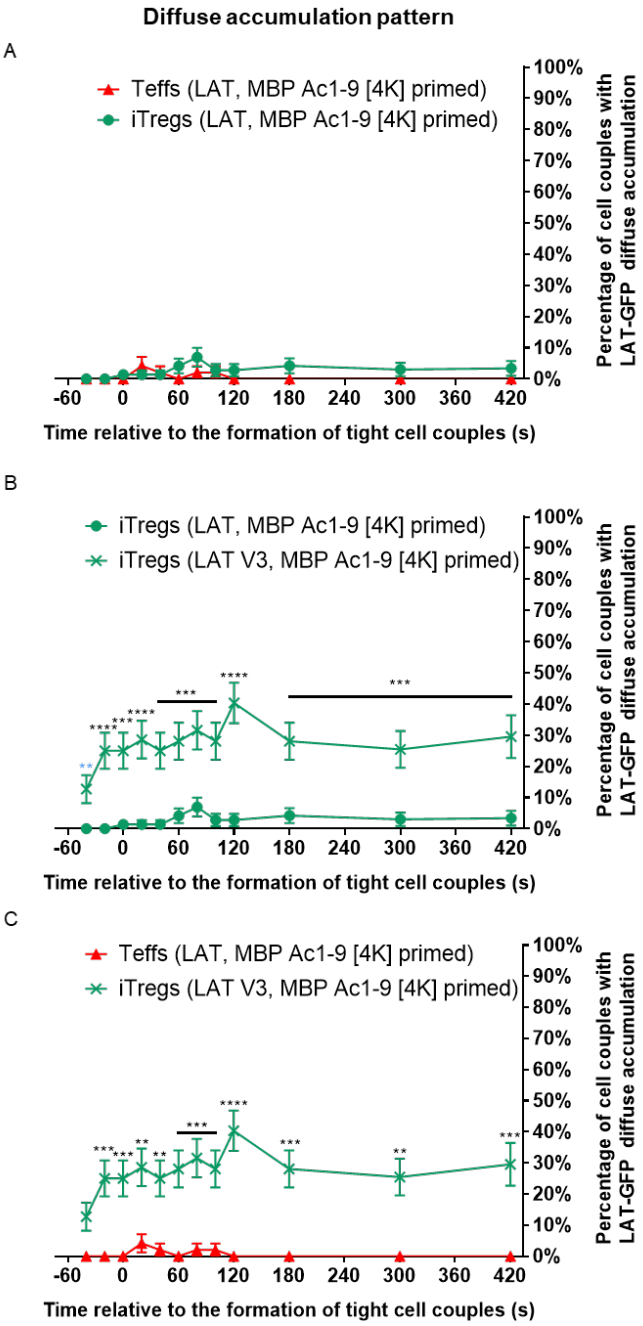

Figure 6.6 LAT V3-GFP shows a much stronger preference for diffuse accumulation than that of LAT-GFP in MBP peptide-primed Teffs and iTregs.

In early activation of MBP Ac1-9 [4K] primed T cells, the percentages of cells with diffuse accumulation of **A)** LAT-GFP in Teffs and iTregs, **B)** LAT-GFP and LAT V3-GFP in iTregs and **C)** LAT-GFP in Teffs and LAT V3-GFP in iTregs were compared. Data of LAT-GFP transduced Teffs (n=49, four experiments) and iTregs (n=72, two experiments) refer to Figure 4.11, and 57 cell couples of LAT V3-GFP expressing iTregs from four experiments were analysed. A two proportion z-test was used to calculate statistical significance. Asterisks indicate p-values and colours indicate whether differences remain significant with the Bonferroni correction (0.004<**<0.01, 0.001<**<0.004, 0.0001<***<0.001, ****<0.0001). Error bars indicate standard error of the mean.

6.5 Computational analyses identify increased accumulation of LAT V3 at the entire and central core of the IS of iTregs

Computational analyses were performed using LAT V3-GFP imaging data to validate observations found in spatiotemporal patterning analyses. A 3D model map showing relative probabilities of LAT V3-GFP accumulation during MBP peptide-primed iTreg activation was generated.

We first compared LAT-GFP and LAT V3-GFP enrichment at the defined IS region showing the top 10% of the fluorescence in corresponding cells. Data showing LAT-GFP enrichment in MBP peptide-primed Teffs and iTregs refer to Figure 4.13, section 4.9. As described before, LAT-GFP enrichment at the IS of Teffs was higher than that of iTregs at all 12 time points and significant difference were found at the 80s, 120s-420s time point ($p<0.05$, Figure 6.7 A). In iTregs, a higher level of LAT V3-GFP enrichment at the IS during early iTreg activation was observed at all 12 time points, compared to that of LAT-GFP enrichment (Figure 6.7 B). However, only one significant difference was observed at the -40s time point ($0.01<p<0.05$). The level of enrichment of LAT-GFP at the IS of Teffs was higher than that of LAT V3-GFP in iTreg at most time points (40s-420s Figure 6.7 C) and the difference was significant at the 420s time point ($0.004<p<0.01$, not significant with the Bonferroni correction). These results together indicate LAT accumulation in the defined IS region in MBP peptide-primed iTregs is upregulated by fusion with PKC-θ V3.

We compared the accumulation of LAT V3-GFP and LAT-GFP at the centre of the interface by focusing on the enrichment inside the central core. As described in section 4.9, the level of LAT-GFP enrichment in the central core of Teffs was higher than that of iTregs at all 12 time points and the differences were significant at the 80s, 120s-420s time point ($0.004<p<0.05$, Figure 6.7 D). In early iTreg activation, more enrichment of LAT V3-GFP in the central core was observed at all time points except one (420s), compared to that of LAT-GFP (Figure 6.7 E). The differences were significant at the -20s and 0s time point ($0.01<p<0.05$). The level of LAT V3-GFP enrichment in the central core of iTregs was comparable to that of LAT-GFP enrichment in the central core of Teffs before the 100s time point (Figure 6.7 F). After that, LAT V3-GFP accumulation in the central core in iTregs gradually decreased while LAT-GFP accumulation remained at the interface centre in Teffs. However, their level of enrichment was only significantly different at the 420s time point ($0.004<p<0.01$). Therefore, fusion of LAT to the PKC-θ V3 domain partially restores its accumulation in the central core of the IS in MBP peptide-primed iTregs.

Being consistent with results from the spatiotemporal distribution analyses, the large-scale computational approach shows that fusing LAT with the PKC-θ V3 domain enhances LAT accumulation at the interface in early activation of MBP peptide-primed iTregs. A higher level of LAT V3-GFP accumulation in the central region of iTregs suggests that fusion with PKC-θ V3 also enhances LAT accumulation at the centre of the interface. In summary, both pattern and computational analyses show that fusion with PKC-θ V3 domain efficiently induces more LAT molecules to the interface and partially restores LAT accumulation in the cSMAC during early activation of Tg4 MBP peptide-primed iTregs.

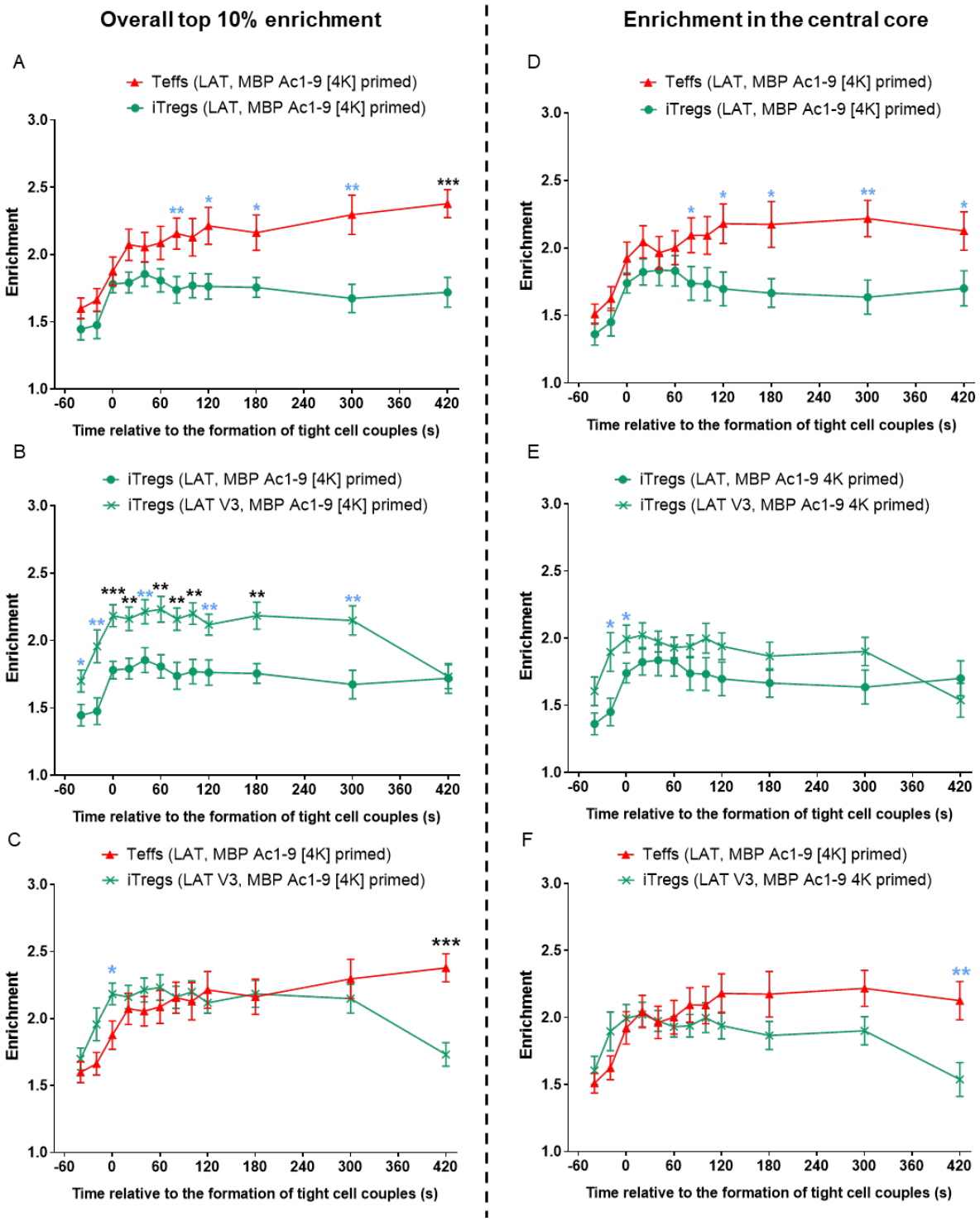
Overall top 10% enrichment
Enrichment in the central core
A
Teffs (LAT, MBP Ac1-9 [4K] primed)
iTregs (LAT, MBP Ac1-9 [4K] primed)
Enrichment
Time relative to the formation of tight cell couples (s)
B
iTregs (LAT, MBP Ac1-9 [4K] primed)
iTregs (LAT V3, MBP Ac1-9 [4K] primed)
C
Teffs (LAT, MBP Ac1-9 [4K] primed)
iTregs (LAT V3, MBP Ac1-9 [4K] primed)
D
Teffs (LAT, MBP Ac1-9 [4K] primed)
iTregs (LAT, MBP Ac1-9 [4K] primed)
E
iTregs (LAT, MBP Ac1-9 4K primed)
iTregs (LAT V3, MBP Ac1-9 4K primed)
F
Teffs (LAT, MBP Ac1-9 [4K] primed)
iTregs (LAT V3, MBP Ac1-9 4K primed)

Figure 6.7 Computational analyses show that when fused to the PKC-θ V3 domain, LAT-GFP overall and central accumulation at the IS are enhanced in early the activation of MBP Ac1-9 [4K]-primed iTregs.

LAT V3-GFP transduced MBP peptide-primed iTregs were computationally analysed to generate 3D model maps which show enrichment of the sensor within a cell. Comparing **A)** LAT-GFP enrichment in Teffs and iTregs, **B)** LAT-GFP and LAT V3-GFP enrichment in iTregs, and **C)** LAT-GFP enrichment in Teffs and LAT V3-GFP enrichment in iTregs, within the IS (top 10% enrichment). Comparing **D)** LAT-GFP enrichment in Teffs and iTregs, **E)** LAT-GFP and LAT V3-GFP enrichment in iTregs, and **F)** LAT-GFP enrichment in Teffs and LAT V3-GFP enrichment in iTregs, within the central core of the IS. Data of LAT-GFP enrichment in Teffs (28 cell couples from four experiments) and iTregs (28 cell couples from two experiments) refer to Figure 4.13 and 4.14, and 22 cell couples from four experiments of LAT V3-GFP transduced iTregs were analysed. Log-transformed data were analysed with unpaired Student's test to calculate statistical significance. Asterisks indicate p-values and colours indicate whether differences remain significant with the Bonferroni correction (0.01<*<0.05, 0.004<**<0.01, 0.001<**<0.004, ***<0.001). Error bars indicate standard error of the mean.

6.6 In early activation of anti-CD3/28-primed iTregs, fusing LAT with the PKC-θ V3 domain strongly enhances LAT overall and central localisation

Additional imaging data of LAT V3-GFP were acquired using anti-CD3/28-primed iTregs, and were compared with that of LAT-GFP accumulation in Teffs and iTregs primed with anti-CD3/28 (refer to Figure 4.10, section 4.8). In anti-CD3/28-primed iTregs, LAT V3-GFP promptly accumulated at the interface upon the IS formation and peaked around the 80s time point with 92% of the cells showing LAT V3-GFP accumulation at the interface (Figure 6.8 C). At the interface, LAT V3-GFP showed mainly central, invagination and diffuse patterning in the first two minutes. The central and invagination accumulation of LAT V3-GFP remained at the interface till the last time point. A low level of distal accumulation of LAT V3-GFP accumulation was observed before the IS formation and diminished after.

In anti-CD3/28-primed iTregs, the percentage of cells with LAT V3-GFP accumulation was higher than that with LAT-GFP accumulation at the interface (Figure 6.8 B) from the 0s to 420s time point. The differences were highly significant from the 20s to 420s time point ($p<0.004$, Figure 6.8 D, the second row). Moreover, the peak of LAT V3-GFP overall accumulation occurred 40 seconds earlier than that of LAT-GFP overall accumulation in iTregs. The overall accumulation at the interface of LAT V3-GFP in iTregs was comparable to that of LAT-GFP in Teff (Figure 6.8 A) during early activation. Only one significant difference was observed at the 120s time point when comparing the percentage of iTregs with LAT V3-GFP accumulation to that of Teffs with LAT-GFP accumulation at the interface, though it was no longer significant with the Bonferroni correction ($0.004<p<0.05$, Figure 6.8 D, the third row). These observations suggest that in early activation of anti-CD3/28-primed iTregs, impaired LAT localisation at the interface can be restored by fusing LAT with the PKC-θ V3 domain.

A

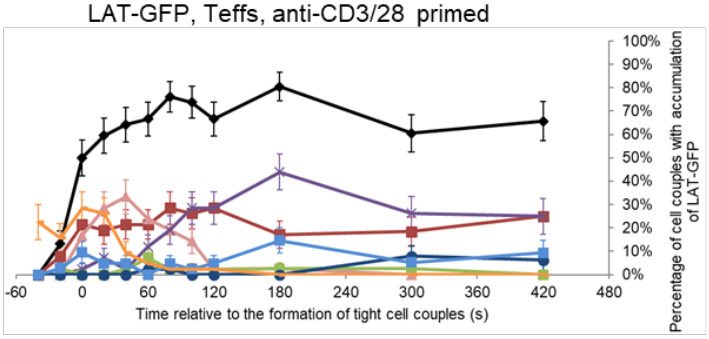

B

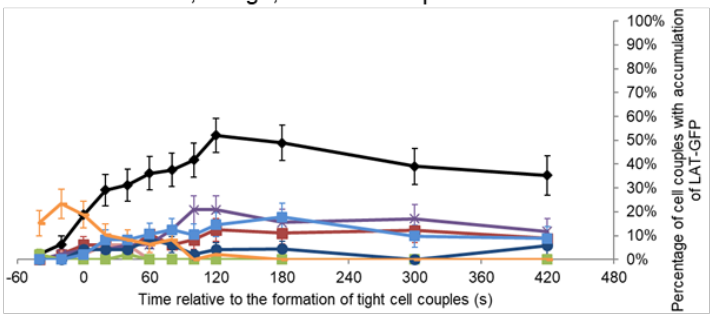

C

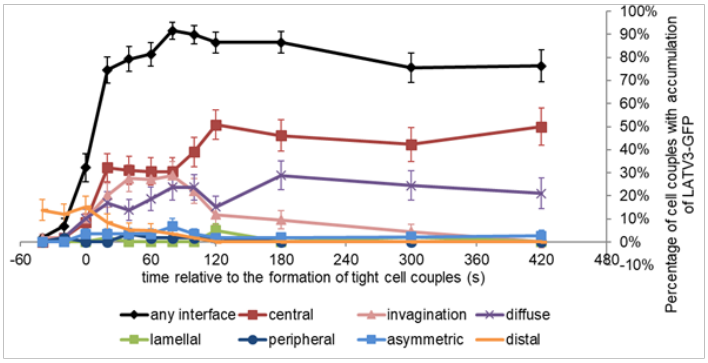

D Statistical comparisons of any interface accumulation

Time (s)	-40	-20	0	20	40	60	80	100	120	180	300	420
Teffs (LAT) vs iTregs (LAT)	0.84	0.49	0.004	0.007	0.003	0.008	0.0005	0.004	0.23	0.005	0.09	0.03
			**	**	**	**	***	**		**		*
iTregs (LAT) vs iTregs (LAT V3)	0.58	0.77	0.18	7.0E-06	1.7E-06	5.5E-06	1.1E-08	3.2E-07	0.0002	0.0002	0.001	0.001
				****	****	****	****	****	***	***	**	**
Teffs (LAT) vs iTregs (LAT V3)	0.75	0.50	0.11	0.17	0.15	0.15	0.06	0.06	0.03	0.61	0.22	0.47
									*			

Figure 6.8 In early activation of anti-CD3/28-primed iTregs, LAT V3-GFP intensively accumulates at the interface with dominant central patterning[†].

LAT V3-GFP expressing anti-CD3/28-primed iTregs were activated by MBP Ac1-9 [4Y]-primed PL8 cells and imaged using spinning disk confocal microscopy for 15 minutes. DIC and GFP images were analysed to determine formations of a tight cell couple (0s). Data of LAT-GFP accumulation in anti-CD3/28-primed **A)** Teffs (n=42, two experiments) and **B)** iTregs (n=48, four experiments) refer to Figure 4.10. **C)** Spatiotemporal distribution patterns of LAT V3-GFP in early activation of anti-CD3/28-primed iTregs (n=58, two experiments). **D)** Comparing the percentages of cells with LAT-GFP or LAT V3-GFP accumulation at the interface during the activation of corresponding cell types using a two proportion z-test. Numerals and asterisks indicate p-values, and asterisk colours denote whether differences remain significant with the Bonferroni correction (0.01<*<0.05, 0.004<**<0.01, 0.001<**<0.004, ***<0.0021, ****<0.0001). Error bars indicate standard error of the mean.

[†] LAT V3-GFP imaging data of Tg4 anti-CD3/28-primed iTregs were analysed by Christoph Wuelfing.

Together the central and invagination patterning of LAT V3-GFP or LAT-GFP in anti-CD3/28-primed T cess during early activation were compared (Figure 6.9). Spatiotemporal accumulation patterns of LAT-GFP during the activation anti-CD3/28-primed cells refer to Figure 4.11 from section 4.8. As described before, the percentage of anti-CD3/28-primed Teffs with central + invagination accumulation of LAT-GFP was higher than that of iTregs at most time points (Figure 6.9 A). Highly significant differences were found at six time points (0s-100s) and all of them remained significant with the Bonferroni correction ($p<0.004$). The percentage of iTregs with LAT V3-GFP central + invagination accumulation was significantly higher than that with LAT-GFP central + invagination accumulation across at most time points (0s to 420s, Figure 6.9 B). Particularly within the first two minutes of activation, the differences were prominent ($p<0.0001$). Moreover, the percentage of iTregs showing LAT V3-GFP central + invagination accumulation was even higher than that of Teffs with LAT-GFP central + invagination accumulation from the 20s to 420s time points (Figure 6.9 C). Significant differences were observed from the 120s to 420s time point ($p<0.05$) and were still significant at the 120s and 180s time point ($p<0.004$). These together reveal that LAT localisation around the interface centre in early activation of anti-CD3/28-primed iTreg is excessively enhanced by fusion with the PKC-θ V3 domain.

We further compared only the central + invagination accumulation of LAT V3-GFP or LAT-GFP in these three conditions. As previously described, less LAT-GFP central accumulation was observed in anti-CD3/28-primed iTregs during early activation, compared to that in Teffs. Significant differences were observed at the 40s, 80s and 180s time point when comparing the percentages of iTregs and Teffs with such accumulation ($0.004<p<0.05$, Figure 6.10 A). In anti-CD3/28-primed iTregs, LAT V3-GFP showed a much stronger preference for central accumulation at the interface than LAT-GFP after the IS was formed (Figure 6.10 B). When comparing the percentages of iTregs with central LAT-GFP and LAT V3-GFP accumulation, highly significant differences were found at most time points ($p<0.004$, 20s, 40s, 80s-180s, 420s). Notably, the percentage of iTregs with central LAT V3-GFP accumulation was higher than that of Teffs with LAT-GFP central accumulation after the IS was formed (20s-420s, Figure 6.10 C). The differences were significant from the 120s to 300s time point but were no longer significant with the Bonferroni correction ($0.004<p<0.05$). These comparisons indicate that LAT accumulation in early activation of anti-CD3/28-primed iTregs is efficiently driven to the centre of the interface by fusion with the PKC-θ V3 domain, and the time range of central accumulation is significantly prolonged.

Barely any LAT-GFP invagination accumulation at the interface was observed during anti-CD3/28-primed iTreg activation, while this was found in Teffs in the first two minutes of

activation (Figure 6.10 D). Differences were significant in the first 100 seconds when comparing their percentage with LAT-GFP invagination patterning ($p<0.05$). The percentage of iTregs with LAT V3-GFP invagination accumulation was higher than that with LAT-GFP invagination accumulation after the IS was formed, and significant differences were observed from the 40s to 100s time point (Figure 6.10 E). The invagination patterning of LAT V3-GFP in iTregs was comparable to that of LAT-GFP in Teffs in early activation (Figure 6.10 F). Therefore, by fusing LAT with the PKC-θ V3 domain, LAT invagination accumulation at the interface is restored.

In summary, during early activation of Tg4 anti-CD3/28-primed iTregs, the impaired LAT overall, central and invagination accumulation is restored by fusing LAT with the PKC-θ V3 domain. Moreover, fusion with PKC-θ V3 exceedingly enhances and prolongs LAT accumulation at the centre of the interface. These observations in anti-CD3/28-primed iTregs are similar to those found in MBP peptide-primed iTregs, except that LAT central localisation driven by the fused PKC-θ V3 domain is more pronounced in the former. This suggests that anti-CD3/28-primed iTregs are more sensitive to the manipulation of LAT polarisation.

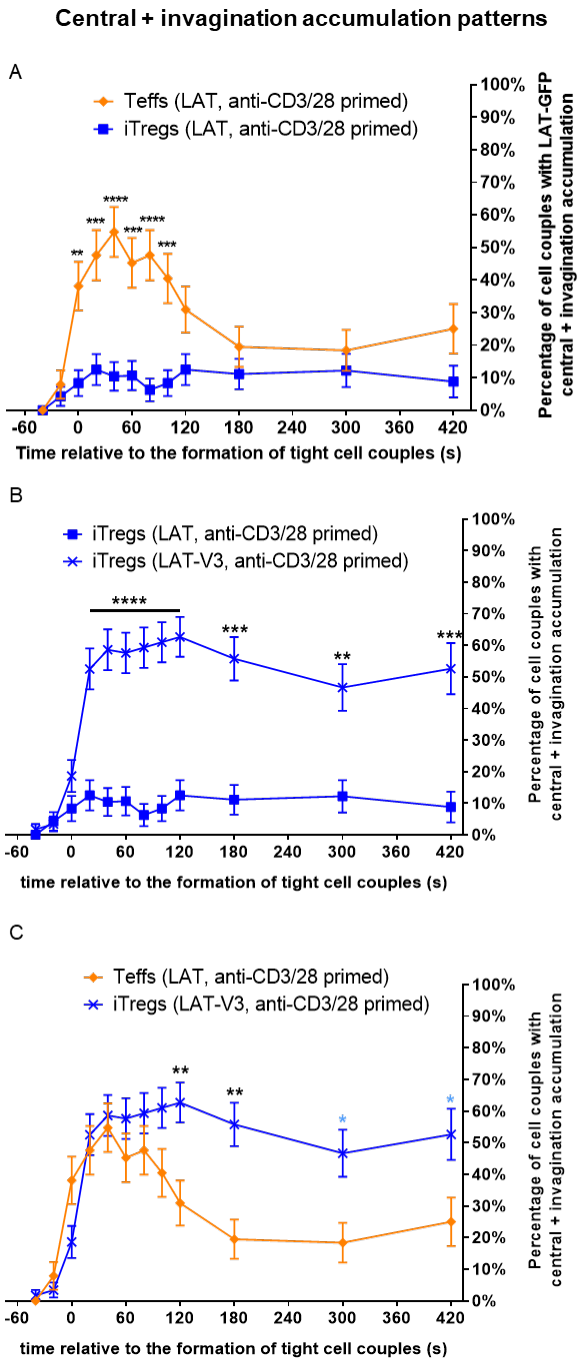

Figure 6.9 LAT V3-GFP shows prominent central and invagination patterning at the IS in the first seven minutes of anti-CD3/28-primed iTreg activation.

In early activation of anti-CD3/28-primed T cells, the percentages of cells with central + invagination accumulation of **A)** LAT-GFP in Teffs and iTregs, **B)** LAT-GFP and LAT V3-GFP in iTregs and **C)** LAT-GFP in Teffs and LAT V3-GFP in iTregs were compared. Data of LAT-GFP transduced Teffs (42 cell couples from two experiments) and iTregs (48 cell couples from four experiments) refer to Figure 4.11, and 58 cell couples of LAT V3-GFP expressing iTregs from two experiments were analysed. A two proportion z-test was used to calculate statistical significance. Asterisks indicate p-values and colours indicate whether differences remain significant with the Bonferroni correction (0.01<*<0.05, 0.001<**<0.004, ***<0.001). Error bars indicate standard error of the mean.

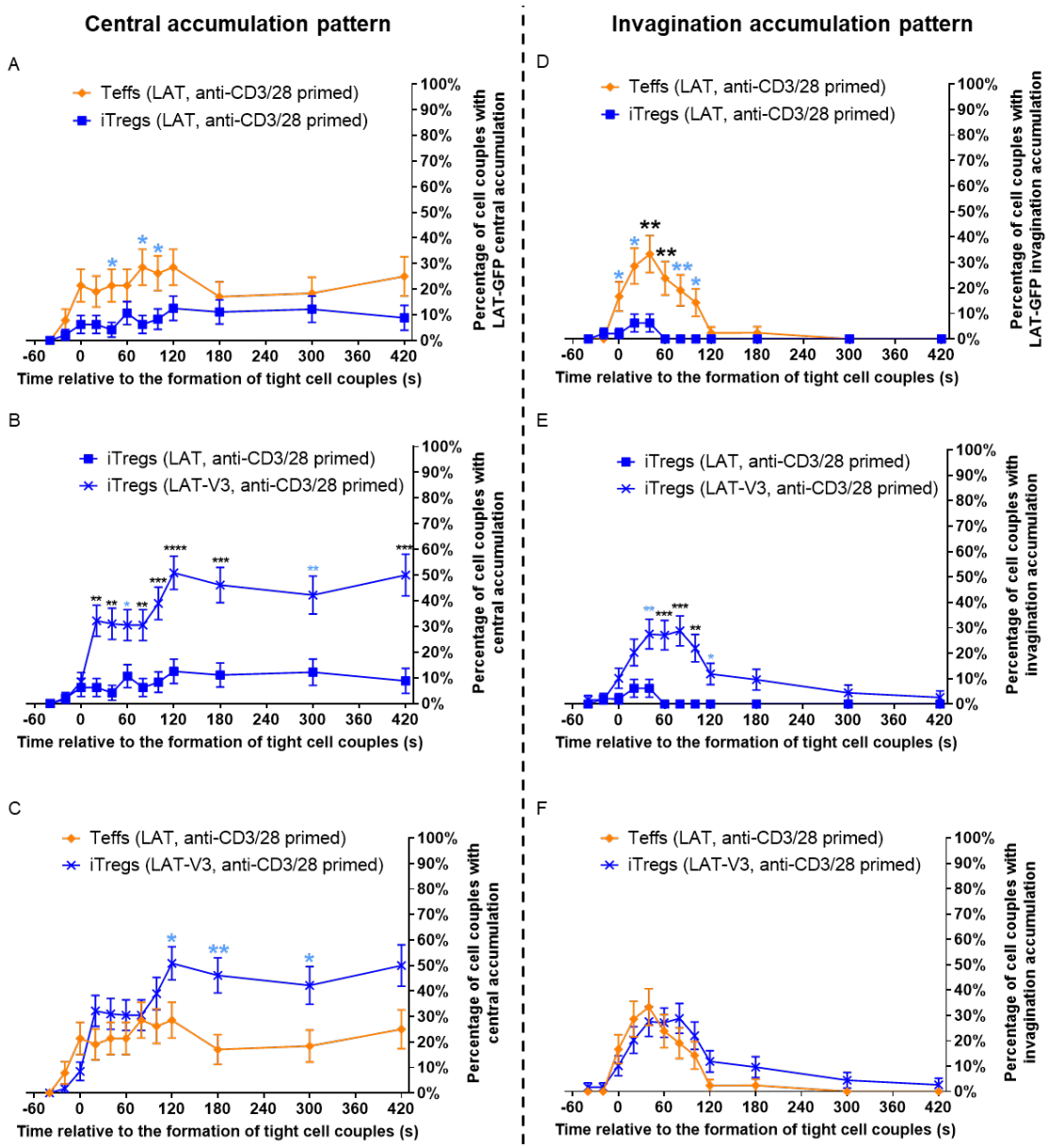

Figure 6.10 Both LAT V3-GFP central and invagination accumulation are significantly enhanced in early activation of anti-CD3/28-primed iTregs, compared to that of LAT-GFP.

In early activation of anti-CD3/28-primed T cells, comparing the percentages of cells with central accumulation of **A)** LAT-GFP in Teffs and iTregs, **B)** LAT-GFP and LAT V3-GFP in iTregs and **C)** LAT-GFP in Teffs and LAT V3-GFP in iTregs, and the percentage of cells with invagination accumulation of **D)** LAT-GFP in Teffs and iTregs, **E)** LAT-GFP and LAT V3-GFP in iTregs and **F)** LAT-GFP in Teffs and LAT V3-GFP in iTregs. Data of LAT-GFP transduced Teffs (42 cell couples from two experiments) and iTregs (48 cell couples from four experiments) refer to Figure 4.11 and 58 cell couples of LAT V3-GFP expressing iTregs from two experiments were analysed. Statistical significance was calculated with a two proportion z-test. Asterisks indicate p-values and colours indicate whether differences remain significant with the Bonferroni correction (0.01<*<0.05, 0.004<**<0.01, 0.001<**<0.004, ***<0.001). Error bars indicate standard error of the mean.

6.7 Fusion with the Vav1 SH3SH2SH3 domain restores overall accumulation and partial central accumulation of LAT in MBP peptide-primed iTregs

SH2 and SH3 domains bind phosphorylated tyrosine residues and proline-rich region respectively and are important modules for protein-protein interactions in signal transduction (274). In addition to PKC-θ V3, Clark *et al* fused LAT with another protein domain, Vav1 SH3SH2SH3, to increase LAT valence under attenuated activation conditions of 5C.C7 transgenic T cells (126). Unlike the exaggerated LAT central localisation induced by the PKC-θ V3 domain, the SH3SH2SH3 domain of Vav1 fairly reconstitutes LAT centrality in early activation of 5C.C7 T cells under costimulation blocked and Itk deficient conditions. Moreover, restoration of LAT central localisation by the fusion with Va1 SH3SH2SH3 significantly enhanced IL-2 mRNA production in these attenuated activation conditions (126). Thus, the expression of LAT Vav leads to better physiological restoration of 5C.C7 T cells under attenuated activation conditions, than that of LAT V3. To investigate whether this domain could also help to restore impaired LAT central localisation in early activation of Tg4 iTregs, we transduced MBP Ac 1-9 [4K]-primed iTregs with the fusion protein LAT Vav-GFP and live-cell imaging was performed to track LAT Vav-GFP accumulation during early activation of iTregs. LAT Vav-GFP transduced iTregs were >75% Foxp3^{+}. Representative images of LAT Vav-GFP transduced iTregs in the first two minutes of T cell activation from the DIC and GFP channel are shown in Figure 6.11.

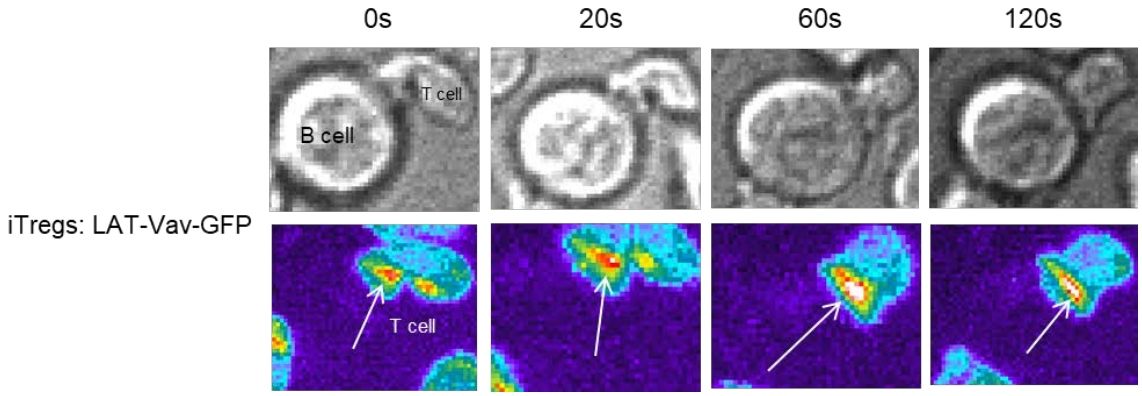

Figure 6.11 Representative live cell images of LAT Vav-GFP expressing Tg4 iTregs at four time points in early T cell activation.

Top: DIC images from four time points. Bottom: matching top-down maximum projections 3D fluorescent images (intensity is encoded in pseudocolour and increases from purple to red). Time is given in seconds relative to the formation of a tight cell couple and arrows show accumulation of the sensor.

The spatiotemporal distributions of LAT Vav-GFP during early activation of MBP peptide-primed iTregs was analysed and the accumulation patterns were compared to that of LAT-GFP in Teffs and iTregs with the same priming and activating condition (Figure 6.12). Data showing LAT-GFP accumulation in MBP peptide-primed Teffs and iTregs refer to Figure 4.10. During early activation of iTregs, LAT Vav-GFP gradually accumulated at the interface from the -40s time point and the accumulation peaked at the 60s time point with 69% of iTregs showing LAT Vav-GFP accumulation at the interface (Figure 6.12 C). The accumulation decreased slowly after and was still observed in 41% of iTregs at the 420s time point. In terms of accumulation patterning, multiple accumulation patterns were observed in LAT Vav-GFP transduced iTregs throughout the time points recorded. Central LAT Vav-GFP accumulation was found from -20s to 420s time point and the percentage of iTregs showing this patterning was around 10-20%. It was still higher than that of iTregs with other patterns from the -20s to 300s time point, although this was not dominant. Invagination accumulation of LAT Vav-GFP was observed mainly before the 180s time point and iTregs with diffuse LAT Vav-GFP accumulation could be found at all time points. Accumulation of LAT Vav-GFP at the distal pole was observed in < 20% of iTregs at early time points but diminished after the IS was formed.

More iTregs showing LAT Vav-GFP accumulation at the interface during early activation was found, compared to that of LAT-GFP, and the differences were prominent (Figure 6.12 D, the second row). The percentage of iTregs with LAT Vav-GFP accumulation at the interface was significantly higher than that with LAT-GFP accumulation at 11 out of 12 time points ($p<0.05$) and the differences were highly significant at the -20s and 20s-420s time point ($p<0.004$). Moreover, this was significantly higher than the percentage of Teffs with LAT-GFP accumulation at the -20s, 180s and 300s time point in early activation ($0.01<p<0.05$, Figure 6.12 D, the third row).

In summary, LAT Vav was found to rapidly accumulate at the interface of the IS in the first minute of iTreg activation and remain at the interface with a slow reduction afterwards. Several accumulation patterns of LAT Vav were observed at the interface in early iTreg activation. Thus, fusion of LAT with the Vav1 SH3SH2SH3 domain significantly enhances LAT localisation at the T cell-APC interface in early activation of MBP peptide-primed iTregs. LAT overall accumulation at the interface is not only restored but also prolonged by this additional domain. However, the overall accumulation of LAT Vav at the interface was largely comparable to that of unaltered LAT in Teffs, which suggests that enhancement of LAT accumulation by Vav1 SH3SH2SH3 is not as excessive as that of PKC-θ V3.

A LAT-GFP, Teffs, MBP Ac1-9 [4K] primed

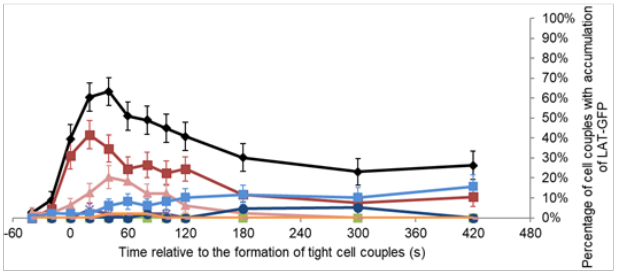

B LAT-GFP, iTregs, MBP Ac1-9 [4K] primed

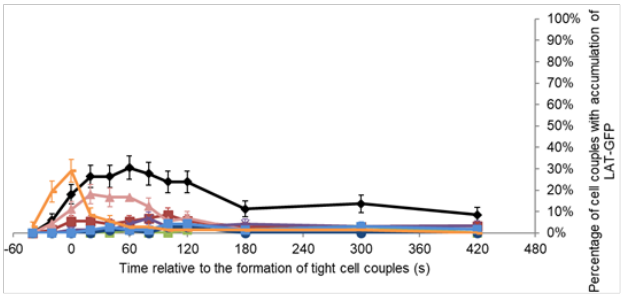

C LAT Vav-GFP, iTregs, MBP Ac1-9 [4K] primed

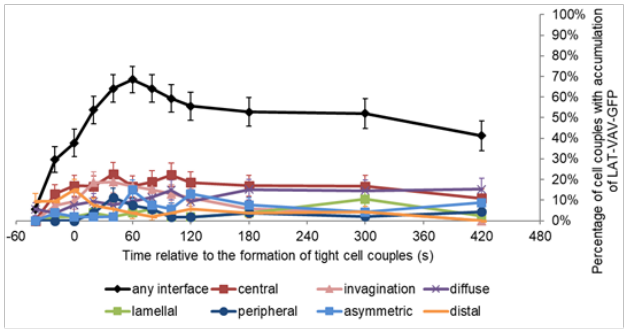

D Statistical comparisons of any interface accumulation

Time (s)	-40	-20	0	20	40	60	80	100	120	180	300	420
Teffs (LAT) vs iTregs (LAT)	0.78	0.83	0.02	0.0004	0.0001	0.04	0.03	0.03	0.08	0.02	0.33	0.04
			*	***	***	*	*	*		*		*
iTregs (LAT) vs iTregs (LAT Vav)	0.18	0.001	0.02	0.003	5.4E-05	5.2E-05	0.00011	0.00013	0.00061	1.3E-06	2.4E-05	0.00018
		**	*	**	****	****	***	***	***	****	****	***
Teffs (LAT) vs iTregs (LAT Vav)	0.9	0.02	0.99	0.63	0.91	0.11	0.18	0.21	0.19	0.04	0.01	0.23
		*								*	*	

Figure 6.12 More LAT Vav-GFP accumulation is found at the interface during early activation of MBP Ac1-9 [4K]-primed iTregs, compared to that of LAT-GFP.

MBP Ac1-9 [4K]-primed iTregs expressing LAT Vav-GFP were activated by MBP Ac1-9 [4Y]-primed PL8 cells and imaged using spinning disk confocal microscopy for 15 minutes. DIC and GFP images were analysed to determine formations of a tight cell couple (0s). Data of LAT-GFP accumulation in MBP Ac1-9 [4K]-primed **A)** Teffs (n=49, four experiments) and **B)** iTregs (n=72, two experiments) refer to Figure 4.10. **C)** Spatiotemporal distribution patterns of LAT Vav-GFP for 12 time points in MBP Ac1-9 [4K]-primed iTregs (n=54, three experiments). **D)** Comparing the percentages of cells with LAT-GFP or LAT Vav-GFP accumulation at the interface during the activation of corresponding cell types using a two proportion z-test. Numerals and asterisks indicate p-values, and asterisk colours denote whether differences remain significant with the Bonferroni correction (0.01<*<0.05, 0.004<**<0.01, 0.001<**<0.004, 0.0001<***<0.001, ****<0.0001). Error bars indicate standard error of the mean.

To investigate LAT Vav-GFP accumulation at the interface centre during early iTreg activation, we first focused on iTregs showing either central or invagination patterning of LAT Vav-GFP in MBP peptide-primed iTregs. As described in Figure 4.10 from section 4.8, the percentage of Teffs showing LAT-GFP central + invagination accumulation at the interface was significantly higher than that of iTregs in the first two minutes of activation ($p<0.05$, Figure 6.13 A). In early iTreg activation, the percentage of iTregs with central + invagination accumulation of LAT V3-GFP was higher than that of LAT-GFP from the -20s to 420s time point (Figure 6.13 B). The differences were significant at the -20s, 40s and 80s-300s time point ($0.004<p<0.05$). The total amount of LAT Vav-GFP central and invagination accumulation in early iTreg activation was comparable to that of LAT-GFP in early Teff activation (Figure 6.13 C). No significant differences were found when comparing the percentages of iTregs showing central + invagination patterning of LAT Vav-GFP and that of Teffs with LAT-GFP central + invagination accumulation at the interface in early activation. These observations indicate that LAT localisation within the central region of the interface is enhanced by fusion with Vav1 SH3SH2SH3 domain.

Then we compared only the central accumulation of LAT V3-GFP and LAT-GFP in corresponding cells. As described in Figure 4.11, section 4.8, more central LAT-GFP accumulation was found in Teffs than that in iTregs at 11 out of 12 time points, and the percentage of Teffs with LAT-GFP central patterning was significantly higher than that of iTreg from in the first two minutes of activation ($p<0.01$, Figure 6.14 A). In early iTreg activation, more central accumulation of LAT Vav-GFP was found from -20s to 420s time point, compared to that of LAT-GFP (Figure 6.14 B). The percentage of iTregs with LAT Vav-GFP central accumulation was significantly higher than that with LAT-GFP central accumulation at the -20s, 40s and 120s-300s time point ($p<0.05$). In Figure 6.14 C, the percentage of Teffs with LAT-GFP central accumulation was higher than that of iTregs showing LAT Vav-GFP central accumulation mainly in the first 40 seconds of activation. The differences were only significant at the 20s time point but not prominent ($0.01<p<0.05$). These comparisons show that fusing LAT with the Vav1 SH3SH2SH3 domain enhances LAT central localisation at the interface in early iTreg activation.

No significant differences were found when comparing the percentage of cells with invagination patterning of LAT-GFP in Teffs and iTregs at all time points (Figure 6.14 D). The percentage of iTregs with LAT Vav-GFP invagination accumulation was also comparable to that of Teffs or iTregs with LAT-GFP invagination accumulation at all time points (Figure 6.14 E and F). Therefore, fusion of LAT with the Vav1 SH3SH2SH3 domain does not have impacts on LAT invagination accumulation in early iTreg activation.

In summary, in early activation of MBP peptide-primed iTregs, fusing LAT with Vav1 SH3SH2SH3 domain restores LAT overall accumulation at the IS and partially restores LAT central localisation, which is likely to enhance cSMAC formation and LAT nucleated signal transduction. The significantly increased localisation of LAT at the interface driven by the Vav1 SH3SH2SH3 domain can also be linked with the improved morphology of LAT Vav transduced iTregs, mostly in the first minute after the formation of tight cell couples (Figure 6.1). These consistent observations suggest that a higher level of LAT accumulation at the interface is positively associated with better T cell-APC interactions, and are both indicative of efficient T cell activation.

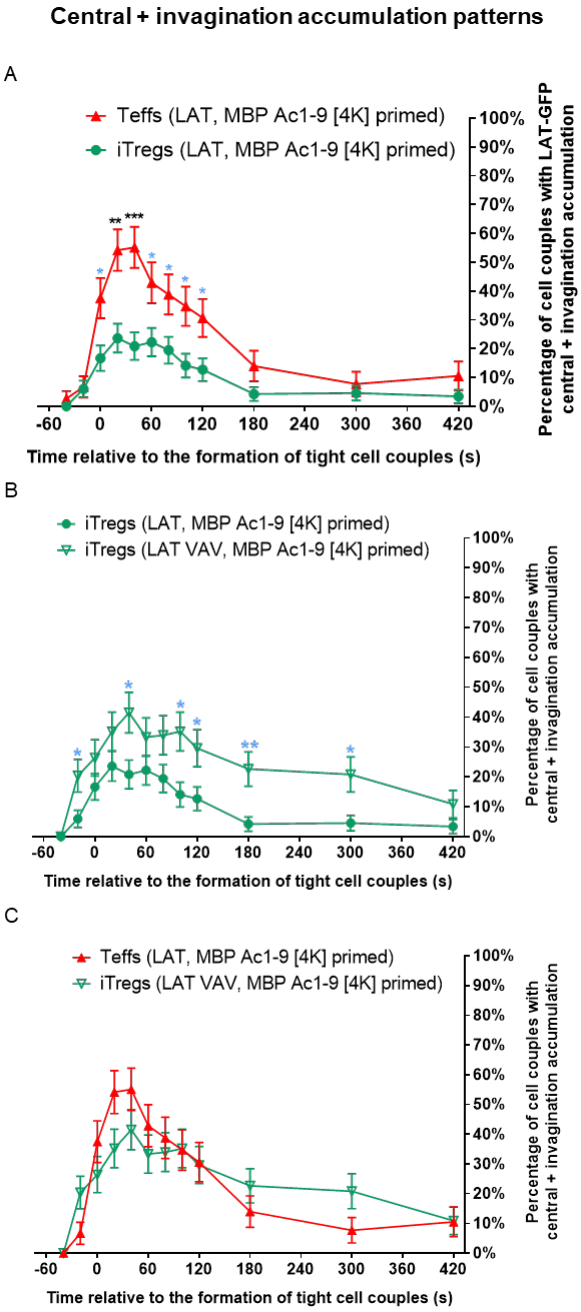

Figure 6.13 During early activation of MBP Ac1-9 [4K]-primed iTregs, the amount of central and invagination accumulation of LAT Vav-GFP at the interface is upregulated, compared to that of LAT-GFP.

In early activation of MBP Ac1-9 [4K] primed T cells, the percentages of cells with central + invagination accumulation of **A)** LAT-GFP in Teffs and iTregs, **B)** LAT-GFP and LAT Vav-GFP in iTregs and **C)** LAT-GFP in Teffs and LAT Vav-GFP in iTregs were compared. Data of LAT-GFP transduced Teffs (n=49, four experiments) and iTregs (n=72, two experiments) refer to Figure 4.11, and 54 cell couples of LAT Vav-GFP expressing iTregs from three experiments were analysed. A two proportion z-test was used to calculate statistical significance. Asterisks indicate p-values and colours indicate whether differences remain significant with the Bonferroni correction (0.01<*<0.05, 0.004<**<0.01, 0.001<**<0.004, ***<0.001). Error bars indicate standard error of the mean.

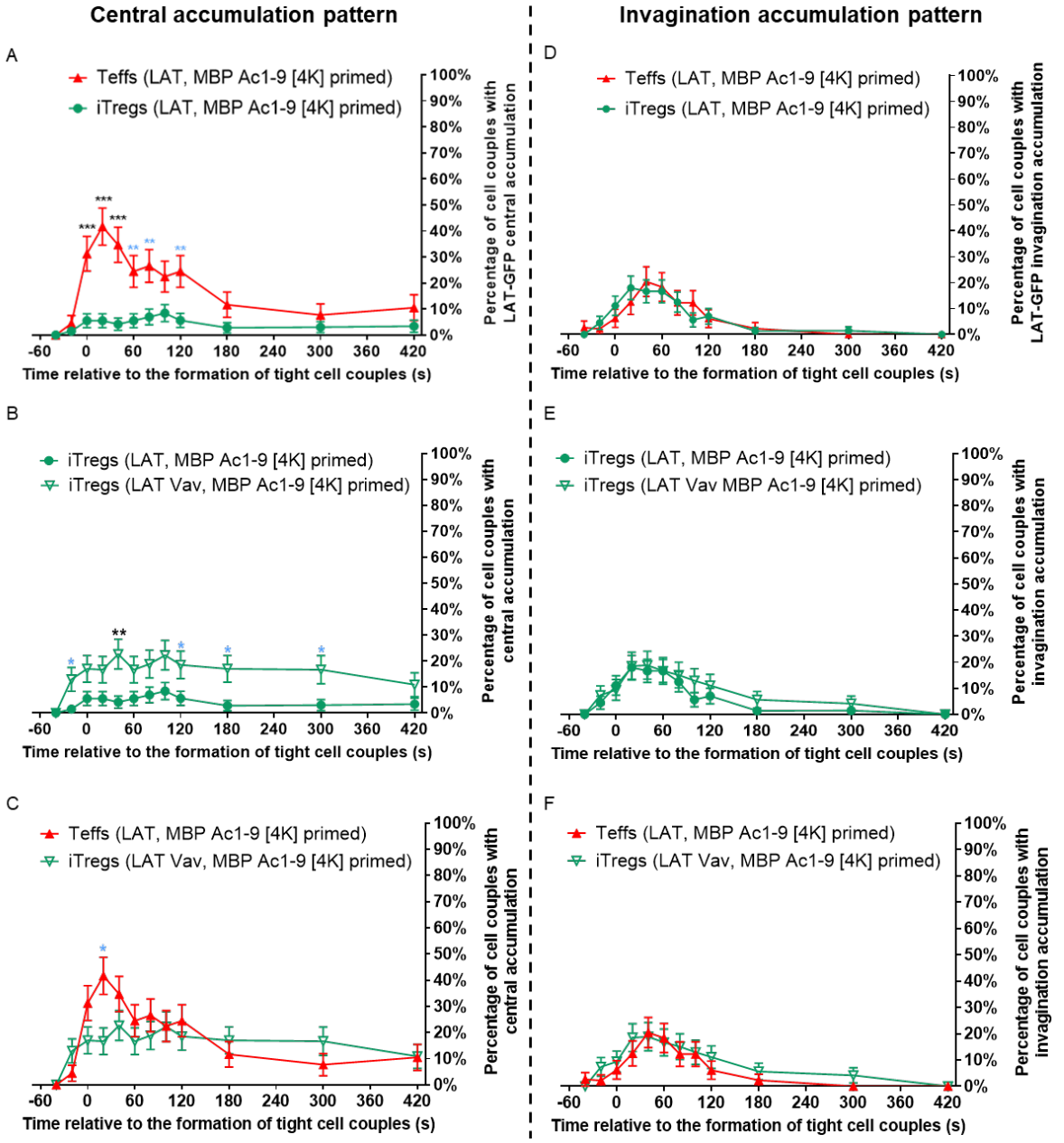

Figure 6.14 LAT Vav-GFP shows increased central patterning at the interface in early activation of MBP peptide-primed iTregs, compared to that of LAT-GFP.

In early activation of MBP peptide-primed T cells, comparing the percentages of cells showing central patterning of **A)** LAT-GFP in Teffs and iTregs, **B)** LAT-GFP and LAT Vav-GFP in iTregs and **C)** LAT-GFP in Teffs and LAT Vav-GFP in iTregs, and the percentage of cells showing invagination patterning of **D)** LAT-GFP in Teffs and iTregs, **E)** LAT-GFP and LAT Vav-GFP in iTregs and **F)** LAT-GFP in Teffs and LAT Vav-GFP in iTregs. Data of LAT-GFP transduced Teffs (n=49, four experiments) and iTregs (n=72, two experiments) refer to Figure 4.11, and 54 cell couples of LAT Vav-GFP expressing iTregs from three experiments were analysed. Statistical significance was calculated with A two proportion z-test. Asterisks indicate p-values and colours indicate whether differences remain significant with the Bonferroni correction (0.01<*<0.05, 0.004<**<0.01, 0.001<**<0.004, ***<0.001). Error bars indicate standard error of the mean.

6.8 Computational analyses show that fusion with Vav1 SH3SH2SH2 significantly increases LAT accumulation at the IS and centre of the interface

In parallel to investigating spatiotemporal distribution patterns, we generated 3D model maps with LAT Vav-GFP imaging data showing relative probabilities of LAT Vav-GFP accumulation within a T cell (sensor enrichment) upon early activation of MBP peptide-primed iTreg. Then we compared the enrichment of sensors of interest within the defined IS area (overall top 10% enrichment) and central core of the interface. Data showing LAT-GFP enrichment in Teffs and iTreg refer to section 4.9.

LAT-GFP enrichment in the defined IS region of Teffs and iTregs were described above in Figure 4.13, section 4.9: compared to that in iTreg, more LAT-GFP accumulation was found in Teffs across all time points and significant differences were identified after the first minute of activation (Figure 6.15 A). In iTregs, the level of enrichment of LAT Vav-GFP at the IS was higher than that of LAT-GFP mainly at the -40s, -20s and 60s-420s time points (Figure 6.15 B). However, the differences were only significant at the -20s time point ($0.004<p<0.01$). Within the defined IS area, the enrichment of LAT Vav-GFP in iTregs was comparable to that of LAT-GFP in Teffs mainly before the 80s time point (Figure 6.15 C). Teffs displayed a higher level of LAT-GFP enrichment than that of LAT Vav-GFP in iTregs from the 80s to 420s time point, and the differences were only significant at the 420s time point ($0.01<p<0.05$). These results show that when fused to the Vav1 SH3SH2SH3 domain, more LAT molecules are driven to the synapse in early activation of iTregs. However, the enhancement does not fully restore LAT accumulation at the IS, as the enrichment of LAT Vav-GFP in iTregs was only partially comparable to that of LAT-GFP in Teffs.

Within the central core of the IS, the level of enrichment of LAT-GFP in Teffs was higher than that in iTregs at all time points (Figure 6.15 D). Significant differences were observed at the 80s and 120s-420s time points ($0.004<p<0.05$). In iTregs, LAT Vav-GFP enrichment in the central core of the IS was higher than that of LAT-GFP at most time points and the differences were significant at the -20s time point ($0.01<p<0.05$, Figure 6.15 E). Inside the central core, LAT Vav-GFP enrichment of iTregs was comparable to that LAT-GFP enrichment at early time points (-40s to 80s, Figure 6.15 F). Although the level of LAT-GFP enrichment in the central core of Teffs was higher than that of LAT Vav-GFP enrichment within this region of iTregs after the 60s time point, no significant differences were identified throughout all time points. These observations suggest that the impaired LAT localisation in the central core of the IS in early activation of iTregs is partially restored by fusing LAT with the Vav1 SH3SH2SH3 domain.

In summary, spatiotemporal distributions of LAT Vav-GFP within the entire and central core of the IS in early iTreg activation was analysed by the systematic computational approach. A higher level of LAT Vav-GFP accumulation at the IS of iTregs was identified, compared to that of LAT-GFP. These results indicate that in early activation of MBP peptide-primed iTregs, LAT overall and central accumulation at the immune synapse is enhanced by fusion of LAT with the Vav1 SH3SH2SH3 domain. However, the enhancement does not fully restore impaired LAT accumulation in iTregs. Again, spatiotemporal pattern-based and computational analysis showed partial consistency in detecting increased LAT Vav-GFP accumulation in early iTreg activation.

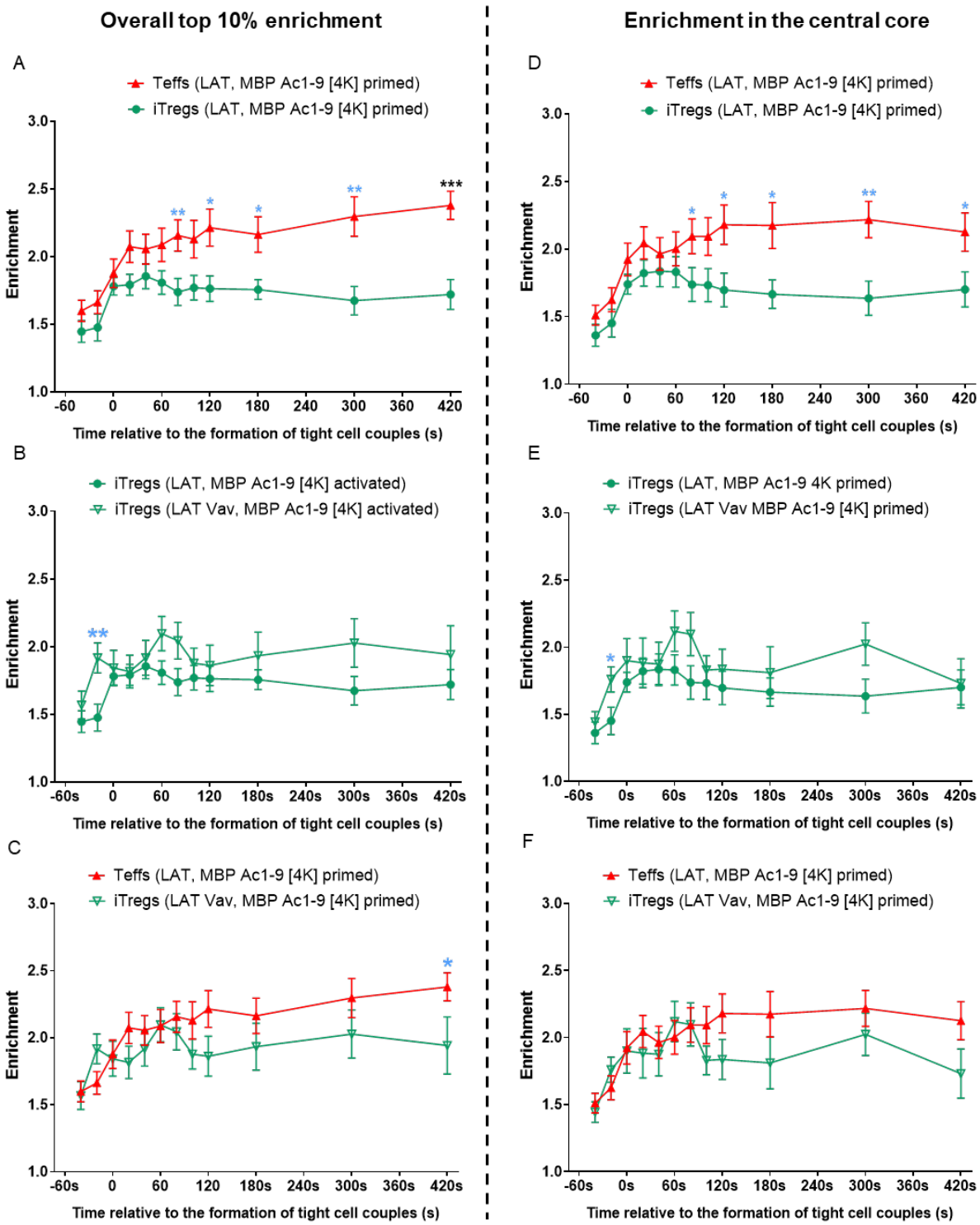
Overall top 10% enrichment
Enrichment in the central core
A
Teffs (LAT, MBP Ac1-9 [4K] primed)
iTregs (LAT, MBP Ac1-9 [4K] primed)
Enrichment
Time relative to the formation of tight cell couples (s)
D
B
iTregs (LAT, MBP Ac1-9 [4K] activated)
iTregs (LAT Vav, MBP Ac1-9 [4K] activated)
E
iTregs (LAT, MBP Ac1-9 4K primed)
iTregs (LAT Vav MBP Ac1-9 [4K] primed)
C
iTregs (LAT Vav, MBP Ac1-9 [4K] primed)
F

Figure 6.15 When fused to the Vav1 SH3SH2SH3 domain, LAT-GFP enrichment within the entire and central core of the IS are enhanced in early the activation of MBP Ac1-9 [4K]-primed iTregs.

Computational analyses were performed on LAT Vav-GFP transduced MBP peptide-primed iTregs to generate 3D model maps, which show enrichment of the sensor within a cell. Comparing **A)** LAT-GFP enrichment in Teffs and iTregs, **B)** LAT-GFP and LAT Vav-GFP enrichment in iTregs, and **C)** LAT-GFP enrichment in Teffs and LAT Vav-GFP enrichment in iTregs, within the IS (top 10% enrichment). Comparing **D)** LAT-GFP enrichment in Teffs and iTregs, **E)** LAT-GFP and LAT Vav-GFP enrichment in iTregs, and **F)** LAT-GFP enrichment in Teffs and LAT Vav-GFP enrichment in iTregs, within the central core of the IS. Data of LAT-GFP enrichment in Teffs (28 cell couples from four experiments) and iTregs (28 cell couples from two experiments) refer to Figure 4.13 and 4.14, and 22 cell couples of LAT Vav-GFP transduced iTregs from three experiments were analysed. Log-transformed data were analysed with unpaired Student's test to calculate statistical significance. Asterisks indicate p-values and colours indicate whether differences remain significant with the Bonferroni correction (0.01<*<0.05, 0.004<**<0.01, ***<0.001). Error bars indicate standard error of the mean.

6.9 LAT V3 tends to reduce IFN-γ and IL-10 production while LAT Vav slightly enhances IL-10 secretion of iTregs upon activation

To investigate whether fusing LAT with the PKC V3 or Vav1 SH3SH2SH3 protein domain can affect the capability of Tg4 iTregs to secrete IFN-γ and IL-10, we transduced Tg4 MBP Ac1-9 [4K]-primed iTregs with LAT-GFP, LAT V3-GFP and LAT Vav-GFP and assessed their production of these two cytokines upon activation by ELISAs. The induction of iTregs and retroviral transduction were performed as described in chapter 3. On day 5 of culture, successful induction of iTregs was confirmed by Foxp3 staining. Then GFP^+ iTregs within a positive FACS gate (1/3 log shift above the negative) were sorted. GFP^+ iTregs were resuspended in Treg medium and transferred to a 96-well round plate. In each well, 0.5-1 x 10^5 cells were restimulated with an equal number of mitomycin C pre-treated PL8 cells and 10 μg/ml MBP Ac1-9 [4K]. The restimulation lasted for 18 hours and cell culture supernatants were collected. ELISAs were performed to quantify the levels of IFN-γ and IL-10. iTregs used for IFN-γ ELISAs were >86% $Foxp3^+$ and for IL-10 ELISAs were >72% $Foxp3^+$. Supernatant samples from untransduced iTregs were used as controls.

Figure 6.1 A show that untransduced iTregs produced significantly more IFN-γ than LAT-GFP, LAT V3-GFP and LAT Vav-GFP expressing iTregs ($p<0.01$) after 18 hours of peptide-induced restimulation. The amount of IFN-γ detected in the cell culture of LAT V3-GFP expressing iTregs was slightly but not significantly reduced, compared to that of LAT-GFP transduced iTregs. The level of IFN-γ secreted by LAT Vav-GFP and LAT-GFP transduced iTregs were comparable. To investigate the relative differences of IFN-γ secretion among transduced iTregs, we compared their relative amount of IFN-γ (Figure 6.16 B). The amount of IFN-γ detected in LAT-GFP expressing iTregs in each experiment was set as control (as "1") and data from the same experiment were normalised to controls. Consistently, no significant differences were observed when comparing the relative IFN-γ production among transduced iTregs, but LAT V3-GFP expressing iTregs showed a trend of secreting less IFN-γ, compared to LAT-GFP transduced iTregs ($p=0.06$).

Results from IL-10 ELISAs (Figure 6.16 C) show that the amount of IL-10 detected in untransduced iTregs upon restimulation was the highest among all four conditions. However, no significant differences were found when comparing IL-10 production in any two of the four conditions. This partially owes to the variability of experiments, as in one repeated experiment, the amount of IL-10 secreted by untransduced iTregs was nearly ten-fold higher than that in the other three experiments. The relatively low levels of IL-10 secreted by LAT-GFP, LAT V3-GFP or LAT Vav-GFP expressing iTregs were comparable. When comparing normalised IL-10 production (Figure 6.16 D), the relative IL-10 amount secreted

by LAT V3-GFP expressing iTregs was significantly lower than that of LAT-GFP expressing iTregs ($p<0.01$). Moreover, the expression of LAT Vav in iTregs slightly but not significantly increased IL-10 production.

In conclusion, retroviral transduction of iTregs with LAT-GFP, LAT V3-GFP or LAT Vav-GFP significantly reduces their ability to produce IFN-γ and IL-10 when activated by MBP peptides. Retroviral transduction or overexpression of LAT is likely to impair cytokine secretion in T cells. When transduced iTregs were restimulated with MBP peptides, the expression of LAT V3 consistently showed a trend of downregulating IFN-γ and IL-10 production. While LAT Vav expression in iTregs barely affected IFN-γ but showed a trend of enhancing IL-10 secretion. These results suggest that fusion of LAT with the PKC-θ V3 and Vav1 SH3SH2SH3 domain affect cytokine secretion differently in iTregs, and LAT Vav tends to induce more IL-10 secretion and possibly better regulatory function of iTregs. Again, these results are consistent with the previous study, where LAT V3 does not affect the amount of IL-2 mRNA and LAT Vav enhances IL-2 mRNA production under attenuated T cell activation conditions in 5C.C7 Teffs (126). Fusion with the PKC-θ V3 domain has been shown to enhance T cell-APC interactions, strongly drives and prolongs LAT localisation at the interface of the IS in early activation of iTregs. Most likely, the excessive LAT polarisation induced by the additional PKC-θ V3 domain disturbs signalling complex spatiotemporal organisation at late time points in the cSMAC and subsequently affect cytokine production of iTregs. In contrast, full but not an excessive restoration of LAT overall accumulation at the IS induced by Vav1 SH3SH2SH3 mildly promotes better iTreg function by enhancing IL-10 production. Hence, increasing LAT valence to a moderate extent in Tg4 iTregs restores impaired LAT overall localisation at the interface and improves iTreg regulatory function, rather than induces iTregs to show more Teff phonotypes.

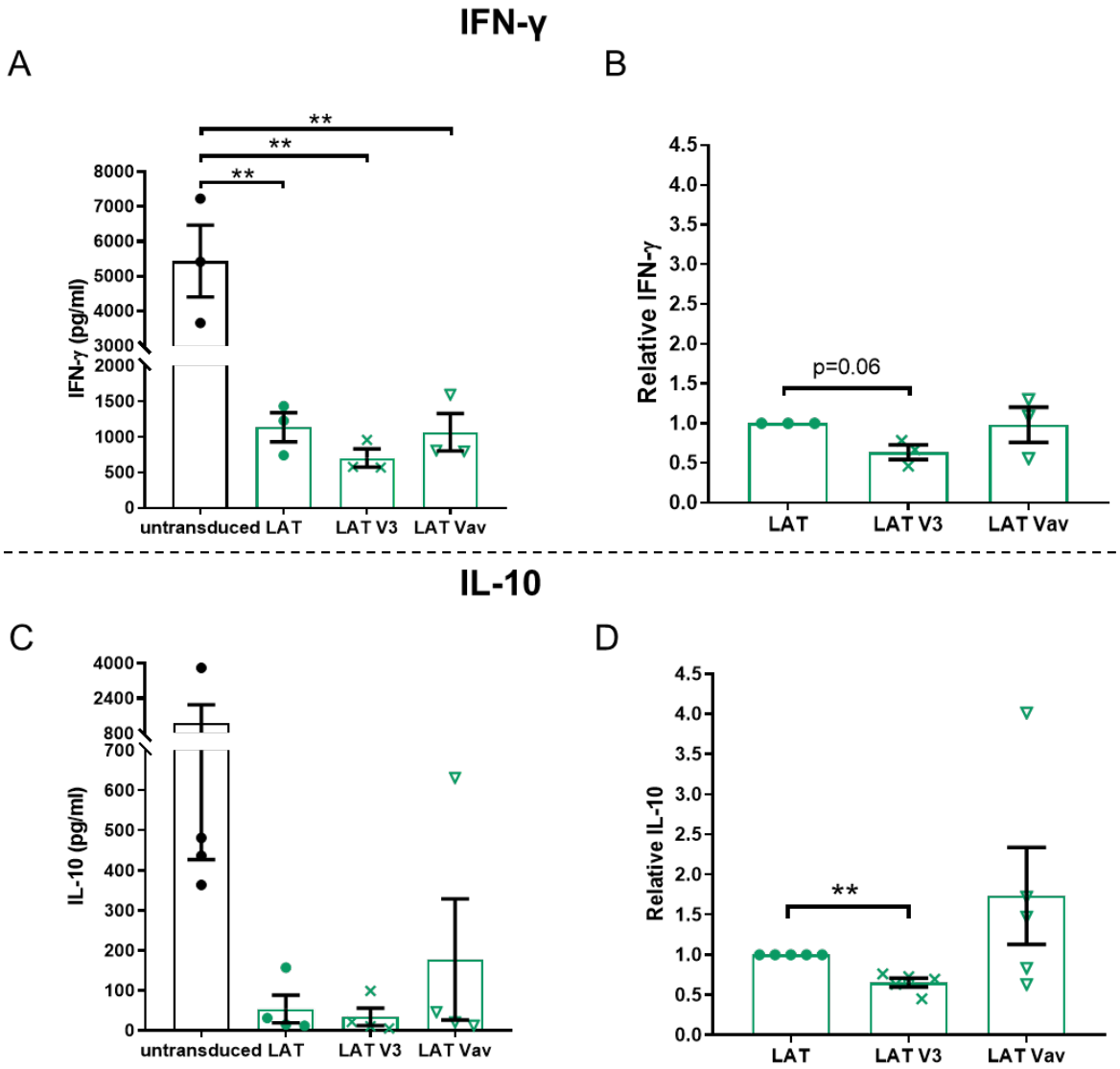

Figure 6.16 Retroviral transduction of iTregs with LAT related sensors impairs cytokine secretion and expression of LAT V3 and LAT Vav iTregs tends to have different impacts on IFN-γ and IL-10 production.

MBP peptide-primed iTregs transduced with LAT-GFP, LAT V3-GFP or LAT Vav-GFP were restimulated on day 5 of culture with MBP peptides and PL8 cells (1:1 ratio, 5-10 x 10^4 cells each) for 18 hours. Cell culture supernatants were collected and used for ELISAs to assess the amount of IFN-γ and IL-10. Untransduced iTregs were used as a control. The level of **A)** IFN-γ (n=3) and **C)** IL-10 (n=4) produced by untransduced, LAT-GFP, LAT V3-GFP and LAT Vav-GFP transduced iTregs when restimulated. Normalised **B)** IFN-γ (n=3) and **D)** IL-10 (n=5) levels among GFP-tagged groups. Statistical significance was calculated using One-way ANOVA (**A** and **C**) and multiple paired Student's T-test (**B** and **D**). Asterisks indicate p-values (**<0.01). Error bars indicate standard error of the mean.

6.10 Discussion

Previous work by Clark *et al* has shown that fusion of LAT with the PKC-θ V3 (LAT V3) and Vav1 SH3SH2SH3 protein domain (LAT Vav) increases LAT valence and restores its centrality upon attenuated activation conditions of 5C.C7 T cells (126). Moreover, restoration of LAT central clustering to a level comparable to that seen under full stimulus conditions by Vav1 SH3SH2SH3 enhances IL-2 mRNA production upon attenuated T cell stimuli, while the excessive LAT V3 central clustering does not. Therefore, complete, but not excessive reconstitution of LAT clustering in the cSMAC promotes better effector function of T cells. In this chapter, we measured morphological parameters, LAT polarisation and cytokine secretion in LAT V3 and LAT Vav expressing Tg4 iTregs to investigate whether increasing LAT valence could change how Tg4 iTregs behave in T cell activation.

6.10.1 LAT V3 and LAT Vav induce iTregs to show more morphological phenotypes of Teffs upon activation

As described in chapter 4, upon IS formation, LAT transduced Tg4 iTregs display a narrow contact interface and are more likely to form an extended lamella, compared to Teffs. Such morphological features are indicative of less effective T cell activation. The expression of LAT V3 in Tg4 iTregs elongates the interface of contact and induces the formation of more compressed cell couples in the first two minutes of activation. LAT V3 transduced iTregs and LAT transduced Teffs are morphologically similar in these two minutes. Therefore, LAT V3 largely restores the morphological changes of iTregs and most likely improves antigen presentation upon activation. However, as mentioned in section 5.9.3, a wide interface of contact is not always needed in early T cell activation. At the stabilisation stage, part of a T cell retracts from a B cell, forming a round cell shape (163). This cell rounding process is partially recovered by the expression of LAT V3. Although the expression of LAT V3 reduces that lamella depth and extends the interface within the first two minutes of activation, it does not reduce the frequency of forming an extended lamella in iTregs. Moreover, the percentage of LAT V3 transduced iTregs showing an extended lamella was the highest among the four types of cells at late time points (60s and 120s), though the difference was not significant. Therefore, the restoration of T cell morphology induced by fusion with the PKC-θ V3 domain is not complete. Sustained extension of the contact interface in LAT V3 expressing iTregs promotes better formation of cell couplings but might impede cell rounding at later stages of T cell-APC interactions.

Morphological alterations induced by LAT V3 and LAT Vav in iTregs are not entirely the same. In terms of widening the interface and shortening the lamella depth at early stages of activation, LAT Vav is not as potent as LAT V3. However, the expression of LAT Vav reduces the frequency of showing an extended lamella in iTregs, particularly in the first 20

seconds of activation, which helps to pull iTregs towards APCs. Overall, they both promote the formation of more stable and compressed T cell-APC conjunctions which are observed in Teffs. Most likely such phenotypes are related to their enhanced LAT accumulation at the interface.

6.10.2 Excessive and full restoration of LAT overall accumulation at the interface are induced by fusion with PKC V3 and Vav1 SH3SH2SH3 respectively

Impaired LAT overall accumulation at the interface of Tg4 MBP peptide-primed iTregs is excessively enhanced by fusing LAT with PKC-θ V3, which is consistent with the previous study (126). The first two minutes of tight cell coupling are characterised by rich accumulation of a large number of signalling intermediates of the cSMAC, including LAT, SLP-76, Grb2, Vav1 and PKC-θ (126, 134, 135). Such a transient peak of this biochemically detectable signalling activity is important for translocation of NFAT and NF-κB (130, 134). Under full and attenuated stimulus conditions, LAT centrality at the interface of 5C.C7 T cells can be exaggeratedly enhanced by fusion with PKC-θ V3 domain. In the former condition, excessively forced LAT central clustering diminishes recruitment of Grb2, Lck and Vav1, thus disturbs the finely regulated signalling system (126). Therefore, Clark *et al* suggest that in the first to two minutes of T cell activation, the cSMAC rapidly recruits key proximal signalling intermediates via multivalent interactions to form supramolecular complexes. Then, a number of these large proteins depart from the cSMAC and form smaller clusters which spread over the entire interface driven by a lamellal actin network(126, 135) Sustained LAT V3 central accumulation in 5C.C7 T cells possibly impedes transformation of these two different roles of the cSMAC and subsequently upset proximal T cell signalling. However, in Tg4 iTregs, impaired LAT central clustering is only partially restored by fusion with PKC-θ V3, mainly in the first two minutes of activation (Figure 6.5 A-C). In addition, fusing LAT with PKC-θ V3 significantly increases LAT diffuse accumulation at most time points. These data suggest that fusion with PKC-θ V3 excessively enhance LAT overall accumulation in iTregs, but does not specifically enhance central LAT accumulation. Notably, in anti-CD3/28-primed iTregs, fusion with PKC V3 excessively enhanced LAT central clustering, particularly after the 120s time point. The reactions of anti-CD3/28 and MBP peptide-primed iTreg to manipulation of LAT localisation are not identical, but comparable. Possibly, less efficiently activated anti-CD3/28-primed iTregs are more sensitive to such manipulation but currently, we do not understand the mechanisms. Given that MBP peptide-primed iTregs are more physiological comparable to Tregs *in vivo* (pTregs), we tend to use peptide-primed iTregs address our research questions.

In contrast, fusing LAT with Vav1 SH3SH2SH3 fully restores LAT overall accumulation at the T cell-APC interface. One key feature of LAT Vav-GFP accumulation at the interface of iTregs is that after reaching the peak at the 60s time point, the accumulation gradually decreased and was comparable to that of LAT-GFP in Teffs at most time points. Impaired central LAT clustering in iTregs is also partially restored by fusion with Vav1 SH3SH2SH3, which slightly increases LAT accumulation with other localisation preferences. These results are partially consistent with the previous study: LAT Vav fully restores overall and central accumulation under attenuated activation conditions of 5C.C7 Teffs (126). However, as a full restoration of central LAT localisation induced by fusion with Vav1 SH3SH2SH3 was not observed in Tg4 iTregs, partially enhanced LAT Vav central accumulation possibly improve cSMAC clustering in a minor fashion. In brief, fusion of LAT with Vav1 SH3SH2SH3 domain restores overall LAT accumulation at the interface with an increased central localisation preference.

Enhanced LAT accumulation at the interface driven by fusion with PKC-θ V3 and Vav1SH3SH2SH3 contributes to morphological alterations of iTregs during T cell-APC interactions via actin network. Tyrosine phosphorylation of LAT results in recruiting SLP-76 and subsequently Nck and Vav1 to the LAT signalosome, and the assembly of a tri-molecular complex of Nck, SLP-76 and Vav1 is required for TCR-induced actin polymerisation (100, 275). More directly, LAT deficient T cells are characterised with irregular and transient T cell spreading driven by the actin cytoskeleton and reconstitution of LAT restores most of the morphological changes in these cells (212). We have also shown in chapter 4 that Tg4 iTregs displayed impaired LAT and delayed F-actin accumulation, particularly in the first two minutes of activation (Figure 4.10 and 4.22). These data suggest that defective LAT accumulation from upstream proximal signalling attenuates subsequent actin polymerisation and result in inefficient T cell spreading and IS formation. Therefore, excessive and full restoration of LAT accumulation at the interface by fusion of PKC-θ V3 and Vav1 SH3SH2SH3 enhance actin polymerisation and help to promote more stable and efficient T cell-APC interactions.

6.10.3 Restoration of LAT accumulation at the interface by fusion with Vav1 SH3SH2SH3 marginally regulates cytokine production of iTregs

Spatiotemporal organisation of T cell signalling intermediates is associated with cell function. As mentioned earlier, the V3 domain of PKC-θ is required for its translocation to cSMAC upon activation, and loss or replacement of this domain abrogates activation of transcription factors including NF-κB, Ap-1 and NFAT (238). Research by Singleton *et al* shows that Itk deficiency in DO11.10 T cells impairs Cdc42 central localisation and actin accumulation at the T cell-APC interface, and reconstituting Cdc42 central accumulation restore actin

accumulation with enhanced peripheral patterning (192). Moreover, Itk deficiency and costimulation blockade both reduces LAT central localisation and IL-2 secretion and mRNA production upon T cell activation, and fusion with Vav1 SH3SH2SH3 domain restores of LAT centrality and consistently enhances the amounts of IL-2 mRNA in both conditions (126)

Results of IFN-γ and IL-10 ELISAs show that retroviral transduction of GFP tagged LAT related sensors significantly reduced IFN-γ and IL-10 production in Tg4 iTregs upon peptide-induced activation. Increasing the total amounts of LAT in T cells by retroviral transduction may change the composition of the cSMAC, and excessive LAT accumulation at the interface drives sequestration of LAT. Among the GFP-labelled iTregs, expression of LAT V3 in iTregs shows a trend of reducing both IFN-γ and IL-10 while LAT Vav tends to enhance IL-10 secretion. As the impacts were both minor, LAT spatiotemporal distribution likely regulates cytokine secretion of iTreg to a small extent. Transcription factors such as E4BP4, IRF4 and Blimp1 may play a more decisive role in regulating IL-10 production by Tregs (276, 277).

Chapter 7 General discussion

$CD4^+$ Teffs and Tregs play different roles in immune responses. Teffs release pro-inflammatory cytokines to activate innate immune cells, enhance antibody production and assist the cytotoxic activity of $CD8^+$ T cells (21). Tregs mediate immune suppression by secreting anti-inflammatory cytokines, expressing coinhibitory molecules and generating immunosuppressive molecules (49). T cell function is closely associated with TCR-induced activation, which is regulated by dynamic spatiotemporal organisation of T cell signalling intermediates (126, 130, 134, 135). Our main research aims were to compare spatiotemporal organisation of T cell signalling molecules in the activation of Tg4 Teffs and iTregs, and investigate how proximal T cell signalling would affect their function. Key signalling intermediates analysed in this study were LAT, TCR-ζ, PKC-θ, Vav1 and F-actin.

7.1 Anti-CD3/28 and MBP peptide-priming generate different iTregs

Tg4 naïve $CD4^+$ T cells were efficiently differentiated into Teffs and iTregs by T cell priming using different cytokines. Transcription factor Foxp3 is specifically expressed by Tregs and indispensable for their suppressive function (46, 48). In this project, we have applied two priming methods to generate $Foxp3^+$ iTregs: priming naive $CD4^+$ T cells with anti-CD3/28 antibodies and priming mixed splenocytes and lymphocytes containing endogenous APCs with MBP Ac1-9 peptides. These two methods both effectively generated $Foxp3^+$ iTregs, and the percentage of $Foxp3^+$ cells induced by the former was significantly higher, as previous studies reported (53, 139). Previously Verhagen and Wraith (148) reported that anti-CD3/28 and MBP peptide-primed iTreg express different levels of Helios, a transcription factor. Here we propose that these two types of iTregs are different for two main reasons: (1) Spatiotemporal distribution patterns of LAT and TCR-ζ in anti-CD3/28 and MBP peptide-primed iTregs are different. In early activation of anti-CD3/28 primed iTregs, more LAT accumulation at the interface was observed after the first 120 seconds of activation, but fewer TCR-ζ molecules localised at the interface at early time points (-40s-40s). (2) When treated with dual CTLA-4 and PD-1 blockade upon activation, they show different phenotypes. Anti-CTLA-4/PD-1 treated anti-CD3/28 primed iTregs showed largely elongated cell shapes with long lamellae, which is indicative of unstable IS formation. In early T cell activation, LAT overall accumulation at the T cell-APC interface of anti-CD3/28 primed iTregs was significantly reduced by the dual blockade. In contrast, cell couples formed by anti-CTLA-4/PD-1 treated MBP peptide-primed iTregs were more compressed, and increased LAT overall and central accumulation at the interface were observed in these iTregs, suggesting their activation was enhanced. To determine whether these two types of iTregs are functionally different, their cytokine profiles, expression of coinhibitory molecules (such as CTLA-4 and PD-1) and suppressive functions should be compared. As MBP

peptide-primed iTregs are more physiologically comparable to naturally occurring Tregs, this research mainly focused on investigating their phenotypes.

7.2 Different IFN-γ and IL-10 production by iTregs

During Tg4 Teff and iTreg generation, Teffs secreted large amounts of IFN-γ at early stages while iTregs produced relatively low levels of IFN-γ throughout induction. IL-10 was initially secreted by both cell types but iTregs maintained IL-10 production at late stages of induction. Tg4 Teffs show a dominant Th1 phenotype (154). IL-10 production of Th1 cells can be induced by IL-12 and a high dose of antigens (236), which might explain transient IL-10 secretion by Teffs. Restimulated iTregs showed a better capability of secreting IL-10 than Teffs, although not significantly. Therefore, mature iTregs develop a reduced ability to promote immune responses and are more likely to induce suppression by secreting IL-10.

7.3 TCR-ζ and PKC-θ accumulation in Tg4 T cells

Among the five signalling intermediates that we have studied, accumulation patterns of TCR-ζ and PKC-θ in Tg4 T cells were found to be different from those in previous research. Lee *et al* investigated conjunctions formed by AND TCR transgenic naive T cells and B10.BR splenic APCs and found that TCR clustering was only observed at the centre of the synapse at relatively late time points (between 15-30 min) (127), unlike that in Tg4 Teffs. We only observed medium levels of TCR central accumulation at the interface 5 minutes after IS formation (Figure 4.16). A similar study using planar bilayers containing adhesion molecules and agonist peptides revealed that TCR microclusters containing phosphorylated Lck, ZAP-70 and LAT localised at the centre of the IS by 5 min in activated AND TCR transgenic T cells (214). Moreover, in 5C.C7 mice, another transgenic model, central TCR-ζ accumulation was also observed within the first 5 minutes of T cell activation (134, 193), which is more comparable to that in Tg4 T cells. In these previous studies, initial peripheral TCR clustering was frequently observed upon early T cell activation, and it later localised at the centre and eventually internalised (after 16 min). Likely, the way of activation and level of stimulation contributes to the different spatiotemporal accumulation patterning of TCR microclusters in these studies. TCR clustering tends to have a delay accumulation pattern in T cells activated by supported planar bilayers, and TCR microclusters under weak Ag stimulation do not promote the development of the cSMAC (278). Moreover, Singleton *et al* have shown that a same sensor could localise differently in T cells from different transgenic mouse models (130).

Significantly more PKC-θ accumulation at the IS of Tg4 iTregs was observed, compared to that of Tg4 Teffs (Figure 4.18). Central PKC-θ accumulation at the IS was comparable in

both cell types but iTregs displayed more PKC-θ accumulation across the whole interface in early activation (i.e. more lamellal and diffuse patterning). However, Zanin-Zhorov *et al* reported that human Tregs activated on planar bilayers shown largely reduced PKC-θ recruitment to the IS than Teffs (201). They found that even in the presence of both anti-CD3 and anti-CD28, human Tregs still had much less PKC-θ accumulation at the IS. Moreover, stronger TCR triggering suppressed PKC-θ recruitment to the synapse in human Tregs but upregulated such accumulation in human Teffs (201). We have mentioned in section 4.14.1 that plate-bound anti-CD3/28 continuously activate target cells and eventually leads to a stronger activation. Most likely, such strong stimuli reduce PKC-θ accumulation at the IS of Tregs but affect Teffs oppositely. Thus relatively defective TCR signalling in Tg4 iTregs might contribute to their increased recruitment and defective clearance of PKC-θ at the IS in early activation. In summary, for Teffs, effective T cell-APC interactions lead to efficient activation, recruitment of PKC-θ to the IS and eventually promote immune responses, but for Tregs, less efficient activation results in defective regulation of PKC-θ localisation at the IS and thus they might display impaired immune responses, shifting towards a regulatory phenotype.

7.4 Regulating iTreg activation and function with dual CTLA-4 and PD-1 blockade

T cells need to be activated to be functional, thus we focused on studying activation of Tg4 Teffs and iTregs by comparing their spatiotemporal organising of proximal T cell signalling intermediates. Live cell imaging analyses reveal that upon TCR-induced activation, iTreg activation is defective from two aspects: (1) iTregs formed unstable T cell-APC junctions, with a narrow interface of contact, long extended lamella and elongated cell shape. (2) At the T cell-APC interface of iTregs, impaired overall and central accumulation of LAT and TCR-ζ, and delayed F-actin polarisation were observed, which indicates assembly of the cSMAC is impaired. We hypothesised that iTreg function is associated with their defective proximal T cell signalling and by enhancing or restoring these signalling events, iTreg function can be tuned.

Our first attempt was to block CTLA-4 and PD-1 coinhibitory pathways during Tg4 iTreg activation. As CTLA-4 and PD-1 are both expressed by Tregs and inhibit costimulation (247), blocking these pathways should promote better iTreg activation. Results show that more stable T cell-APC junctions were formed by iTregs treated with anti-CTLA-4/PD-1 during their activation. The dual blockade partially enhanced LAT overall and central accumulation at the interface in early iTreg activation, but did not affect their IL-10 production. Moreover, blocking CTLA-4 and PD-1 significantly inhibited the generation of

Foxp3$^+$ iTregs during iTreg induction, suggesting CTLA-4 and PD-1 pathways positively regulate iTreg development. Dual CTLA-4 and PD-1 blockade also slightly enhanced IL-10 but barely affected IFN-γ secretion by iTregs during induction. Together these data indicate that dual blockade of CTLA-4 and PD-1 promotes Tg4 iTreg activation but marginally affects their IFN-γ and IL-10 production.

7.5 Regulating iTreg activation and function by manipulating LAT spatiotemporal organisation

As dual CTLA-4 and PD-1 blockade only partially restored LAT localisation, we then directly targeted LAT to regulate iTreg activation. The adaptor protein LAT is important for promoting the formation of the cSMAC which is required for efficient T cell activation (121, 185). Upon TCR-induced activation, phosphorylated LAT rapidly localises at the interface centre and recruits multiple signalling intermediates including Grb2, Gads, PLC-γ1 and SLP-76 to the interface, forming a LAT signalosome (126, 185). These signalling events are critical for actin polymerisation, translocation and activation of key transcription factors such as NFAT and NF-κB (237). In particular, central LAT accumulation at the interface in the first two minutes is important for IL-2 mRNA production (126). Spatiotemporal patterning of LAT in Tg4 iTreg activation is defective. Previous work by Clark *et al* showed that impaired LAT central accumulation upon attenuated T cell activation can be consistently enhanced and largely restored by fusion of LAT with PKC-θ V3 domain (LAT V3) and Vav1 SH3SH2SH3 domain (LAT Vav), respectively (126). Thus we transduced iTregs with GFP-tagged LAT V3 and LAT Vav respectively and investigated whether we could reconstitute cSMAC formation in iTregs and regulate iTreg function.

Results show that LAT V3 and LAT Vav stabilised T cell-APC interactions upon iTreg activation but the former continuously enhanced cell spreading and pulled iTregs towards APCs during the first two minutes of iTreg activation. Fusion with the PKC-θ V3 and Vav1 SH3SH2SH3 domain both partially restored LAT central accumulation at the interface in iTreg activation. Moreover, the former excessively enhanced LAT overall accumulation, while the latter led to a full restoration. These observations indicate that fusing LAT to the PKC-θ V3 or Vav1 SH3SH2SH3 domain increases its total functional protein interaction motifs, thus enhances assembly of LAT signalosome at the interface in early iTreg activation. However, fusion with PKC-V3 excessively maintained LAT accumulation at the interface in iTregs to higher levels than that observed in Teffs, leading to sequestration of LAT. LAT is one of the key components of the cSMAC. Previous work (126) and this study both show that the composition of the cSMAC changes in a time-dependent manner and the two-minute borderline is critical. In early Teff activation, key signalling intermediates such as

LAT, Grb2, Gads and PKC-θ localise to the interface within the first two minutes to efficiently transduce activation signals, and many of them leave the cSMAC afterwards so that T cell activation signalling can be controlled and attenuated (126, 130, 134). Sequestration of LAT at the interface after the first two minutes would change the composition of the cSMAC and affect T cell function. Clark *et al* showed that full restoration of LAT central accumulation by the Vav1 SH3SH2SH3 domain enhances IL-2 mRNA production under attenuated T cell stimulation, but excessively enhanced LAT central accumulation by the PKC-θ V3 domain does not (126). Although in this study, fusion of LAT with PKC-θ V3 and Vav1 SH3SH2SH3 domain excessively enhanced and fully restored overall LAT accumulation in iTreg activation respectively, but their enhancement on central LAT accumulation were both partial. Possibly different cell types used contribute to the variance, as they used 5C.C7 Teffs and we used Tg4 iTregs.

Upon activation, LAT Vav transduced iTregs secreted slightly more IL-10, while LAT V3 transduced iTregs secreted less, compared to LAT transduced iTregs. IFN-γ secretion upon iTreg activation was less affected by fusing LAT with PKC-θ V3 or Vav1 SH3SH2SH3 domain. Therefore, the excessive enhancement of LAT overall accumulation induced by the PKC-θ V3 domain is more likely to upset cytokine secretion of iTregs, while reasonably restored LAT overall accumulation by the Vav1 SH3SH2SH3 domain promotes IL-10 production of iTregs to a minor extent.

7.6 Tregs in immunotherapy and clinical applications

Owing to the roles Tregs play in preventing autoimmunity and maintaining immune homeostasis, various therapeutic approaches targeting Tregs have been developed. For cell-based Treg therapies, *ex vivo*-expanded Tregs could be infused to treat autoimmune diseases such as type 1 diabetes (279). However, therapies using polyclonal Tregs tend to induce global immunosuppression and infections could occur in treated patients (280). To increase their specificity, Tregs can be modified to express an antigen-specific TCR or chimeric antigen receptor (CAR) and several studies have explored their applications in treating MS, type 1 diabetes and acquired factor VIII deficiency (281). Non-cell-based Treg therapies mainly aim to expand Tregs *in vivo* while maintaining their suppressive phenotypes. For example, a low dose of IL-2 can expand Tregs as they are more responsive to IL-2 than other T cells owing to their high surface expression of CD25 (282). An mTOR inhibitor, rapamycin blocks T cell responses to cytokines or growth factors and induces T cell anergy and deletion (283). It can also induce immune tolerance by enhancing Treg induction and proliferation (281).

A previous study reported that adoptive transfer of Tg4 iTregs could delay disease progression of EAE in Tg4 mice (268). In this project, we have shown that by transducing Tg4 iTregs with LAT V3 or LAT Vav, defective LAT localisation could be partially restored. However, the impacts of such LAT manipulation on the regulatory function of Tregs have not been directly assessed. Overall, results from ELISAs support that enhancing LAT accumulation at the IS is likely to promote a better suppressive function of Tg4 iTregs. Therefore, to further verify how such manipulation will affect T cell function and EAE progression, adoptive transfer of Tg4 cells transduced with LAT V3 or LAT Vav into Tg4 mice could be performed. Disease progression can be recorded in Tg4 recipients to determine their efficacy. Likely, transduced Teffs and iTregs may have different responses to LAT manipulation, thus they should be transferred in parallel for better understanding of LAT function in Teffs and iTregs. We expect to observe relieved EAE progression in Tg4 mice transferred with LAT Vav transduced iTregs while Teffs bearing the same sensor might exacerbate EAE. Results from such *in vivo* experiments shall provide another prospective for cell-based therapies.

7.7 Conclusions

In summary, Tg4 Foxp3^{+} iTregs can be generated successfully using MBP peptides and endogenous APCs in the presence of IL-2 and TGF-β. Activated Tg4 iTregs show a reduced ability of secrete IFN-γ and more sustained ability to produce IL-10. Live cell imaging shows that in early T cell activation iTregs form unstable T cell-APC junctions, and spatiotemporal distribution of signalling intermediates including LAT, TCR-ζ, F-actin at the T cell-APC interface are defective, compared to that of Teffs. To explore the relationship between activation and immune suppressive function of iTregs, coinhibitory pathways and LAT localisation of iTregs were manipulated.

Blocking CTLA-4 and PD-1 pathways significantly inhibit the generation of iTregs and enhance IL-10 production by iTregs to a small extent. In early iTreg activation, dual blockade of CTLA-4 and PD-1 stabiles cell coupling and partially enhances LAT overall and central accumulation at the interface and therefore enhances iTreg activation. Fusion of LAT with the PKC-θ V3 and Vav1 SH3SH2SH3 domain both stabilise cell coupling and partially restore LAT accumulation at the interface centre during iTreg activation. However, fusion with PKC-θ V3 excessively enhances LAT overall accumulation at the interface, which slightly reduces IFN-γ and IL-10 secretion by iTregs. Fusion with Vav1 SH3SH2SH3 fully restores LAT overall accumulation at the interface, which slightly increases IL-10 production by iTregs. These data suggest that blocking coinhibitory pathways and restoring LAT spatiotemporal patterning enhance activation of iTregs, but regulate their immunosuppressive function to a lesser extent. Likely, the suppressive function of Tregs is

mainly conducted via cell to cell contact. As a variety of cells are capable of secreting IL-10 (156), its role in immunosuppression induced by Tregs might be limited.

Further spatiotemporal patterning analyses of more key signalling intermediates of the cSMAC such as Grb2, Gads, SLP-76 will be required to better understand proximal T cell signalling events upon iTreg activation. LAT phosphorylation needs to be examined to validate their impaired function in iTreg activation. The *in vitro* suppression assay requires further optimisation to better assess the suppressive function of Teffs and iTreg more specifically. Using irradiated endogenous Tg4 APCs or anti-CD3 only for activation and membranes that block cell contact may lead to clearer results. Last but not least, optimising IL-10 detection, determining CTLA-4, PD-1 and TGF-β expression by Tg4 iTregs will provide a better understanding of iTreg-mediated suppression.

Chapter 8 References

1. Janeway CA, Jr., Medzhitov R. Innate immune recognition. Annual review of immunology. 2002;20:197-216.
2. Walsh D, McCarthy J, O'Driscoll C, Melgar S. Pattern recognition receptors—Molecular orchestrators of inflammation in inflammatory bowel disease. Cytokine & Growth Factor Reviews. 2013;24(2):91-104.
3. Medzhitov R, Janeway CA. Innate immunity: impact on the adaptive immune response. Current Opinion in Immunology. 1997;9(1):4-9.
4. Bonilla FA, Oettgen HC. Adaptive immunity. The Journal of allergy and clinical immunology. 2010;125(2 Suppl 2):S33-40.
5. Hardy RR, Hayakawa K. B cell development pathways. Annual review of immunology. 2001;19:595-621.
6. Harwood NE, Batista FD. Early Events in B Cell Activation. Annual review of immunology. 2010;28(1):185-210.
7. Rodríguez-Pinto D. B cells as antigen presenting cells. Cellular immunology. 2005;238(2):67-75.
8. Wieczorek M, Abualrous ET, Sticht J, Álvaro-Benito M, Stolzenberg S, Noé F, et al. Major Histocompatibility Complex (MHC) Class I and MHC Class II Proteins: Conformational Plasticity in Antigen Presentation. Frontiers in immunology. 2017;8:292-.
9. Germain RN. T-cell development and the CD4-CD8 lineage decision. Nat Rev Immunol. 2002;2(5):309-22.
10. Robey E, Fowlkes BJ. Selective Events in T Cell Development. Annual review of immunology. 1994;12(1):675-705.
11. Krangel MS. Mechanics of T cell receptor gene rearrangement. Current opinion in immunology. 2009;21(2):133-9.
12. Klein L, Kyewski B, Allen PM, Hogquist KA. Positive and negative selection of the T cell repertoire: what thymocytes see (and don't see). Nature Reviews Immunology. 2014;14(6):377-91.
13. Derbinski J, Gäbler J, Brors B, Tierling S, Jonnakuty S, Hergenhahn M, et al. Promiscuous gene expression in thymic epithelial cells is regulated at multiple levels. The Journal of experimental medicine. 2005;202(1):33-45.
14. Takada K, Kondo K, Takahama Y. Generation of Peptides That Promote Positive Selection in the Thymus. The Journal of Immunology. 2017;198(6):2215-22.
15. Jordan MS, Boesteanu A, Reed AJ, Petrone AL, Holenbeck AE, Lerman MA, et al. Thymic selection of CD4+CD25+ regulatory T cells induced by an agonist self-peptide. Nat Immunol. 2001;2(4):301-6.
16. Andersen MH, Schrama D, Thor Straten P, Becker JC. Cytotoxic T cells. J Invest Dermatol. 2006;126(1):32-41.
17. Luckheeram RV, Zhou R, Verma AD, Xia B. CD4(+)T cells: differentiation and functions. Clin Dev Immunol. 2012;2012:925135.
18. Evans CM, Jenner RG. Transcription factor interplay in T helper cell differentiation. Brief Funct Genomics. 2013;12(6):499-511.
19. Zhu J, Yamane H, Paul WE. Differentiation of effector CD4 T cell populations (*). Annual review of immunology. 2010;28:445-89.
20. Tao X, Constant S, Jorritsma P, Bottomly K. Strength of TCR signal determines the costimulatory requirements for Th1 and Th2 CD4+ T cell differentiation. The Journal of Immunology. 1997;159(12):5956-63.
21. Wan YY, Flavell RA. How diverse--CD4 effector T cells and their functions. J Mol Cell Biol. 2009;1(1):20-36.
22. Szabo SJ, Kim ST, Costa GL, Zhang X, Fathman CG, Glimcher LH. A novel transcription factor, T-bet, directs Th1 lineage commitment. Cell. 2000;100(6):655-69.
23. Bosisio D, Polentarutti N, Sironi M, Bernasconi S, Miyake K, Webb GR, et al. Stimulation of toll-like receptor 4 expression in human mononuclear phagocytes by interferon-γ: a molecular basis for priming and synergism with bacterial lipopolysaccharide. Blood. 2002;99(9):3427-31.

24. Schroder K, Hertzog PJ, Ravasi T, Hume DA. Interferon-gamma: an overview of signals, mechanisms and functions. J Leukoc Biol. 2004;75(2):163-89.
25. Newburger PE, Ezekowitz RA, Whitney C, Wright J, Orkin SH. Induction of phagocyte cytochrome b heavy chain gene expression by interferon gamma. Proc Natl Acad Sci U S A. 1988;85(14):5215-9.
26. Peng SL, Szabo SJ, Glimcher LH. T-bet regulates IgG class switching and pathogenic autoantibody production. Proceedings of the National Academy of Sciences. 2002;99(8):5545-50.
27. Whitmire JK, Tan JT, Whitton JL. Interferon-γ acts directly on CD8+ T cells to increase their abundance during virus infection. Journal of Experimental Medicine. 2005;201(7):1053-9.
28. Kimura H, Caturegli P, Takahashi M, Suzuki K. New Insights into the Function of the Immunoproteasome in Immune and Nonimmune Cells. J Immunol Res. 2015;2015:541984.
29. Ma W, Lehner PJ, Cresswell P, Pober JS, Johnson DR. Interferon-γ Rapidly Increases Peptide Transporter (TAP) Subunit Expression and Peptide Transport Capacity in Endothelial Cells. Journal of Biological Chemistry. 1997;272(26):16585-90.
30. Raphael I, Nalawade S, Eagar TN, Forsthuber TG. T cell subsets and their signature cytokines in autoimmune and inflammatory diseases. Cytokine. 2015;74(1):5-17.
31. Constantinescu CS, Farooqi N, O'Brien K, Gran B. Experimental autoimmune encephalomyelitis (EAE) as a model for multiple sclerosis (MS). Br J Pharmacol. 2011;164(4):1079-106.
32. Dos Passos GR, Sato DK, Becker J, Fujihara K. Th17 Cells Pathways in Multiple Sclerosis and Neuromyelitis Optica Spectrum Disorders: Pathophysiological and Therapeutic Implications. Mediators Inflamm. 2016;2016:5314541-.
33. McGinley AM, Edwards SC, Raverdeau M, Mills KHG. Th17 cells, γδ T cells and their interplay in EAE and multiple sclerosis. Journal of Autoimmunity. 2018;87:97-108.
34. Rostami A, Ciric B. Role of Th17 cells in the pathogenesis of CNS inflammatory demyelination. J Neurol Sci. 2013;333(1-2):76-87.
35. Lloyd CM, Hessel EM. Functions of T cells in asthma: more than just T(H)2 cells. Nature reviews Immunology. 2010;10(12):838-48.
36. Mills KH. Induction, function and regulation of IL-17-producing T cells. Eur J Immunol. 2008;38(10):2636-49.
37. Schwarzenberger P, Huang W, Ye P, Oliver P, Manuel M, Zhang Z, et al. Requirement of endogenous stem cell factor and granulocyte-colony-stimulating factor for IL-17-mediated granulopoiesis. Journal of immunology. 2000;164(9):4783-9.
38. von Vietinghoff S, Ley K. Homeostatic regulation of blood neutrophil counts. Journal of immunology. 2008;181(8):5183-8.
39. Leonard WJ, Spolski R. Interleukin-21: a modulator of lymphoid proliferation, apoptosis and differentiation. Nature Reviews Immunology. 2005;5(9):688-98.
40. Aujla SJ, Chan YR, Zheng M, Fei M, Askew DJ, Pociask DA, et al. IL-22 mediates mucosal host defense against Gram-negative bacterial pneumonia. Nature Medicine. 2008;14(3):275-81.
41. Cipollini V, Anrather J, Orzi F, Iadecola C. Th17 and Cognitive Impairment: Possible Mechanisms of Action. Frontiers in Neuroanatomy. 2019;13(95).
42. Constantinescu CS, Farooqi N, O'Brien K, Gran B. Experimental autoimmune encephalomyelitis (EAE) as a model for multiple sclerosis (MS). Br J Pharmacol. 2011;164(4):1079-106.
43. Stromnes IM, Cerretti LM, Liggitt D, Harris RA, Goverman JM. Differential regulation of central nervous system autoimmunity by T(H)1 and T(H)17 cells. Nature medicine. 2008;14(3):337-42.
44. Gershon RK, Kondo K. Cell interactions in the induction of tolerance: the role of thymic lymphocytes. Immunology. 1970;18(5):723-37.
45. Sakaguchi S, Sakaguchi N, Asano M, Itoh M, Toda M. Immunologic self-tolerance maintained by activated T cells expressing IL-2 receptor alpha-chains (CD25). Breakdown of a single mechanism of self-tolerance causes various autoimmune diseases. Journal of immunology. 1995;155(3):1151-64.

46. Fontenot JD, Gavin MA, Rudensky AY. Foxp3 programs the development and function of CD4+CD25+ regulatory T cells. Nat Immunol. 2003;4(4):330-6.
47. Wolf D, Sopper S, Pircher A, Gastl G, Wolf AM. Treg(s) in Cancer: Friends or Foe? J Cell Physiol. 2015;230(11):2598-605.
48. Hori S, Nomura T, Sakaguchi S. Control of regulatory T cell development by the transcription factor Foxp3. Science. 2003;299(5609):1057-61.
49. Schmidt A, Oberle N, Krammer PH. Molecular mechanisms of treg-mediated T cell suppression. Front Immunol. 2012;3:51.
50. Ovcinnikovs V, Ross EM, Petersone L, Edner NM, Heuts F, Ntavli E, et al. CTLA-4-mediated transendocytosis of costimulatory molecules primarily targets migratory dendritic cells. Sci Immunol. 2019;4(35).
51. Chen W, Jin W, Hardegen N, Lei KJ, Li L, Marinos N, et al. Conversion of peripheral CD4+CD25- naive T cells to CD4+CD25+ regulatory T cells by TGF-beta induction of transcription factor Foxp3. The Journal of experimental medicine. 2003;198(12):1875-86.
52. Apostolou I, von Boehmer H. In vivo instruction of suppressor commitment in naive T cells. The Journal of experimental medicine. 2004;199(10):1401-8.
53. Shevach EM, Thornton AM. tTregs, pTregs, and iTregs: similarities and differences. Immunol Rev. 2014;259(1):88-102.
54. Floess S, Freyer J, Siewert C, Baron U, Olek S, Polansky J, et al. Epigenetic control of the foxp3 locus in regulatory T cells. PLoS biology. 2007;5(2):e38.
55. Ohkura N, Hamaguchi M, Morikawa H, Sugimura K, Tanaka A, Ito Y, et al. T cell receptor stimulation-induced epigenetic changes and Foxp3 expression are independent and complementary events required for Treg cell development. Immunity. 2012;37(5):785-99.
56. Sakaguchi S, Mikami N, Wing JB, Tanaka A, Ichiyama K, Ohkura N. Regulatory T Cells and Human Disease. Annual review of immunology. 2020;38:541-66.
57. Itoh M, Takahashi T, Sakaguchi N, Kuniyasu Y, Shimizu J, Otsuka F, et al. Thymus and autoimmunity: production of CD25+CD4+ naturally anergic and suppressive T cells as a key function of the thymus in maintaining immunologic self-tolerance. Journal of immunology. 1999;162(9):5317-26.
58. Tai X, Cowan M, Feigenbaum L, Singer A. CD28 costimulation of developing thymocytes induces Foxp3 expression and regulatory T cell differentiation independently of interleukin 2. Nat Immunol. 2005;6(2):152-62.
59. Kanamori M, Nakatsukasa H, Okada M, Lu Q, Yoshimura A. Induced Regulatory T Cells: Their Development, Stability, and Applications. Trends Immunol. 2016;37(11):803-11.
60. Wawman RE, Bartlett H, Oo YH. Regulatory T Cell Metabolism in the Hepatic Microenvironment. Front Immunol. 2017;8:1889.
61. Kretschmer K, Apostolou I, Hawiger D, Khazaie K, Nussenzweig MC, von Boehmer H. Inducing and expanding regulatory T cell populations by foreign antigen. Nat Immunol. 2005;6(12):1219-27.
62. Molinero LL, Miller ML, Evaristo C, Alegre ML. High TCR stimuli prevent induced regulatory T cell differentiation in a NF-kappaB-dependent manner. Journal of immunology. 2011;186(8):4609-17.
63. Semple K, Nguyen A, Yu Y, Wang H, Anasetti C, Yu XZ. Strong CD28 costimulation suppresses induction of regulatory T cells from naive precursors through Lck signaling. Blood. 2011;117(11):3096-103.
64. Wakamatsu E, Omori H, Kawano A, Ogawa S, Abe R. Strong TCR stimulation promotes the stabilization of Foxp3 expression in regulatory T cells induced in vitro through increasing the demethylation of Foxp3 CNS2. Biochem Biophys Res Commun. 2018;503(4):2597-602.
65. Koenecke C, Czeloth N, Bubke A, Schmitz S, Kissenpfennig A, Malissen B, et al. Alloantigen-specific de novo-induced Foxp3+ Treg revert in vivo and do not protect from experimental GVHD. European Journal of Immunology. 2009;39(11):3091-6.
66. Davidson TS, DiPaolo RJ, Andersson J, Shevach EM. Cutting Edge: IL-2 is essential for TGF-beta-mediated induction of Foxp3+ T regulatory cells. Journal of immunology. 2007;178(7):4022-6.

67. Groux H, O'Garra A, Bigler M, Rouleau M, Antonenko S, de Vries JE, et al. A CD4+ T-cell subset inhibits antigen-specific T-cell responses and prevents colitis. Nature. 1997;389(6652):737-42.
68. Vieira PL, Christensen JR, Minaee S, O'Neill EJ, Barrat FJ, Boonstra A, et al. IL-10-secreting regulatory T cells do not express Foxp3 but have comparable regulatory function to naturally occurring CD4+CD25+ regulatory T cells. Journal of immunology. 2004;172(10):5986-93.
69. Gagliani N, Magnani CF, Huber S, Gianolini ME, Pala M, Licona-Limon P, et al. Coexpression of CD49b and LAG-3 identifies human and mouse T regulatory type 1 cells. Nat Med. 2013;19(6):739-46.
70. Chen Y, Kuchroo VK, Inobe J, Hafler DA, Weiner HL. Regulatory T cell clones induced by oral tolerance: suppression of autoimmune encephalomyelitis. Science. 1994;265(5176):1237-40.
71. Duan W, So T, Mehta AK, Choi H, Croft M. Inducible CD4+LAP+Foxp3- regulatory T cells suppress allergic inflammation. Journal of immunology. 2011;187(12):6499-507.
72. Zhao H, Liao X, Kang Y. Tregs: Where We Are and What Comes Next? Front Immunol. 2017;8:1578.
73. Liu GY, Fairchild PJ, Smith RM, Prowle JR, Kioussis D, Wraith DC. Low avidity recognition of self-antigen by T cells permits escape from central tolerance. Immunity. 1995;3(4):407-15.
74. Mueller DL. Mechanisms maintaining peripheral tolerance. Nat Immunol. 2010;11(1):21-7.
75. Theofilopoulos AN, Kono DH, Baccala R. The multiple pathways to autoimmunity. Nat Immunol. 2017;18(7):716-24.
76. Dendrou CA, Fugger L, Friese MA. Immunopathology of multiple sclerosis. Nat Rev Immunol. 2015;15(9):545-58.
77. Compston A, Coles A. Multiple sclerosis. Lancet. 2008;372(9648):1502-17.
78. Katz Sand I. Classification, diagnosis, and differential diagnosis of multiple sclerosis. Curr Opin Neurol. 2015;28(3):193-205.
79. Frischer JM, Bramow S, Dal-Bianco A, Lucchinetti CF, Rauschka H, Schmidbauer M, et al. The relation between inflammation and neurodegeneration in multiple sclerosis brains. Brain. 2009;132(Pt 5):1175-89.
80. Sun JB. Autoreactive T and B cells in nervous system diseases. Acta neurologica Scandinavica Supplementum. 1993;142:1-56.
81. Bernard CC, Johns TG, Slavin A, Ichikawa M, Ewing C, Liu J, et al. Myelin oligodendrocyte glycoprotein: a novel candidate autoantigen in multiple sclerosis. Journal of molecular medicine (Berlin, Germany). 1997;75(2):77-88.
82. Kurland LT. Trauma and multiple sclerosis. Annals of neurology. 1994;36 Suppl:S33-7.
83. Goodin DS, Ebers GC, Johnson KP, Rodriguez M, Sibley WA, Wolinsky JS. The relationship of MS to physical trauma and psychological stress. Report of the Therapeutics and Technology Assessment Subcommittee of the American Academy of Neurology. 1999;52(9):1737-.
84. Cepok S, Zhou D, Srivastava R, Nessler S, Stei S, Büssow K, et al. Identification of Epstein-Barr virus proteins as putative targets of the immune response in multiple sclerosis. The Journal of clinical investigation. 2005;115(5):1352-60.
85. Grigoriadis N, van Pesch V, Paradig MSG. A basic overview of multiple sclerosis immunopathology. Eur J Neurol. 2015;22 Suppl 2:3-13.
86. t Hart BA, Gran B, Weissert R. EAE: imperfect but useful models of multiple sclerosis. Trends Mol Med. 2011;17(3):119-25.
87. Libbey JE, Fujinami RS. Experimental autoimmune encephalomyelitis as a testing paradigm for adjuvants and vaccines. Vaccine. 2011;29(17):3356-62.
88. Lafaille JJ, Nagashima K, Katsuki M, Tonegawa S. High incidence of spontaneous autoimmune encephalomyelitis in immunodeficient anti-myelin basic protein T cell receptor transgenic mice. Cell. 1994;78(3):399-408.
89. Pollinger B, Krishnamoorthy G, Berer K, Lassmann H, Bosl MR, Dunn R, et al. Spontaneous relapsing-remitting EAE in the SJL/J mouse: MOG-reactive transgenic T cells

recruit endogenous MOG-specific B cells. The Journal of experimental medicine. 2009;206(6):1303-16.
90. Burkhart C, Liu GY, Anderton SM, Metzler B, Wraith DC. Peptide-induced T cell regulation of experimental autoimmune encephalomyelitis: a role for IL-10. International immunology. 1999;11(10):1625-34.
91. Wraith D. Autoimmunity: Antigen-specific immunotherapy. Nature. 2016;530(7591):422-3.
92. Gabrysova L, Nicolson KS, Streeter HB, Verhagen J, Sabatos-Peyton CA, Morgan DJ, et al. Negative feedback control of the autoimmune response through antigen-induced differentiation of IL-10-secreting Th1 cells. The Journal of experimental medicine. 2009;206(8):1755-67.
93. Alcover A, Alarcon B, Di Bartolo V. Cell Biology of T Cell Receptor Expression and Regulation. Annual review of immunology. 2018;36:103-25.
94. Courtney AH, Lo WL, Weiss A. TCR Signaling: Mechanisms of Initiation and Propagation. Trends Biochem Sci. 2018;43(2):108-23.
95. Esensten JH, Helou YA, Chopra G, Weiss A, Bluestone JA. CD28 Costimulation: From Mechanism to Therapy. Immunity. 2016;44(5):973-88.
96. Pitcher LA, van Oers NS. T-cell receptor signal transmission: who gives an ITAM? Trends Immunol. 2003;24(10):554-60.
97. Zhang W, Trible RP, Zhu M, Liu SK, McGlade CJ, Samelson LE. Association of Grb2, Gads, and phospholipase C-gamma 1 with phosphorylated LAT tyrosine residues. Effect of LAT tyrosine mutations on T cell angigen receptor-mediated signaling. The Journal of biological chemistry. 2000;275(30):23355-61.
98. Liu SK, Fang N, Koretzky GA, McGlade CJ. The hematopoietic-specific adaptor protein gads functions in T-cell signaling via interactions with the SLP-76 and LAT adaptors. Current biology : CB. 1999;9(2):67-75.
99. Turner SD, Yeung D, Hadfield K, Cook SJ, Alexander DR. The NPM-ALK tyrosine kinase mimics TCR signalling pathways, inducing NFAT and AP-1 by RAS-dependent mechanisms. Cellular Signalling. 2007;19(4):740-7.
100. Samelson LE. Signal transduction mediated by the T cell antigen receptor: the role of adapter proteins. Annual review of immunology. 2002;20:371-94.
101. Billadeau DD, Burkhardt JK. Regulation of cytoskeletal dynamics at the immune synapse: new stars join the actin troupe. Traffic (Copenhagen, Denmark). 2006;7(11):1451-60.
102. Billadeau DD, Nolz JC, Gomez TS. Regulation of T-cell activation by the cytoskeleton. Nat Rev Immunol. 2007;7(2):131-43.
103. Zeng R, Cannon JL, Abraham RT, Way M, Billadeau DD, Bubeck-Wardenberg J, et al. SLP-76 Coordinates Nck-Dependent Wiskott-Aldrich Syndrome Protein Recruitment with Vav-1/Cdc42-Dependent Wiskott-Aldrich Syndrome Protein Activation at the T Cell-APC Contact Site. The Journal of Immunology. 2003;171(3):1360-8.
104. Dombroski D, Houghtling RA, Labno CM, Precht P, Takesono A, Caplen NJ, et al. Kinase-Independent Functions for Itk in TCR-Induced Regulation of Vav and the Actin Cytoskeleton. The Journal of Immunology. 2005;174(3):1385-92.
105. Bogin Y, Ainey C, Beach D, Yablonski D. SLP-76 mediates and maintains activation of the Tec family kinase ITK via the T cell antigen receptor-induced association between SLP-76 and ITK. Proceedings of the National Academy of Sciences. 2007;104(16):6638-43.
106. Balagopalan L, Coussens NP, Sherman E, Samelson LE, Sommers CL. The LAT story: a tale of cooperativity, coordination, and choreography. Cold Spring Harb Perspect Biol. 2010;2(8):a005512.
107. Krishna S, Zhong X. Role of diacylglycerol kinases in T cell development and function. Crit Rev Immunol. 2013;33(2):97-118.
108. Hogan PG, Chen L, Nardone J, Rao A. Transcriptional regulation by calcium, calcineurin, and NFAT. Genes Dev. 2003;17(18):2205-32.
109. Acuto O, Michel F. CD28-mediated co-stimulation: a quantitative support for TCR signalling. Nat Rev Immunol. 2003;3(12):939-51.
110. Sharpe AH, Freeman GJ. The B7–CD28 superfamily. Nature Reviews Immunology. 2002;2(2):116-26.

111. Lenschow DJ, Walunas TL, Bluestone JA. CD28/B7 SYSTEM OF T CELL COSTIMULATION. Annual review of immunology. 1996;14(1):233-58.
112. Rudd CE, Taylor A, Schneider H. CD28 and CTLA-4 coreceptor expression and signal transduction. Immunol Rev. 2009;229(1):12-26.
113. Shahinian A, Pfeffer K, Lee KP, Kündig TM, Kishihara K, Wakeham A, et al. Differential T cell costimulatory requirements in CD28-deficient mice. Science. 1993;261(5121):609-12.
114. Green JM, Noel PJ, Sperling AI, Walunas TL, Gray GS, Bluestone JA, et al. Absence of B7-dependent responses in CD28-deficient mice. Immunity. 1994;1(6):501-8.
115. King CL, Xianli J, June CH, Abe R, Lee KP. CD28-deficient mice generate an impaired Th2 response to Schistosoma mansoni infection. Eur J Immunol. 1996;26(10):2448-55.
116. Chen L, Flies DB. Molecular mechanisms of T cell co-stimulation and co-inhibition. Nat Rev Immunol. 2013;13(4):227-42.
117. Curtsinger JM, Schmidt CS, Mondino A, Lins DC, Kedl RM, Jenkins MK, et al. Inflammatory cytokines provide a third signal for activation of naive CD4+ and CD8+ T cells. Journal of immunology. 1999;162(6):3256-62.
118. Curtsinger JM, Valenzuela JO, Agarwal P, Lins D, Mescher MF. Cutting Edge: Type I IFNs Provide a Third Signal to CD8 T Cells to Stimulate Clonal Expansion and Differentiation. The Journal of Immunology. 2005;174(8):4465-9.
119. Tewari K, Nakayama Y, Suresh M. Role of Direct Effects of IFN-γ on T Cells in the Regulation of CD8 T Cell Homeostasis. The Journal of Immunology. 2007;179(4):2115-25.
120. Grakoui A, Bromley SK, Sumen C, Davis MM, Shaw AS, Allen PM, et al. The immunological synapse: a molecular machine controlling T cell activation. Science. 1999;285(5425):221-7.
121. Monks CR, Freiberg BA, Kupfer H, Sciaky N, Kupfer A. Three-dimensional segregation of supramolecular activation clusters in T cells. Nature. 1998;395(6697):82-6.
122. Monks CR, Kupfer H, Tamir I, Barlow A, Kupfer A. Selective modulation of protein kinase C-theta during T-cell activation. Nature. 1997;385(6611):83-6.
123. Freiberg BA, Kupfer H, Maslanik W, Delli J, Kappler J, Zaller DM, et al. Staging and resetting T cell activation in SMACs. Nat Immunol. 2002;3(10):911-7.
124. Costello PS, Gallagher M, Cantrell DA. Sustained and dynamic inositol lipid metabolism inside and outside the immunological synapse. Nat Immunol. 2002;3(11):1082-9.
125. Bunnell SC, Hong DI, Kardon JR, Yamazaki T, McGlade CJ, Barr VA, et al. T cell receptor ligation induces the formation of dynamically regulated signaling assemblies. J Cell Biol. 2002;158(7):1263-75.
126. Clark DJ, McMillan LE, Tan SL, Bellomo G, Massoue C, Thompson H, et al. Transient protein accumulation at the center of the T cell antigen-presenting cell interface drives efficient IL-2 secretion. Elife. 2019;8.
127. Lee KH, Holdorf AD, Dustin ML, Chan AC, Allen PM, Shaw AS. T cell receptor signaling precedes immunological synapse formation. Science. 2002;295(5559):1539-42.
128. Cemerski S, Das J, Giurisato E, Markiewicz MA, Allen PM, Chakraborty AK, et al. The balance between T cell receptor signaling and degradation at the center of the immunological synapse is determined by antigen quality. Immunity. 2008;29(3):414-22.
129. Cemerski S, Das J, Locasale J, Arnold P, Giurisato E, Markiewicz MA, et al. The stimulatory potency of T cell antigens is influenced by the formation of the immunological synapse. Immunity. 2007;26(3):345-55.
130. Singleton KL, Roybal KT, Sun Y, Fu G, Gascoigne NR, van Oers NS, et al. Spatiotemporal patterning during T cell activation is highly diverse. Sci Signal. 2009;2(65):ra15.
131. Alarcon B, Mestre D, Martinez-Martin N. The immunological synapse: a cause or consequence of T-cell receptor triggering? Immunology. 2011;133(4):420-5.
132. Brossard C, Feuillet V, Schmitt A, Randriamampita C, Romao M, Raposo G, et al. Multifocal structure of the T cell - dendritic cell synapse. Eur J Immunol. 2005;35(6):1741-53.
133. Dustin ML, Cooper JA. The immunological synapse and the actin cytoskeleton: molecular hardware for T cell signaling. Nature Immunology. 2000;1(1):23-9.

134. Roybal KT, Sinai P, Verkade P, Murphy RF, Wulfing C. The actin-driven spatiotemporal organization of T-cell signaling at the system scale. Immunol Rev. 2013;256(1):133-47.
135. Roybal KT, Mace EM, Mantell JM, Verkade P, Orange JS, Wulfing C. Early Signaling in Primary T Cells Activated by Antigen Presenting Cells Is Associated with a Deep and Transient Lamellal Actin Network. PLoS One. 2015;10(8):e0133299.
136. Ambler R, Ruan X, Murphy RF, Wulfing C. Systems Imaging of the Immune Synapse. Methods Mol Biol. 2017;1584:409-21.
137. Wraith DC, Smilek DE, Webb S. MHC-binding peptides for immunotherapy of experimental autoimmune disease. J Autoimmun. 1992;5 Suppl A:103-13.
138. Shintani T, Klionsky DJ. Autophagy in health and disease: a double-edged sword. Science. 2004;306(5698):990-5.
139. Verhagen J, Burton BR, Britton GJ, Shepard ER, Anderton SM, Wraith DC. Modification of the FoxP3 transcription factor principally affects inducible T regulatory cells in a model of experimental autoimmune encephalomyelitis. PLoS One. 2013;8(4):e61334.
140. Lafferty KJ, Prowse SJ, Simeonovic CJ, Warren HS. Immunobiology of tissue transplantation: a return to the passenger leukocyte concept. Annual review of immunology. 1983;1:143-73.
141. Curtsinger JM, Mescher MF. Inflammatory cytokines as a third signal for T cell activation. Curr Opin Immunol. 2010;22(3):333-40.
142. Davis MM, Krogsgaard M, Huppa JB, Sumen C, Purbhoo MA, Irvine DJ, et al. Dynamics of cell surface molecules during T cell recognition. Annu Rev Biochem. 2003;72:717-42.
143. Bettelli E, Carrier Y, Gao W, Korn T, Strom TB, Oukka M, et al. Reciprocal developmental pathways for the generation of pathogenic effector TH17 and regulatory T cells. Nature. 2006;441(7090):235-8.
144. Heufler C, Koch F, Stanzl U, Topar G, Wysocka M, Trinchieri G, et al. Interleukin-12 is produced by dendritic cells and mediates T helper 1 development as well as interferon-gamma production by T helper 1 cells. Eur J Immunol. 1996;26(3):659-68.
145. Heinen AP, Wanke F, Moos S, Attig S, Luche H, Pal PP, et al. Improved method to retain cytosolic reporter protein fluorescence while staining for nuclear proteins. Cytometry A. 2014;85(7):621-7.
146. Akkaya B, Holstein AH, Isaac C, Maz MP, Glass DD, Shevach EM, et al. Ex-vivo iTreg differentiation revisited: Convenient alternatives to existing strategies. J Immunol Methods. 2017;441:67-71.
147. Thornton AM, Korty PE, Tran DQ, Wohlfert EA, Murray PE, Belkaid Y, et al. Expression of Helios, an Ikaros transcription factor family member, differentiates thymic-derived from peripherally induced Foxp3+ T regulatory cells. Journal of immunology. 2010;184(7):3433-41.
148. Verhagen J, Wraith DC. Comment on "Expression of Helios, an Ikaros transcription factor family member, differentiates thymic-derived from peripherally induced Foxp3+ T regulatory cells". Journal of immunology. 2010;185(12):7129; author reply 30.
149. Thornton AM, Lu J, Korty PE, Kim YC, Martens C, Sun PD, et al. Helios(+) and Helios(-) Treg subpopulations are phenotypically and functionally distinct and express dissimilar TCR repertoires. Eur J Immunol. 2019;49(3):398-412.
150. Kishimoto T. The biology of interleukin-6. Blood. 1989;74(1):1-10.
151. Annunziato F, Cosmi L, Liotta F, Maggi E, Romagnani S. Defining the human T helper 17 cell phenotype. Trends Immunol. 2012;33(10):505-12.
152. Lee GR. The Balance of Th17 versus Treg Cells in Autoimmunity. Int J Mol Sci. 2018;19(3).
153. Laurence A, Tato CM, Davidson TS, Kanno Y, Chen Z, Yao Z, et al. Interleukin-2 signaling via STAT5 constrains T helper 17 cell generation. Immunity. 2007;26(3):371-81.
154. Gabrysova L, Wraith DC. Antigenic strength controls the generation of antigen-specific IL-10-secreting T regulatory cells. Eur J Immunol. 2010;40(5):1386-95.
155. Abbas AK, Murphy KM, Sher A. Functional diversity of helper T lymphocytes. Nature. 1996;383(6603):787-93.

156. Ng THS, Britton G, Hill E, Verhagen J, Burton B, Wraith D. Regulation of Adaptive Immunity; The Role of Interleukin-10. Frontiers in Immunology. 2013;4(129).
157. Berg DJ, Leach MW, Kuhn R, Rajewsky K, Muller W, Davidson NJ, et al. Interleukin 10 but not interleukin 4 is a natural suppressant of cutaneous inflammatory responses. The Journal of experimental medicine. 1995;182(1):99-108.
158. Kuhn R, Lohler J, Rennick D, Rajewsky K, Muller W. Interleukin-10-deficient mice develop chronic enterocolitis. Cell. 1993;75(2):263-74.
159. Chaudhry A, Samstein RM, Treuting P, Liang Y, Pils MC, Heinrich JM, et al. Interleukin-10 signaling in regulatory T cells is required for suppression of Th17 cell-mediated inflammation. Immunity. 2011;34(4):566-78.
160. Uhlig HH, Coombes J, Mottet C, Izcue A, Thompson C, Fanger A, et al. Characterization of Foxp3+CD4+CD25+ and IL-10-secreting CD4+CD25+ T cells during cure of colitis. Journal of immunology. 2006;177(9):5852-60.
161. Rubtsov YP, Rasmussen JP, Chi EY, Fontenot J, Castelli L, Ye X, et al. Regulatory T cell-derived interleukin-10 limits inflammation at environmental interfaces. Immunity. 2008;28(4):546-58.
162. Donnadieu E, Bismuth G, Trautmann A. Antigen recognition by helper T cells elicits a sequence of distinct changes of their shape and intracellular calcium. Current biology : CB. 1994;4(7):584-95.
163. Negulescu PA, Krasieva TB, Khan A, Kerschbaum HH, Cahalan MD. Polarity of T cell shape, motility, and sensitivity to antigen. Immunity. 1996;4(5):421-30.
164. Lin W, Suo YZ, Deng YT, Fan ZC, Zheng YJ, Wei XB, et al. Morphological change of CD4(+) T cell during contact with DC modulates T-cell activation by accumulation of F-actin in the immunology synapse. Bmc Immunol. 2015;16.
165. Roybal KT, Mace EM, Clark DJ, Leard AD, Herman A, Verkade P, et al. Modest Interference with Actin Dynamics in Primary T Cell Activation by Antigen Presenting Cells Preferentially Affects Lamellal Signaling. PLoS One. 2015;10(8):e0133231.
166. Zhang W, Sloan-Lancaster J, Kitchen J, Trible RP, Samelson LE. LAT: the ZAP-70 tyrosine kinase substrate that links T cell receptor to cellular activation. Cell. 1998;92(1):83-92.
167. Lin J, Weiss A. Identification of the minimal tyrosine residues required for linker for activation of T cell function. The Journal of biological chemistry. 2001;276(31):29588-95.
168. Beemiller P, Krummel MF. Mediation of T-cell activation by actin meshworks. Cold Spring Harb Perspect Biol. 2010;2(9):a002444.
169. Kumari S, Curado S, Mayya V, Dustin ML. T cell antigen receptor activation and actin cytoskeleton remodeling. Biochim Biophys Acta. 2014;1838(2):546-56.
170. Singleton K, Parvaze N, Dama KR, Chen KS, Jennings P, Purtic B, et al. A large T cell invagination with CD2 enrichment resets receptor engagement in the immunological synapse. Journal of immunology. 2006;177(7):4402-13.
171. Tskvitaria-Fuller I, Rozelle AL, Yin HL, Wulfing C. Regulation of sustained actin dynamics by the TCR and costimulation as a mechanism of receptor localization. Journal of immunology. 2003;171(5):2287-95.
172. Cullinan P, Sperling AI, Burkhardt JK. The distal pole complex: a novel membrane domain distal to the immunological synapse. Immunol Rev. 2002;189:111-22.
173. Roybal KT, Buck TE, Ruan X, Cho BH, Clark DJ, Ambler R, et al. Computational spatiotemporal analysis identifies WAVE2 and cofilin as joint regulators of costimulation-mediated T cell actin dynamics. Sci Signal. 2016;9(424):rs3.
174. Thornton AM, Shevach EM. CD4+CD25+ immunoregulatory T cells suppress polyclonal T cell activation in vitro by inhibiting interleukin 2 production. The Journal of experimental medicine. 1998;188(2):287-96.
175. Morgan DJ, Liblau R, Scott B, Fleck S, McDevitt HO, Sarvetnick N, et al. CD8(+) T cell-mediated spontaneous diabetes in neonatal mice. Journal of immunology. 1996;157(3):978-83.
176. Ai W, Li H, Song N, Li L, Chen H. Optimal method to stimulate cytokine production and its use in immunotoxicity assessment. Int J Environ Res Public Health. 2013;10(9):3834-42.

177. Chattopadhyay G, Shevach EM. Antigen-specific induced T regulatory cells impair dendritic cell function via an IL-10/MARCH1-dependent mechanism. Journal of immunology. 2013;191(12):5875-84.
178. Delon J, Bercovici N, Liblau R, Trautmann A. Imaging antigen recognition by naive CD4+ T cells: compulsory cytoskeletal alterations for the triggering of an intracellular calcium response. Eur J Immunol. 1998;28(2):716-29.
179. Finco TS, Kadlecek T, Zhang W, Samelson LE, Weiss A. LAT is required for TCR-mediated activation of PLCgamma1 and the Ras pathway. Immunity. 1998;9(5):617-26.
180. Zhang W, Irvin BJ, Trible RP, Abraham RT, Samelson LE. Functional analysis of LAT in TCR-mediated signaling pathways using a LAT-deficient Jurkat cell line. International immunology. 1999;11(6):943-50.
181. Zhang W, Trible RP, Samelson LE. LAT palmitoylation: its essential role in membrane microdomain targeting and tyrosine phosphorylation during T cell activation. Immunity. 1998;9(2):239-46.
182. Lin J, Weiss A, Finco TS. Localization of LAT in glycolipid-enriched microdomains is required for T cell activation. The Journal of biological chemistry. 1999;274(41):28861-4.
183. Zhu M, Shen S, Liu Y, Granillo O, Zhang W. Cutting Edge: Localization of linker for activation of T cells to lipid rafts is not essential in T cell activation and development. Journal of immunology. 2005;174(1):31-5.
184. Hundt M, Harada Y, De Giorgio L, Tanimura N, Zhang W, Altman A. Palmitoylation-dependent plasma membrane transport but lipid raft-independent signaling by linker for activation of T cells. Journal of immunology. 2009;183(3):1685-94.
185. Balagopalan L, Kortum RL, Coussens NP, Barr VA, Samelson LE. The linker for activation of T cells (LAT) signaling hub: from signaling complexes to microclusters. The Journal of biological chemistry. 2015;290(44):26422-9.
186. Liu S, Chen J, Cai X, Wu J, Chen X, Wu Y-T, et al. MAVS recruits multiple ubiquitin E3 ligases to activate antiviral signaling cascades. eLife. 2013;2:e00785.
187. Franklin BS, Bossaller L, De Nardo D, Ratter JM, Stutz A, Engels G, et al. The adaptor ASC has extracellular and 'prionoid' activities that propagate inflammation. Nature Immunology. 2014;15(8):727-37.
188. Gentle IE. Supramolecular Complexes in Cell Death and Inflammation and Their Regulation by Autophagy. Frontiers in Cell and Developmental Biology. 2019;7(73).
189. Rodina A, Wang T, Yan P, Gomes ED, Dunphy MPS, Pillarsetty N, et al. The epichaperome is an integrated chaperome network that facilitates tumour survival. Nature. 2016;538(7625):397-401.
190. Banani SF, Rice AM, Peeples WB, Lin Y, Jain S, Parker R, et al. Compositional Control of Phase-Separated Cellular Bodies. Cell. 2016;166(3):651-63.
191. Shin Y, Brangwynne CP. Liquid phase condensation in cell physiology and disease. Science. 2017;357(6357):eaaf4382.
192. Singleton KL, Gosh M, Dandekar RD, Au-Yeung BB, Ksionda O, Tybulewicz VL, et al. Itk controls the spatiotemporal organization of T cell activation. Sci Signal. 2011;4(193):ra66.
193. Krummel MF, Sjaastad MD, Wulfing C, Davis MM. Differential clustering of CD4 and CD3zeta during T cell recognition. Science. 2000;289(5483):1349-52.
194. Melowic HR, Stahelin RV, Blatner NR, Tian W, Hayashi K, Altman A, et al. Mechanism of diacylglycerol-induced membrane targeting and activation of protein kinase Ctheta. The Journal of biological chemistry. 2007;282(29):21467-76.
195. Wang X, Chuang H-C, Li J-P, Tan T-H. Regulation of PKC-θ function by phosphorylation in T cell receptor signaling. Frontiers in Immunology. 2012;3(197).
196. Chuang HC, Lan JL, Chen DY, Yang CY, Chen YM, Li JP, et al. The kinase GLK controls autoimmunity and NF-kappaB signaling by activating the kinase PKC-theta in T cells. Nat Immunol. 2011;12(11):1113-8.
197. Coudronniere N, Villalba M, Englund N, Altman A. NF-κB activation induced by T cell receptor/CD28 costimulation is mediated by protein kinase C-θ. Proceedings of the National Academy of Sciences. 2000;97(7):3394-9.

198. Baier-Bitterlich G, Uberall F, Bauer B, Fresser F, Wachter H, Grunicke H, et al. Protein kinase C-theta isoenzyme selective stimulation of the transcription factor complex AP-1 in T lymphocytes. Mol Cell Biol. 1996;16(4):1842-50.
199. Pfeifhofer C, Kofler K, Gruber T, Tabrizi NG, Lutz C, Maly K, et al. Protein kinase C theta affects Ca2+ mobilization and NFAT cell activation in primary mouse T cells. The Journal of experimental medicine. 2003;197(11):1525-35.
200. Gupta S, Manicassamy S, Vasu C, Kumar A, Shang W, Sun Z. Differential requirement of PKC-theta in the development and function of natural regulatory T cells. Mol Immunol. 2008;46(2):213-24.
201. Zanin-Zhorov A, Ding Y, Kumari S, Attur M, Hippen KL, Brown M, et al. Protein kinase C-theta mediates negative feedback on regulatory T cell function. Science. 2010;328(5976):372-6.
202. Ma J, Ding Y, Fang X, Wang R, Sun Z. Protein kinase C-θ inhibits inducible regulatory T cell differentiation via an AKT-Foxo1/3a-dependent pathway. Journal of immunology (Baltimore, Md : 1950). 2012;188(11):5337-47.
203. Brezar V, Tu WJ, Seddiki N. PKC-Theta in Regulatory and Effector T-cell Functions. Front Immunol. 2015;6:530.
204. Ksionda O, Saveliev A, Kochl R, Rapley J, Faroudi M, Smith-Garvin JE, et al. Mechanism and function of Vav1 localisation in TCR signalling. J Cell Sci. 2012;125(Pt 22):5302-14.
205. Reynolds LF, Smyth LA, Norton T, Freshney N, Downward J, Kioussis D, et al. Vav1 Transduces T Cell Receptor Signals to the Activation of Phospholipase C-γ1 via Phosphoinositide 3-Kinase-dependent and -independent Pathways. Journal of Experimental Medicine. 2002;195(9):1103-14.
206. Costello PS, Walters AE, Mee PJ, Turner M, Reynolds LF, Prisco A, et al. The Rho-family GTP exchange factor Vav is a critical transducer of T cell receptor signals to the calcium, ERK, and NF-κB pathways. Proceedings of the National Academy of Sciences. 1999;96(6):3035-40.
207. Tybulewicz VL. Vav-family proteins in T-cell signalling. Curr Opin Immunol. 2005;17(3):267-74.
208. Houlard M, Arudchandran R, Regnier-Ricard F, Germani A, Gisselbrecht S, Blank U, et al. Vav1 is a component of transcriptionally active complexes. The Journal of experimental medicine. 2002;195(9):1115-27.
209. Fischer KD, Kong YY, Nishina H, Tedford K, Marengère LE, Kozieradzki I, et al. Vav is a regulator of cytoskeletal reorganization mediated by the T-cell receptor. Current biology : CB. 1998;8(10):554-62.
210. Ardouin L, Bracke M, Mathiot A, Pagakis SN, Norton T, Hogg N, et al. Vav1 transduces TCR signals required for LFA-1 function and cell polarization at the immunological synapse. Eur J Immunol. 2003;33(3):790-7.
211. Vicente-Manzanares M, Sanchez-Madrid F. Role of the cytoskeleton during leukocyte responses. Nat Rev Immunol. 2004;4(2):110-22.
212. Bunnell SC, Kapoor V, Trible RP, Zhang W, Samelson LE. Dynamic actin polymerization drives T cell receptor-induced spreading: a role for the signal transduction adaptor LAT. Immunity. 2001;14(3):315-29.
213. Babich A, Li S, O'Connor RS, Milone MC, Freedman BD, Burkhardt JK. F-actin polymerization and retrograde flow drive sustained PLCgamma1 signaling during T cell activation. J Cell Biol. 2012;197(6):775-87.
214. Campi G, Varma R, Dustin ML. Actin and agonist MHC-peptide complex-dependent T cell receptor microclusters as scaffolds for signaling. The Journal of experimental medicine. 2005;202(8):1031-6.
215. Ritter AT, Asano Y, Stinchcombe JC, Dieckmann NM, Chen BC, Gawden-Bone C, et al. Actin depletion initiates events leading to granule secretion at the immunological synapse. Immunity. 2015;42(5):864-76.
216. Valitutti S, Dessing M, Aktories K, Gallati H, Lanzavecchia A. Sustained signaling leading to T cell activation results from prolonged T cell receptor occupancy. Role of T cell actin cytoskeleton. The Journal of experimental medicine. 1995;181(2):577-84.

217. Zhang J, Shehabeldin A, da Cruz LAG, Butler J, Somani A-K, McGavin M, et al. Antigen Receptor–Induced Activation and Cytoskeletal Rearrangement Are Impaired in Wiskott-Aldrich Syndrome Protein–Deficient Lymphocytes. Journal of Experimental Medicine. 1999;190(9):1329-42.
218. Wülfing C, Bauch A, Crabtree GR, Davis MM. The vav exchange factor is an essential regulator in actin-dependent receptor translocation to the lymphocyte–antigen-presenting cell interface. Proceedings of the National Academy of Sciences. 2000;97(18):10150-5.
219. Zeng R, Cannon JL, Abraham RT, Way M, Billadeau DD, Bubeck-Wardenberg J, et al. SLP-76 coordinates Nck-dependent Wiskott-Aldrich syndrome protein recruitment with Vav-1/Cdc42-dependent Wiskott-Aldrich syndrome protein activation at the T cell-APC contact site. Journal of immunology. 2003;171(3):1360-8.
220. Gomez TS, McCarney SD, Carrizosa E, Labno CM, Comiskey EO, Nolz JC, et al. HS1 functions as an essential actin-regulatory adaptor protein at the immune synapse. Immunity. 2006;24(6):741-52.
221. Gomez TS, Hamann MJ, McCarney S, Savoy DN, Lubking CM, Heldebrant MP, et al. Dynamin 2 regulates T cell activation by controlling actin polymerization at the immunological synapse. Nature Immunology. 2005;6(3):261-70.
222. Yi J, Wu XS, Crites T, Hammer JA, 3rd. Actin retrograde flow and actomyosin II arc contraction drive receptor cluster dynamics at the immunological synapse in Jurkat T cells. Mol Biol Cell. 2012;23(5):834-52.
223. Takahashi T, Kuniyasu Y, Toda M, Sakaguchi N, Itoh M, Iwata M, et al. Immunologic self-tolerance maintained by CD25+CD4+ naturally anergic and suppressive T cells: induction of autoimmune disease by breaking their anergic/suppressive state. International immunology. 1998;10(12):1969-80.
224. Malek TR. The biology of interleukin-2. Annual review of immunology. 2008;26:453-79.
225. Boyman O, Sprent J. The role of interleukin-2 during homeostasis and activation of the immune system. Nat Rev Immunol. 2012;12(3):180-90.
226. Barthlott T, Moncrieffe H, Veldhoen M, Atkins CJ, Christensen J, O'Garra A, et al. CD25+CD4+ T cells compete with naive CD4+ T cells for IL-2 and exploit it for the induction of IL-10 production. International immunology. 2005;17(3):279-88.
227. Glimcher LH, McKean DJ, Choi E, Seidman JG. Complex regulation of class II gene expression: analysis with class II mutant cell lines. Journal of immunology. 1985;135(5):3542-50.
228. Shevach EM. Foxp3(+) T Regulatory Cells: Still Many Unanswered Questions-A Perspective After 20 Years of Study. Front Immunol. 2018;9:1048.
229. Collison LW, Vignali DAA. In vitro Treg suppression assays. Methods in molecular biology (Clifton, NJ). 2011;707:21-37.
230. Kelchtermans H, De Klerck B, Mitera T, Van Balen M, Bullens D, Billiau A, et al. Defective CD4+CD25+ regulatory T cell functioning in collagen-induced arthritis: an important factor in pathogenesis, counter-regulated by endogenous IFN-gamma. Arthritis Res Ther. 2005;7(2):R402-15.
231. Sawitzki B, Kingsley CI, Oliveira V, Karim M, Herber M, Wood KJ. IFN-gamma production by alloantigen-reactive regulatory T cells is important for their regulatory function in vivo. The Journal of experimental medicine. 2005;201(12):1925-35.
232. Wei G, Wei L, Zhu J, Zang C, Hu-Li J, Yao Z, et al. Global mapping of H3K4me3 and H3K27me3 reveals specificity and plasticity in lineage fate determination of differentiating CD4+ T cells. Immunity. 2009;30(1):155-67.
233. Koenecke C, Lee C-W, Thamm K, Föhse L, Schafferus M, Mittrücker H-W, et al. IFN-γ Production by Allogeneic Foxp3⁺ Regulatory T Cells Is Essential for Preventing Experimental Graft-versus-Host Disease. The Journal of Immunology. 2012;189(6):2890-6.
234. Wood KJ, Sawitzki B. Interferon gamma: a crucial role in the function of induced regulatory T cells in vivo. Trends Immunol. 2006;27(4):183-7.

235. Mitchell RE, Hassan M, Burton BR, Britton G, Hill EV, Verhagen J, et al. IL-4 enhances IL-10 production in Th1 cells: implications for Th1 and Th2 regulation. Sci Rep. 2017;7(1):11315.
236. Saraiva M, Christensen JR, Veldhoen M, Murphy TL, Murphy KM, O'Garra A. Interleukin-10 production by Th1 cells requires interleukin-12-induced STAT4 transcription factor and ERK MAP kinase activation by high antigen dose. Immunity. 2009;31(2):209-19.
237. Gaud G, Lesourne R, Love PE. Regulatory mechanisms in T cell receptor signalling. Nat Rev Immunol. 2018;18(8):485-97.
238. Kong KF, Yokosuka T, Canonigo-Balancio AJ, Isakov N, Saito T, Altman A. A motif in the V3 domain of the kinase PKC-theta determines its localization in the immunological synapse and functions in T cells via association with CD28. Nat Immunol. 2011;12(11):1105-12.
239. Kiani A, García-Cózar FJ, Habermann I, Laforsch S, Aebischer T, Ehninger G, et al. Regulation of interferon-γ gene expression by nuclear factor of activated T cells. Blood. 2001;98(5):1480-8.
240. Lucca LE, Dominguez-Villar M. Modulation of regulatory T cell function and stability by co-inhibitory receptors. Nature Reviews Immunology. 2020.
241. Alsaab HO, Sau S, Alzhrani R, Tatiparti K, Bhise K, Kashaw SK, et al. PD-1 and PD-L1 Checkpoint Signaling Inhibition for Cancer Immunotherapy: Mechanism, Combinations, and Clinical Outcome. Front Pharmacol. 2017;8:561.
242. Keir ME, Butte MJ, Freeman GJ, Sharpe AH. PD-1 and Its Ligands in Tolerance and Immunity. Annual review of immunology. 2008;26(1):677-704.
243. Rotte A. Combination of CTLA-4 and PD-1 blockers for treatment of cancer. J Exp Clin Cancer Res. 2019;38(1):255.
244. Chambers CA, Kuhns MS, Egen JG, Allison JP. CTLA-4-mediated inhibition in regulation of T cell responses: mechanisms and manipulation in tumor immunotherapy. Annual review of immunology. 2001;19:565-94.
245. Perkins D, Wang Z, Donovan C, He H, Mark D, Guan G, et al. Regulation of CTLA-4 expression during T cell activation. Journal of immunology. 1996;156(11):4154-9.
246. Takahashi T, Tagami T, Yamazaki S, Uede T, Shimizu J, Sakaguchi N, et al. Immunologic self-tolerance maintained by CD25(+)CD4(+) regulatory T cells constitutively expressing cytotoxic T lymphocyte-associated antigen 4. The Journal of experimental medicine. 2000;192(2):303-10.
247. Buchbinder EI, Desai A. CTLA-4 and PD-1 Pathways: Similarities, Differences, and Implications of Their Inhibition. Am J Clin Oncol. 2016;39(1):98-106.
248. Fallarino F, Fields PE, Gajewski TF. B7-1 engagement of cytotoxic T lymphocyte antigen 4 inhibits T cell activation in the absence of CD28. The Journal of experimental medicine. 1998;188(1):205-10.
249. Schneider H, Downey J, Smith A, Zinselmeyer BH, Rush C, Brewer JM, et al. Reversal of the TCR Stop Signal by CTLA-4. Science. 2006;313(5795):1972.
250. Wing K, Onishi Y, Prieto-Martin P, Yamaguchi T, Miyara M, Fehervari Z, et al. CTLA-4 control over Foxp3+ regulatory T cell function. Science. 2008;322(5899):271-5.
251. Freeman GJ, Long AJ, Iwai Y, Bourque K, Chernova T, Nishimura H, et al. Engagement of the PD-1 immunoinhibitory receptor by a novel B7 family member leads to negative regulation of lymphocyte activation. The Journal of experimental medicine. 2000;192(7):1027-34.
252. Latchman Y, Wood CR, Chernova T, Chaudhary D, Borde M, Chernova I, et al. PD-L2 is a second ligand for PD-1 and inhibits T cell activation. Nat Immunol. 2001;2(3):261-8.
253. Yamazaki T, Akiba H, Iwai H, Matsuda H, Aoki M, Tanno Y, et al. Expression of programmed death 1 ligands by murine T cells and APC. Journal of immunology. 2002;169(10):5538-45.
254. Zhong X, Tumang JR, Gao W, Bai C, Rothstein TL. PD-L2 expression extends beyond dendritic cells/macrophages to B1 cells enriched for V(H)11/V(H)12 and phosphatidylcholine binding. Eur J Immunol. 2007;37(9):2405-10.
255. Sheppard KA, Fitz LJ, Lee JM, Benander C, George JA, Wooters J, et al. PD-1 inhibits T-cell receptor induced phosphorylation of the ZAP70/CD3zeta signalosome and downstream signaling to PKCtheta. FEBS letters. 2004;574(1-3):37-41.

256. Sharpe AH, Pauken KE. The diverse functions of the PD1 inhibitory pathway. Nat Rev Immunol. 2018;18(3):153-67.
257. Wang L, Pino-Lagos K, de Vries VC, Guleria I, Sayegh MH, Noelle RJ. Programmed death 1 ligand signaling regulates the generation of adaptive Foxp3⁺CD4⁺ regulatory T cells. Proceedings of the National Academy of Sciences. 2008;105(27):9331.
258. Francisco LM, Salinas VH, Brown KE, Vanguri VK, Freeman GJ, Kuchroo VK, et al. PD-L1 regulates the development, maintenance, and function of induced regulatory T cells. The Journal of experimental medicine. 2009;206(13):3015-29.
259. Leach DR, Krummel MF, Allison JP. Enhancement of Antitumor Immunity by CTLA-4 Blockade. Science. 1996;271(5256):1734-6.
260. Hirano F, Kaneko K, Tamura H, Dong H, Wang S, Ichikawa M, et al. Blockade of B7-H1 and PD-1 by Monoclonal Antibodies Potentiates Cancer Therapeutic Immunity. Cancer Research. 2005;65(3):1089-96.
261. Selby MJ, Engelhardt JJ, Quigley M, Henning KA, Chen T, Srinivasan M, et al. Anti-CTLA-4 Antibodies of IgG2a Isotype Enhance Antitumor Activity through Reduction of Intratumoral Regulatory T Cells. Cancer Immunology Research. 2013;1(1):32-42.
262. Yoshida K, Okamoto M, Sasaki J, Kuroda C, Ishida H, Ueda K, et al. Anti-PD-1 antibody decreases tumour-infiltrating regulatory T cells. BMC cancer. 2020;20(1):25.
263. Sharma A, Subudhi SK, Blando J, Scutti J, Vence L, Wargo J, et al. Anti-CTLA-4 Immunotherapy Does Not Deplete FOXP3⁺ Regulatory T Cells (Tregs) in Human Cancers. Clinical Cancer Research. 2019;25(4):1233-8.
264. Tang AL, Teijaro JR, Njau MN, Chandran SS, Azimzadeh A, Nadler SG, et al. CTLA4 expression is an indicator and regulator of steady-state CD4+ FoxP3+ T cell homeostasis. Journal of immunology (Baltimore, Md : 1950). 2008;181(3):1806-13.
265. Kavanagh B, O'Brien S, Lee D, Hou Y, Weinberg V, Rini B, et al. CTLA4 blockade expands FoxP3+ regulatory and activated effector CD4+ T cells in a dose-dependent fashion. Blood. 2008;112(4):1175-83.
266. Verhagen J, Gabrysova L, Minaee S, Sabatos CA, Anderson G, Sharpe AH, et al. Enhanced selection of FoxP3+ T-regulatory cells protects CTLA-4-deficient mice from CNS autoimmune disease. Proc Natl Acad Sci U S A. 2009;106(9):3306-11.
267. Verhagen J, Genolet R, Britton GJ, Stevenson BJ, Sabatos-Peyton CA, Dyson J, et al. CTLA-4 controls the thymic development of both conventional and regulatory T cells through modulation of the TCR repertoire. Proc Natl Acad Sci U S A. 2013;110(3):E221-30.
268. Verhagen J, Gabrysova L, Shepard ER, Wraith DC. Ctla-4 modulates the differentiation of inducible Foxp3+ Treg cells but IL-10 mediates their function in experimental autoimmune encephalomyelitis. PLoS One. 2014;9(9):e108023.
269. Park HJ, Park JS, Jeong YH, Son J, Ban YH, Lee BH, et al. PD-1 upregulated on regulatory T cells during chronic virus infection enhances the suppression of CD8+ T cell immune response via the interaction with PD-L1 expressed on CD8+ T cells. Journal of immunology. 2015;194(12):5801-11.
270. Montler R, Bell RB, Thalhofer C, Leidner R, Feng Z, Fox BA, et al. OX40, PD-1 and CTLA-4 are selectively expressed on tumor-infiltrating T cells in head and neck cancer. Clin Transl Immunology. 2016;5(4):e70-e.
271. Wei SC, Anang NAS, Sharma R, Andrews MC, Reuben A, Levine JH, et al. Combination anti-CTLA-4 plus anti-PD-1 checkpoint blockade utilizes cellular mechanisms partially distinct from monotherapies. Proc Natl Acad Sci U S A. 2019;116(45):22699-709.
272. Houtman JC, Yamaguchi H, Barda-Saad M, Braiman A, Bowden B, Appella E, et al. Oligomerization of signaling complexes by the multipoint binding of GRB2 to both LAT and SOS1. Nat Struct Mol Biol. 2006;13(9):798-805.
273. Zhu J, Paul WE. CD4 T cells: fates, functions, and faults. Blood. 2008;112(5):1557-69.
274. Schlessinger J. SH2/SH3 signaling proteins. Curr Opin Genet Dev. 1994;4(1):25-30.
275. Bubeck Wardenburg J, Pappu R, Bu JY, Mayer B, Chernoff J, Straus D, et al. Regulation of PAK activation and the T cell cytoskeleton by the linker protein SLP-76. Immunity. 1998;9(5):607-16.

276. Cretney E, Xin A, Shi W, Minnich M, Masson F, Miasari M, et al. The transcription factors Blimp-1 and IRF4 jointly control the differentiation and function of effector regulatory T cells. Nature Immunology. 2011;12(4):304-11.
277. Kubo M, Motomura Y. Transcriptional regulation of the anti-inflammatory cytokine IL-10 in acquired immune cells. Front Immunol. 2012;3:275.
278. Hashimoto-Tane A, Saito T. Dynamic Regulation of TCR-Microclusters and the Microsynapse for T Cell Activation. Front Immunol. 2016;7:255.
279. Bluestone JA, Buckner JH, Fitch M, Gitelman SE, Gupta S, Hellerstein MK, et al. Type 1 diabetes immunotherapy using polyclonal regulatory T cells. Sci Transl Med. 2015;7(315):315ra189-315ra189.
280. Terry LV, Oo YH. The Next Frontier of Regulatory T Cells: Promising Immunotherapy for Autoimmune Diseases and Organ Transplantations. Front Immunol. 2020;11:565518.
281. Eggenhuizen PJ, Ng BH, Ooi JD. Treg Enhancing Therapies to Treat Autoimmune Diseases. Int J Mol Sci. 2020;21(19).
282. Tang Q. Therapeutic window of interleukin-2 for autoimmune diseases. Diabetes. 2015;64(6):1912-3.
283. Thomson AW, Turnquist HR, Raimondi G. Immunoregulatory functions of mTOR inhibition. Nat Rev Immunol. 2009;9(5):324-37.